Analysing an unbiased forward genetic screen for longevity: Inhibiting the integrated stress response extends lifespan through selective mRNA translation

Laura Wester

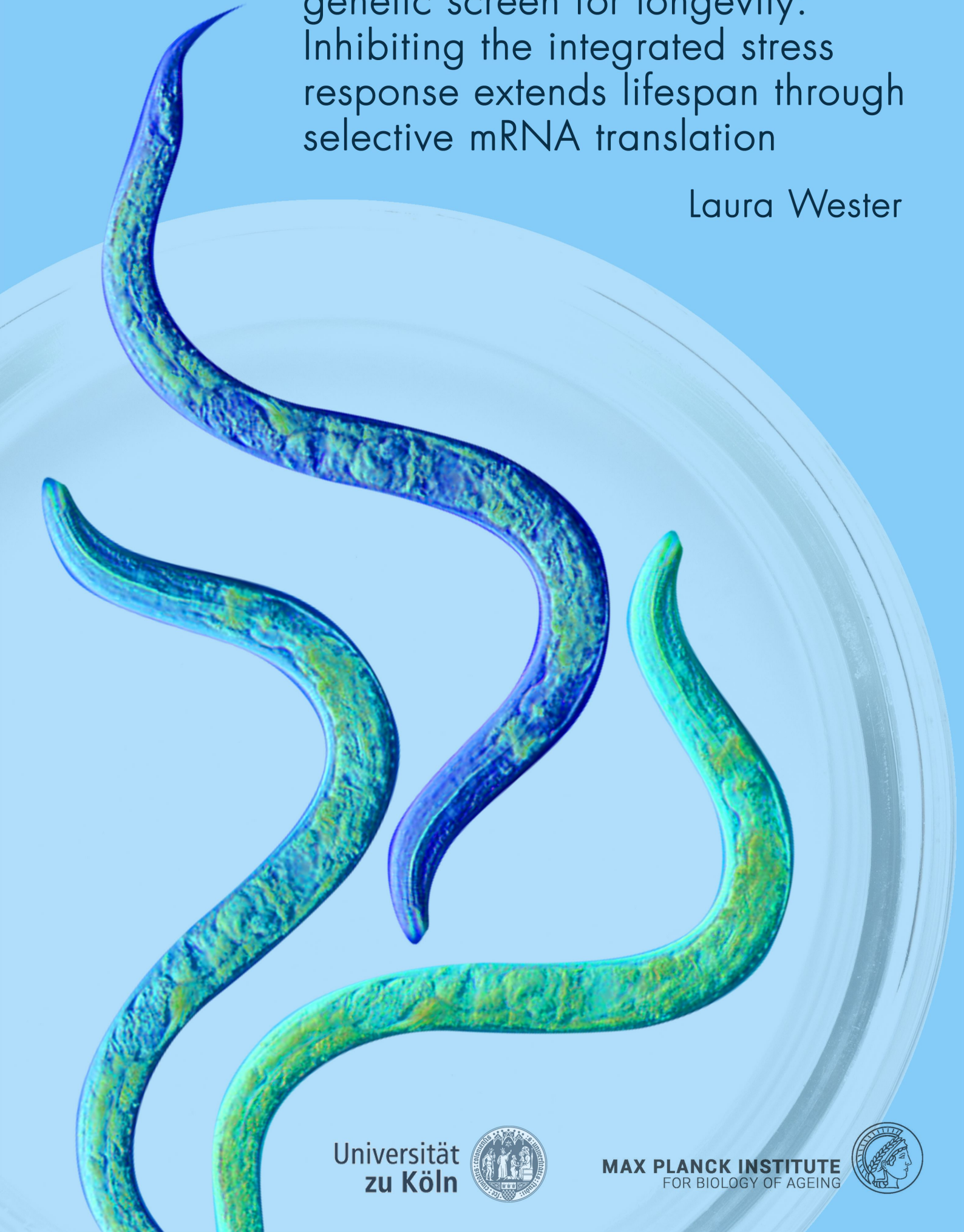

Universität zu Köln

MAX PLANCK INSTITUTE FOR BIOLOGY OF AGEING

Analysing an unbiased forward genetic screen for longevity: Inhibiting the integrated stress response extends lifespan through selective mRNA translation

Inaugural - Dissertation
zur
Erlangung des Doktorgrades
der Mathematisch-Naturwissenschaftlichen Fakultät
der Universität zu Köln

vorgelegt von
Laura Elisabeth Wester
aus Mainz

Köln, 2021

Gutachter: Dr. Martin Denzel & Prof. Dr. Andreas Beyer

Tag der mündlichen Prüfung: 19. Juli 2021

The work described in this dissertation was conducted from October 2016 until May 2021 under the supervision of Dr. Martin Denzel at the Max Planck Institute for Biology of Ageing, Joseph-Stelzmann-Straße 9b, D-50931, Cologne, Germany. Part of this work was conducted in collaboration with associate Prof. William Mair and Anne Lanjuin, PhD, at Harvard T.H. Chan School of Public Health, Department of Molecular Metabolism, 665 Huntington Avenue, Boston, Massachusetts 02115, USA.

Die in dieser Dissertation beschriebenen Arbeiten wurden zwischen Oktober 2016 und Mai 2021 unter der Leitung von Dr. Martin Denzel am Max-Planck-Institut für Biologie des Alterns, Joseph-Stelzmann-Straße 9b, D-50931, Köln, Deutschland, durchgeführt. Teile dieser Arbeit wurden in Zusammenarbeit mit associate Prof. William Mair and Anne Lanjuin, PhD, an der Harvard T.H. Chan School of Public Health, Department of Molecular Metabolism, 665 Huntington Avenue, Boston, Massachusetts 02115, USA, durchgeführt.

Parts of this work have been published:
Teile dieser Arbeit wurden bereits veröffentlicht:

M Derisbourg, **L Wester**, R Baddi, M Denzel. Mutagenesis screen uncovers lifespan extension through integrated stress response inhibition without reduced mRNA translation. *Nature Communications*. DOI: 10.1038/s41467-021-21743-x. **2021**. Equal contribution.

Contents

Abstract

Living a long and healthy life is a central human desire. While the human average age has been increasing since generations, age-associated pathologies comprising cancer and cardiovascular diseases are the main cause of death in Western countries. This makes biological ageing, which is defined as a progressive decline of function in cells and tissues throughout an organism over time, a major challenge for society. Using forward genetic screens in the nematode *Caenorhabditis elegans* (*C. elegans*), genetic signalling pathways have been identified to control the ageing process, such as the insulin/IGF-like signalling (IIS) pathway. In the past decade, genetic techniques have improved massively and nowadays allow the combination of chemical mutagenesis and whole genome sequencing. To uncover novel genes that modulate the process of ageing, Dr. Martin Denzel and his team performed the first forward genetic screen in *C. elegans*, directly aiming for enhanced lifespan in mutant worms, and combined it with whole genome sequencing of the long-lived animals. This strategy allowed screening at amino acid resolution, generated loss- and gain-of-function mutations and affected non-essential and essential genes. The overall research aim of this PhD project was the identification of novel conserved biological mechanisms of ageing, making use of the forward longevity screen.

From the described screen, we identified over 100 worm lines with a mean lifespan extension of 18 % and more compared to a control and sequenced their whole genomes. Using a stringent pipeline to identify candidate longevity genes from the sequencing data, we were able to find novel alleles of known longevity genes, for example within the IIS pathway, validating our approach. We further found mutations in genes belonging to the translation initiation pathway and the integrated stress response (ISR) to be causative for longevity. The process of mRNA translation initiation relies on the activity of the eukaryotic translation initiation factor 2 (eIF2) and it's guanine nucleotide exchange factor eIF2B. Upon organismal stress, different kinases can phosphorylate eIF2. The kinases thereby inhibit eIF2 and eIF2B function and thus down-regulate global protein synthesis. This mediates further downstream effects in form of a transcriptional reprogramming, all together forming the ISR and adapting the animals to cellular stress. A reduction of global mRNA translation was shown to be associated with longevity in multiple research lines. From the forward longevity screen, we revealed a mutation in *iftb-1*, the β subunit of the eIF2 complex, that decreased mRNA translation and therefore extended lifespan. Strikingly, we further identified mutations in the worm eIF2 kinases *gcn-2* and *pek-1* as well as in *ppp-1*, the γ subunit of eIF2B. These mutations caused longevity without a reduction of overall protein synthesis. While global mRNA translation remained unchanged in the *ppp-1* mutants, we identified the specific translation of selected mRNAs to be altered. We further identified the selective translation of uncharacterised *kin-35* to be required for longevity in *ppp-1* animals.

We showed that the mutations in *gcn-2*, *pek-1* and *ppp-1* likewise inhibited ISR activity. We therefore speculated that a full genetic ISR inhibition causes longevity in *C. elegans*. We generated a phosphorylation-deficient S51A mutation in eIF2 that fully impaired the ISR in the respective worms. This full ISR inhibition strikingly caused longevity. We further provided evidence that pharmacological ISR inhibition extends lifespan in the nematode.

Phenocopying the *ppp-1* animals, during full genetic or partial pharmacological inhibition of the ISR, bulk protein synthesis was unaffected. However, the longevity relied on *kin-35* in all cases. In sum, we showed that a genetic or pharmacological inhibition of the ISR affects worm survival without suppression of global mRNA translation. Instead, we showed that a translational switch is required for the observed lifespan extension. From our results, we speculate that ISR inhibition and a tuning of mRNA translation might be a viable option to also promote healthy ageing in higher organisms including mammals and potentially humans.

While strong genetic and biochemical research techniques come to use in *C. elegans*, tissue-specific studies are limited due to the small size of the worm. Hence, our studies on the role of a translational switch in longevity during ISR inhibition were restricted to whole body analyses. Another aim of my dissertation therefore was the generation of novel research tools to enable the comprehensive analysis of tissue-specific translation from *C. elegans*. Together with the team of assoc. Prof. William Mair (Harvard T.H. Chan School of Public Health), we used the CRISPR/Cas9 technology to generate worms with a biochemically tagged ribosomal protein expressed either endogenously or within selected tissues only. We deeply characterised the effects of the biochemical ribosome tags (RiboTags) regarding worm health or changes in translation without detecting any undesired phenotypes or side-effects. Finally, the endogenously or tissue-specifically expressed RiboTags enabled us to pull down fully assembled ribosomes including the translated mRNA from co-immuno-precipitations (co-IPs). The quality of the eluted RNA was sufficient for subsequent RNA sequencing. The sequencing and analysis of purified RNA from RiboTag co-IPs of neuron-specifically tagged ribosomes confirmed the tissue-specificity of the approach. We aim to generate more worm lines expressing a RiboTag in different tissues such as the muscle or intestine. We provide a clean neuronal RiboTag model that was characterised in depth and will be used to study the role of tissue-specific translation in the context of ageing and longevity, for example during ISR inhibition in *ppp-1*-mutant animals.

Zusammenfassung

Ein langes und gesundes Leben zu führen ist ein zentraler Wunsch des Menschen. Während das Durchschnittsalter der Menschen seit Generationen ansteigt, sind alters-assoziierte Krankheiten wie Krebs und Herz-Kreislauf-Erkrankungen die Haupttodesursache in westlichen Ländern. So wird das hohe gesellschaftliche Durchschnittsalter zu einer großen Herausforderung für die Gesellschaft. Biologisch gesehen ist das Altern definiert als ein fortschreitender Funktionsrückgang von Zellen und Geweben im gesamten Organismus im Laufe der Zeit. Mit Hilfe von genetischen Mutagenese-Screens im Fadenwurm *Caenorhabditis elegans* (*C. elegans*) wurden genetische Signalwege identifiziert, die den Alterungsprozess kontrollieren, wie zum Beispiel der Insulin/IGF-like Signalweg (IIS). Im letzten Jahrzehnt haben sich die genetischen Labortechniken massiv verbessert und erlauben heute die Kombination von chemischer Mutagenese und Hochdurchsatz-Sequenzierung. Um neue Gene zu entdecken, die den Alterungsprozess modulieren, führten Dr. Martin Denzel und sein Team den ersten genetischen Mutagenese-Screen in *C. elegans* durch, der direkt auf eine erhöhte Lebensspanne in mutierten Würmern abzielte und mit einer Hochdurchsatz-Sequenzierung der langlebigen Tiere kombiniert wurde. Diese Strategie ermöglichte ein Mutagenese-Screening mit einer Auflösung im Aminosäure Bereich, generierte Loss- und Gain-of-Function Mutationen und beeinflusste nicht-essentielle sowie essentielle Gene. Das übergeordnete Forschungsziel dieses Projekts war die Identifizierung neuer konservierter biologischer Mechanismen des Alterns unter Nutzung des Mutagenese-Screens für Langlebigkeit in *C. elegans*.

Aus dem beschriebenen Screen identifizierten wir über 100 Wurmlinien mit einer mittleren Lebensverlängerung von 18 % und mehr im Vergleich zu nicht-mutagenisierten Tieren. Anschließend sequenzierten wir das Genom der langlebigen Tiere. Mithilfe einer stringenten Strategie zur Identifizierung von Kandidatengenen aus den Sequenzierungsdaten konnten wir neue Allele bekannter Langlebigkeitsgene finden, zum Beispiel innerhalb des IIS-Signalwegs. Dies validierte unseren Ansatz. Darüber hinaus fanden wir Mutationen in Genen, die zur Initiation der Translation von mRNA und zur integrierten Stressreaktion (ISR) gehören. Wir konnten zeigen, dass die entsprechenden Mutationen Langlebigkeit in Würmern verursachen. Der Prozess der mRNA-Translations-Initiation beruht auf der Aktivität des eukaryotischen Translations-Initiations Faktors 2 (eIF2) und seines Guanin-Nukleotid-Austauschfaktors eIF2B. Unter zellulärem Stress wird eIF2 durch verschiedene Kinasen phosphoryliert. So hemmen die Kinasen die Funktion von eIF2 und eIF2B und regulieren damit die globale Proteinsynthese herunter. Dies vermittelt weitere Downstream-Effekte in Form einer transkriptionellen Umprogrammierung, welche die Tiere an den zellulären Stress adaptiert. Eine Reduktion der globalen mRNA-Translation wurde bereits mit Langlebigkeit in Verbindung gebracht. Aus dem Mutagenese-Screen für Langlebigkeit haben wir eine Mutation in *iftb-1*, der β-Untereinheit des eIF2-Komplexes, entdeckt, welche die mRNA-Translation verringerte und damit die Lebensspanne der Würmer verlängerte. Weiterhin identifizierten wir Mutationen in den eIF2-Kinasen *gcn-2* und *pek-1* des Wurms, sowie in *ppp-1*, der γ-Untereinheit von eIF2B. Interessanterweise verursachten diese Mutationen Langlebigkeit ohne eine Reduktion der gesamten Proteinsynthese. Während die globale mRNA-Translation in den *ppp-1* Mutanten unverändert blieb, konnten wir aufzeigen, dass

die Translation ausgewählter mRNAs in den *ppp-1* Tieren verändert war. Weiterhin zeigten wir, dass die selektive Translation von *kin-35*, einem bislang uncharakterisierten Gen, für die Langlebigkeit in *ppp-1* Tieren erforderlich ist.

Die Mutationen in *gcn-2*, *pek-1* und *ppp-1* hemmten die Aktivität der ISR. Wir spekulierten daher, dass eine vollständige genetische ISR-Inhibition Langlebigkeit in *C. elegans* verursacht. Wir erzeugten eine phosphorylierungs-defiziente S51A-Mutation in eIF2, welche die ISR in den entsprechenden Würmern vollständig hemmte. Diese vollständige ISR-Inhibition führte ebenso zu Langlebigkeit wie die Mutationen in *ppp-1*. Wir konnten außerdem nachweisen, dass auch eine pharmakologische ISR-Inhibition die Lebensspanne im Fadenwurm verlängert. Wie beobachtet in den *ppp-1* Tieren, war während der vollständigen genetischen oder teilweisen pharmakologischen Hemmung der ISR die Gesamt-Proteinsynthese unbeeinflusst. Die Langlebigkeit hing jedoch in allen Fällen von der selektiven Translation von *kin-35* ab. Zusammenfassend konnten wir zeigen, dass ein Fine-tuning von eIF2 durch genetische oder pharmakologische Hemmung der ISR das überleben der Würmer beeinflusst, ohne dabei die gesamte Proteinsynthese zu modifizieren. Wir konnten zeigen, dass die Translation spezifischer mRNAs für die beobachtete Lebensverlängerung erforderlich ist. Aufgrund unserer Ergebnisse spekulieren wir, dass die Hemmung der ISR und ein Fine-tuning der mRNA-Translation eine praktikable Option sein könnte, um auch in höheren Organismen, einschließlich Säugetieren und Menschen, gesundes Altern zu fördern.

Während in *C. elegans* verschiedenste genetische und biochemische Forschungstechniken zum Einsatz kommen, sind gewebespezifische Studien aufgrund der geringen Größe des Wurms begrenzt. Daher beschränkten sich unsere Untersuchungen zur Rolle der selektiven Translation in Alterungsprozessen auf Ganzkörperanalysen des Wurms. Ein weiteres Ziel meiner Dissertation war daher die Generierung neuartiger Forschungswerkzeuge, die eine umfassende Analyse der gewebespezifischen Translation in *C. elegans* ermöglichen. Zusammen mit dem Team von Assoc. Prof. William Mair (Harvard T.H. Chan School of Public Health) verwendeten wir die CRISPR/Cas9-Technologie, um Würmer mit einem biochemisch markierten ribosomalen Protein auszustatten, das entweder endogen oder nur in ausgewählten Geweben exprimiert wird. Wir charakterisierten die Auswirkungen der biochemisch getaggten Ribosomen (RiboTags) auf die Gesundheit der Würmer und auf Veränderungen der Translation, ohne unerwünschte Phänotypen oder Nebenwirkungen festzustellen. Schließlich konnten wir die endogen und gewebespezifisch exprimierten RiboTags dazu nutzen, vollständig assemblierte Ribosomen einschließlich der translatierten mRNA aus Co-Immuno-Präzipitationen (Co-IPs) zu isolieren. Die Qualität der eluierten RNA war ausreichend für eine anschließende RNA-Sequenzierung. Die Sequenzierung und Analyse der eluierten RNA aus RiboTag-Co-IPs von Neuronen-spezifisch markierten Ribosomen bestätigte die Gewebespezifität des Ansatzes. Unser Ziel ist es, weitere Wurmlinien zu generieren, die einen RiboTag in verschiedenen Geweben wie dem Muskel oder dem Verdauungstrakt exprimieren. Wir stellen hiermit ein neuronales RiboTag-Modell zur Verfügung, das eingehend charakterisiert wurde. Perspektivisch soll es dazu verwendet werden, die Rolle der gewebespezifischen Translation im Zusammenhang mit Alterung und Langlebigkeit zu untersuchen, zum Beispiel während der ISR-Hemmung in *ppp-1*-mutanten Würmern.

List of Figures

List of Tables

Abbreviations

^{FLAG}RPL-22	3xFLAG::RPL22
4E-BP	eIF4E-binding protein
A-site	aminoacyl-site
AMP	adenosine monophosphate
ApoE	Apolipoprotein E
ATF	activating transcription factor
ATP	adenosine triphosphate
bp	base pair
cDNA	complementary DNA
CDS	coding sequence
C. elegans	*Caenorhabditis elegans*
CHOP	C/EBP homology protein
cIAP	cellular inhibitor of apoptosis protein
co-IP	co-immuno-precipitation
CReP	constitutive repressor of eIF2α phosphorylation
CRISPR	clustered regularly interspaced short palindromic repeat
Cryo-EM	cryogenic electron microscopy
DAF	abnormal dauer formation
DHPC	1,2-diheptanoyl-sn-glycero-3-phosphocholine
DMSO	dimethyl sulfoxide
DNA	deoxyribonucleic acid
DR	dietary restriction
dsRNA	doublestranded RNA
DTT	dithiothreitol
E-site	exit-site
e.g.	*exempli gratia*
eGFP	enhanced green fluorescent protein
eIF	eukaryotic initiation factor
elu	elution
EMS	ethyl methanesulfonate
ER	endoplasmic reticulum
eRF	eukaryotic protein release factor
E. coli	*Escherichia coli*
FOX	forkhead box
FOXO	forkhead box class O
FUDR	5-Fluoro-2´-deoxyuridine
GADD34	growth arrest DNA-inducible gene 34
GCN	general control non-derepressible
GDP	guanosine diphosphate
GEF	guanine nucleotide exchange factor
GFAT	glutamine-fructose 6-phosphate aminotransferase
GFP	green fluorescent protein
GO	gene ontology
GTP	guanosine triphosphate
GWAS	genome-wide association studies
HDR	homology directed repair
HEPES	4-(2-hydroxyethyl)-1- piperazineethanesulfonic acid
HIF	hypoxia-inducible factor
HRI	heme regulated inhibitor
IGF	insulin-like growth factor
IGF1R	insulin/IGF receptor 1
IIS	insulin/IGF-like signalling
IPTG	isopropyl β-D-1-thiogalactopyranoside
IRE1	inositol-requiring protein 1
IRES	internal ribosomal entry site
ISR	integrated stress response
L1 - L4	larval stages of *C. elegans*

MEF	mouse embryonic fibroblast
Met-tRNAi	methionyl tRNA specialised for translation initiation
miRISC	miRNA-induced silencing complex
miRNA	micro RNA
mORF	main ORF
mRNA	messenger RNA
mRNP	messenger ribonucleoproteins
mTORC	mammalian target of rapamycin complex
mut	mutant
NAD	nicotinamide adenine dinucleotide
NGM	nematode growth medium
Nrf	nuclear respiratory factor
nt	nucleotide
OE	overexpression
ORF	open reading frame
P-site	peptidyl-site
PABP	poly(A)-binding protein
PAM	protospacer-adjacent motif
PCA	principle compoment analysis
PERK	PKR-like endoplasmic reticulum kinase
phospho-eIF2	phosphorylated eIF2
PIC	pre-initiation complex
PKB	protein kinase B
PKR	protein kinase R
polyQ	polyglutamine
PP	protein phosphatase
qPCR	quantitative PCR
RiboTag	ribosome tag
RINe	RNA integrity number equivalent
RNA	ribonucleic acid
RNAi	RNA interference
RNAseq	RNA sequencing
RPL	ribosomal protein of the large subunit
RPS	ribosomal protein of the small subunit
rRNA	ribosomal RNA
RVC	ribonucleoside vanadyl complex
S51A	serine 51 alanine exchange
S51D	serine 51 aspartic acid exchange
S6K	ribosomal protein S6 kinase
SD	standard deviation
SEM	standard error of the mean
SKI LODGE	single-copy knock-in loci for defined gene expression
SL	spliced leader
SNP	single nucleotide polymorphism
SUnSET	surface sensing of translation
syn	synuclein
TC	ternary complex
TCA	trichloroacetic acid
TM	tunicamycin
TOR	target of rapamycin
tRNA	transfer RNA
uAUG	upstream AUG start codon
uORF	upstream ORF
UPR	unfolded protein response
UPR^{ER}	unfolded protein response of the ER
UTR	untranslated region
UV	ultraviolet
VWM	vanishing white matter disease
WT	wildtype
XBP1	X-box binding protein 1

1 Introduction

Having a long and healthy life mesmerises humankind since ancient times and longevity myths exist for a similar timespan. In the Chinese philosophical tradition Taoism, the legendary long-lived figure Peng Zu supposedly lived for 834 years and his figure is worshipped for his happy and healthy long life (so in E. Wongs "Tales of the Dancing Dragon: Stories of the Tao", 2007). The Hebrew Bible describes Methuselah to have lived for 969 years and the name has become a synonym for longevity in Western culture ("as old as Methuselah") and science (for example in the long-lived *Drosophila* mutant *methuselah* and a corresponding gene class; Lin et al. (1998)). Legendary lifespan-prolonging interventions have found their way into many myths with the fountain of youth being mentioned as early as the 5th century BC (Herodotus, The Histories Book III: 23) and the philosopher's stone, also called the elixir of life, being implemented in modern pop culture (so in J.K. Rowlings "Harry Potter and the Philosopher's Stone", 1997). The many myths around old ages and longevity show that having a long and healthy life is a central human desire.

Surprisingly, it was only in the early 20^{th} century that studies on ageing collectively were defined as gerontology (Achenbaum and Levin, 1989). Gerontologic research shows that ageing is a multifaceted progress in life comprising biological, psychological and social mechanisms. Hence, how we age is influenced by external and internal circumstances that can be of social, organismal or cellular nature (Kruse and Wahl, 2010). In terms of individual ageing processes, ageing starts with one's birth and it ends with one's death. It affects everyone through all age groups. Biologically, ageing is understood as the irreversible change in one's physical substance as a function of time (Bürger, 1960). More focussing on changes that occur late in life, ageing can also be characterised as the progressive loss of physiological function and integrity of cells, tissues and organs that continually increases the risk of death (Lopez-Otin et al., 2013; Hayflick, 1985). These days, understanding ageing and its mechanisms is of increased importance. There has never been before a society with such a high life expectancy as today and the human average age is constantly increasing. At the same time, age-related human pathologies such as cardiovascular diseases and cancer are main causes of death in the modern western civilisation (data from Germany, Plötzsch and Rößger (2015); Bundesamt (2017)). The discovery that the rate of ageing is partially controlled by genetic and biochemical processes further increased the significance of ageing research in all sciences (Lopez-Otin et al., 2013). The deep biological processes which lead to ageing and its phenotypes, as well as how ageing can be modulated on a cellular and organismal level are still not fully understood and hence main scientific questions. In this context, the main objective of my PhD project is the identification of novel conserved biological mechanisms of ageing in the model organism *Caenorhabditis elegans* (*C. elegans*).

1.1 Ageing: A biological point of view

1.1.1 Theories of ageing

The human desire for a long and healthy life prompts a so far unresolved question: Why do we age after all? Understanding the processes of ageing from an evolutionary point of view can help to better integrate the ageing and longevity regimes described throughout this work into a more global picture. It might further help to understand old and new biological ageing mechanisms and to place them within the complex network of ageing phenotypes and interventions. Amongst many, three classical evolutionary theories of ageing exist that are widely considered: The theories of mutation accumulation, disposable soma and antagonistic pleiotropy. They are all based on the hypothesis that ageing is a feature of organisms with a germ line that is separable from the soma (Reichard, 2017).

The 'mutation accumulation theory' poses that during ageing, harmful mutations with individual effects, for example on health, occur. They accumulate in the genome when they are expressed late in life, because they are not selected against. In other words, during ageing the organismal performance might be impaired due to the accumulation of senescent changes and natural selection fails to scavenge these mutations from a population (Reichard, 2017). However, while some studies with conflicting results exist, this theory is hard to be experimentally tested and concrete evidence for the 'mutation accumulation theory' is weak (Partridge, 2001). While this holds true to date, mutation accumulation studies analysed the effects of spontaneous mutation accumulation over many generations, for example in *C. elegans* (Estes et al., 2005). The results indicate that the accumulated mutations have an extremely wide window of effects across all life stages, positively as well as negatively (Maklakov et al., 2015). Subsequently, a 'modified mutation accumulation theory' proposes the existence of mutations with negative effects that have an impact throughout life with an increased emphasis towards the late life. The steeper the increase of the negative effect is during age, the less likely the variation is selected against and the more likely it affects the ageing process (Maklakov et al., 2015). Still, the 'modified mutation accumulation theory' remains to be elaborated in ageing model organisms as well (Maklakov et al., 2015; Reichard, 2017).

The 'ageing theory of the disposable soma' directly looks at the distinction between germ line and somatic tissues, depicting the germ line as immortal lineage, passing on genes from generation to generation (Reichard, 2017; Kirkwood, 2017). Therefore, the 'disposable soma theory' speculates that deleterious changes in the germ line should be prevented under all circumstances by the organism. Somatic cells also can accumulate maladaptive mutations throughout life leading to cellular dysfunctions. While the repair of such maladaptation might be possible in somatic tissues, the energetic cost for such a repair might be too high to implement it. The key hypothesis behind the 'disposable soma theory' is a direct trade-off between reproduction and survival with a strong focus on the protection and maintenance of the germ line only. Experimental support for this theory is abundant in studies using different lower model organisms (Kirkwood, 2017; Arantes-Oliveira et al., 2002; Sgro and Partridge, 1999).

The third classical evolutionary ageing theory is the antagonistic pleiotropy one. In part

overlapping with the earlier theories, here it is assumed that ageing occurs due to a decline in the strength of natural selection late in life. In the 'antagonistic pleiotropy theory', the focus lies on pathways involved in reproduction and fitness that are closely linked to a loss of homeostasis and loss of cellular maintenance when de-regulated. Through low natural selection, in a trade-off, the negative consequences of these pathways are tolerated later in life (Mitteldorf, 2019). While the findings supporting the 'disposable soma theory' in part also support the antagonistic pleiotropy one (Sgro and Partridge, 1999), the complexity of antagonistic pleiotropic effects makes it experimentally complicated to consequently prove this theory (Leroi et al., 2005). However, it was shown on multiple occasions that processes that favour growth and reproduction early in life can contribute to defects post-reproductively during ageing. It was further shown that the modulation of such processes can promote longevity. In turn, this means that pleiotropic ageing- and longevity interventions that increase lifespan might have deleterious effects early in life (Leroi et al., 2005). Studying such effects in detail and potentially fine-tuning ageing and longevity pathways towards a sweet spot of activity therefore marks an intriguing possibility to postpone ageing. The molecular and genetic processes behind organismal and cellular ageing will be introduced in detail in the following chapters.

1.1.2 Biological hallmarks of ageing

What is ageing, from a biologists point of view, in terms of cellular and molecular processes? In agreement with the basic biological definition that ageing is the accumulation of cellular damage over time, the main phenotypes of ageing have been intensely studied. Nine molecular and cellular hallmarks of ageing have been suggested. While these hallmarks were tailored to mammalian ageing, many of them are very conserved through evolution. For a phenotype to become a hallmark of ageing, it was postulated that the respective trait should occur during the normal ageing process and an experimental exacerbation should further enhance the ageing process while an amelioration of the phenotype should slow ageing down. The final hallmarks include genomic instability, telomere attrition, epigenetic alterations, loss of protein homeostasis, deregulated nutrient sensing, mitochondrial dysfunction, cellular senescence, stem cell exhaustion and altered intercellular communication (Lopez-Otin et al., 2013).

Primary hallmarks of ageing are considered to directly act negative on cellular health and integrity. Examples are genomic and epigenetic damage and a reduction in protein homeostasis. Antagonistic hallmarks comprise the responses to the age-related cellular damage and can have positive cellular effects until an excessive activation of these responses becomes pathological. In other words, these hallmarks can be seen as protective until their overactivation reverts their purpose and exaggerated responses generate more damage compared to their absence. The deregulation of many nutrient sensing pathways belongs to the class of antagonistic ageing hallmarks. Integrative hallmarks of ageing such as stem cell exhaustion and mis-regulated intercellular communication finally cause a functional decline in tissue- and organismal homeostasis (Lopez-Otin et al., 2013). In sum, these hallmarks explain the cellular basis for the organismal reduction in fitness and increased risk of disease during older ages. Understanding these and other, yet unknown, age-associated molecular and cellular

processes causing age-related phenotypes is crucial. This can accelerate the development of preventive or acute actions and treatments against age-associated functional decline or pathologies. Ultimately, successfully preventing detrimental age-associated phenotypes and finding effective treatments for age-dependent diseases is one of the main goals of gerontologic research. This will lead to multiple benefits not only on the personal but also on the demographic level in an ageing society (Pakulski, 2016).

1.1.3 Shifting the balance from growth and reproduction to stress-resistance slows the ageing process

For a long time, the cellular ageing process was seen as passive and spontaneous. Entropic exogenous and endogenous factors, for example UV radiation and the production of reactive oxygen species leading to increased DNA lesions, were assumed as sole causative triggers for cellular ageing. Instead, although it is an extremely multifaceted process, the rate of ageing was more and more shown to be regulated by classical signalling pathways in the past decades (Kenyon, 2010). Many of these pathways and their regulating roles in ageing were discovered in small and short-lived model organisms such as yeast, worms, and flies (Kenyon, 2010). One could wonder about the conservation of such ageing-regulating pathways in higher organisms, since ageing rates vary in a very large range between them: While worms live for three weeks on average, mice live for around three years and humans have an average lifespan of 80 years (Pitt and Kaeberlein, 2015). Strikingly, most pathways and interventions of ageing were shown to be deeply conserved throughout many species, making the mentioned model organisms excellent for studying the ageing process (Pitt and Kaeberlein, 2015). Diverse studies prove the existence of environmental and genetic ageing modifiers causing longevity when tuned in the right way from yeast to mammals. Interestingly, most of the known conserved pathways found to regulate the ageing process affect stress-responses or nutrient sensing. These pathways seem to balance organismal growth and reproduction with environmental and physiological stresses (Pitt and Kaeberlein, 2015). While growth and reproduction are promoted under un-stressed conditions, during cellular stress a physiological shift bolsters molecular processes for cellular protection and homeostasis (Kenyon, 2010). For example heat stress can induce longevity by activating stress resistance pathways (Shama et al., 1998). Different master-regulators of stress response pathways and protein folding homeostasis, such as heat shock factors and other molecular chaperones, were shown to regulate longevity (Morley and Morimoto, 2004). Protein quality control pathways and their enhancement have been linked to an extension in lifespan (Taylor and Dillin, 2013; Denzel et al., 2014). The roles of overall protein homeostasis in ageing and longevity will be described in more detail in a following chapter (see 1.2.4).

Nutrient sensing and longevity One of the most studied environmental ageing interventions is dietary restriction (DR) in form of a reduction in calorie or food consumption. Controlled DR was shown to extend the lifespan of a variety of model organisms (Partridge et al., 2005; Masoro, 2005). Interestingly, this extension of lifespan was shown to function in an acute way by reducing the short-term death risk shortly after starting the DR intervention

(Mair et al., 2003). Along with extended lifespan, also the onset of age-related diseases was slowed down under DR conditions. For example, intermittent fasting in rats was shown to protect the heart from ischaemic injury, likely through anti-apoptotic and anti-inflammatory mechanisms (Ahmet et al., 2005; Mattson and Wan, 2005). During ageing in rhesus monkeys, intermittent fasting was shown to prevent diabetes and further increased general organismal health (Bodkin et al., 2003). While ethical and logistical limitations complicate the research of DR in humans, a variety of studies found favourable alterations in biomarkers upon DR, often related to the function of cardiovascular and glucoregulatory systems (Trepanowski et al., 2011). In accordance with the correlation of DR-mediated longevity and effects in the glucoregulatory system, the longevity in response to DR was shown to be molecularly linked to the insulin/IGF-like signalling (IIS) pathway (Fig. 1; Honjoh et al. (2009)).

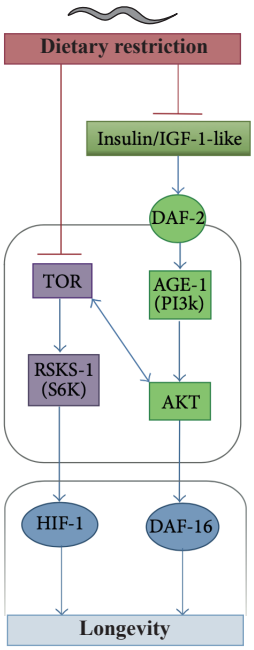

Figure 1: Scheme of the IIS and TOR signalling pathways during DR in *C. elegans*. Depicted are central key factors that are conserved through many organisms and were shown to modulate lifespan upon DR. Figure modified from Santos et al. (2016).

The IIS pathway was one of the first molecular pathways linked to ageing regulation. Within the IIS network, for the first time, single mutations in key genes were found to induce longevity (Kenyon et al., 1993). This marked the first evidence for a direct genetic regulation of ageing. The very conserved IIS pathway senses and connects nutrient levels to the metabolic activity in growth, development and ageing. By ligand-binding of insulin-like peptides to the insulin/IGF-1 receptor (IGF1R), this receptor regulates a diverse downstream cascade. The active IIS promotes growth and development. Concerning ageing and longevity, one of the major outputs of the IIS is the regulation of the transcription factor FOXO. FOXO activation during an inactive IIS triggers a broad transcriptional response in target gene expression to mediate general stress resistance (Wang et al., 2008; Curran et al., 2009). The first mutations that were found to cause longevity were identified in the *C. elegans* IIS genes *age-1* (PI-3 kinase in mammals) and *daf-2*/IGF1R, which nearly doubled the worm's lifespans (Friedman and Johnson, 1988a; Kenyon et al., 1993). Further, the lifespan extension seen under reduced IIS conditions was shown to be dependent on DAF-16/FOXO (Kenyon et al., 1993; Ogg et al., 1997). In accordance with an evolutionary conserved genetic and biochemical regulation of ageing, the observation that mutations in the IIS pathway can prolong lifespan and increase stress resistance holds true for a variety of IIS-related genes in worms, flies and higher organisms such as mice (Kenyon, 2005; Tatar et al., 2003; Mathew et al., 2017). Next to a proposed role of DR-mediated longevity in humans (Trepanowski et al., 2011), mutations have been identified in IIS components including FOXO in centenarians, and were correlated to low IGF-1 plasma levels (van Heemst et al., 2005; Kenyon, 2010). In sum, the above-described findings in the IIS pathway not only related classical signalling pathways with the regulation of ageing and longevity. They also showed that genetic variations can cause longevity in a variety of model organisms and potentially humans.

Next to the IIS pathway, the target of rapamycin (TOR) signalling is another pathway regulating ageing and longevity based on nutrient sensing (Fig. 1). In conditions of nutrient supply, the essential Ser/Thr protein kinase TOR senses amino acids. In mammals, TOR consists of two complexes that differ in their functions, the mammalian target of rapamycin complex mTORC1 and mTORC2. Upstream effects such as IIS activity modulate mTORC1 through a complex signalling cascade, for example mediated by the insulin-stimulated protein kinase B (PKB, also known as Akt; Yoon (2017); Vander Haar et al. (2007)). As downstream effects, active TOR signalling promotes growth while inhibiting degrading systems such as autophagy (Bjedov et al., 2010). Similarly to FOXO activation during inactive IIS, the inhibition of TOR signalling promotes resistance to stress and cellular maintenance via a reprogramming of a transcriptional response through factors such as Nrf, HIF1α and FOXA (Robida-Stubbs et al., 2012; Dekanty et al., 2005; Sheaffer et al., 2008). The genetic and pharmacologic inhibition of TOR signalling causes lifespan-extension in many model organisms (Santos et al., 2016). Next to a regulation of autophagy (Bjedov et al., 2010), TOR signalling is considered as a master regulator of translation. The active TOR signalling during nutrient-rich conditions promotes translation through inactivation of specific translation inhibiting proteins (eIF4E-binding proteins, 4E-BPs) and activation of the ribosomal subunit S6 kinase (S6K). During low nutrient availability, TOR signalling is inactive and therefore fails to promote translation (Proud, 2007; Hay and Sonenberg, 2004; Kapahi et al., 2010). The down-regulation of protein synthesis has not only been described as feature of longevity during DR and low TOR activity. Lowering translation levels interestingly also mediates a lifespan extension by itself. Therefore, the inhibition of translation *per se* depicts a longevity regime that shifts the cellular state from growth to stress resistance and cellular maintenance (Hansen et al., 2007; Syntichaki et al., 2007; Tohyama et al., 2008; Pan et al., 2007).

Further nutrient and energy sensing pathways were connected to longevity and DR-mediated cellular changes. Examples are the processes mediated by the AMP kinase and sirtuins. The AMP kinase senses cellular energy levels via AMP/ATP ratio and mediates anabolic processes upon ATP depletion. Genetic and pharmacological AMP kinase activation were shown to extend lifespan (Apfeld et al., 2004; Anisimov et al., 2008; Zhou et al., 2001). Sirtuins belong to the class of NAD^+-dependent acetylases with a wide range of targets (Houtkooper et al., 2010a). Sirtuins were shown to mediate longevity under DR conditions (Lin et al., 2000; Moroz et al., 2014) and to improve healthspan upon their over-expression (Tissenbaum and Guarente, 2001; Herranz et al., 2010). While the function of sirtuins in longevity is still under debate, a close interaction between sirtuins and AMP kinase was shown to improve mitochondrial function (Price et al., 2012). Furthermore, the AMP kinase signalling was connected to FOXO activation and S6K-mediated longevity (Canto et al., 2009; Selman et al., 2009). These interactions show that while different longevity regimes have specific nodes of action, many ageing regulatory pathways are inter-connected. Such connections comprise partly overlapping metabolic signalling networks, for example through shared downstream mediators (Houtkooper et al., 2010b; Denzel et al., 2019). This was shown to hold true for human ageing genes as assessed by a systems-level analysis. It revealed that many ageing genes and pathways are organised in overlapping hubs and within them are more functionally

connected (Zhang et al., 2016; Lee et al., 2003).

Further processes, although less tightly connected to nutrient sensing, have been described to play a role in the ageing process and during longevity. Often, they also converge with some of the above-named longevity regimes. For example, the direct inhibition of mitochondrial respiration extends lifespan (Copeland et al., 2009), in part by activating AMP kinase and the transcription factor HIF1α (Hwang et al., 2012). Furthermore, signals from the reproductive system in *C. elegans* were reported to extend lifespan via activation of DAF-16/FOXO (Hsin and Kenyon, 1999). In sum, the here described observations prove a role of classical signalling pathways in the regulation of ageing. It was shown that the down-regulation of pathways that promote growth and development often extends lifespan. These pathways can be modulated by different interventions including DNA mutations and thus induce longevity.

In comparison to lower organisms, studying ageing and longevity in humans is challenging because of the higher complexity of signalling pathways. Confounding environmental factors including lifestyle behaviour affect individual ageing processes greatly. Furthermore, many experimental perturbations are not feasible in human research (Houtkooper et al., 2010b). Overcoming some of these problems, human genetic lifespan regulation was analysed in several genome-wide association studies (GWAS), identifying genetic ageing regulators in humans (Deelen et al., 2019). Variants in two genes have been strongly associated with human longevity: Apolipoprotein E (ApoE) and FOXO3A (Schachter et al., 1994; Deelen et al., 2019). ApoE is a cholesterol carrier involved in lipid transport mechanisms and a polymorphic gene in humans. ApoE function is connected to ageing-associated diseases such as Alzheimer's and cardiovascular disease. Different ApoE alleles were associated with reduced and increased likelihood of longevity (Shadyab and LaCroix, 2015; Deelen et al., 2019). Being involved in the IIS pathway, the identification of FOXO3A and its implication in human longevity further shows the evolutionary conservation of longevity mechanisms (Shadyab and LaCroix, 2015; Deelen et al., 2019). Finally, different studies estimate a genetic proportion of ageing control in humans that ranges between 10 % and 25 % (Herskind et al., 1996; Ruby et al., 2018; van den Berg et al., 2017).

Together, conserved pathways regulate cellular processes contributing to ageing and longevity. Among others, the most conserved longevity regimes include reduced IIS and TOR signalling, enhanced protein homeostasis and reduced mRNA translation. It was shown, not only in model organisms but also in humans, that ageing is genetically controlled, at least in part. However, the ageing process is still an area of many open questions and under active investigation. Many ageing regulating pathways were identified in the context of stress and nutrient sensing pathways and a strong correlation between stress resistance and longevity was shown. Therefore, most of the known longevity interventions modulate pathways in the class of antagonistic ageing hallmarks and can be connected to the 'antagonistic pleiotropy theory' of ageing. Next to the well-established longevity mechanisms, it will be of interest to identify a role of further pathways in longevity processes within antagonistic or other hallmark processes during ageing. Identifying and integrating crucial nodes of ageing to the landscape of known longevity mediators is therefore the superordinate goal of this work.

1.2 From mRNA to protein: A tightly regulated process

1.2.1 The molecular processes of mRNA translation and protein synthesis

Genes encoded within the DNA are transcribed to messenger RNA (mRNA), which is processed and finally translated to a protein. Francis Crick described this mechanism in 1958 as the "central dogma of molecular biology" (Crick, 1970). Gene expression and protein synthesis are regulated on many levels. During transcription, RNA polymerases read the DNA sequence and upon transcription start site selection transcribe it into mRNAs or other non-coding RNAs. The generated mRNA acts as template during protein synthesis via translation. Here, the ribosome decodes the mRNA using transfer RNAs (tRNAs) by matching amino acids to three mRNA nucleotides at a time according to the genetic code (Urry et al., 2016). mRNA translation is divided into three sub-processes: Initiation, elongation and termination. During the initiation process, the ribosome, as cellular hub of protein synthesis, assembles around the mRNA and starts translation at the translation start site. During elongation, the amino acid chain of the synthesised protein gets elongated through peptide bond formation, building the heart of the protein synthesis process. The termination describes the release of the synthesised polypeptide and the disassembly of the ribosomal complex from the mRNA (Sonenberg and Hinnebusch, 2009; Fabian et al., 2010).

The cellular nanomachine executing the protein synthesis process is the ribosome, which is a ribonucleoprotein complex. In eukaryotes, fully assembled and functional 80S ribosomes consist of two subunits: the small ribosomal 40S subunit is comprised of 33 ribosomal proteins and the 18S ribosomal RNA (rRNA); the large ribosomal 60S subunit contains 46 ribosomal proteins and three different rRNA species, the 25S, the 5.8S and the 5S rRNAs (Ben-Shem et al., 2011). The initiation of translation is the rate-limiting step under most circumstances. In eukaryotes, to initiate translation the ternary complex (TC) is formed consisting of the eukaryotic initiation factor 2 (eIF2, consisting of an α, β and γ subunit), GTP and a loaded methionyl tRNA that is specialised for initiation (Met-tRNAi, Fig. 2). Subsequently, the 43S pre-initiation complex (PIC) is formed by the TC and the small ribosomal (40S) subunit, stimulated by other initiation factors such as eIF1, eIF1a, eIF3 and eIF5 (Hinnebusch et al., 2016). This PIC binds to the mRNA at the m^7G-capped 5'-untranslated region (5'-UTR). This process is facilitated by the eIF4F complex, which comprises the RNA helicase eIF4A, cap-binding proteins eIF4E and eIF4G and the poly(A)-binding protein PABP (Hinnebusch et al., 2016). Downstream of the capped 5'end of the mRNA, the PIC scans nucleotide triplets in the P(eptidyl)-site of the 40S ribosome, while the Met-tRNAi is fixed in the PIC by eIF2-GTP. Finally, the PIC identifies and decodes the initiating start codon, which usually is an AUG and rarely can differ as near-cognate alternative start codon (Sonenberg and Hinnebusch, 2009). The GTPase-activating protein eIF5 then releases eIF2-GDP and other factors from the mRNA-40S-complex by hydrolysis of GTP. In the final step of the initiation process, the large ribosomal (60S) subunit completes the full translation-mediating ribosomal (80S) complex, catalysed by eIF5B. The initiation process is completed when the Met-tRNAi is positioned at the P-site of the ribosome and the first binding site in the ribosome, the A(minoacyl)-site, is ready for the next charged aminoacyl-tRNA (Hinnebusch et al., 2016; Urry et al., 2016). For each round of translation initiation, the TC needs to reform with an

exchange of GDP to GTP at the regulating factor eIF2. This reaction is catalysed by the heterodecameric guanine nucleotide exchange factor (GEF) eIF2B, therefore depicting a key regulating factor of translation initiation (Pavitt et al., 1998).

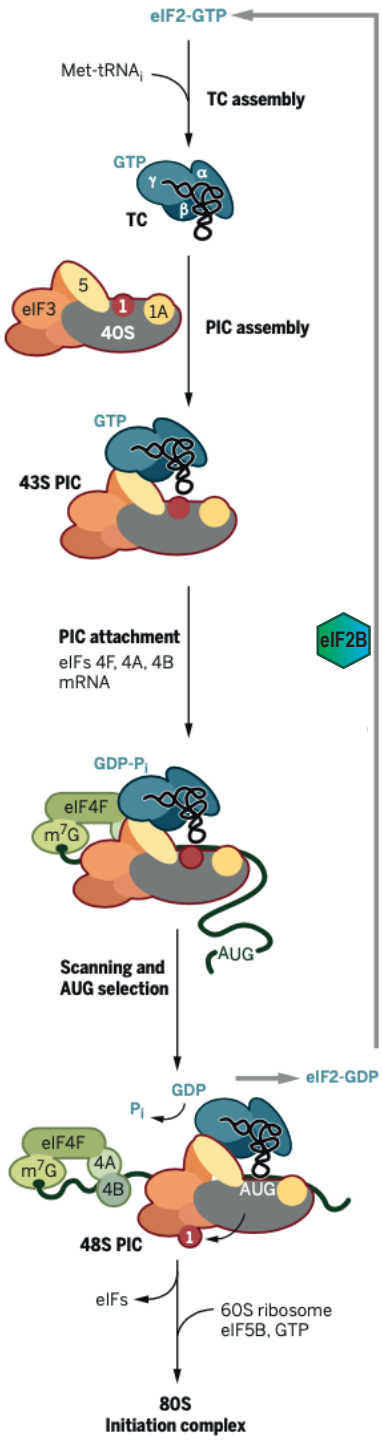

Figure 2: The mechanism of translation initiation. The simple 5-subunit version of eIF3 in yeast is depicted. Figure modified from Hinnebusch et al. (2016).

At the start of the translation elongation process, the second codon of the mRNA open reading frame (ORF) is positioned in the ribosomal A-site. A cognate aminoacyl-tRNA is delivering the next amino acid, a process mediated by the translation elongation factor eEF1A. After the release of the elongation factor, a peptide bond is formed between the two consecutive amino acids from the aminoacyl- and peptidyl-tRNAs, catalysed by the peptidyl transferase centre of the 80S ribosome. This process is promoted by the factor eEF5A, located in the ribosomal E(xit)-site. Here, it promotes the peptide bond formation through substrate positioning. The nascent peptide chain is transferred from the P-site to the aminoacyl-tRNA at the A-site which results in an elongated polypeptide. During this process, the tRNAs are translocated from the A- to the P-site and from the P- to the E-site, mediated by eEF2. As a result, the deacetylated tRNA sits at the E-site and the elongated peptidyl-tRNA at the P-site. Upon release of the deacetylated tRNA from the E-site, the elongation process can be repeated with the next aminoacyl-tRNA waiting in the A-site (Dever et al., 2018). Once a stop codon is read in the A-site, the translational process is terminated. This is mainly mediated by two eukaryotic protein release factors (eRFs). Upon stop codon recognition, eRF1 promotes the hydrolysis of the polypeptide chain from the peptidyl-tRNA, while eRF3 is involved by its GTPase activity on eRF1. Lastly, after completing the polypeptide chain, the 80S ribosome and the deacetylated tRNA are released from the mRNA and recycled for subsequent translation processes (Dever and Green, 2012; Hellen, 2018). When the translation from the mRNA sequence to a linear amino acid chain is finished, the protein has to fold into a three-dimensional structure to gain its full biological function. This process is determined by the amino acid sequence and starts already during elongation of the nascent amino acid chain. It further depends on the cellular milieu and molecular

chaperones, proteins which assist the correct folding of other proteins (Dobson, 2003). Next to the correct folding state, other post-translational modifications affect protein function and comprise phosphorylation, acetylation and glycosylation of selected amino acid positions within a protein, mediating both activating and inhibiting effects on protein function (Khoury et al., 2011).

1.2.2 The regulation of mRNA translation and protein synthesis

The regulation of mRNA translation and therefore protein synthesis is a crucial mechanism to maintain or modulate the cellular metabolism in adaptation to different circumstances. While growth requires high protein synthesis rates, exaggerated levels of protein production cause tissue hypertrophy or tumour growth, for example (Hannan et al., 2003; Inoki et al., 2005). Furthermore, gene expression is not only regulated transcriptionally. It was shown that cellular protein levels are controlled translationally to a vast extent (de Godoy et al., 2008; Schwanhausser et al., 2011). Lastly, protein synthesis is one of the most energy consuming processes within the cell, which is another reason why translation needs to be tightly regulated (Proud, 2007). mRNA translation can be regulated globally and specifically. General translation factors can regulate global protein synthesis, leading to changes in cell proliferation. Moreover, the translation, transport or stability of specific mRNAs can be regulated, for example through selected translation factors or RNA-binding proteins. This transcript-specific regulation can rapidly activate the production of specific proteins, which are needed to adapt the cell to quickly changing conditions (Proud, 2007). Within these two categories, there are several mechanisms of translational regulation. Some of the most common ones will be briefly introduced here.

Several mRNA structures can serve as regions for translational regulation of specific mRNAs. Most of these translational control elements reside within the 5'- and 3'-UTRs (Wilkie et al., 2003). 3'-UTRs are known to harbour binding sites for micro RNAs (miRNAs). These small non-coding RNAs can constitute a miRNA-induced silencing complex (miRISC), which silences mRNAs in a targeted way by both translational repression and mRNA destabilisation (Jonas and Izaurralde, 2015). Within the 5'-UTR, one basic regulatory element is the m^7G cap that is needed to be recognised by translation initiation factor eIF4F to initiate cap-dependent translation. Internal ribosomal entry sites (IRES) can initiate translation independently of the m^7G cap scanning, a mechanism that plays a crucial role in gene regulation of viral and mammalian genes (Wilkie et al., 2003; Weingarten-Gabbay et al., 2016). Moreover, the formation of secondary structures or the binding of regulatory proteins at specific 5'-UTR structures often repress translation of the respective mRNA. Further repressing elements are upstream ORFs (uORFs) and upstream AUG start codons (uAUGs), usually down-regulating translation of the main ORF by an alternative translation start site selection (Wilkie et al., 2003). When the uAUG is in-frame with the actual start codon and there is no stop codon between both, two isoforms of one protein can be produced, one carrying an N-terminal extension. In this case, the different isoforms are often targeted to specific cellular locations. However, if the uAUG is followed by an in-frame stop codon, the translation initiation at this uORF can diminish translation of the following main ORF due to an ineffi-

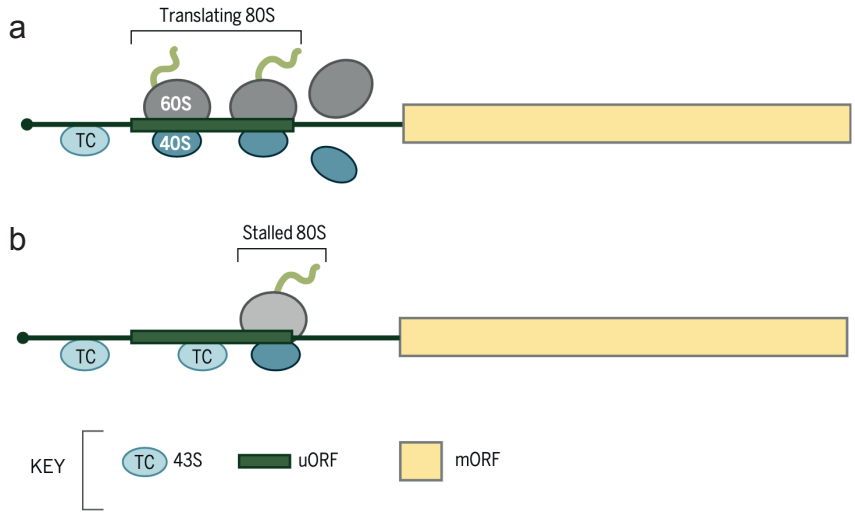

Figure 3: Mechanisms of translational control through uORFs. **a** After scanning an uORF, the ribosome dissociates from the mRNA. The poor re-initiation inhibits the translation of the main ORF (mORF). **b** Ribosome stalling at the uORF inhibits translation initiation at the mORF. Figure adapted from Hinnebusch et al. (2016).

cient re-initiation of the translational machinery (Fig. 3a). Furthermore, uORFs can inhibit translation of a downstream ORF by ribosomal stalling and thereby preventing the PIC to scan the actual ORF start codon (Fig. 3b; Hinnebusch et al. (2016)). Interestingly, uORF sequences were detected in a majority of mRNAs (Lee et al., 2012; Johnstone et al., 2016). However, only a small fraction of them produces peptides that can be detected (Vanderperre et al., 2013; Hinnebusch et al., 2016). While uORF sequences were found in many mRNAs, direct evidence for uORF-mediated translation regulation only exists for a small number of genes. For example, uORF translation followed by ribosomal stalling was observed in the mRNA of the gene *AMD1* encoding the S-adenosylmethionine decarboxylase. A shift from uORF to main ORF translation was shown to be modulated by pathway-related ligands such as spermidine (Raney et al., 2002). One well known uORF regulated mRNA is the transcript of the mammalian gene activating transcription factor 4 (*ATF4*), which will be introduced in detail in a following section (see chapter 1.2.3).

In contrast to the translational modification of specific mRNAs, general protein synthesis regulation is often mediated by upstream signalling pathways to the translational machinery. Such pathways have been described before in the context of ageing regulating pathways and comprise the IIS and TOR pathways (see chapter 1.1.3). Both can regulate overall translation by modulating the activity of translation initiation factors and the TOR complex is considered as master regulator of translation (Proud, 2007). Upon TOR activation, mTORC1 phosphorylates S6K, which further phosphorylates the protein S6 of the small ribosomal subunit, promoting the global biogenesis of ribosomes (Proud, 2007; Shimobayashi and Hall, 2014). Furthermore, mTORC1 phosphorylates the translation-inhibitory 4E-BPs. They subsequently dissociate from the translation initiation factor eIF4E. This de-repression promotes eIF4E- and eIF4G-mediated cap-dependent translation initiation, as described in section 1.2.1 (Proud, 2007; Shimobayashi and Hall, 2014). In sum, overall translation rates can be modulated by upstream signalling pathways through the regulation of ribosomal protein biogenesis via S6K or translation initiation via eIF4E. Another mechanism that controls

bulk protein synthesis through the modulation of translation initiation is the regulation of eIF2 via phosphorylation. This is the first step in a signalling cascade termed the integrated stress response (ISR). Since the ISR and its regulation play a crucial role within this thesis, it will be described in the following, separate chapter.

1.2.3 The integrated stress response

The ISR is a deeply conserved master regulating pathway of global mRNA translation. At the same time, the ISR regulates translation of selected mRNAs through specific uORF-mediated mechanisms. The overall biological function of the ISR is the restoration of cellular homeostasis during diverse stress conditions. The core event of the ISR is the phosphorylation of eIF2. Phospho-eIF2 becomes an inhibitor of eIF2B, its very own GEF. Thereby, TC-formation is attenuated upon the activation of the ISR, causing a reduction of cap-dependent mRNA translation. At the same time, the decrease of TC formation paradoxically de-represses the translation of a defined class of mRNAs that carry specific uORFs, such as ATF4 (Fig. 4). These translationally up-regulated factors upon high ISR levels further activate mechanisms to cope with the cellular stress (Costa-Mattioli and Walter, 2020).

In mammals, the ISR can be activated upon stress by four different eIF2 kinases: heme regulated inhibitor (HRI), protein kinase R (PKR), general control non-derepressible 2 (GCN2) and PKR-like endoplasmic reticulum kinase (PERK). Canonically, they are activated by iron deficiency, viral infection, amino acid deprivation and accumulation of mis-folded proteins in the endoplasmic reticulum (ER), respectively (Pakos-Zebrucka et al., 2016). By PERK sensing un- or mis-folded proteins in the ER, the ISR becomes part of the conserved unfolded protein response of the ER (UPR^{ER}). This general reaction of cells to ER stress regulates a broad transcriptional reprogramming to overcome the protein folding stress. Next to the PERK arm activating the ISR, the UPR^{ER} comprises signalling through IRE1-mediated cleavage and ATF6 translocation (Hetz et al., 2020).

Coming back to the ISR, all eIF2 kinases have a high sequence identity in their catalytic kinase domains and each of them has to dimerise and auto-phosphorylate to be fully active. They differ in their regulatory domains, reflecting their unique responsiveness to different stress sources (Pakos-Zebrucka et al., 2016). Still, the eIF2 kinases were described to also have overlapping functions, an example is the activation of all four kinases by oxidative stress (Pakos-Zebrucka et al., 2016). Furthermore, the kinases were shown to compensate for each other. Phosphorylation of eIF2 upon ER stress in *Perk*$^{-/-}$ MEFs is, at least partially, mediated by GCN2 in a compensatory way (Hamanaka et al., 2005). Moreover, PERK was suggested to *vice versa* compensate a loss of GCN2 (Lehman et al., 2015). Upon ER stress, the knockdown of one of the two kinases PERK or GCN2 resulted in a compensatory up-regulation of the respective other kinase (Roobol et al., 2015). Hence, the knowledge on the ISR and its activating kinases is being constantly expanded. Recently, it has been described that HRI can be triggered by mitochondrial stress through an OMA1/DELE1 axis in mammalian cells (Fessler et al., 2020; Guo et al., 2020).

Upon their respective stress-mediated activation, the ISR kinases converge on the phosphorylation of serine 51 of the α subunit of eIF2. This modification rearranges eIF2 struc-

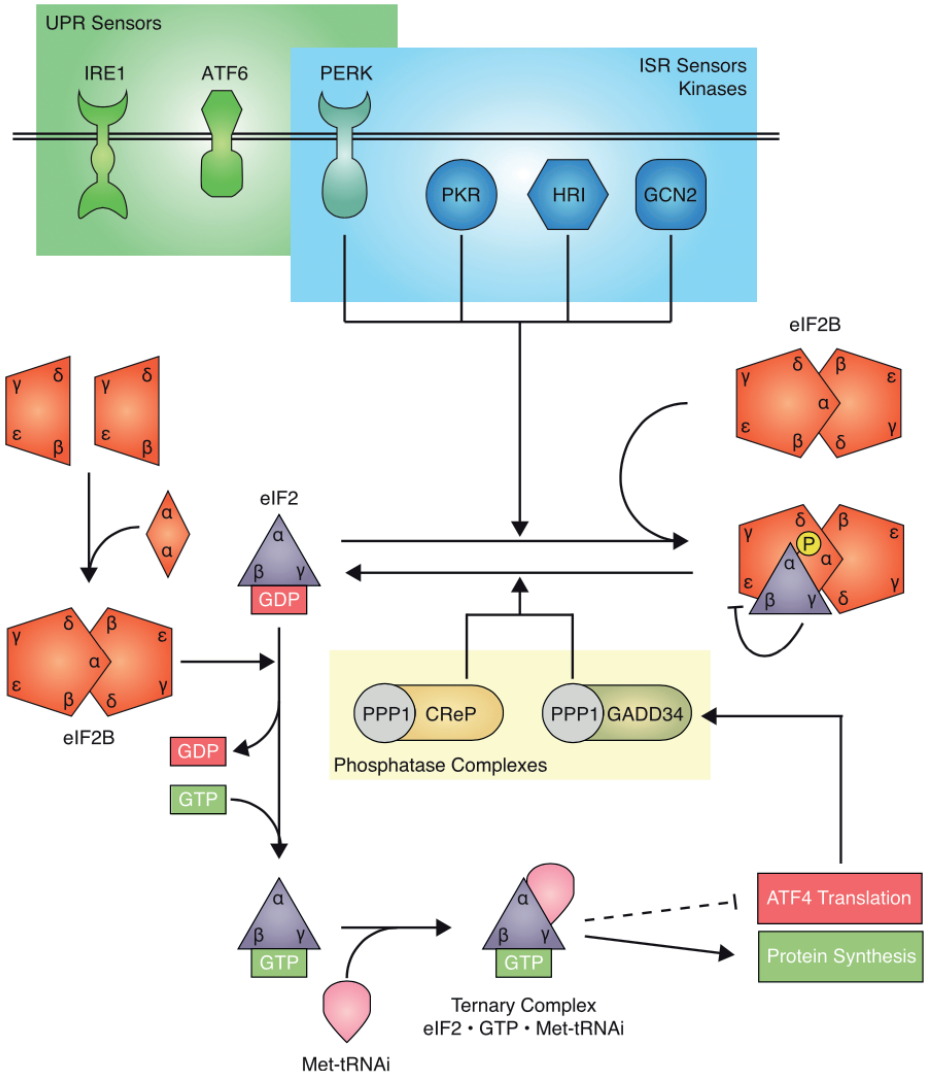

Figure 4: Schematic depiction of the ISR. The activation, the complex molecular wiring and the cellular outcomes of the ISR are described in detail in the main text. Figure adapted from Costa-Mattioli and Walter (2020).

turally and turns it from a substrate into an inhibitor of eIF2B (Fig. 4; Costa-Mattioli and Walter (2020)). eIF2B is a symmetric heterodecamer comprised of two copies each of the subunits α, β, γ, δ and ϵ. Before building the fully active complex, stable subunits are formed as two heterotetramers formed by eIF2Bβ, γ, δ and ϵ and one homodimer formed by two eIF2Bα subunits. The catalytic centre is comprised by eIF2Bϵ which interacts closely with eIF2Bγ. The core of the enzymatic complex is formed by eIF2Bβ and eIF2Bδ with the eIF2Bα homodimer bridging the core of the complex. In the heterodecamer, the catalytic eIF2Bϵ subunits are located at the opposing sites of the complex. To mediate the guanine nucleotide exchange at the substrate eIF2, eIF2γ localises between two eIF2Bϵ domains, where the dissociation of GDP and the loading of GTP takes place at eIF2 (Fig. 5). To be stably associated with eIF2B, eIF2α binds across the symmetrical interface of eIF2B, explaining why only the fully assembled eIF2B heterodecamer has the full GEF activity (Kenner et al., 2019; Kashiwagi et al., 2019; Adomavicius et al., 2019; Costa-Mattioli and Walter, 2020). During the active ISR, the phosphorylation of eIF2α causes a structural rearrangement of eIF2 including a new hydrophobic site with a strong affinity for eIF2B. Upon binding of this re-structured phospho-eIF2 to eIF2B, eIF2γ cannot appropriately locate to the catalytic eIF2Bϵ subunit. As a result, phospho-eIF2 inhibits the GEF activity of eIF2B and at the same time binds eIF2B with a higher affinity in an inhibitory way (Fig. 5, Costa-Mattioli and Walter (2020); Pakos-Zebrucka et al. (2016)). In sum, the eIF2 kinases, eIF2 itself and eIF2B are central nodes of the ISR.

Global and specific translation regulation upon ISR activation The inhibition of an eIF2B-mediated exchange of GDP to GTP at phospho-eIF2 during the active ISR blocks the formation of the TC and the 43S PIC and therefore prevents global translation initiation. The outcome is a down-regulation of cap-dependent mRNA translation. At the same time, the translation of a subset of mRNAs is up-regulated during the active ISR even though TC levels are diminished. These specific mRNAs contain small uORFs that prevent translation initiation at the canonical AUG upon high TC levels. Paradoxically, while TC amounts are low, the PIC has a higher chance to read the main start codon. Therefore, translation rates of these selected mRNAs are high during conditions of low overall translation initiation rates (Hinnebusch et al., 2016; Sonenberg and Hinnebusch, 2009). The transcription factor ATF4 (Gcn4 in yeast) is a well-known example of such a selectively translated factor upon ISR activity. ATF4/Gcn4 was first identified within the stress response pathway in yeast and subsequently was shown to be conserved in higher organisms (Hinnebusch, 2005). The uORF-mediated translation regulation of ATF4 has been intensely studied (Abastado et al., 1991; Vattem and Wek, 2004; Lu et al., 2004). In the 5'-UTR of *ATF4*, the specific properties of two uORFs mediate the translational repression under regular conditions and the de-repression upon stress (Fig. 6). A first uORF in the *ATF4* mRNA generally enhances translation initiation. It is optimised to promote re-initiation downstream of uORF1: It is proposed that the 40S ribosomal subunit keeps scanning the mRNA after uORF1 and therefore can quickly gather a new TC upon high TC abundance (Wek, 2018). This mediates the re-initiation of translation at uORF2. This second uORF overlaps with the main ORF of *ATF4* in an out-of-frame manner. As a consequence, the translation of uORF2 inhibits the

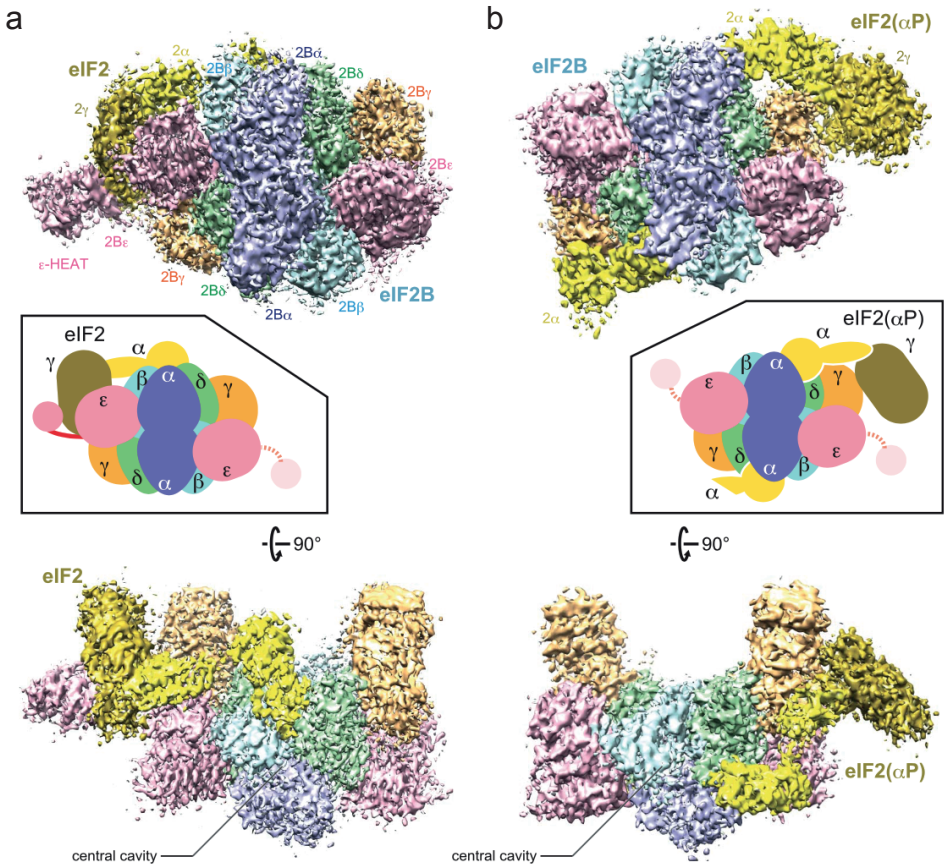

Figure 5: Cryo-EM structure and model of human eIF2-eIF2B complexes. The catalytic eIF2Bϵ subunit is depicted in pink. **a** Unphosphorylated eIF2-eIF2B complex. **b** Phosphorylated eIF2-eIF2B complex. Figure adapted from Kashiwagi et al. (2019).

translation initiation at the main *ATF4* start codon and ATF4 protein levels are depleted under conditions of high TC levels. During the active ISR, TC levels get depleted. Now, after scanning uORF1 of the *ATF4* mRNA, it takes longer for the 40S ribosomal subunit to acquire a fully assembled TC. Therefore, the start codon of uORF2 often is bypassed by the 40S ribosome. Instead, the chances are higher for the main start codon of *ATF4* to get recognised by the 43S PIC. As a result, ATF4 gets synthesised with a higher abundance when global TC levels are low (Wek, 2018; Hinnebusch et al., 2016).

Next to *ATF4*, other uORF regulated mRNAs get translated in response to ISR activation. The transcription factor C/EBP homology protein (CHOP) is required for stress-induced apoptosis and its transcription and translation were reported to be up-regulated through the ISR (Harding et al., 2000; Palam et al., 2011). The *CHOP* mRNA carries one uORF that was described to stall elongating ribosomes and thereby prevent translational re-initiation at the *CHOP* main ORF. Upon high phospho-eIF2 and low TC levels, the uORF is by-passed and translation is initiated at the *CHOP* main ORF start codon (Palam et al., 2011). Similarly to translational CHOP regulation, the mRNA of the growth arrest DNA-inducible gene 34 (*GADD34*) is also regulated through the bypassing of an uORF upon eIF2 phosphorylation. GADD34 is a negative feedback inhibitor of the ISR and is regulated transcriptionally and translationally by ISR activity (Lee et al., 2009). In sum, while global protein synthesis is down-regulated by the active ISR, specific mRNAs are translated preferentially. The products

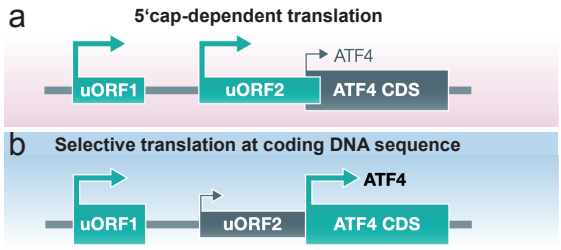

Figure 6: Scheme of uORF-mediated translation of *ATF4*. **a** During conditions of regular 5'cap-dependent mRNA translation, translation initiation at uORF2 inhibits translation of the main *ATF4* ORF. **b** When TC levels are depleted, the start codon of uORF2 is often bypassed. Instead, translation re-initiation at the main *ATF4* ORF occurs with a higher prevalence, leading to an increase of main *ATF4* ORF translation. Figure modified from Pakos-Zebrucka et al. (2016).

are involved in cellular mechanisms adapting the organism to the stress sensed by the ISR kinases.

Downstream consequences of ISR activation As described, the ISR is a master regulator of translational and transcriptional reprogramming, leading to several downstream effects. The ISR-induced transcription factors can either activate stress-related, protective mechanisms to prevent and resolve cellular damage; otherwise, apoptosis is induced when cellular homeostasis cannot be maintained (Pakos-Zebrucka et al., 2016). One global ISR outcome to promote maintenance during stress conditions is the reduction of overall translation rates by eIF2 phosphorylation. This is of specific importance when ISR signalling is induced via protein folding stress sensed by PERK to reduce the burden of mis-folded proteins (Ron, 2002). Nutrient stress is detected by GCN2. The following reduced translation levels are accompanied with a lowered consumption of amino acids which are in short supply under starvation conditions (Vazquez de Aldana et al., 1994). In mammals, HRI is activated by low heme levels. Heme is bound by globins and globins devoid of heme form detrimental aggregates. The attenuation of mRNA translation through HRI balances the synthesis of globins with the availability of heme (Han et al., 2001). During viral infection sensed by PKR, the down-regulated protein synthesis prevents the translation of viral mRNA (Garcia et al., 2007).

The active ISR further mediates its downstream effects through the activation of transcription factors. As mentioned above, the best studied one is ATF4, translational de-repression of which causes a complex fine-tuning of the cellular transcription towards stress regulating genes. ATF4 binds specific sequences of its target genes and therefore mediates their expression (Kilberg et al., 2009). One prominent ATF4 target gene is CHOP, which makes CHOP not only a translationally, but also a transcriptionally regulated factor through the ISR. ATF4 is further acting in combination with other proteins, often forming heterodimers with other DNA-binding proteins. These complexes further specify the outcome of the active ISR. While ATF4 in combination with ATF3 promotes cellular maintenance, an ATF4-CHOP complex is driving apoptosis (Fawcett et al., 1999; Matsumoto et al., 2013). This ability of ATF4 to drive a diverse range of transcriptional reprogrammings makes the ISR very specific upon different stress stimuli.

To maintain physiological homeostasis, downstream reactions of the active ISR include an

induction of autophagy, modulation of the UPR and a down-regulation of cell death pathways such as apoptosis. Specifically, upon ER stress, the activation of PERK was shown to regulate several stages of autophagy and both PERK and GCN2 activity were shown to cause increased autophagic flux (Deegan et al., 2013; Ye et al., 2010). In sum, the ISR can induce autophagy to overcome cellular stress. ISR activity was further shown to inhibit apoptosis through the up-regulation of cellular inhibitor of apoptosis protein 1 (cIAP1) and cIAP2 (Hamanaka et al., 2009). In the UPR^{ER}, PERK acts in parallel with IRE1 and ATF6 to cope with protein folding stress. As for the ISR, the overall outcome of an active UPR^{ER} is a transcriptional re-programming of chaperones and genes involved in the degradation of mis-folded proteins. All three UPR^{ER} branches show an interplay with each other. For example, the transcription of XBP1, a critical downstream factor of the IRE1 branch, depends on the ISR (Ron, 2002). It is further discussed that the timely interplay of the different UPR^{ER} branches dictates the outcome of the pathway. In this context, sustained PERK activation can promote apoptosis whereas IRE1 activation triggers cellular maintenance (Lin et al., 2007, 2009). Therefore, the cellular outcome of the active UPR^{ER} depends on the interplay of the ISR with the two other UPR^{ER} branches. Not only sustained PERK activity can induce apoptosis. If the cellular stress sensed by any ISR kinase cannot be resolved, cell death is induced through apoptosis mainly by the ATF4-CHOP axis with CHOP acting as transcriptional inducer for a variety of genes involved in apoptosis (Matsumoto et al., 2013; Pakos-Zebrucka et al., 2016). The ISR was shown to further induce other forms of cell death such as necrosis (Leon-Annicchiarico et al., 2015). Together, the ISR mediates cellular reactions to stress that have to be balanced between cell survival and cell death, depending on the severity of the stress and disturbance of the homeostasis. While not being specified for the ISR, this is in line with a mathematical model of the UPR^{ER}. It proposes that states of low, intermediate and high UPR^{ER} activity are associated with stress adaptation, tolerance and initiation of apoptosis (Erguler et al., 2013).

While the sustained ISR activation was shown to induce cell death, ISR activity has to be finely controlled and terminated to ensure sufficient translation of essential proteins to promote cell survival. Furthermore, to ensure a proper outcome of the transcriptional re-programming that is mediated by ATF4, CHOP *et cetera*, sufficient levels of TC need to be restored for the translation of the respective transcriptional targets (Costa-Mattioli and Walter, 2020; Pakos-Zebrucka et al., 2016). To reset the ISR, in the mammalian system two phosphatase complexes are known to de-phosphorylate phospho-eIF2 and therefore restore eIF2 for regular TC formation and translation initiation. The basis of these phosphatase complexes is set by protein phosphatase 1 (PP1), which contains the catalytic core for the de-phosphorylation process. To specify the complex to eIF2, two different regulatory subunits can bind to PP1: the constitutive repressor of eIF2α phosphorylation (CReP) or the growth arrest and DNA damage-inducible protein 34 (GADD34). CReP was shown to regulate basal levels of eIF2 phosphorylation and CReP expression was not changed upon stress that successfully induced the ISR (Jousse et al., 2003). To re-start translation upon conditions of high stress and high ISR activity, eIF2 is de-phosphorylated by GADD34. GADD34 expression is mediated in a feedback loop by the ISR to prevent its over-activation. As described above,

GADD34 is up-regulated translationally in states of low TC availability through a specific uORF-dependent mechanism. Additionally, ATF4 increases the transcription of *GADD34* (Lee et al., 2009; Novoa et al., 2001). Together, CReP controls eIF2 phosphorylation on a basal level, while GADD34 promotes recovery from translational inhibition during a highly active ISR. In sum, the ISR and mRNA translation initiation are finely balanced processes that provide robustness, cellular maintenance and eventually controlled cell death under different stress stimuli.

1.2.4 Protein homeostasis and longevity

As outlined in chapter 1.1.2, the loss of protein homeostasis depicts a hallmark of ageing (Lopez-Otin et al., 2013). Protein homeostasis describes the maintenance and balancing of protein synthesis, fidelity, folding, localisation, modification and degradation (Basisty et al., 2018). Maintenance of protein homeostasis is a crucial feature of any cell to retain overall resilience. Therefore, several cellular stress response pathways directly regulate protein homeostasis, integrating and processing internal and external stress stimuli. Failure of protein homeostasis begins early during ageing. Multiple lines of evidence show that healthy ageing and longevity rely on the fidelity of cellular stress response pathways in general, and on interventions that promote or maintain protein homeostasis specifically (Kourtis and Tavernarakis, 2011; Basisty et al., 2018). Many of these pathways have been introduced already in the previous chapters.

The TOR pathway mediates mRNA translation and protein degradation depending on nutrient availability and its modulation promotes longevity (Kenyon, 2010). The down-regulation of translation by itself was shown to mediate a lifespan extension (Hansen et al., 2007). A variety of molecular chaperones assists in protein folding and stress induced degradation of mis-folded proteins. Upon cellular stress, many pathways involved in the maintenance of protein homeostasis induce the synthesis and activation of chaperones (Dobson, 2003). Chaperones were shown to be required for the longevity mediated by reduced IIS (Morley and Morimoto, 2004). The above mentioned UPR^{ER} is an organelle-specific stress response pathway sensing protein folding stress, inhibiting protein synthesis and activating chaperones (Hetz et al., 2020). The UPR^{ER} promotes longevity when activated through IRE1/XBP1 signalling (Taylor and Dillin, 2013). Moreover, enhanced protein quality control through activation of the hexosamine pathway extends lifespan (Denzel et al., 2014). Autophagy is a major pathway of bulk protein degradation in the cell. Its activation was shown to be involved in processes mediating longevity such as the TOR and UPR^{ER} signalling pathways (Martina et al., 2012; Deegan et al., 2013). Furthermore, the over-expression of Atg5, a protein essential for autophagosome formation, has been shown to activate autophagy and extend lifespan in mice (Pyo et al., 2013). Together, longevity relies on the maintenance of protein homeostasis on several levels and the fidelity of corresponding stress response mechanisms. The ISR is one of the major cellular stress sensing pathways regulating protein synthesis. Mutations in the ISR have been shown to cause diseases in humans (van der Knaap et al., 2002) and maladaptive changes in ISR activity were associated with a variety of age-associated pathologies, including cancer, neurodegenerative and metabolic disorders

(Costa-Mattioli and Walter, 2020). However, the direct roles of the ISR during healthy ageing and longevity remain largely unexplored.

1.3 The model organism *Caenorhabditis elegans*

The small worm *C. elegans* was introduced by Sydney Brenner as model organism to study basic genetics in 1974 (Brenner, 1974). The 1 mm small post-mitotic animals are non-parasitic, multicellular nematodes containing 959 somatic cells forming different organs and tissues including a nervous system containing 302 neurons. Their life cycle from a fertilised egg to an adult is completed after three days when the animals are grown at 20 °C. The worm development comprises four larval stages. Under stress conditions such as heat stress or starvation, the nematodes can enter an alternative larval stage called the dauer stage, priming the animals to survive harsh conditions while keeping them in a type of stasis (Fig. 7; Meneely et al. (2019)). The mean lifespan of *C. elegans* is 21 days at 20 °C under laboratory conditions, making it easy to study their whole life cycle (Meneely et al., 2019). The worms are genetically well studied. They have five pairs of autosomes and one pair of sex chromosomes. *C. elegans* was the first multi-cellular organism to ever have its genome fully sequenced (Consortium, 1998), comprising about 20 000 protein-coding genes according to the WormBase data release WS280. The animals are hermaphrodites. They reproduce by self-fertilisation and therefore produce offspring which is genetically mostly identical with their parent. However, male animals occur due to non-disjunction of the sex chromosomes during meiosis with a chance of about 0.2 % and can be used for genetic crossing experiments (Hodgkin and Doniach, 1997).

A plethora of genetic experimental methods can be used within *C. elegans* research. RNA interference (RNAi) can be induced in worms by ingestion of bacteria containing double-stranded RNA (dsRNA) in form of specific plasmids (Fire et al., 1998; Timmons et al., 2001). Forward genetic screens, traditional transgenesis via extrachromosomal arrays and genetic modifications using CRISPR/Cas9 are routinely being performed (Meneely et al., 2019; Paix et al., 2017). Furthermore, the animals are frequently used to study the effects of environmental stress including heat shock, oxidative stress, and ER stress, for example using fluorophore reporter constructs as stress markers (Meneely et al., 2019; Morley and Morimoto, 2004). The worm's cuticle is transparent, making it easy to track such *in vivo* fluorescent markers. In addition, biochemical research techniques get more and more adapted by the worm community. One example is the analysis of global translation using the separation of ribosomes on a sucrose gradient in polysome profiling experiments (Großhans and Ding, 2009). However, tissue-specific analyses from the small worms remain rare and are complicated by the small size of the animals, making tissue dissections tricky.

The genetic conservation between worms and higher organisms including mammals is surprisingly high with 60-80 % of human genes having homologues in *C. elegans*. This is also reflected in a high conservation of cellular pathways (Kaletta and Hengartner, 2006), including a wide range of pathways involved in the regulation of ageing and longevity such as the TOR and IIS pathways (Kenyon, 2010). Three Nobel prizes have been awarded for research conducted with *C. elegans*. In 2002, Sydney Brenner, Robert Horvitz and John

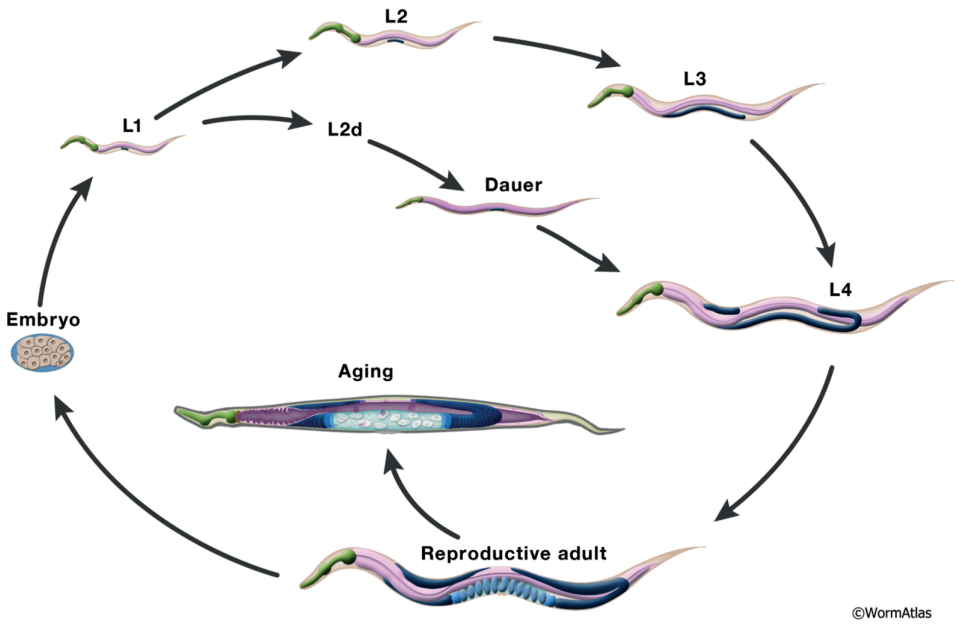

Figure 7: The life cycle of *C. elegans*. Worms develop from an embryonic state through four larval stages into adults within three days upon favourable conditions. During harsh environmental conditions, dauer larvae develop which are adapted for long-term survival. During their life-cycle, *C. elegans* show a wide range of ageing phenotypes. Figure adapted from Herndon et al. (2018), in WormAtlas.

Sulston shared the Nobel prize for their discoveries in the fields of genetic regulation of organ development and programmed cell death using the nematode. Andrew Fire and Craig Mello were awarded a Nobel Prize for the discovery of RNA interference in *C. elegans* in 2006. For the discovery of green fluorescent protein (GFP) and its utilisation as research tool e.g. in *C. elegans*, Osamu Shimomura, Martin Chalfie and Roger Tsien were awarded the Nobel prize in 2008. Together, these points underline the suitability of *C. elegans* as model organism to study molecular and genetic mechanisms in general and the ageing process in particular.

1.3.1 Conserved pathways in *C. elegans*: The IIS and ISR pathways

As mentioned above, many important signalling pathways are conserved between *C. elegans* and higher organisms. As in mammals, the fundamental IIS pathway is regulated by insulin-like peptides in the worm. In *C. elegans*, DAF-2 is the ortholog of the mammalian insulin receptor IGFR1 (Kimura et al., 1997). Like in higher organisms, DAF-2 regulates a downstream cascade involving AGE-1, the worm version of the PI3-kinase (Morris et al., 1996; Murphy and Hu, 2013). The important FOXO transcription factor regulated by IIS activity is termed DAF-16 in the worm and was shown to act downstream of DAF-2/AGE-1 (Lin et al., 1997; Ogg et al., 1997). Mutations in many *C. elegans* genes involved in the IIS pathway were shown to cause longevity (Murphy and Hu, 2013).

Moreover, the ISR is an evolutionary conserved pathway and the *C. elegans* genome contains orthologs of the key genes and corresponding proteins involved in the ISR (Fig. 8). In worms, the two known eIF2 kinases are GCN-2 and PEK-1, which are orthologs of mammalian GCN2 and PERK, respectively. In accordance with the canonical knowledge on the ISR, upon amino acid starvation, GCN-2 was shown to mediate phosphorylation of eIF2 in *C. elegans* (Rousakis et al., 2013). Upon ER stress, PEK-1 phosphorylates eIF2 in worms

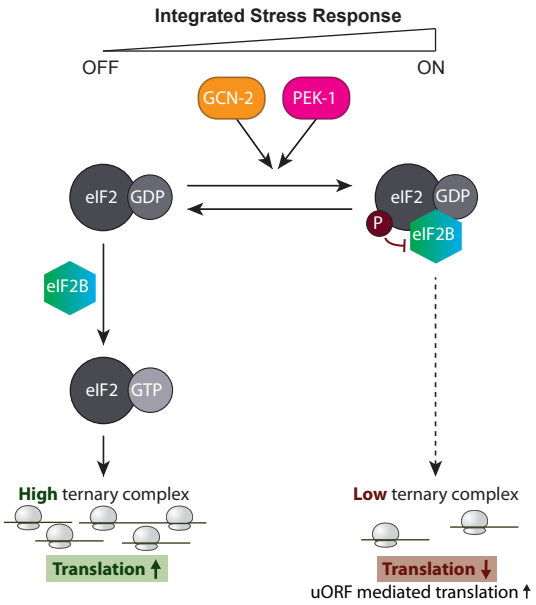

Figure 8: The ISR in *C. elegans*. Schematic depiction of the translation initiation pathway and the ISR as described in the nematode *C. elegans*.

(Richardson et al., 2011). The phosphorylation site around Serine 51 at eIF2α is conserved between the worm and human protein sequences. Inhibition of the β subunit of eIF2 and the δ subunit of eIF2B have been shown to reduce overall translation rates and thereby extend lifespan of worms (Hansen et al., 2007; Tohyama et al., 2008). Furthermore, *ATF4* is conserved and its worm ortholog is *atf-4* (previously named *atf-5*). As in other organisms, in *C. elegans*, *atf-4* is proposed to be regulated by the presence of two uORFs. Reporter worms express constructs with the *atf-4* promotor including the two uORFs, followed by either the main *atf-4* sequence including a C-terminally fused GFP or a GFP directly inserted after the promotor. Both reporter lines showed a stress induced increase of the GFP signal, proving that ATF4 protein levels are induced upon cellular stress as for the yeast and mammalian versions (Rousakis et al., 2013; Statzer et al., 2020). Rousakis *et al.* (2013) further could show that the translational repression of *atf-4* under non-stress conditions depends on the uORF sequences. They also showed that the induction of *atf-4* under amino acid starvation depends on the ISR kinase GCN-2 (Rousakis et al., 2013). Therefore, as in the yeast and mammalian orthologs, the uORFs of *C. elegans atf-4* regulate its translation in response to different stresses. The protein phosphatase GSP-1 is discussed to be required for eIF2 dephosphorylation in the worm (Baker et al., 2012). In sum, many main actors of the ISR are conserved between *C. elegans* and other organisms, making the worm a suitable model to study the ISR and its related cellular mechanisms.

1.3.2 Studying ageing in *C. elegans*

C. elegans is a popular model to study ageing and many key discoveries in ageing and longevity research have been made using the small nematode. Next to the earlier mentioned features making the worm a suitable model organism in general, the short lifespan of the animals makes them particularly valuable for the ageing research field. Moreover, worms show a wide range

of ageing phenotypes, including a decline in tissue integrity, motility, memory and immunity; also complex changes at the cellular and molecular level were observed during worm ageing such as fragmentation of mitochondria, a decline of protein homeostasis or global changes in gene expression (Son et al., 2019). The first signalling pathway shown to modulate ageing was discovered in *C. elegans*: The IIS pathway. Kenyon *et al.* (1993) showed that partial loss of function mutations in *daf-2/IGFR1* extend worm lifespan (Kenyon et al., 1993).

In the search of genetic ageing regulators, genetic screens for the phenotype of longevity have been performed very successfully in *C. elegans* and led to the discovery of multiple genes associated to ageing and longevity processes (Klass, 1983; Friedman and Johnson, 1988a,b; Lee et al., 2003; Hamilton et al., 2005; Hansen et al., 2005). These screens for longevity can be assigned to two classes. In early screens, parental worm populations were mutagenised with chemical agents inducing point mutations to the DNA in an unbiased way, for example using ethyl methanesulfonate (EMS). The offspring of these mutagenised animals was analysed for the phenotype of longevity. To identify genes causing the lifespan extension, associated phenotypes and gene segregation were analysed. The first forward genetic screen for longevity in *C. elegans* by Michael Klass (1983) identified eight mutant worm lines each with a lifespan extension of at least 20 % (Klass, 1983). This initial screen led to the identification of *age-1*/PI3-kinase, one of the first ever identified longevity genes, that was later shown to be part of the IIS pathway (Friedman and Johnson, 1988a,b; Murphy and Hu, 2013). Of the eight mutants, all fell into one of the two phenotype categories of spontaneous dauer formation or reduced food intake and ingestion. From these results, Klass concluded that longevity genes must be rare. After the discovery of RNAi in *C. elegans* (Fire et al., 1998), RNAi clone libraries targeting most of all known *C. elegans* genes enabled functional, genome-wide RNAi screens for longevity genes (Lee et al., 2003; Hamilton et al., 2005; Hansen et al., 2005). These successful RNAi screens led to the identification of numerous genes causing significant longevity upon their knockdown. The vast majority of these genes was involved in three processes: the IIS pathway, mitochondrial processes or the response to dietary restriction. It was hence concluded that the major biological pathways causing lifespan extension by their inhibition in *C. elegans* were discovered (Hansen et al., 2005). However, RNAi remains limited in the context of genetic screens. It causes variable degrees of mRNA knockdown and does not have the resolution to induce other genetic alterations such as point mutations, potentially leading to gain-of-function mutations. Furthermore, functions of essential genes cannot be investigated in genetic screens using RNAi.

While the processes behind ageing and longevity are still not fully understood, the advanced sequencing analysis methods available nowadays provide ground-breaking new possibilities when it comes to the performance and analysis of genetic screens. Through the combination of random chemical mutagenesis with whole genome sequencing, a deep screening resolution is enabled: Mutations in essential genes can be investigated, for example resulting in separation-of-function mutations (Allmeroth et al., 2020; Horn et al., 2018). Further, the point mutagenesis combined with sequencing can lead to the identification of single amino acid substitutions causing gain-of-function mutations. For example, a *C. elegans* screen, using resistance to ER stress as proxy phenotype, identified a gain-of-function mechanism in

GFAT-1 that improved protein quality control and therefore extended worm lifespan (Denzel et al., 2014). Random chemical mutagenesis combined with high throughput sequencing has thus been proven to identify relevant phenotypes in the past in worms and other model systems (Denzel et al., 2014; Allmeroth et al., 2020; Horn et al., 2018). However, an unbiased forward genetic screen using chemical mutagenesis in combination with whole genome sequencing has not been performed to date directly analysing the phenotype of longevity.

1.4 Aims of this study

The human average age has been increasing for generations and the main causes of death in the modern western civilisation are cardiovascular diseases and cancer, pathologies which are highly associated with ageing (Plötzsch and Rößger, 2015; Bundesamt, 2017). Ageing concerns all humankind. In this context, I want to make a contribution to the field of ageing research. Therefore, the main objective of my PhD project is the identification of new conserved biological mechanisms of ageing in the model organism *C. elegans*. So far, genetic screens for the phenotype of longevity in *C. elegans* (1) identified longevity without having access to whole genome sequencing (Klass, 1983), (2) identified mainly loss of function longevity alleles using RNAi (Lee et al., 2003; Hamilton et al., 2005; Hansen et al., 2005) or (3) used proxy phenotypes not directly aiming towards longevity (Denzel et al., 2014). To uncover novel genes that modulate the process of ageing, Dr. Martin Denzel and his team set out to perform the first unbiased forward genetic screen in *C. elegans*, directly aiming for enhanced lifespan in mutant worms, combining it with whole genome sequencing. This screening workflow enabled the unrestricted analysis of loss- and gain-of-function mutations in non-essential and essential genes causing an extension of worm lifespan. Making use of this unbiased forward genetic screen, the overall research aim of my PhD project was the identification and characterisation of novel genes implicated in the process of ageing. At the same time, I aimed to generate research tools to comprehensively study age-associated phenotypes in the nematode. In sum, I addressed the following major aims during my doctoral study:

(1) Identifying novel genetic regulators of the ageing process using an unbiased forward longevity screen in *C. elegans*.

(2) Unraveling the cellular mechanism of action behind the novel longevity genes identified in (1).

(3) Raising the bar of tissue-specific experimental techniques in *C. elegans* to improve biochemical ageing research using the worm.

Together, following the fundamental ideas behind this research project, I aim to identify novel genetic ageing regulators, fine-tuning of which can ultimately prevent detrimental age-associated phenotypes or diseases not only in the nematode, but potentially also in higher organisms up to humans.

2 Results

2.1 An unbiased forward longevity genetic screen in *C. elegans*

2.1.1 The forward longevity screen: Overview and results

To uncover novel regulators that modulate the process of ageing, we optimised an unbiased forward longevity genetic screen in *C. elegans*, directly aiming for enhanced lifespan in mutant worms (Klass, 1983; Friedman and Johnson, 1988b), by combining it with deep sequencing. A parental population of the conditionally sterile CF512 strain [*fer-15(b26)*; *fem-1(hc17)*] was mutagenised with 0.3 % ethyl methanesulfonate (EMS). As an alkylating reagent, EMS induces mostly nucleotide substitutions in form of transitions. Animals of the F2 generation were collected, carrying homozygous mutations for a given allele. The clonal individual F3 populations were then tested for extended lifespan after inducing sterility by growth at non-permissive temperature until the L4 larval stage. Of 28 000 tested genomes, 283 mutant strains showed an increase in their maximum lifespan of at least 2 days compared to a CF512 control (Fig. 9a). Verifying these results, full demographic lifespan analyses were performed and confirmed an enrichment in mutant worm lines with extended lifespan from the forward longevity screen (Fig. 9a and 9b). We aimed to perform whole genome sequencing of all mutants with at least 18 % mean lifespan extension. From the frozen worm stocks, we were able to recover 101 mutant worm lines from the originally 127 strains fulfilling our criteria of 18 % mean lifespan extension and more. Thus, 101 genomes were sequenced. All single-nucleotide polymorphisms (SNPs) within the long-lived EMS-mutant strains were mapped and identified, resulting in a list of potential longevity variants, encompassing loss- and gain-of-function alleles. Taken together, the sequencing of 101 long-lived *C. elegans* genomes resulted in over 30 000 SNPs including non-synonymous, frameshift and start/stop codon mutations in over 5000 genes. To exclude unknown but common *C. elegans* variants that did not arise from the EMS, we only incorporated unique SNPs for further analyses.

Making use of this forward longevity screen combined with deep sequencing, the overall research aim of my PhD project was the identification and characterisation of novel genes

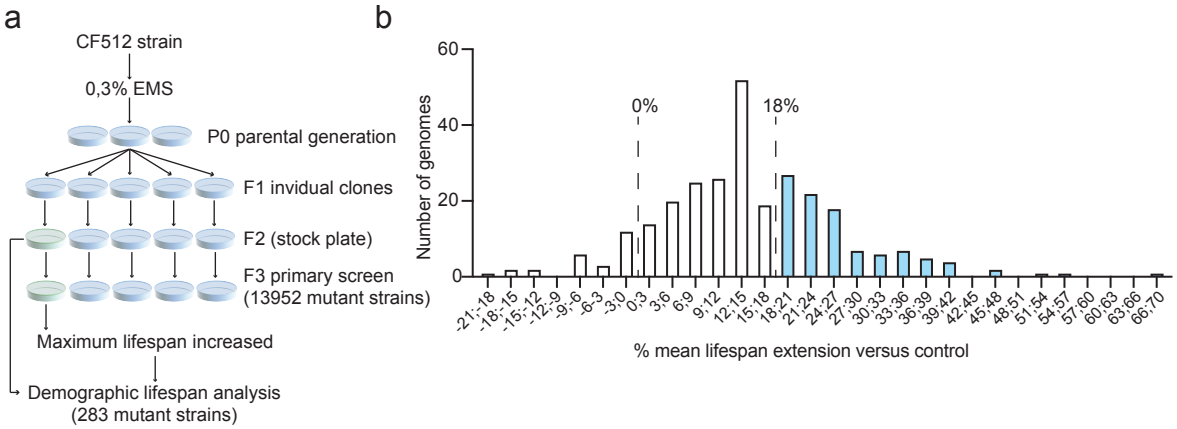

Figure 9: Unbiased forward longevity screen in *C. elegans*. **a** Mutagenesis screening strategy. **b** Mean lifespan extension (normalized to temperature sensitive sterile CF512 control) visualized as the number of tested genomes in 3 % bins. Worm strains with a mean lifespan extension of at least 18 % compared to CF512 control animals were further analysed (corresponding bins depicted in light blue).

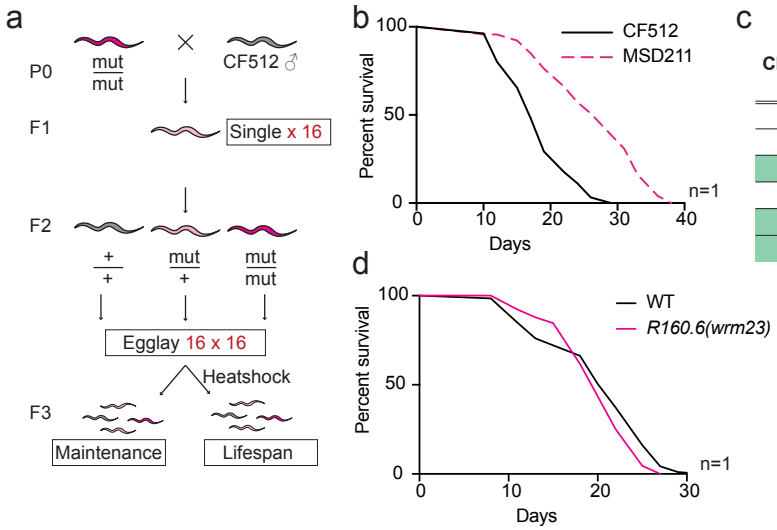

c

Chromosome	SNPs after outcrossing compared to MSD211 SNPs per Chr. normalised in %
Chr. I	-2,59
Chr. II	-5,41
Chr. III	3,28
Chr. IV	-3,73
Chr. V	3,28
Chr. X	5,17 → *R160.6*

Figure 10: Outcrossing for longevity. **a** Outcrossing strategy following the phenotype of longevity. **b** Survival of the original EMS mutagenised strain MSD211. **c** Remaining common EMS SNPs in long-lived and individually out-crossed F3 animals were compared to original MSD211 EMS SNPs. The distribution of the remaining SNPs on the *C. elegans* chromosomes was normalised to the chromosomal distribution of original EMS SNPs of the strain MSD211 and the change is depicted in percent. **d** Survival of CRISPR/Cas9-generated *R160.6(wrm23)* animals compared to WT controls. Mut = mutant. See Tab. 8 in appendix for survival statistics.

implicated in the process of ageing and longevity. One of the most challenging parts of this project was the identification of the variants causing lifespan extension in the EMS mutagenised worms. For this purpose, we developed two distinct strategies of (1) analysing separate long-lived strains and (2) pooling and analysing all sequencing data of the strains with lifespan extension. Both methods and their results will be introduced in the following chapters. The underlying assumption for both strategies is that the lifespan extension was caused by a single SNP present in distinct worm stains as seen with *gfat-1* mutants, where three independent point mutations were shown to enhance lifespan by activating the hexosamine pathway and thereby improving protein quality control (Denzel et al., 2014).

2.1.2 Outcrossing for longevity reduces the number of SNPs in the CDS

The aim of strategy (1) for the identification of novel longevity alleles was to reduce the number of EMS SNPs in single worm strains while preserving the mutated locus causative for the lifespan extension. A selected long-lived worm strain from the forward longevity screen was outcrossed to a wildtype Bristol N2 *C. elegans* strain (hereafter referred to as wildtype), following the phenotype of longevity. Subsequently, the outcrossed worm genomes were sequenced and analysed for remaining EMS SNPs. To ensure a sufficient decrease in EMS SNPs, several outcrossing events needed to occur between the mutant and wildtype genomes. Starting with a parental cross between mutant and wildtype strains, up to the F2 generation every worm underwent two distinct outcrossing events. To increase the number of these events without consecutively repeating such crosses, we aimed for a high number of outcrossed and long-lived worm lines within the F3 generation. This strategy increased the outcrossing events in a parallel manner (Fig. 10a). We performed whole genome sequencing of pooled DNA from heterogenous long-lived and individually out-crossed F3 animals. We

then looked for remaining common EMS SNPs in the long-lived lines after outcrossing.

This approach was performed on the EMS-mutant strain MSD211, which is one of the most long-lived worm lines generated in the forward longevity screen (long-lived by 46 % compared to a CF512 control, Fig. 10b). Therefore, screening for conserved longevity after outcrossing was possible by analysing maximum lifespans. Furthermore, the EMS mutagenised line MSD211 has no mutations in known longevity pathways. After two outcrossing events each, twelve distinct worm lines could be identified to be long-lived in the F3 generation. Hence, the genomic DNA of these lines was prepared, pooled and whole genome sequencing was performed. The subsequent SNP analysis revealed a reduction of EMS SNPs by ∼87 % from 994 EMS SNPs within the original EMS mutant line to 126 common EMS SNPs in the outcrossed lines. To genetically map the longevity-causing variants, we analysed the remaining EMS SNPs for an enrichment within a specific chromosome. However, a chromosome-specific enrichment could not be observed (Fig. 10c). Of the remaining 126 EMS SNPs, one fell into the coding DNA sequence, namely the coding region of the uncharacterised *C. elegans* gene *R160.6*. The EMS variation within *R160.6* could be generated in wildtype worms by using the CRISPR/Cas9 technology and a lifespan analysis of the resulting worm strain *R160.6(wrm23)* was performed. Compared to a wildtype control, the *R160.6* mutant worms did not show a lifespan extension (Fig. 10d).

These results indicate, that either the longevity causing allele of the strain MSD211 resides within the non-coding region of the genome or that a combination of SNPs within or outside the CDS cause the longevity. Hence, a general assumption that the forward longevity screen mainly produced mutations in the coding region of the genome causative for lifespan extension cannot be made.

2.1.3 Selection of candidate genes by allelism enables identification of known longevity genes

In strategy (2), we analysed the pooled EMS variant data of all 101 sequenced strains with at least 18 % lifespan extension compared to control (Fig. 9b). From the over 5000 genes hit by the EMS mutagenesis, we aimed for a universal list of high-confidence candidate longevity genes and corresponding alleles, which could subsequently be tested for an effect on worm lifespan. While the "outcrossing for longevity" strategy described above indicates, that the lifespan-extension causing variants can reside within the non-coding sequence, previous targeted screens in worms and mammalian cells prove the successful identification of SNPs causing defined phenotypes by analysing the coding sequence (CDS) only (Denzel et al., 2014; Horn et al., 2018; Allmeroth et al., 2020). Hence, we created a pipeline for candidate longevity gene identification from EMS SNPs within the CDS. The overall basis of this pipeline was the assumption, that one mutant gene per genome is driving longevity. Further selection criteria for high-confidence candidate genes were the following: A high-confidence candidate gene was represented by at least two different alleles in independent mutant worm lines (allelism). We next produced a score indicating the probability of a given mutation having an influence on the function of the gene, dividing the size of the coding sequence of a given gene by the number of times it was independently mutagenised in total. Last, we manually analysed the

a

Chromosome	Position	Nucleotide substitution	Gene name	AA substitution	AA position	Strain name
III	3016950	C/T	*daf-2*	L/F	162	MSD104
III	3016315	G/A	*daf-2*	V/M	181	MSD212
III	3000601	T/A	*daf-2*	M/K	1406	MSD305
III	3000581	C/T	*daf-2*	H/Y	1413	MSD167
III	3000560	G/A	*daf-2*	G/S	1420	MSD055
III	2997074	A/G	*daf-2*	Y/C	1805	MSD155

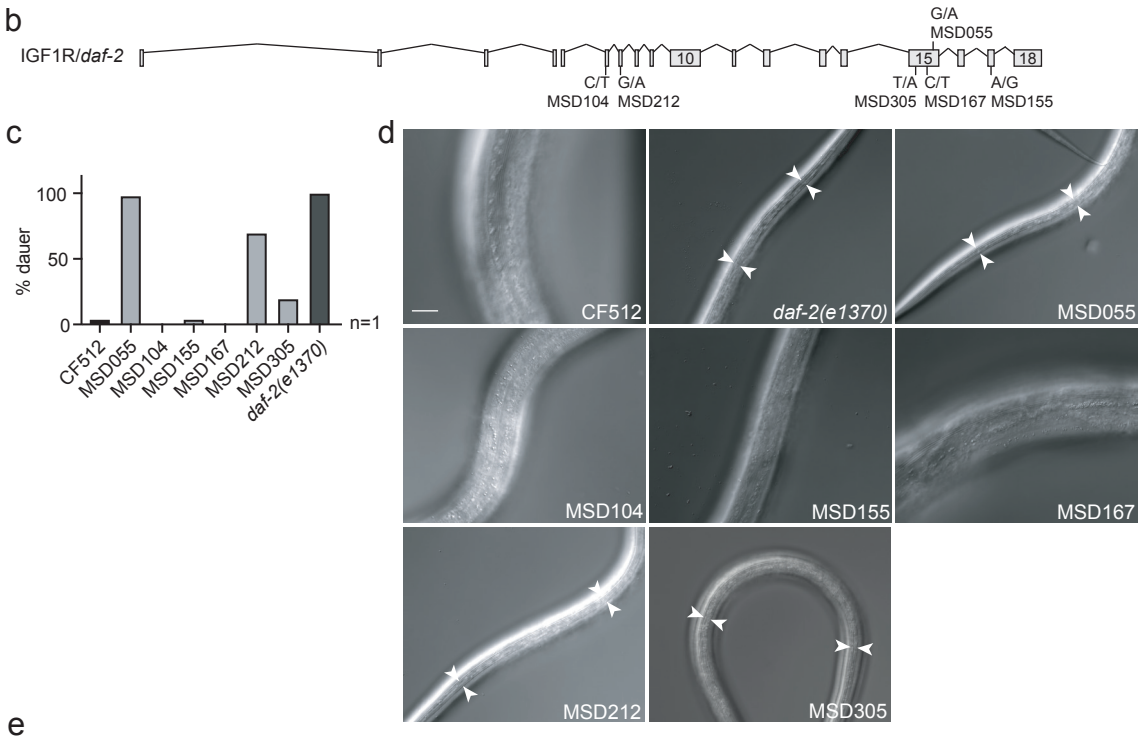

e

Chromosome	Position	Nucleotide substitution	Gene name	AA substitution	AA position	Strain name
I	8063756	T/A	*che-3*	N/I	3849	MSD121
I	8064225	G/A	*che-3*	S/F	3708	MSD202
I	8067069	C/T	*che-3*	A/T	3200	MSD097
I	8071899	T/A	*che-3*	E/V	2188	MSD215
IV	3798574	C/T	*osm-3*	A/T	140	MSD009
X	381554	C/T	*ife-2*	E/K	221	MSD218
X	382676	C/T	*ife-2*	G/E	10	MSD306
II	8220548	C/T	*ifg-1*	P/S	560	MSD295
II	8221040	G/A	*ifg-1*	E/K	685	MSD076

Figure 11: Mutations in known longevity genes identified through a mutagenesis screen for longevity. **a** Detailed overview of identified alleles in the *daf-2* insulin/insulin-like growth factor 1 (IGF-1) receptor gene. **b** Schematic representation of the *daf-2* gene and corresponding alleles identified in the screen, also shown in (**a**). **c** Percentage of worms entering the dauer stage upon development at 27 °C. Analyzed were CF512 control worms, mutant strains from the screen carrying *daf-2* mutations (MSD strains shown in **a** and **b**), and a dauer constitutive (daf-c) *daf-2(e1370)* control strain (n=1 with $\geq$50 animals per genotype). **d** Microscopic analysis of dauer alae. Analysed were control and mutant worm strains depicted in (**c**). White arrows indicate dauer alae. **e** Detailed overview of alleles in known longevity genes *che-3*, *osm-3*, *ife-2*, and *ifg-1* identified in the screen.

list of candidate alleles for clusters of candidate genes in specific pathways.

From the high-confidence candidate gene list we identified variants of genes that are known to modulate lifespan in *C. elegans*, validating this approach (Tacutu et al., 2018). Such a gene is for example the insulin/IGF receptor ortholog *daf-2*, specific knockdown alleles of which are known to enhance lifespan in worms and higher organisms via reduction of the insulin signalling pathway. Exemplary is the canonical allele *daf-2(e1370)*, extending worm lifespan by ∼100 % compared to wildtype control worms (Kenyon et al., 1993). In the forward longevity screen, we identified six novel *daf-2* alleles in six independent long-lived worm lines (Fig. 11a and b). Therefore, the *daf-2* gene appeared on top of the high-confidence candidate gene list (see Tab. 4 in appendix). A specific phenotype of *daf-2* mutants is their ability to enter the developmental dauer state: 100 % of *daf-2(e1370)* larvae enter the dauer state if grown at 27 °C (temperature-sensitive dauer-constitutive mutants), whereas wildtype worms remain in a conventional developmental cycle (Gems et al., 1998). To verify that the newly identified mutations have an effect on DAF-2 function, we directly checked if the EMS mutant worms are temperature-sensitive dauer-constitutive. We quantified heat-induced dauer formation and observed enhanced dauer formation in three out of six *daf-2* mutant worm lines (Fig. 11c). We further analysed a dauer-specific trait of the worm cuticle called dauer alae. While a CF512 control develops regular cuticle alae if grown at 27 °C, the three above identified dauer-constitutive *daf-2* mutants also developed dauer alae (forward longevity screen lines MSD055, MSD212 and MSD305; Fig. 11d). Hence, they can be considered functional *daf-2* mutants. From these results, we conclude that in these strains, longevity is likely obtained via reduction of insulin/IGF signalling activity by insulin/IGF receptor mutations.

Next to the *daf-2* gene, we identified genes in pathways known to drive longevity through reduced mRNA translation (two mutations each in *ifg-1* and *ife-2*; Hansen et al. (2007); Rogers et al. (2011)), and in pathways that extend lifespan by regulating chemosensation (four mutations in *che-3* and one mutation in *osm-3*; Fig. 11e; Apfeld and Kenyon (1999)). Together, these results validate the forward longevity screen and the high-confidence candidate gene list as combined approach to identify longevity genes. To avoid the dilution of the high-confidence candidate gene list, we excluded worm lines with SNPs in already known longevity genes from the analysis. These criteria led to a total of 303 high-confidence candidate genes from a total of 101 sequenced long-lived worm lines.

2.2 Mutations in the translation initiation machinery cause longevity without reduction in overall protein synthesis

2.2.1 From the forward longevity screen to translation initiation

To identify novel longevity alleles from the high-confidence candidate genes conveyed from the forward longevity screen, we aimed to validate the top candidates. To analyse the lifespan effect of candidate mutations in a clean genetic background, we either outcrossed the corresponding EMS mutagenised strain at least 4 times to wildtype animals, or we recapitulated the respective genetic change using the CRISPR/Cas9 technology in wildtype worms. Due to our high-confidence candidate gene criteria, all genes on our list were represented with at

a

Chromosome	Position	Nucleitode substitution	Gene name	AA substitution	AA position	Allele name
II	6966468	T/A	*ppp-1*	N/I	295	*ppp-1(wrm10)II*
II	6966802	G/A	*ppp-1*	L/F	216	*ppp-1(wrm15)II*
II	13088136	G/A	*gcn-2*	D/N	1217	*gcn-2(wrm4)II*
X	11414450	C/T	*pek-1*	D/N	81	*pek-1(wrm7)X*
	8026808	C/T	*iftb-1*	E/K	244	*iftb-1(wrm53)I*

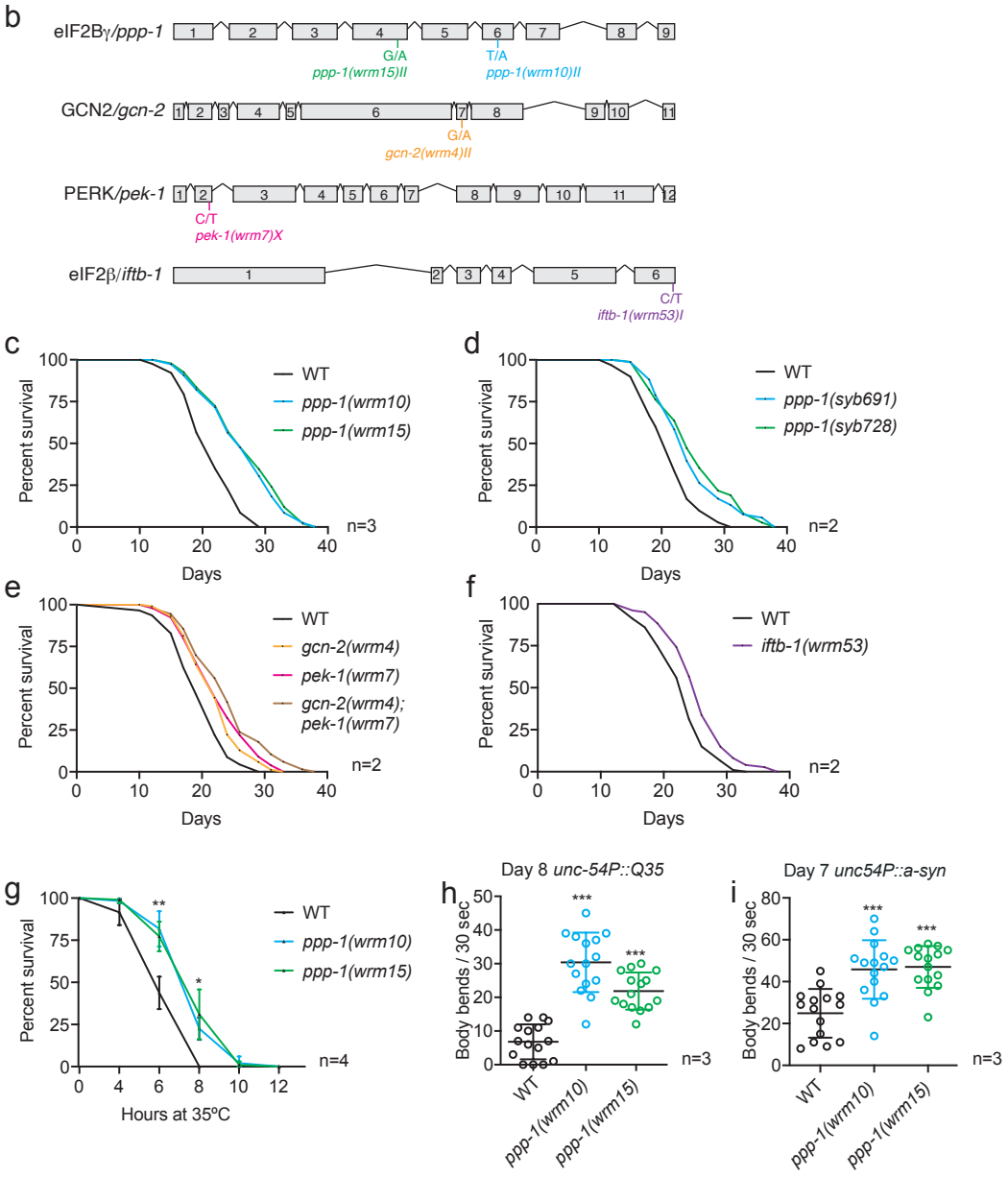

Figure 12: Mutations in ISR components identified in the forward longevity screen in *C. elegans*. **a** Detailed overview of identified longevity alleles clustering in the ISR identified in the screen. **b** Schematic representation of identified ISR genes and corresponding longevity alleles. **c** Survival of outcrossed *ppp-1(wrm10)* and *ppp-1(wrm15)* mutants compared to WT controls (representative data from n=3 independent experiments). **d** Survival of CRISPR/Cas9-generated *ppp-1* alleles *syb691* and *syb728* compared to WT controls (representative data from n=2 independent experiments). *syb691* corresponds to *wrm10* and *syb728* to *wrm15*. **e** Survival of outcrossed *gcn-2(wrm4)*, *pek-1(wrm7)*, and *gcn-2(wrm4); pek-1(wrm7)* double mutants compared to WT controls (representative data from n=2 independent experiments). **f** Survival of outcrossed *iftb-1(wrm53)* mutants compared to WT controls (representative data from n=2 independent experiments). **g** Thermotolerance assays of day 1 *ppp-1* mutant worms compared to WT controls (error bars represent means ±SD, two-way ANOVA Dunnett's post hoc test with *p<0.05 and **p<0.01 versus WT controls at respective time points; n=4 independent experiments with 50 animals each). **h** Motility assays using day 8 WT animals and *ppp-1* mutants with *unc-54P*-driven muscle-specific expression of polyQ35 YFP fusion protein (error bars represent means ±SD, one-way ANOVA Dunnett's post hoc test with ***p<0.001 versus WT controls; n=3 independent experiments with ≥12 animals each). **i** Motility assays using day 7 WT animals and *ppp-1* mutants with *unc-54P*-driven muscle-specific expression of α-synuclein (α-syn; error bars represent means ±SD, one-way ANOVA Dunnett's post hoc test with ***p<0.001 versus WT controls; n=3 independent experiments with 15 worms each).

least two independent alleles. To test as many genes as possible, we decided to validate one allele per candidate gene. Using these strategies, we analysed a total of 20 isolated mutations from the EMS background, which turned out as false candidates not causing longevity (see Tab. 4 in appendix).

Notably, we next identified a cluster of genes that control the process of mRNA translation initiation and the ISR (Fig. 8). As described in detail in the introduction (see chapter 1.2.3), one of the key factors during translation initiation is eIF2-GTP, which is a primary constituent of the TC. For each translation initiation process, a guanine nucleotide exchange at eIF2 is mediated by eIF2B, a second key regulator of translation initiation. During the active ISR, in worms eIF2 is phosphorylated by one of its stress-sensing kinases GCN-2 or PEK-1, making phospho-eIF2 an inhibitor of its own GEF eIF2B. As a result, TC formation and overall translation are down-regulated during the active ISR. We initially found the gene *ppp-1*/eIF2Bγ ranking high on the candidate list with two independent alleles. We further identified one mutation each in *gcn-2*/GCN-2, *pek-1*/PEK-1 and *iftb-1*/eIF2β (Fig. 12a and b). Strikingly, the outcrossed alleles *ppp-1(wrm10)* and *ppp-1(wrm15)* led to an increase in lifespan by over 20 % compared to wildtype controls (Fig. 12c). The longevity of both *ppp-1* alleles could be confirmed in corresponding CRISPR/Cas9-generated mutants *ppp-1(syb691)* and *ppp-1(syb728)* (Fig. 12d). Furthermore, the outcrossed mutants *gcn-2(wrm4)* and *pek-1(wrm7)*, the double mutant *gcn-2(wrm4); pek-1(wrm7)* and finally the outcrossed *iftb-1(wrm53)* strain were long-lived compared to controls (Fig. 12e and f). These results prove the successful identification of novel longevity variants from the forward longevity screen using our high-confidence candidate gene list. Furthermore, we found an unknown link between ISR regulation and lifespan extension in *C. elegans*.

Longevity is often associated with an increase in protein homeostasis (Denzel et al., 2014; Ben-Zvi et al., 2009; Pyo et al., 2013). Hence, we analysed the *ppp-1* mutants with their robust lifespan extension for phenotypes upon proteotoxic conditions. Upon heat stress at 35 °C, both *ppp-1* strains showed an increase in survival compared to wildtype animals (Fig. 12g). We further crossed the *ppp-1* mutants in backgrounds expressing muscle-specific tagged polyglutamine stretches (polyQ35, Morley et al. (2002)) or muscle-specific tagged α-synuclein (van Ham et al., 2008). Both transgenic constructs decrease the motility of wildtype worms drastically. Strikingly, the *ppp-1* mutations rescued these paralysis phenotypes and increased motility significantly compared to controls (Fig. 12h and i). Hence, the identified *ppp-1* alleles cause not only a robust lifespan extension but also an increased resistance to proteotoxic stresses.

2.2.2 Attenuated mRNA translation does not drive *ppp-1* longevity

It is a widely accepted longevity regime that reducing protein production by down-regulating mRNA translation can lead to an extension of lifespan (Hansen et al., 2007; Syntichaki et al., 2007; Tohyama et al., 2008; Pan et al., 2007). The identified longevity alleles of *ppp-1* and *iftb-1* reside within critical subunits of key regulators eIF2B and eIF2 of the translation initiation process (Fig. 8). Hence, we carefully analysed mRNA translation and protein synthesis in these mutants.

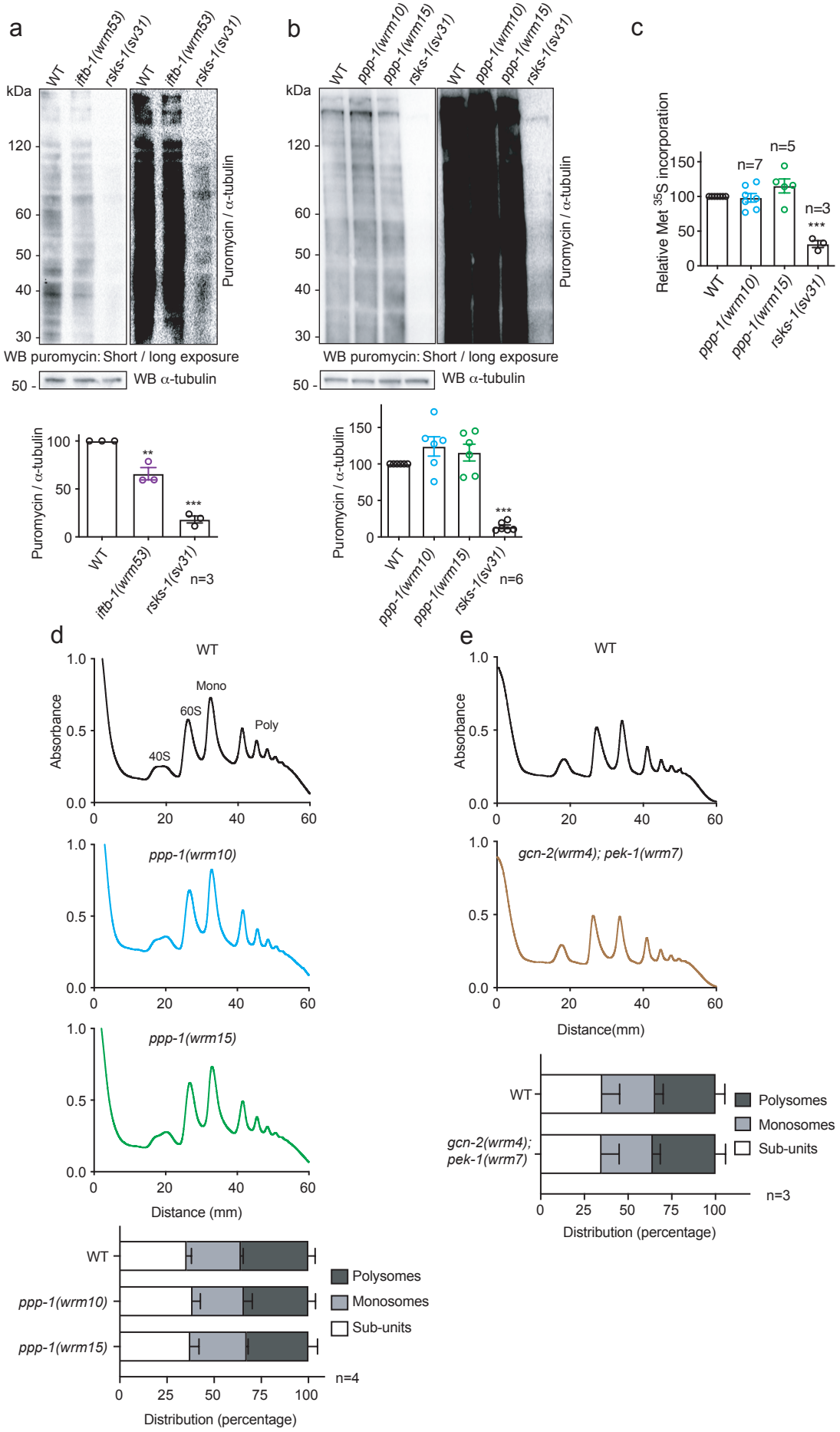

Figure 13: (Caption next page.)

Figure 13: Mutations in *ppp-1* do not attenuate global protein synthesis (previous page). **a** Puromycin incorporation followed by Western blot analysis using antibodies detecting puromycin and α-tubulin in day 1 WT animals, *iftb-1(wrm53)* mutants, and control *rsks-1(sv31)* mutants. Images of the same membrane are shown with short and long exposures (error bars represent means ±SEM, one-way ANOVA Dunnett's post hoc test with **p<0.01 and ***p<0.001 versus WT control; n=3 independent experiments). **b** Puromycin incorporation assay in day 1 WT animals, *ppp-1* mutants, and *rsks-1(sv31)* controls as described in (**a**). Images of the same membrane are shown with short and long exposures (error bars represent means ±SEM, one-way ANOVA Dunnett's post hoc test with ***p<0.001 versus WT control; n=6 independent experiments). **c** Quantification of methionine ^{35}S labelling of day 1 WT worms, *ppp-1* mutants, and control *rsks-1(sv31)* mutants (error bars represent means ±SEM, one-way ANOVA Dunnett's post hoc test with ***p<0.001 versus WT; number of independent experiments (n) indicated in the figure). **d** Polysome profiling and quantification of day 1 WT and *ppp-1* animals. Quantification represents the relative abundance of ribosomal subunits (40S, 60S), monosomes (mono) and polysomes (poly; error bars represent means +SD, two-way ANOVA Dunnett's post hoc test; n=4 independent experiments; no significant changes were detected). **e** Polysome profiling and quantification of day 1 WT and *gcn-2(wrm4); pek-1(wrm7)* animals as explained in (**d**) (error bars represent means +SD, two-way ANOVA Dunnett's post hoc test; n=3 independent experiments; no significant changes were detected).

Surface sensing of translation (SUnSET) is a method based on the incorporation of the compound puromycin into actively synthesised proteins. The incorporated puromycin can be immunologically detected with a monoclonal antibody during Western blotting. Hence, it gives direct and quantifiable insight into protein synthesis rates (Schmidt et al., 2009). The *iftb-1* mutants showed a significant reduction in puromycin incorporation compared to wildtype worms (Fig. 13a). In consistence, RNAi-mediated knockdown of *iftb-1* was previously reported to reduce protein synthesis rates and to extend lifespan in *C. elegans* (Hansen et al., 2007). Surprisingly, puromycin incorporation assays in *ppp-1* mutants did not show changes in translation rates compared to wildtype animals, while control *rsks-1*/S6K mutants displayed a strong reduction in incorporated puromycin (Fig. 13b). To verify these results, we measured protein synthesis via the incorporation of radioactive isotope ^{35}S-methionine tracers. In consistence with the previous SUnSET measurements, *ppp-1* mutants did not show a reduction in protein synthesis using isotopic protein labelling, while in *rsks-1*/S6K control animals a strong reduction of ^{35}S-methionine incorporation was measured (Fig. 13c).

To deeper understand the activity of the translational machinery of *ppp-1* mutants, we performed polysome profiling. In this method, ribosomal complexes including bound mRNAs are separated on a sucrose gradient during ultracentrifugation due to differences in density. Hence, free ribosomal subunits can be divided from translating monosomes (one actively translating ribosome per mRNA) and polysomes (two and more actively translating ribosomes per mRNA). Again, in *ppp-1* mutants no differences in ribosome distribution could be detected in comparison to wildtype animals (Fig. 13d). We also analysed the translational machinery of the *gcn-2(wrm4); pek-1(wrm7)* double mutant using polysome profiling and did not detect changes in translation compared to wildtype worms (Fig. 13e). Therefore, the analysis of the forward longevity screen revealed two classes of mutations in key enzymes of the translation initiation process that can be linked to lifespan extension. First, animals with a novel mutation in *iftb-1*/eIF2β are long-lived while showing reduced protein synthesis rates. Next, the *ppp-1*/eIF2Bγ mutants with extended lifespan and increased protein homeostasis do not display changes in mRNA translation rates or the ribosomal machinery.

Translational activity can be modulated by inactivation of eIF2 via phosphorylation through ISR activity. eIF2B regulates eIF2 and can be inhibited in a feed-back loop by phosphorylated eIF2. To analyse if the *ppp-1*/eIF2Bγ mutations affect eIF2 phosphorylation, we monitored eIF2α phosphorylation in *ppp-1* animals on day 1 and day 6 of adulthood. While phos-

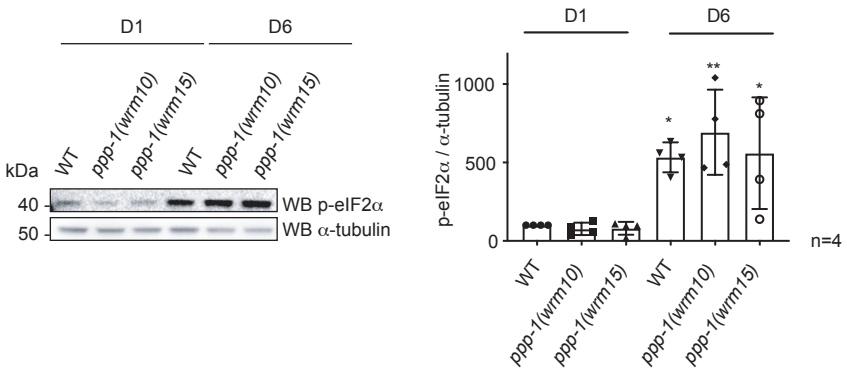

Figure 14: ISR analysis in aged ppp-1 mutants. Representative Western blot and quantification of day 1 and day 6 WT animals and *ppp-1* mutants detecting phospho-eIF2α (Ser51) normalized to α-tubulin (error bars represent means ±SEM, one-way ANOVA Tukey's post hoc test with *p<0.05 and **p<0.01 versus WT day 1; n=4 independent experiments).

phorylated eIF2α levels were consistently increased upon ageing, no differences between *ppp-1* mutants and wildtype animals could be detected (Fig. 14). Overall, *ppp-1* longevity and increased protein homeostasis are not driven by attenuated mRNA translation.

2.2.3 *ppp-1* longevity is driven by translation of specific mRNAs

While *ppp-1* mutants did not display changes in global protein synthesis, we hypothesised that translational efficiency of specific mRNAs might be changed. To analyse translational efficiency, we used polysome profiling followed by RNA sequencing. We specifically analysed mRNAs associated with polysomes (>3 ribosomes/mRNA), since these can be considered as efficiently translated transcripts. The detected levels of polysome-bound mRNAs were normalised to total RNA levels, which led to the translational efficiency levels (Fig. 15a). The polysome fractions of *ppp-1* mutants showed a significant de-enrichment of 336 mRNAs and an enrichment of 72 mRNAs (Fig. 15b) compared to wildtype worms. In the set of all significantly changed mRNAs, a GO term analysis of the corresponding genes revealed an over-representation of annotations regarding phosphorylation processes (Fig. 15c).

We next analysed if the enhanced translational efficiency of specific mRNAs contributes to *ppp-1* longevity and increased protein homeostasis. Therefore, we individually knocked down the candidate mRNAs that we found to be enriched in *ppp-1* mutants using RNAi in *ppp-1(wrm10)* animals. We used the resistance to polyQ35-mediated paralysis as a proxy-phenotype for general increased protein homeostasis and longevity. At day 8 of adulthood, polyQ transgenic worms were paralysed and did not move outside an area of 1 cm^2, while the *ppp-1(wrm10)* allele rescued this phenotype in an easily quantifiable way (Fig. 15d). We screened for candidate mRNAs, knockdown of which would reduce the motility in polyQ transgenic *ppp-1(wrm10)* mutants towards wildtype levels. The RNAi treatment against 7 mRNA candidates suppressed the *ppp-1(wrm10)* motility on plates by at least 50 % (Fig. 15d, depicted in yellow). To validate the effect of these 7 top suppressor mRNAs, we performed body bending assays in liquid in both *ppp-1* mutants upon RNAi-mediated knockdown of the given mRNAs. All treatments led at least to a mild suppression of motility compared to the *luciferase*-targeting control RNAi treatment with some reaching significance in *ppp-1*

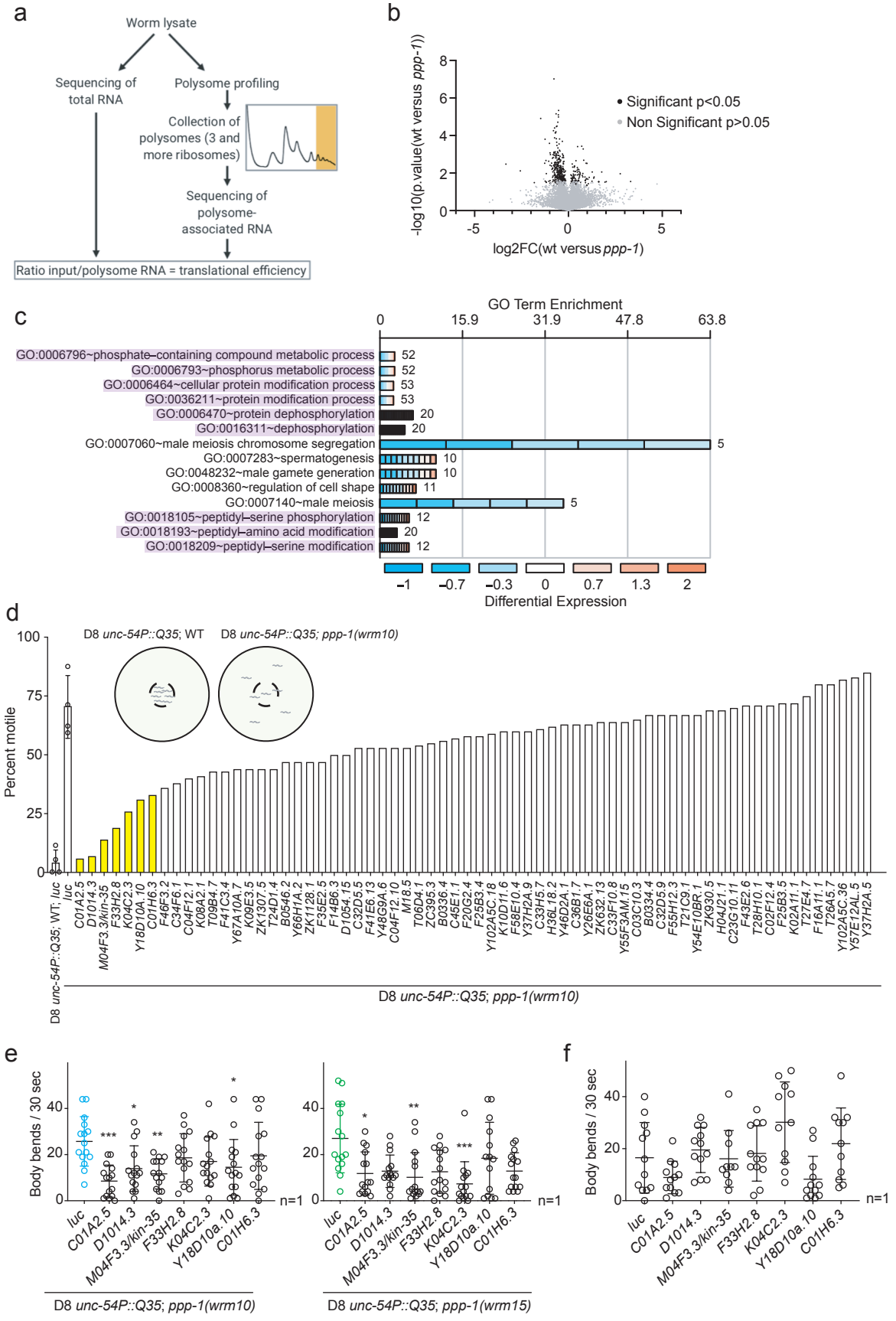

Figure 15: (Caption next page.)

Figure 15: Translational efficiency is altered in *ppp-1* mutants (previous page). **a** Polysome sequencing strategy. **b** Volcano plot of polysome-associated mRNAs normalised to total mRNA levels between WT animals and *ppp-1* mutants. All displayed mRNAs were found in both *ppp-1* mutants. Mean p-values and mean log 2-fold change of both *ppp-1* mutants were used (Student's two-sided t test, significance is reached for $p<0.05$). FC=fold change. **c** DAVID gene ontology (GO) analysis of significantly changed mRNAs shown in (**b**). Processes involved in phosphorylation are highlighted in purple. **d** RNAi screen for suppressors of polyQ35; *ppp-1(wrm10)* motility. For reliability, assays of polyQ35 WT animals and polyQ35; *ppp-1(wrm10)* mutants on *luciferase* RNAi were performed four times (error bars represent means ±SD). Bars highlighted in yellow indicate RNAi treatments with a reduction of motility of at least 50 % compared to the *luciferase* control treatment of polyQ35; *ppp-1(wrm10)* worms. **e** Motility assays of day 8 polyQ35 transgenic animals, polyQ35; *ppp-1(wrm10)* and polyQ35; *ppp-1(wrm15)* mutants after indicated RNAi treatments (error bars represent means ±SD, one-way ANOVA Kruskal Wallis test with *$p<0.05$, **$p<0.01$ and ***$p<0.001$ versus respective *luciferase* control treatments; n=1 with ≥14 animals per treatment). **f** Control motility assays of day 6 polyQ35 transgenic worms after indicated RNAi treatments (error bars represent means ±SD, one-way ANOVA Dunnett's post hoc test, no significant changes were detected; n=1 with ≥10 worms per RNAi treatment).

worms (Fig. 15e), while the RNAi treatments did not significantly change motility in polyQ35 wildtype animals (Fig. 15f). The candidate RNAi clones C01A2.5 and M04F3.3 were the only ones that caused significant results independently in both *ppp-1(wrm10)* and *ppp-1(wrm15)* mutants compared to *luciferase*-targeting control clones (Fig. 15e). Therefore, we analysed *ppp-1* lifespans upon knockdown of C01A2.5 and M04F3.3. RNAi treatment against C01A2.5 rescued the lifespan extension of both *ppp-1* mutants, but also reduced wildtype lifespan suggesting general toxicity (Fig. 16a). Strikingly, knockdown of M04F3.3 fully suppressed the lifespan extension of *ppp-1* mutants without showing effects on wildtype lifespan (Fig. 16b). M04F3.3 is a so far uncharacterised *C. elegans* gene with a predicted protein kinase activity. We hence termed it *kin-35*. We validated the RNAi-mediated knockdown of *kin-35* by qPCR (Fig. 16c). Importantly, the increased association of *kin-35* to polysomes in *ppp-1* animals compared to wildtype could be confirmed by qPCR, while baseline levels of *kin-35* transcripts were not changed in the mutants (Fig. 16d). These results suggest that altered translational efficiency of *kin-35* is required for *ppp-1* longevity.

To address if *kin-35* is not only required for the lifespan-extension in *ppp-1* animals but also sufficient to cause longevity in wildtype animals, we generated three independent transgenic lines over-expressing *kin-35* through an extrachromosomal array. qPCR analysis confirmed the over-expression of *kin-35* in all three lines compared to transgenic lines not carrying the array (Fig. 16e). The independent over-expression of *kin-35* alone did not cause longevity (Fig. 16f) or an increase in protein homeostasis measured by survival during heat stress compared to controls (Fig. 16g). Together, our results demonstrate that while elevated *kin-35* transcript levels alone are not sufficient to induce longevity, the selective translation of *kin-35* is a driver of longevity in *ppp-1* mutants.

2.2.4 Mutations in *ppp-1* inhibit the ISR

To better understand the effects of the identified *ppp-1* alleles, we further characterised their functional relevance. Heterozygous *ppp-1* strains were long-lived, demonstrating genetic dominance of the *ppp-1* mutations (Fig. 17a). Furthermore, RNAi mediated knockdown of *ppp-1* in wildtype animals did not change their lifespan or response to heat stress compared to *luciferase*-targeting RNAi control treatments. Instead, *ppp-1* silencing fully abolished the longevity of both *ppp-1* mutants as well as their increased heat resistance (Fig. 17b and c). Together, these results suggest that the *ppp-1* mutations do not fall into the class of

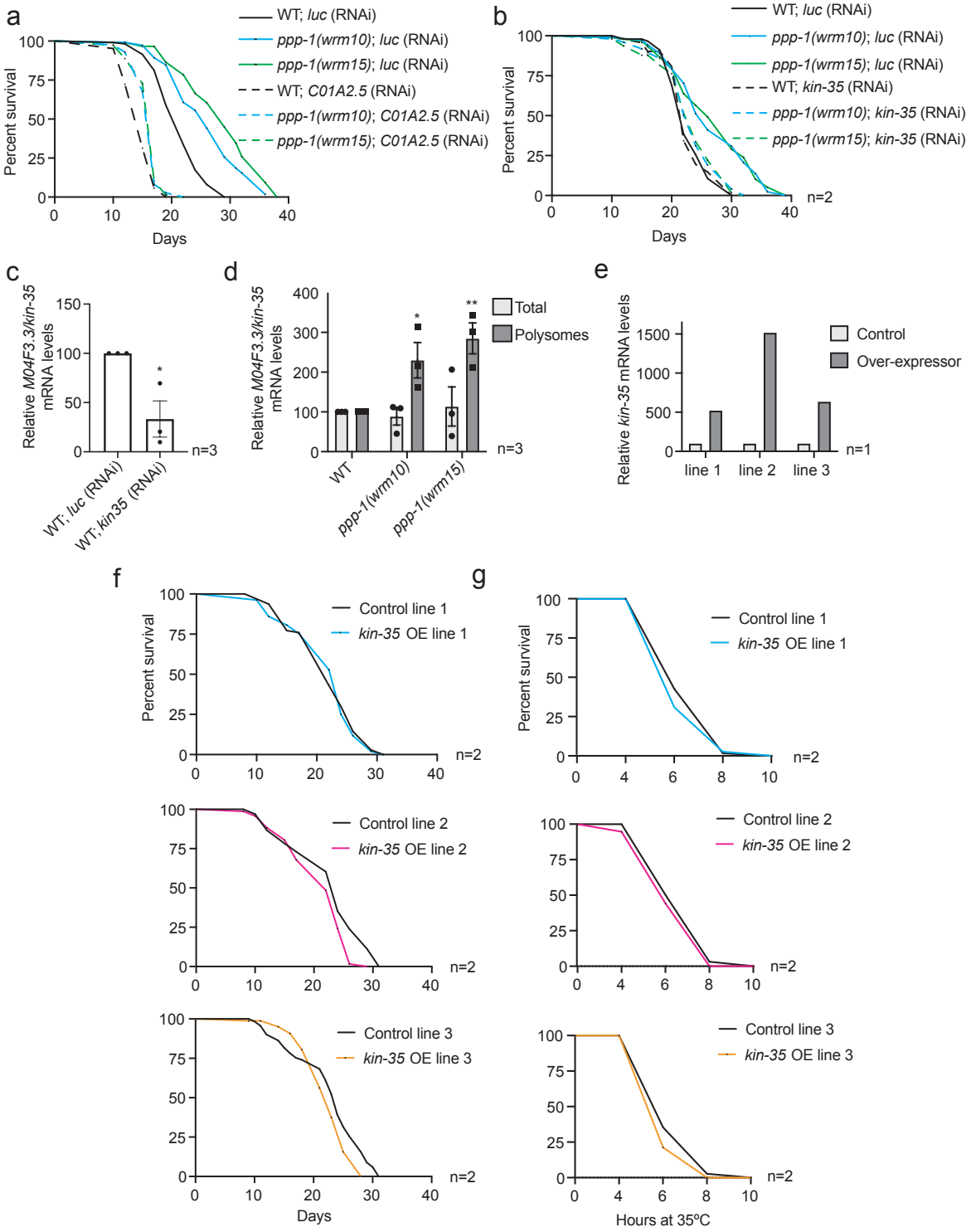

Figure 16: *kin-35* translation is required for *ppp-1* longevity. **a** Survival of WT animals and *ppp-1* mutants upon RNAi knockdown of C01A2.5 and control *luciferase* (n=1). **b** Survival of WT animals and *ppp-1* mutants upon *kin-35* or control *luciferase* RNAi knockdown (representative data from n=2 independent experiments). **c** qPCR for *kin-35* mRNA in WT animals using *luciferase* control or *kin-35* RNAi (error bars represent means ±SEM, unpaired two-tailed t-test with *p<0.05 versus *luciferase* control; n=3 independent experiments). **d** mRNA distribution of *kin-35* mRNA in total worm extracts and polysomes of day 1 WT and *ppp-1* animals measured by qPCR (error bars represent means±SEM, two-way ANOVA Tukey's post hoc test with *p<0.05 and **p<0.01 versus WT control; n=3 independent experiments). **e** Relative *kin-35* mRNA levels measured by qPCR in *kin-35* over-expressing worm lines 1, 2, and 3 compared to the respective non-transgenic littermate controls (n=1). **f** Survival of *kin-35* over-expressing worms (lines 1, 2 and 3) compared to respective control animals not over-expressing the extrachromosomal array (representative data from n=2 independent experiments). **g** Thermotolerance assay of day 1 *kin-35* over-expressing mutants (lines 1, 2 and 3) compared to respective controls as described in (**f**) (representative data from n=2 independent experiments with ≥30 worms each). OE=Over-expressor.

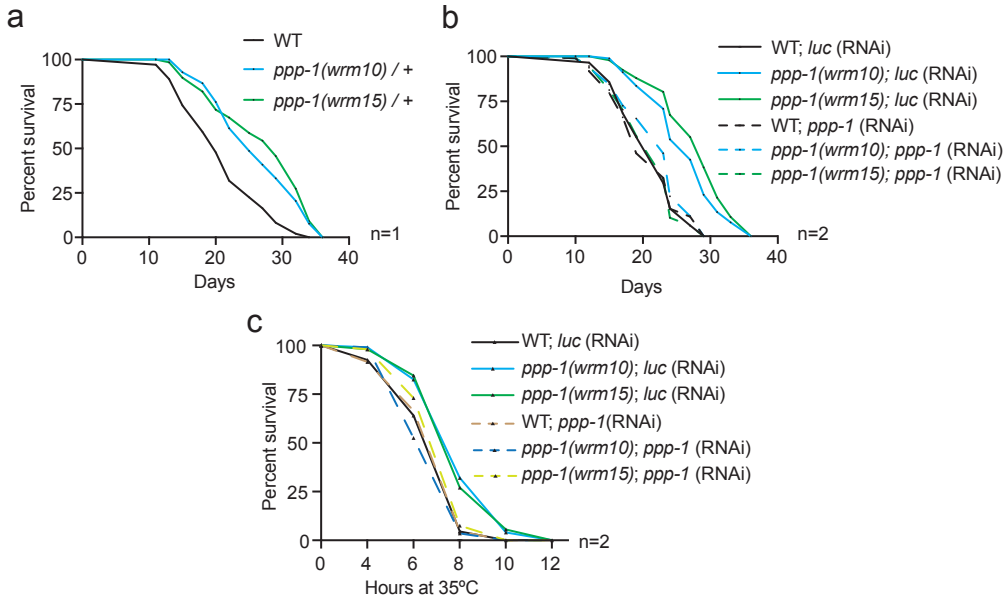

Figure 17: A knockdown of *ppp-1* does not mediate longevity. **a** Survival of heterozygous *ppp-1* mutants compared to WT control animals. **b** Survival of WT animals and *ppp-1* mutants upon RNAi treatment targeting *ppp-1* or control *luciferase* (representative data from n=2 independent experiments). **c** Thermotolerance assays of day 1 WT animals and *ppp-1* mutants upon *ppp-1* RNAi treatment (representative data from n=2 independent experiments with $\geq$30 worms each).

casual loss-of-function alleles, since the activity of *ppp-1* was required for the observed phenotypes. Consequently, we hypothesised that gain-of-function mutations in *ppp-1* might lead to an increased activity of the full eIF2B complex. Enhanced eIF2B activity would increase eIF2 function and hence counter the effects of eIF2α-phosphorylation and general ISR activity (Fig. 8). While eIF2α-phosphorylation levels were not changed in *ppp-1* animals during un-stressed conditions (Fig. 14), we now aimed to closely investigate the ISR upon stress conditions. While the active ISR inhibits mRNA translation globally, a small sub-set of mRNAs is translationally de-repressed upon ISR activity through special uORF mechanisms (see chapter 1.2.3). Therefore, we used translational activation of the uORF-controlled gene *atf-4* as canonical ISR activity readout. We induced ER stress using dithiothreitol (DTT), which disturbs protein structures by reducing disulfide bonds, and tunicamycin (TM), which inhibits N-linked glycosylation-mediated protein maturation. For quantification of *atf-4* translation, we used an *atf-4*::GFP reporter strain crossed to the *ppp-1* mutants. In accordance with our previous results regarding eIF2α-phosphorylation (Fig. 14), under non-stressed conditions, no changes in *atf-4*::GFP signals could be detected between wildtype and *ppp-1* animals by microscopy (Fig. 18a) and Western blotting using anti-GFP antibody (Fig. 18b). Strikingly, while in wildtype *atf-4*::GFP reporter lines DTT treatment led to a substantial increase in GFP signal, this response was significantly blunted in the *ppp-1* animals (Fig. 18a and b). These results could be independently confirmed using TM at varying doses. Interestingly, *atf-4*::GFP levels reached a plateau at high TM concentrations, suggesting that the ISR reached an activity maximum. Independent of TM doses, the *ppp-1* mutants down-regulated *atf-4*::GFP signals significantly (Fig. 18c and d). We conclude from these data that specific mutations in *ppp-1* inhibit the ISR during stress.

To test if ISR activity is similarly blunted in long-lived strains carrying the eIF2 kinase

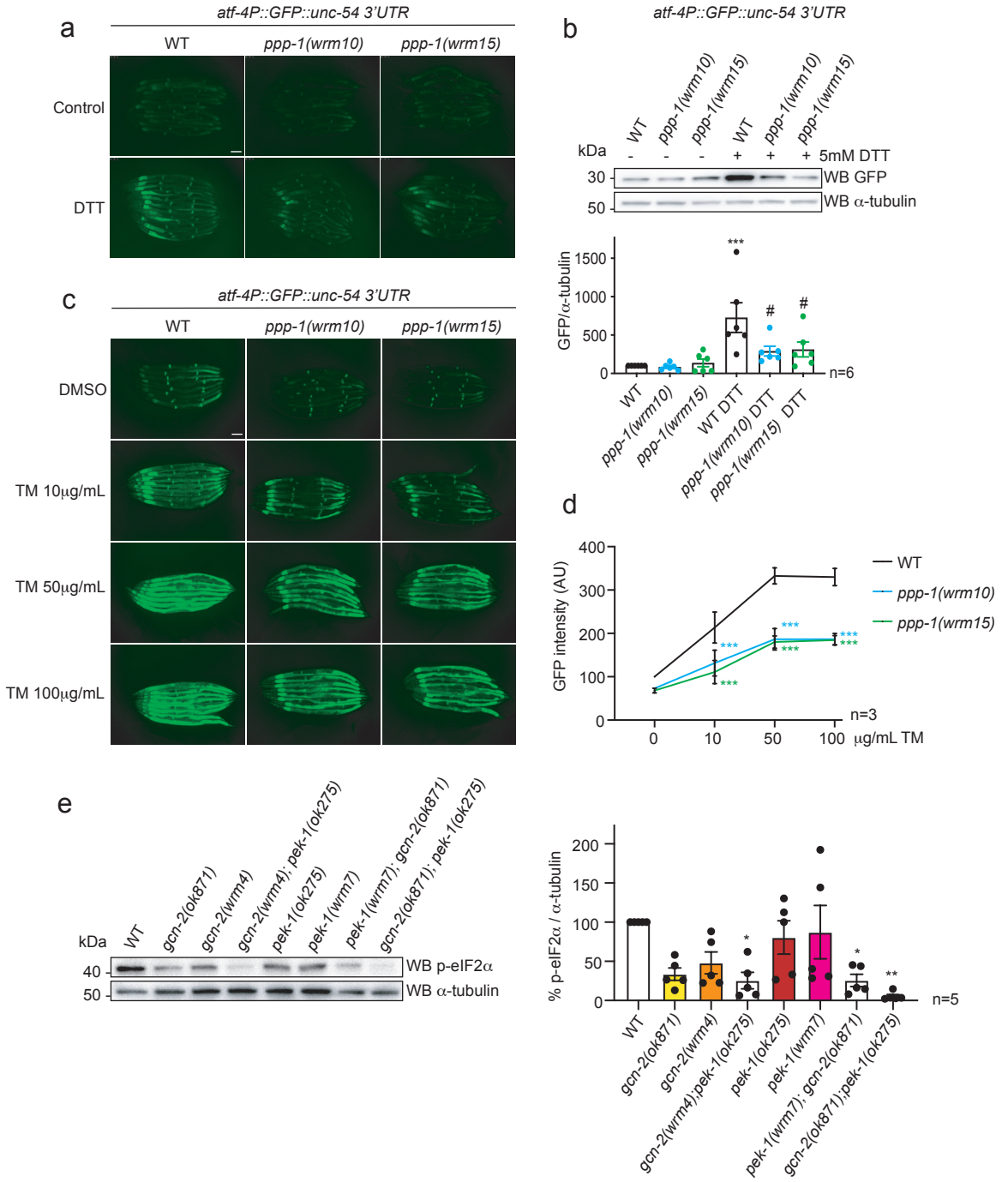

Figure 18: Mutations in *ppp-1* and in eIF2 kinases reduce ISR activity. a Representative fluorescence images of day 1 WT animals and *ppp-1* mutants in the *atf-4P*::GFP::*unc-54* 3'UTR background, incubated without (control) or with 5 mM DTT for 2 h. Scale bar is 75 μm, n=3 independent experiments. **b** Representative Western blot of day 1 WT animals and *ppp-1* mutants in the *atf-4P*::GFP::*unc-54* 3'UTR reporter background treated with 5 mM DTT for 2 h, using anti-GFP and anti-α-tubulin antibodies. GFP levels were normalized to α-tubulin (error bars represent means $\pm$SEM, one-way ANOVA Tukey's post hoc test, ***p<0.001 versus WT(-DTT) and #p<0.05 versus WT(+DTT); n=6 independent experiments). **c** Fluorescence images of day 1 WT animals and *ppp-1* mutants in the *atf-4P*::GFP::*unc-54* 3'UTR reporter background. Worms were treated with DMSO only (control) or with the indicated tunicamycin (TM) concentrations (10, 50, or 100 μg/mL) for 6 h each (scale bar 75 μm; representative data from n=3 independent experiments with $\geq$7 animals each). **d** Quantification of GFP intensity in (**c**). Error bars represent means $\pm$SD, two-way ANOVA Dunnett's post hoc test with ***p<0.001 versus WT (n=3 independent experiments with $\geq$7 animals each). **e** Representative Western blot and quantification of day 1 worms of indicated genotypes detecting phospho-eIF2α (Ser51) and α-tubulin. Levels of phospho-eIF2α were normalized to α-tubulin (error bars represent means $\pm$SEM, one-way ANOVA Dunnett's post hoc test, *p<0.05 and **p<0.01 versus WT control; n=5 independent experiments).

alleles *gcn-2(wrm4)* and *pek-1(wrm7)*, we analysed eIF2α-phosphorylation levels as direct output of the kinase activity. Since *C. elegans* has only the two eIF2 kinases GCN-2 and PEK-1, we aimed to isolate the *gcn-2(wrm4)* and *pek-1(wrm7)* alleles from the respective other kinase. We therefore used the full knock-out mutants *gcn-2(ok871)* and *pek-1(ok275)* and generated the following double-mutants: The *gcn-2(wrm4)*; *pek-1(ok275)* strain has only the remaining GCN-2 activity and displays a strong reduction in baseline eIF2α-phosphorylation compared to wildtype worms and the *pek-1(ok275)* strain (Fig. 18e). *Vice versa*, this is true for the *pek-1(wrm7)*; *gcn-1(ok275)* double mutant. This strain has only the remaining kinase activity of PEK-1 and shows a down-regulation of eIF2α-phosphorylation compared to the wildtype and *gcn-2(ok871)* strains (Fig. 18e). Together, these results show that the *gcn-2(wrm4)* and *pek-1(wrm7)* alleles reduce the respective kinase function and therefore inhibit the ISR. Collectively, these data demonstrate that by analysing the forward longevity screen we identified different longevity genes that lead to a reduction in ISR activity.

2.2.5 Inhibiting the ISR does not alter UPR^{ER} or IIS pathways

The ISR is part of the conserved UPR^{ER}, the general reaction of cells to ER stress, which regulates a transcriptional reprogramming of the cell by IRE-1/IRE1 cleavage, ATF-6/ATF6 translocation and via the ISR by PEK-1/PERK activation (Hetz et al., 2020). We therefore hypothesised that the *ppp-1* allele-mediated ISR regulation results in a compensatory change in the signalling of other UPR^{ER} branches. We measured the states of the constitutive and inducible UPR^{ER} by analysing the expression of UPR^{ER} target genes without and with application of TM stress, respectively (Shen et al., 2005). We did not observe changes of UPR target gene expression in *ppp-1* animals compared to wildtype worms (Fig. 19a and b).

We next asked if *ppp-1* mutants show alterations in the insulin signalling pathway. We assessed heat-induced dauer formation without detecting changes compared to wildtype worms, while *daf-2(e1370)* control animals constitutively formed dauer larvae under the same conditions (Fig. 19c). Furthermore, we measured the expression levels of *daf-16*/FOXO target genes *dod-8* and *sod-3*. While in *daf-2(e1370)* mutants with reduced insulin receptor function *dod-8* and *sod-3* levels were elevated, in *daf-16(mu86)* deletion mutants the respective target gene levels were low. However, in *ppp-1* animals, no changes could be detected compared to wildtype controls (Fig. 19d), showing that the *ppp-1* mutations specifically affect the ISR without altering the UPR or insulin signalling pathways.

2.2.6 Pharmacological ISR inhibition promotes lifespan extension

To verify the results of genetic ISR inhibition causing longevity, we hypothesised that *C. elegans* lifespan could be extended by pharmacologically reducing ISR activity. We re-analysed a set of compounds that were described as UPR^{ER} modulators in worms before (Halliday et al., 2017). We used the *atf-4::GFP* reporter line upon tunicamycin stress and could validate estradiol valerate as ISR inhibiting compound, while propafenone hydrochloride elevated *atf-4::GFP* levels (Fig. 20a). ISRIB, a well described ISR inhibitor of the mammalian ISR, did neither affect *atf-4::GFP* levels (Fig. 20a), nor lifespan in *C. elegans* (Fig. 20b; Sidrauski et al. (2015); Sekine et al. (2015)). In accordance with our genetic ISR inhibition models,

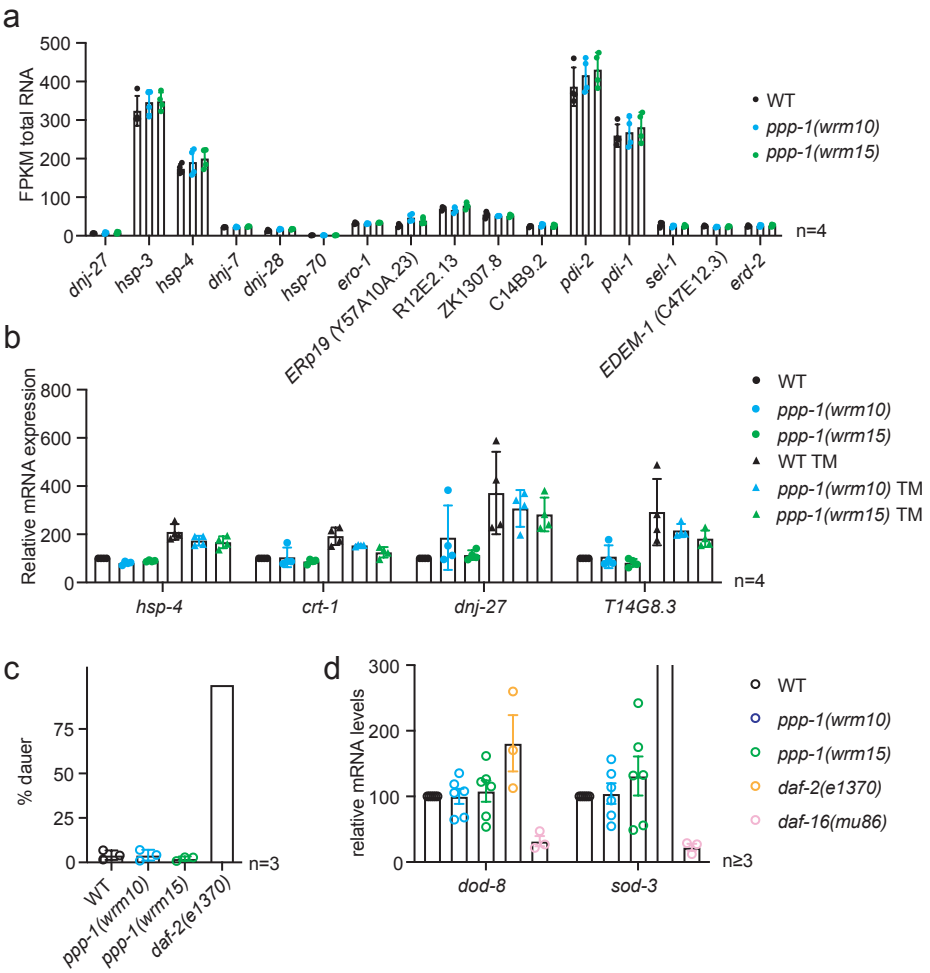

Figure 19: Inhibiting the ISR through *ppp-1* mutations does not activate UPR or IIS pathways. a mRNA levels of indicated UPR genes measured by RNA sequencing in un-stressed WT and *ppp-1* animals depicted as fragments per kilo base per million mapped reads (FPKM; n=4 independent experiments). **b** Relative mRNA levels of indicated UPR genes measured by qPCR in WT animals and *ppp-* mutants. Day 1 animals were treated with 1 % DMSO control or 10 μg/mL tunicamycin (TM) for 6 h (n=4 independent experiments). **c** Percentage of worms entering the dauer stage upon development at 27 °C. Analyzed were WT, *ppp-1* and dauer constitutive *daf-2(e1370)* control animals (n=3 independent experiments with $\geq$30 animals each). **d** Relative mRNA levels of indicated *daf-16*/FOXO target genes measured by qPCR in WT animals, *ppp-1* mutants, and *daf-2(e1370)* and *daf-16(mu86)* controls (n$\geq$3 independent experiments).

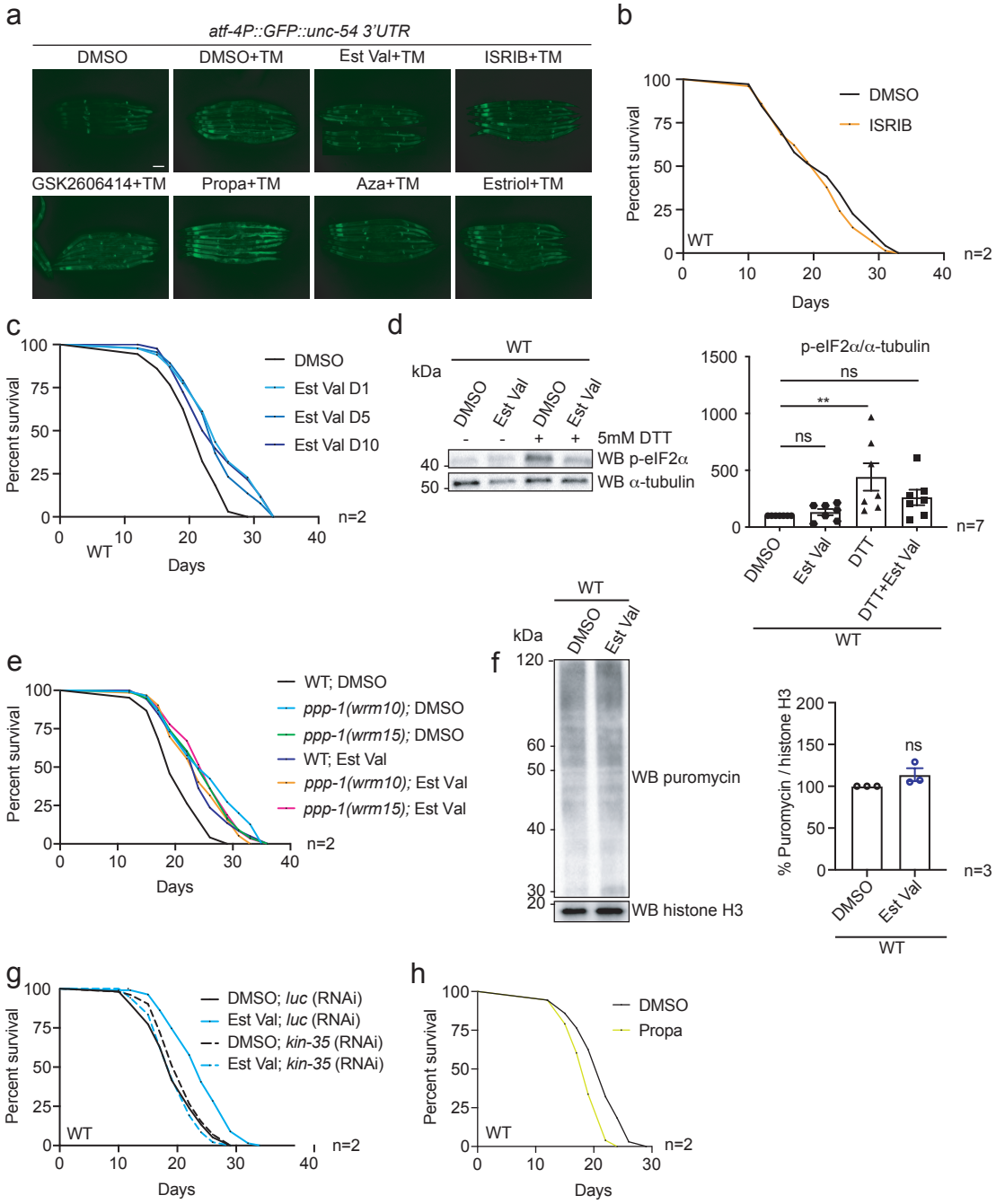

Figure 20: Estradiol Valerate inhibits the ISR and extends lifespan. **a** Fluorescence images of *atf-4P*::GFP::*unc-54* 3'UTR reporter animals grown on NGM plates supplemented with 10 μg/mL tunicamycin (TM) and with the indicated compounds (20 μM) or 1 % DMSO vehicle control (Est Val=estradiol valerate, Propa=propafenone hydrochloride, Aza=azadirachtin). Scale bar is 75 μm, n=1. **b** Survival of WT worms grown on NGM plates supplemented with 1 % DMSO or 20 μM ISRIB (n=2 independent experiments). **c** Survival of WT worms treated with 1 % DMSO (control) or 20 μM estradiol valerate from day 1 (D1), day 5 (D5), or day 10 (D10) (representative data from n=2 independent experiments). **d** Representative Western blot of day 1 worms treated with 1 % DMSO (control) or 20 μM estradiol valerate. Worms were incubated without (-) or with 5 mM DTT (+) for 2 h. Levels of phospho-eIF2α (Ser51) were normalized to α tubulin (error bars represent means ±SEM, one-way ANOVA Dunnett's post hoc test, **p<0.01 DTT versus DMSO; ns=not significant versus DMSO; n=7 independent experiments). **e** Survival of *ppp-1* mutants and WT controls treated with 1 % DMSO (control) or 20 μM estradiol valerate from day 1 of adulthood (representative data from n=2 independent experiments). **f** Puromycin incorporation followed by Western blot analysis using antibodies detecting puromycin and histone H3 in day 1 WT animals treated with DMSO (control) or 20 μM estradiol valerate (error bars represent means ±SEM, unpaired two-tailed t-test; n=3 independent experiments; no significant changes were detected). **g** Survival of WT worms treated with 1 % DMSO (control) or 20 μM estradiol valerate from day 1 of adulthood upon RNAi treatment targeting *kin-35* or control *luciferase* (representative data from n=2 independent experiments). **h** Survival of WT worms grown on NGM plates supplemented with 1 % DMSO or 20 μM propafenone hydrochloride (n=2 independent experiments).

estradiol valerate significantly extended lifespan in wildtype worms (Fig. 20c). Surprisingly, longevity was not only caused when the treatment was initiated at day one of adulthood, but also when started at day five or ten (Fig. 20c). These results suggest that pharmacological inhibition of the ISR is sufficient for lifespan extension and an effective treatment can be initiated late in life. To validate that estradiol valerate acts through the ISR, we measured eIF2α phosphorylation levels. Upon DTT stress, untreated worms showed a strong induction of phosphorylated eIF2α levels, whereas estradiol valerate treatment blunted this induction (Fig. 20d). Also, estradiol valerate treatment and *ppp-1* mutations did not show additive effects regarding worm lifespan, further supporting a role of estradiol valerate in ISR regulation (Fig. 20e). At the same time, other estradiol derivatives do not affect the ISR, suggesting specificity of the estradiol valerate mode of action (Halliday et al., 2017). In accordance with the *ppp-1* phenotypes, estradiol valerate treatment did not affect overall protein synthesis levels (Fig. 20f). Upon RNAi mediated knockdown of *kin-35*, estradiol valerate did not cause an extension of lifespan, while worms grown on luciferase control RNAi conditions still were long-lived (Fig. 20g). These results are in further congruence with the *ppp-1* phenotypes and confirm the role of *kin-35* in longevity through reduced ISR activity. In contrast to the lifespan-extending prospects of ISR inhibition, when growing wildtype animals on the ISR activating compound propafenone hydrochloride, their lifespan is shortened compared to a control treatment (Fig. 20h). All together, these results show that pharmacological ISR inhibition led to longevity in the worm, while ISR activation was detrimental.

2.2.7 Full genetic ISR inhibition promotes lifespan extension

To mechanistically validate our hypothesis that ISR inhibition causes longevity, we engineered an *eIF2*αS51A mutant worm strain [Y37E3.10a(*syb1385*)] with full ablation of eIF2α phosphorylation (Fig. 21a). Homozygous animals were viable with unchanged pharyngeal pumping rates, generation time and brood sizes compared to wildtype worms (Fig. 21b, c and d). Since phosphorylation of eIF2α is required for PEK-1 signalling during the ER stress response, we hypothesised that *eIF2*αS51A mutants would be hypersensitive to ER stress. Therefore, we tested the development of *eIF2*αS51A worms on TM. With increasing TM doses, the mutants were hypersensitive to the treatment compared to wildtype worms (Fig. 21e), highlighting the role of a functional ISR upon stress conditions during development specifically. Strikingly, if grown in absence of stress, the lifespan of *eIF2*αS51A worms was extended compared to wildtype animals (Fig. 21f), demonstrating that full genetic ISR inhibition causes longevity in *C. elegans*. We hypothesised, that the longevity might come in a trade-off with hypersensitivity to chronic stress during adulthood. To test this, we assessed survival on TM starting the treatment post-developmentally at day 1 of adulthood. Expectedly, wildtype animals showed a reduced lifespan upon TM compared to DMSO control treatment. Also the *eIF2*αS51A worms depicted a reduced lifespan on TM compared to DMSO control conditions. To our surprise, on TM the *eIF2*αS51A lifespan was not shorter than the wildtype one (Fig. 21g). Hence, we conclude that genetic ISR ablation does not lead to hypersensitivity to ER stress in adult *eIF2*αS51A animals. To further assess similarities between *eIF2*αS51A and *ppp-1* animals, we analysed heat shock survival on day 1 of

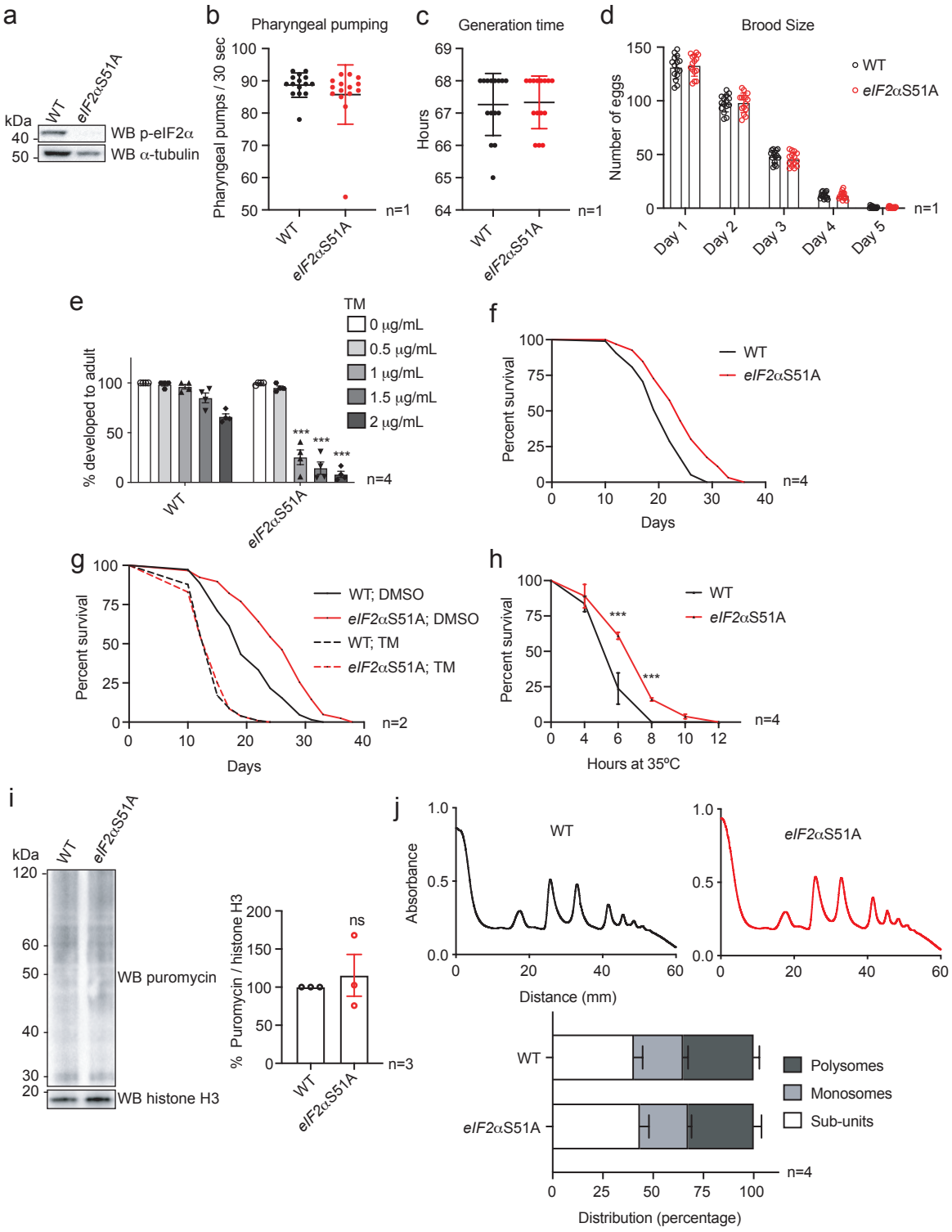

Figure 21: (Caption next page.)

Figure 21: Direct ISR inhibition through phospho-defective *eIF2*αS51A mutations mimicks *ppp-1* mutations and extends lifespan (Previous page). **a** Western blot of day 1 WT animals and *eIF2*αS51A mutants using anti-phospho eIF2α (Ser51) and anti-α-tubulin antibodies. **b** Pharyngeal pumping rates of day 1 WT animals and *eIF2*αS51A mutants (error bars represent means ±SD; n=1 with ≥15 animals per genotype). **c** Generation time of WT animals and *eIF2*αS51A mutants (error bars represent means ±SD; n=1 with ≥15 animals per genotype). **d** Brood size of WT and *eIF2*αS51A animals (error bars represent means ±SD; n=1 with ≥15 animals per genotype). **e** Developmental tunicamycin (TM) resistance assay of WT animals and *eIF2*αS51A mutants treated with tunicamycin at the indicated concentrations (error bars represent means ±SEM, two-way ANOVA Sidak's post hoc test, ***p<0.001 versus WT at respective tunicamycin concentration; n=4 independent experiments with ≥20 animals each). **f** Survival of *eIF2*αS51A mutants compared to WT control animals (Representative data from n=4 independent experiments). **g** Survival of WT animals and *eIF2*αS51A mutants treated with 1 % DMSO (vehicle control) or 20 μg/mL tunicamycin (TM) from day 1 of adulthood (n=2 independent experiments). **h** Thermotolerance assays of *eIF2*αS51A mutants compared to WT animals (error bars represent means ±SD, two-way ANOVA Sidak's post hoc test with ***p<0.001 versus WT controls; n=4 independent experiments with 50 animals each). **i** Puromycin incorporation followed by Western blot analysis using antibodies detecting puromycin and histone H3 in day 1 WT animals and *eIF2*αS51A mutants (error bars represent means ±SEM, unpaired two-tailed t-test; n=3 independent experiments; no significant changes were detected). **j** Polysome profiling and quantification of day 1 WT worms and *eIF2*αS51A mutants (error bars represent means +SD, two-way ANOVA Dunnett's post hoc test; n=4 independent experiments, no significant changes were detected).

adulthood. Mimicking the *ppp-1* mutants, *eIF2*αS51A worms were resistant to heat stress (Fig. 21h). Despite the crucial role of eIF2α in translation initiation, the animals showed no changes in overall protein synthesis and translation rates compared to wildtype worms as measured by puromycin incorporation (Fig. 21i) and polysome profiling (Fig. 21j). Interestingly, RNAi-mediated *kin-35* knockdown showed that the lifespan extension of *eIF2*αS51A worms was partially dependent on *kin-35* (Fig. 22a), phenocopying *ppp-1* animals. To mechanistically pinpoint the mode of action of longevity in *eIF2*αS51A worms, we investigated the genetic interaction between *ppp-1*/eIF2Bγ and eIF2α. Upon RNAi-mediated *ppp-1* silencing, the longevity of the *eIF2*αS51A mutants was fully abolished (Fig. 22b). We conclude that *eIF2*αS51A mediated longevity is dependent on *ppp-1*/eIF2Bγ function and that eIF2B is a general mediator of longevity in the context of ISR inhibition through genetic and pharmacological interventions.

Since pharmacological ISR activation shortened wildtype lifespan (Fig. 20h), we lastly aimed to test the effect of genetic ISR activation on *C. elegans* health and lifespan. Using the CRISPR/Cas9 technology, we generated an *eIF2*αS51D mutant [Y37E3.10a(*syb1567*)], in which a constitutive eIF2α phosphorylation is mimicked. Surprisingly, homozygous animals were not viable, so the worms were maintained in a heterozygous state using the genetic ht2 balancer. The heterozygous *eIF2*αS51D/+ worms showed slow generation time and low brood size phenotypes compared to wildtype animals (Fig. 22c and d). In consistence with the shortened worm lifespan on the ISR activating compound propafenone hydrochloride (Fig. 20h), genetic ISR activation in heterozygous *eIF2*αS51D/+ animals reduced their lifespan (Fig. 22e).

Summarising, by performing and extensively analysing a forward longevity screen in *C. elegans*, we could identify modulators of eIF2 function as novel longevity genes in the worm. The respective mutants from the screen showed an extended lifespan and increased resistance to protein toxicity, without having reduced overall protein synthesis. Instead, the mutants had reduced ISR activity. Strikingly, both pharmacological and direct genetic ISR inhibition could be linked to the described phenotypes depending on eIF2B function, while ISR activation was detrimental in the worm. Furthermore, selective translation of *kin-35* was required for the lifespan extension mediated by ISR inhibition. Overall, we found that fine tuning of

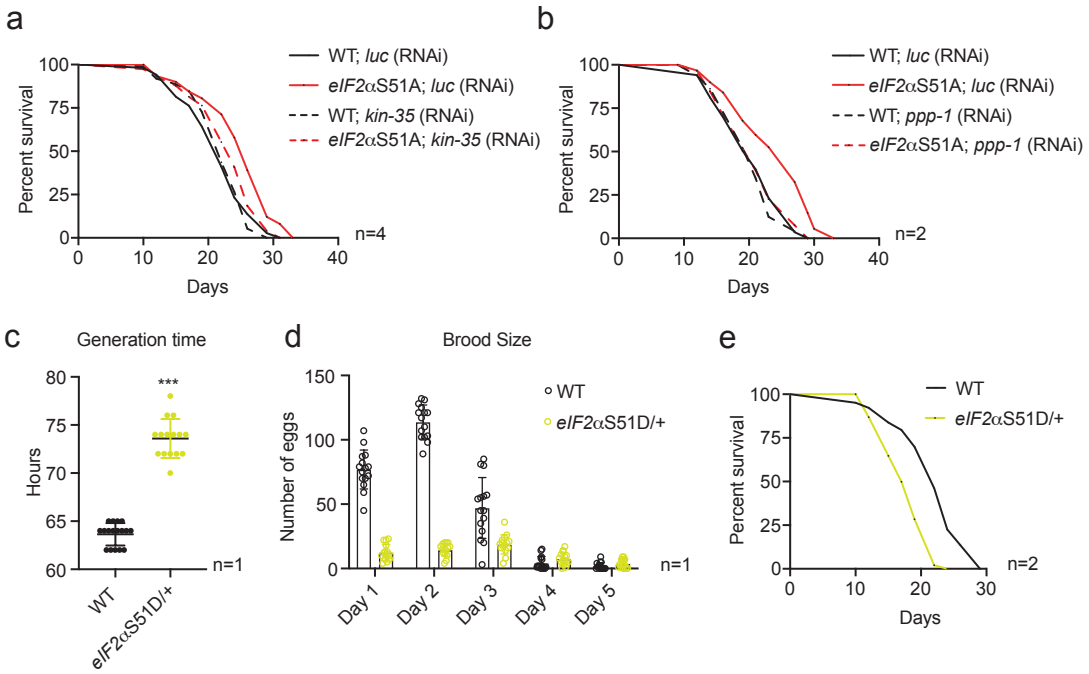

Figure 22: *eIF2*αS51A mutant longevity depends on *kin-35* and *ppp-1*; constitutive ISR activation via phospho-mimic *eIF2*αS51D/+ mutations shortens *C. elegans* lifespan. **a** Survival of WT worms and *eIF2*αS51A mutants upon RNAi treatment targeting *kin-35* or control *luciferase* (representative data from n=4 independent experiments). **b** Survival of WT animals and *eIF2*αS51A mutants upon RNAi treatment targeting *ppp-1* or control *luciferase* (representative data from n=2 independent experiments). **c** Generation time of WT animals and heterozygous phospho-mimic *eIF2*αS51D/+ mutants (error bars represent means ±SD, unpaired two-tailed t-test ***p<0.001 versus WT; n=1 with ≥15 animals per genotype). **d** Brood size of WT and heterozygous phospho-mimic *eIF2*αS51D/+ animals (error bars represent means ±SD; n=1 with ≥15 animals per genotype). **e** Survival of heterozygous phospho-mimic *eIF2*αS51D/+ mutants compared to WT control animals (representative data from n=2 independent experiments).

eIF2 function causes longevity in *C. elegans*.

2.3 Development of a novel RiboTag tool to investigate tissue-specific translation

We could not detect changes in overall protein production but found significant differences in the selective translation of specific mRNAs in the *ppp-1*/eIF2Bγ mutants. However, these analyses were performed on a whole body level and hence draw a very global picture of translation in the animals (Fig. 13). We speculate that the effects of genetic and pharmacological eIF2 modulation on translation as seen in the *ppp-1* mutants might occur selectively or with higher prevalence in defined tissues as compared to others.

To analyse the translatome from *in vitro* and *in vivo* model systems, powerful methods have been developed before and were adapted for this study, including SUnSET, ^{35}S-methionine incorporation, and polysome profiling and sequencing (Schmidt et al., 2009; Hansen et al., 2007; Großhans and Ding, 2009). However, analysing the translatome tissue-specifically was not achieved using these techniques. In small model organisms such as *C. elegans*, studying mRNA translation from different tissue-types is complicated by the presence of neighbouring tissues and cells during the tissue isolation processes. We hence aimed to develop a worm model for tissue-specific affinity purification of ribosomes. Ribosomal proteins therefore are tagged end expressed endogenously or in defined tissues. During a co-immuno-precipitation (co-IP), fully assembled ribosomes including associated mRNAs can be purified from the tagged ribosomal protein. Subsequent sequencing of the co-purified mRNA can provide information of the cell type-specific translatome (King and Gerber, 2016). Initial ribosome tagging (RiboTag) techniques were established in mice using tagged Ribosomal Protein of the Large subunit (RPL) 20a (Heiman et al., 2008) or RPL22 (Sanz et al., 2009), generated with the well-characterized Cre/LoxP system. The approach was adapted to *Drosophila melanogaster* (Thomas et al., 2012; Desplan et al., 2017) and *C. elegans* (Gracida et al., 2017; Gracida and Calarco, 2017; Rhoades et al., 2019; McLachlan and Flavell, 2019). All current *C. elegans* RiboTag models were designed using extrachromosomal arrays to tissue-specifically express tagged ribosomal subunits (Gracida and Calarco, 2017; Rhoades et al., 2019; McLachlan and Flavell, 2019). While being a standard worm technique for generating transgenic lines, the use of extrachromosomal arrays can lead to a variability in copy number and mosaicism in gene expression. Furthermore, the stable integration of the transgene

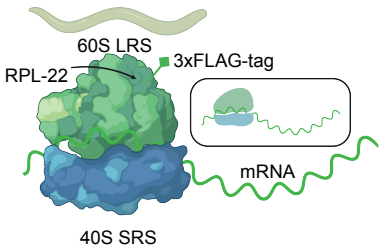

Figure 23: FLAG-tagging a ribosome. Model of an assembled ribosome with associated mRNA embedded between the 40S small ribosomal subunit and the 60S large ribosomal subunit, schematically depicting FLAG-tagged RPL-22 at the ribosomal surface.

into the genome is not a targeted process and the genetic locus of integration cannot be controlled. For these reasons, we decided to generate the first *C. elegans* RiboTag toolkit using the CRISPR/Cas9 technology with controlled expression of a tagged ribosomal protein sufficient for co-IPs from defined tissues. We therefore expressed an N-terminal FLAG tagged version of the conserved 60S ribosomal subunit protein RPL-22 in *C. elegans* by making use of the CRISPR/Cas9 based Single-copy Knock-In LOci for Defined Gene Expression (SKI LODGE) system (Fig. 23; Silva-Garcia et al. (2019)). The final aim was the generation and full characterisation of tissue-specific RiboTag lines for all major worm tissues to enable their use for the whole *C. elegans* community. Here I show the proof-of-principle results for a control worm line carrying a FLAG tag at the genomic RPL-22 locus and the first tissue-specific RiboTag worm expressing tagged RPL-22 in neurons exclusively.

2.3.1 Characterisation of endogenous FLAG::RPL-22 RiboTag worms

RPL22 was used for co-IPs in the initial RiboTag mice and its *C. elegans* ortholog RPL-22 was tagged before in the extrachromosomal RiboTag worms (Sanz et al., 2009; Rhoades et al., 2019). We hence decided to place a 3xFLAG epitope tag at the N-terminus of *C. elegans* RPL-22 as general concept for the CRISPR/Cas9 generated RiboTag worms (Fig. 23). With our RiboTag lines, we aimed to investigate small changes in tissue-specific translation between different genetic worm lines or during pharmacological treatments. We hence pursued a stringent systematic characterisation of FLAG-tagged RPL-22 worms. First, we intended to analyse the effect of the tag on ribosome assembly and mRNA translation under wildtype conditions, as well as its incorporation into actively translating ribosomes. Therefore, we generated an endogenous 3xFLAG::RPL22 (^{FLAG}RPL-22) knock-in strain *rpl-22(wbm58)* at the genomic RPL-22 locus using the standard CRISPR/Cas9 technology.

We first analysed the fitness of *rpl-22(wbm58)* animals and did not detect any changes in their health- and lifespan, generation time, and brood size compared to wildtype worms (Fig. 24a, b and c). To analyse the canonical mRNA translation process in worms endogenously expressing ^{FLAG}RPL-22, we performed polysome profiling after separation on a sucrose gradient (Fig. 24d). Comparing *rpl-22(wbm58)* and wildtype animals, no differences in ribosomal distribution could be detected (Fig. 24e). To demonstrate the incorporation of ^{FLAG}RPL-22 into actively translating ribosomes, we extracted the proteins from respective sucrose gradient fractions of the polysome profiling experiments and performed Western blot analyses using antibodies binding to the FLAG epitope. The corresponding FLAG signal could be detected in the fractions of the 60S large ribosomal subunit and in polysomal fractions (Fig. 24e). First, these results show that animals expressing ^{FLAG}RPL-22 are healthy and display a functional translation machinery. Second, our data prove that ^{FLAG}RPL-22 is incorporated in translating ribosomes in the 80S monosome and polysome states.

We next investigated if the tag on RPL-22 influences mRNA association to ribosomes. We therefore compared the mRNAs actively translated in wildtype and *rpl-22(wbm58)* worms. We performed RNA sequencing of ribosome-associated mRNAs extracted from polysome profiling fractions. For the planned co-IP experiments from RiboTag worms, we expected to co-immuno-purify assembled monosomes and polysomes using ^{FLAG}RPL-22, but also unas-

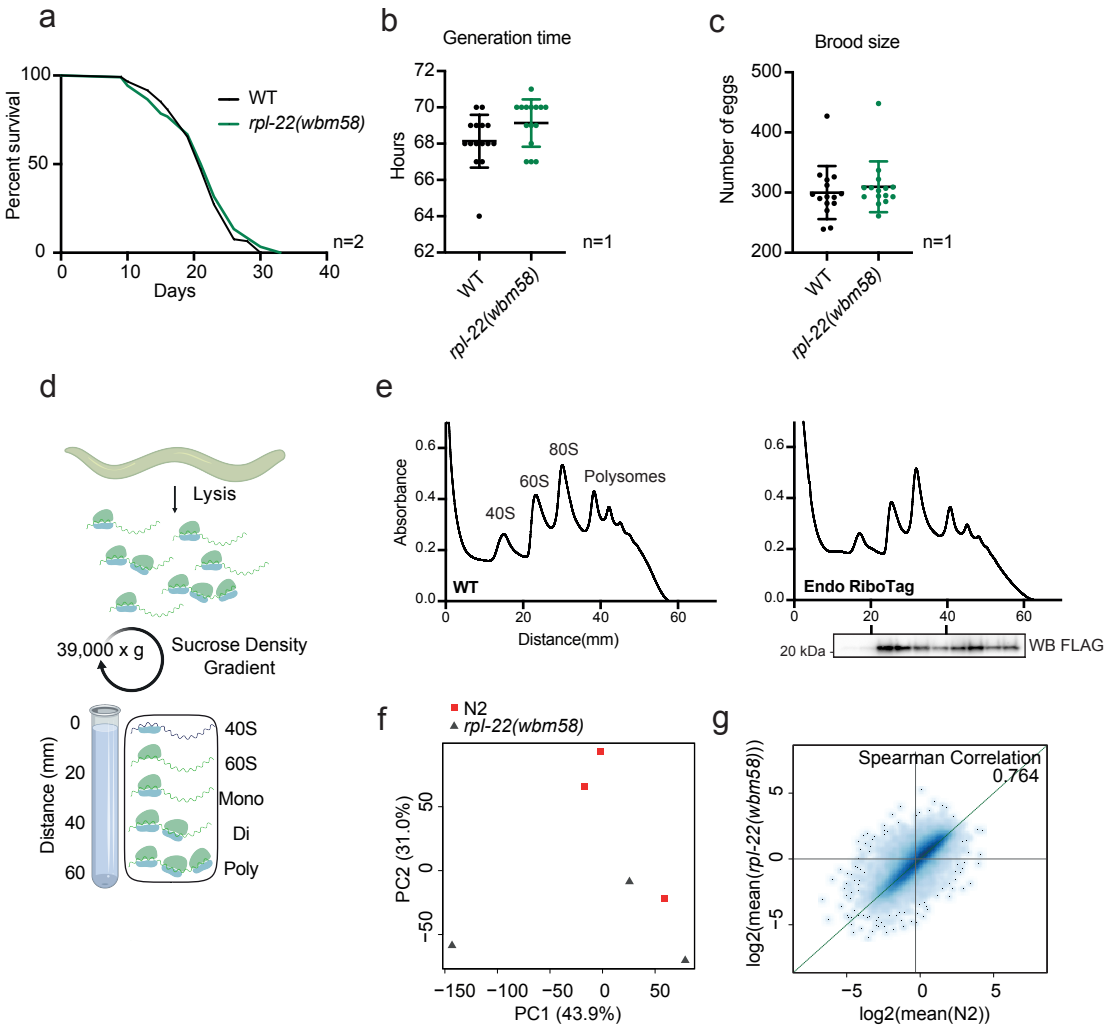

Figure 24: Adding an N-terminal FLAG tag to RPL-22 does not impact worm health or overall mRNA translation. **a** Survival of endogenously FLAG-tagged *rpl-22(wbm58)* animals compared to WT controls. **b** Generation time of WT animals and *rpl-22(wbm58)* mutants (error bars represent means ±SD; n=1 with ≥15 animals per genotype). **c** Brood size of WT and *rpl-22(wbm58)* animals as total number of viable progeny per individual parental worm (error bars represent means ±SD; n=1 with ≥15 animals per genotype). **d** Schematic depiction of the polysome profiling process. **e** Polysome profiling of day 1 WT and *rpl-22(wbm58)* animals. Western blot of extracted proteins from respective polysome profiling fractions from *rpl-22(wbm58)* worms as indicated in the figure. Anti-FLAG antibodies were used. **f and g** RNA sequencing was performed of RNA captured from pooled 60S, 80S, monosomal and polysomal profiling fractions and normalised to total RNA from WT and *rpl-22(wbm58)* worms. **f** PCA using log2(ratios) of RNA expression values comparing WT and *rpl-22(wbm58)* samples. **g** Scatter plot showing mean log2(ratios) only of RNAs detected in both WT and *rpl-22(wbm58)* samples. See Tab. 8 in appendix for survival statistics.

sembled 60S large ribosomal subunits might be pulled down. For the RNA sequencing after polysome profiling, we therefore selected all corresponding polysome profiling fractions from the 60S subunit to polysomal peaks and pooled them before performing RNA extraction and sequencing. To assess translational efficiency of specific mRNAs, we compared the expression values of ribosome-associated mRNAs normalised to respective total mRNA levels of the wildtype and *rpl-22(wbm58)* animals. We performed a principle component (PC) analysis to test for sample similarity. The samples of the two worm lines could not be separated by either of the PCs, indicating a highly similar translatome between the two strains (Fig. 24f). The majority of actively translated mRNAs could be identified in both sample sets and the commonly detected mRNAs in wildtype and *rpl-22(wbm58)* worms showed similar expression values (Fig. 24g; Spearman correlation coefficient of 0,764). We conclude that the translatome of *rpl-22(wbm58)* worms cannot be distinguished from the wildtype translatome regarding transcript identities and respective translation quantity.

2.3.2 Immuno-precipitation of functional ribosomes from endogenous RiboTag worms

The heart of the RiboTag protocol is the pulldown of fully assembled ribosomes including associated mRNAs using ^{FLAG}RPL-22 (Fig. 25a). We aimed to use the endogenously tagged ^{FLAG}RPL-22 from the *rpl-22(wbm58)* worms to perform initial proof-of-principle RiboTag co-IP experiments. Therefore, *rpl-22(wbm58)* samples were homogenised and protein G-coated magnetic beads covered with FLAG-antibodies were used to immuno-absorb ribosomes. After the co-IP, protein or RNA were extracted from the samples (see methods chapter 5.2.8). To validate the successful co-IP of ribosomes, we performed Western blot analyses on the purified co-IP eluate. ^{FLAG}RPL-22 could be detected by anti-FLAG antibodies in the elution fractions of *rpl-22(wbm58)* samples, while being absent in wildtype controls (Fig. 25b). To assess whether the co-IP strategy was sufficient to immuno-precipitate assembled ribosomes, we performed Western blotting using antibodies detecting ribosomal protein S6 (RPS-6), a protein of the untagged small ribosomal subunit. RPS-6 was detected along the ^{FLAG}RPL-22 pattern in the elution fraction of *rpl-22(wbm58)* samples, while the signal was absent in wildtype elution fractions (Fig. 25b). This suggests the successful purification of intact ribosomes from ^{FLAG}RPL-22 worms.

The final aim of the co-IPs from RiboTag worms was the purification of actively translated mRNAs for RNA sequencing or qPCR analyses. We hence extracted the RNA from co-IP elution fractions of wildtype and *rpl-22(wbm58)* animals. First, we measured RNA quality by analysing ribosomal RNA (rRNA) fractions in the samples. Ribosomes contain different rRNA species of specific lengths in the small and large ribosomal subunits. Using the Agilent 2100 bioanalyzer TapeStation, we could detect the respective 18S and 28S rRNA species after ^{FLAG}RPL-22 co-IP in samples of *rpl-22(wbm58)* animals (Fig. 25c). The RNA integrity number equivalent (RINe) obtained from TapeStation experiments measures RNA quality according to the gradual shift towards shorter fragment sizes during degradation. RINe values range from 1 (very degraded) to 10 (fully intact). The high RINe of RNA obtained from the RiboTag co-IP of *rpl-22(wbm58)* worms further shows that this method is suitable to pull down RNA of high quality from assembled ribosomes (Fig. 25c). We

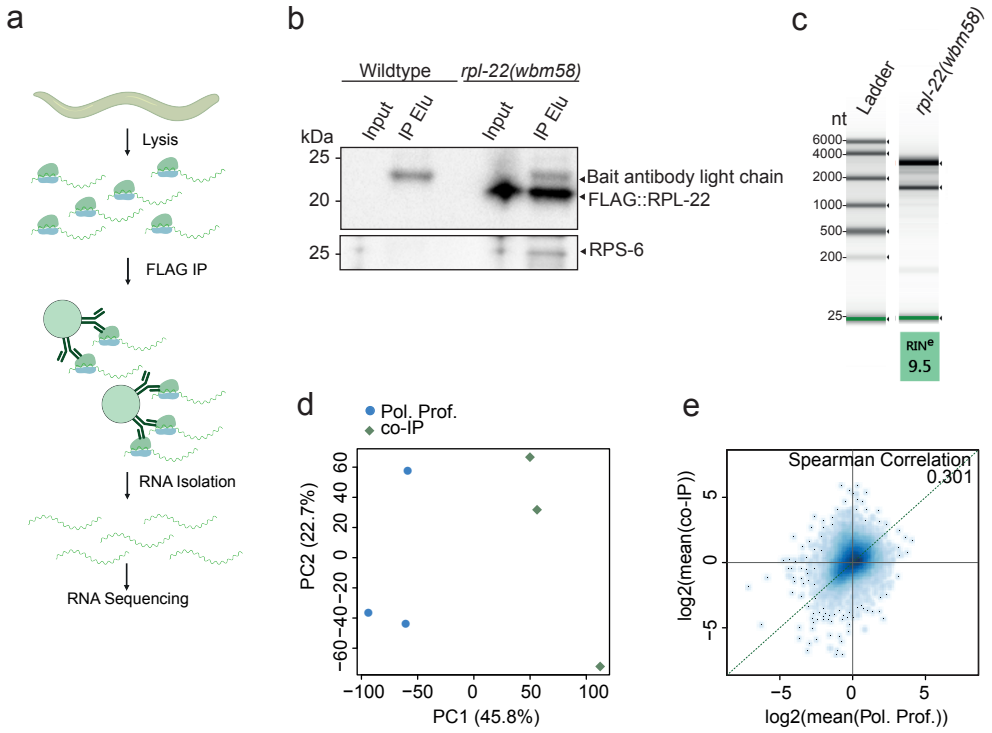

Figure 25: RiboTag co-IP from endogenously FLAG-tagged *rpl-22(wbm58)* animals and analysis of eluted protein and RNA. a Schematic depiction of the RiboTag co-IP experiment. **b** Western blot of day 1 WT animals and *rpl-22(wbm58)* mutants after RiboTag co-IP using anti-FLAG and anti-RPS-6 antibodies. Shown are co-IP input and elution (elu) fractions. **c** On-chip electrophoresis of eluted RNA from RiboTag co-IP of *rpl-22(wbm58)* animals including calculated RINe. **d and e** From *rpl-22(wbm58)* worms, RNA sequencing was performed (1) of RNA captured from pooled 60S, 80S, monosomal and polysomal profiling fractions and (2) of RNA eluted after RiboTag co-IP and normalised to respective input total RNA samples each. **d** PCA using log2(ratios) comparing RNA obtained from polysome profiling to RNA eluted from RiboTag co-IPs of *rpl-22(wbm58)* samples. **e** Scatter plot showing mean log2(ratios) only of RNAs detected in both polysome profiling and RiboTag IP samples of *rpl-22(wbm58)* animals.

wanted to compare the RiboTag co-IP method with existing strategies assessing the *C. elegans* translatome. Therefore, we analysed the mRNAs of *rpl-22(wbm58)* animals purified from the FLAG antibody-based co-IP method next to mRNAs of the same worm strain captured by polysome profiling after separation on a sucrose gradient. We found differences not only in the identity of transcripts but also in transcript quantities (Fig. 25d, e). These results might arise due to variations in sample handling, since both methods require separate buffers and use different homogenisation techniques. Taken together, both methods shed lights on partially distinct pools of translated mRNAs. Further analyses will need to be performed to investigate these variances. Collectively, our results show that ^{FLAG}RPL-22 can be used for the co-IP of assembled ribosomes along with associated RNA of high quality. We conclude that the RiboTag method can enable the comparison of differently translated mRNAs e.g. in independent worm strains, potentially also in tissue-specific RiboTag models.

2.3.3 Design and generation of tissue-specific RiboTag worm strains

To generate the novel tissue-specific RiboTag worm lines, we used the *C. elegans* SKI LODGE system based on the CRISPR/Cas9 technology (Silva-Garcia et al., 2019). Here, a single copy of the desired DNA edit can be inserted into defined engineered loci that are controlled by well-characterised tissue-specific promoters. To prevent the interference with endogenous gene expression, the SKI LODGE cassettes were inserted to intergenic regions. The cassettes include a trans-spliced wrmScarlet fluorophore which verifies the tissue specific SKI LODGE expression. The final genomic constructs of the tissue-specific RiboTag strains follow the initial ^{FLAG}RPL-22 design of the endogenously tagged *rpl-22(wbm58)* line. The respective tissue-specific SKI-LODGE constructs hence consist of a tissue-specific promoter followed by sequences for an N-terminal 3xFLAG tag, full-length *rpl-22* cDNA, a spliced leader (SL) RNA coupled with a wrmScarlet fluorophore and a *rab-3* or *unc-54* 3'UTR, depending on the cassette (Fig. 26a). We so far generated and fully characterised the NeuroRiboTag line (strain WBM1340), expressing ^{FLAG}RPL-22 exclusively in neuronal tissues (Fig. 26b). Further work is planned to insert *rpl-22* into other SKI LODGE lines, enabling specific expression of ^{FLAG}RPL-22 in somatic, muscle or intestinal tissues (Fig. 26b). Our goal is to generate a

a

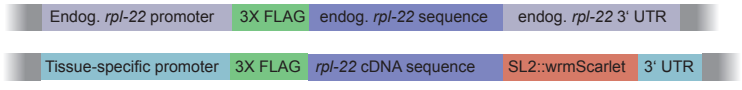

b

Strain	Allele	Description	Expression	Chr
Endogenous FLAG tag at *rpl-22* genomic locus:				
WBM1344	*wbm58*	3xFLAG::*rpl-22*	Endogenous	II
SKI LODGE knock-in alleles:				
WBM1340	*wbmIs99*	*rab-3p*::3xFLAG::*rpl-22*::SL2::wrmScarlet::*rab-3* 3'UTR	Neurons	IV
WBM1364	*wbmIs119*	*eft-3p*::3xFLAG::*rpl-22*::SL2::wrmScarlet::*unc-54* 3'UTR	Soma	V
WBM1339	*wbmIs118*	*myo-3p*::3xFLAG::*rpl-22*::SL2::wrmScarlet::*unc-54* 3'UTR	Muscle	I
WBM1458	*wbmIs131*	*nep-17p*::3XFLAG::*rpl-22*::SL2::wrmScarlet::*unc-54* 3'UTR	Intestine	V

Figure 26: Design of endogenously and tissue-specifically tagged ^{FLAG}RPL-22 RiboTag worms. a Schematic overview of the genetic RiboTag constructs. **b** Detailed overview of all RiboTag worm lines that are already generated and characterised (WBM1344, WBM1340) or planned for publication (WBM1364, WBM1339, WBM1458).

library of tissue-specific RiboTag worm strains with defined gene expression in a clean genetic background generated by the SKI LODGE system including full functional characterisations.

2.3.4 The NeuroRiboTag enables analysis of the neuronal translatome

To analyse the translatome of neuronal tissues from *C. elegans*, we used the SKI LODGE system to generate the worm strain WBM1340 with the genotype *wbmIs99*[*rab-3p*::3XFLAG::*rpl-22*::SL2::wrmScarlet::*rab-3* 3'UTR] IV, hereafter referred to as NeuroRiboTag worms. These animals express ^{FLAG}RPL-22 in a SKI LODGE cassette under the control of the *rab-3* promoter and 3'UTR. *rab-3* is the worm ortholog of human ras-related proteins in brain (RAB) 3A and 3C and is expressed particularly in the nervous system. In analogy to the full charac-

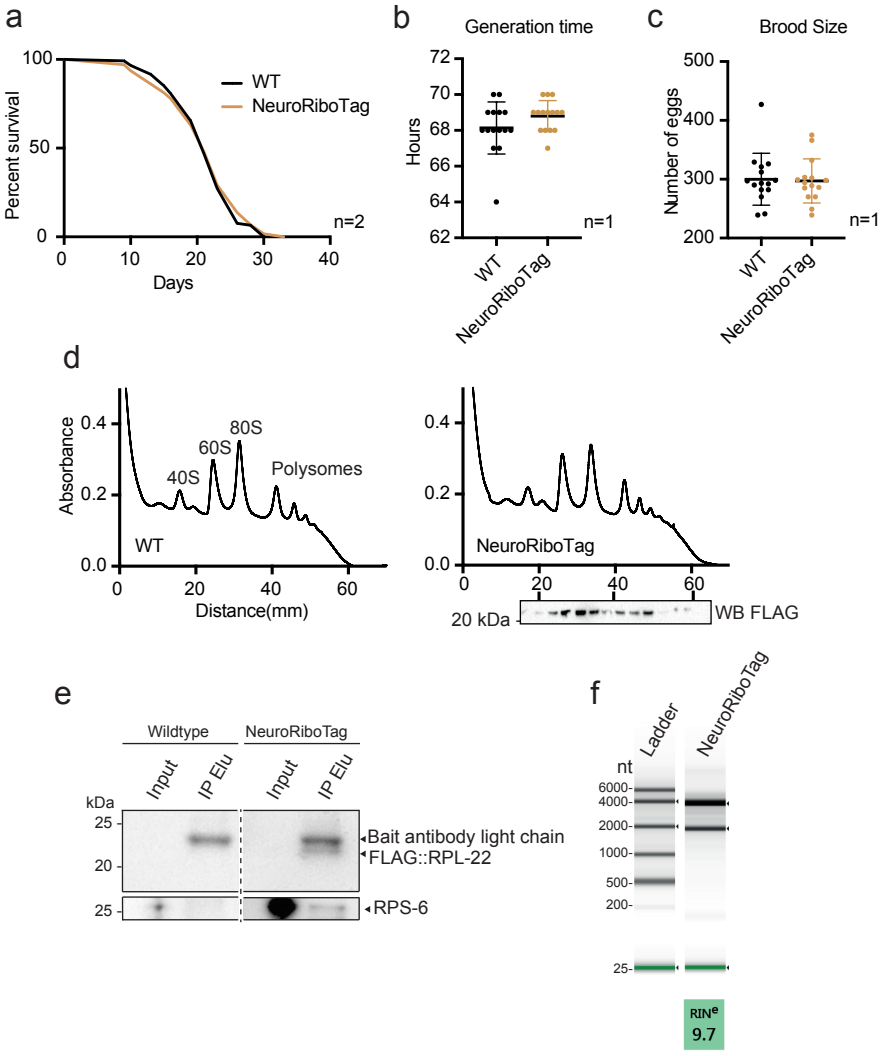

Figure 27: Neuron-specific expression of ^{FLAG}RPL-22 does not impact worm health or overall translation and is sufficient for RiboTag co-IPs. a Survival of NeuroRiboTag animals compared to WT controls. **b** Generation time of WT animals and NeuroRiboTag mutants (error bars represent means ±SD; n=1 with ≥15 animals per genotype). **c** Brood size of WT and NeuroRiboTag animals as total number of viable progeny per individual parental worm (error bars represent means ±SD; n=1 with ≥15 animals per genotype). **d** Polysome profiling of day 1 WT and NeuroRiboTag animals. Western blot of extracted proteins from respective polysome profiling fractions from NeuroRiboTag worms as indicated in the figure, using anti-FLAG antibodies. **e** Western blot of day 1 WT animals and NeuroRiboTag mutants after RiboTag co-IP using anti-FLAG and anti-RPS-6 antibodies. Shown are co-IP input and elution (elu) fractions. **f** On-chip electrophoresis of eluted RNA from RiboTag co-IP of NeuroRiboTag animals including calculated RINe. See Tab. 8 in appendix for survival statistics.

terisation of the endogenously ^{FLAG}RPL-22 expressing *rpl-22(wbm58)* worms, we performed a broad analysis of general health of the NeuroRiboTag worms. Comparing NeuroRiboTag with wildtype animals, no significant changes were observed regarding health- and lifespan, generation time, and brood size (Fig. 27a, b, c). Next, polysome profiles of NeuroRiboTag worms and wildtype controls did not show any differences in ribosomal distribution, indicating that there is no effect of the neuronal RiboTag on overall mRNA translation (Fig. 27d). We further extracted proteins from fractions of the polysome profiling experiment and performed Western blot analyses. Using anti-FLAG antibodies, ^{FLAG}RPL-22 could be detected in the 60S, monosomal and polysomal fractions (Fig. 27d). This verified the incorporation of FLAG-tagged RPL-22 expressed from the neuron-specific SKI LODGE locus into actively translating ribosomes. We then tested whether performing a co-IP from NeuroRiboTag worms was sufficient to immuno-precipitate assembled ribosomes in adequate amounts and quality for further experiments. We performed Western blot analyses of the elution fraction after co-IP and detected neuronal ^{FLAG}RPL-22 and untagged RPS-6 using the respective antibodies (Fig. 27e). We further purified RNA from co-IP elution fractions of NeuroRiboTag worms. In TapeStation analyses we obtained 28S and 18S rRNA bands with a high RINe value indicating sufficient RNA quality and integrity for further experiments (Fig. 27f).

To get a global picture of the mRNAs captured by the NeuroRiboTag co-IP, we performed RNA sequencing and set out different comparisons. We first compared RNA sequencing

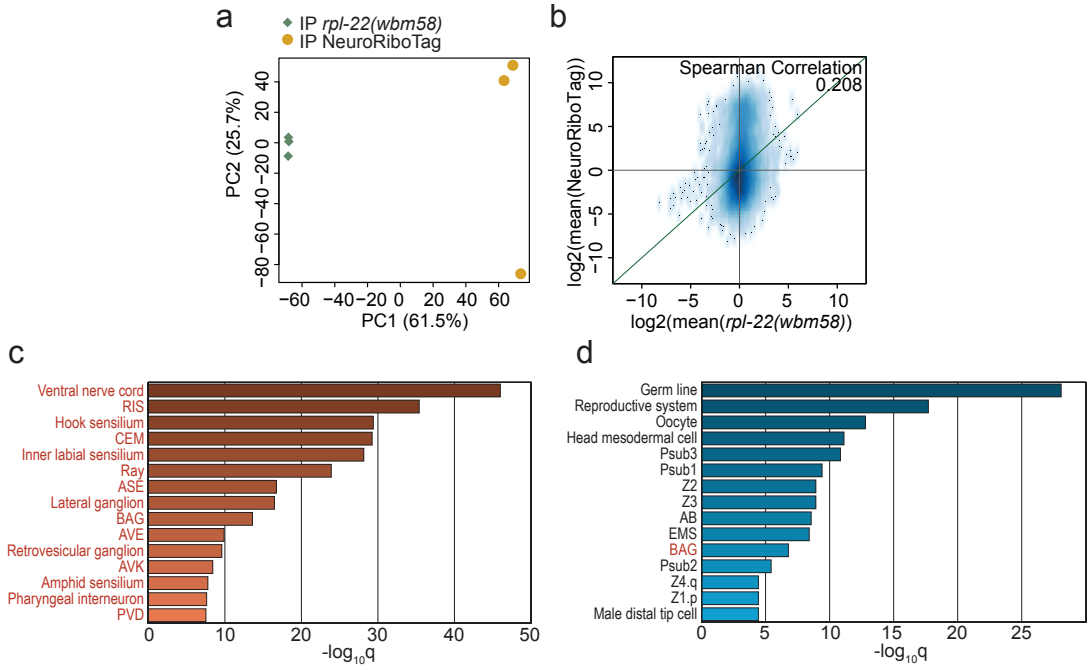

Figure 28: Co-IPs from NeuroRiboTag worms are sufficient to isolate and analyse mRNAs specifically translated in neuronal tissues. a and b RNA sequencing from endogenously tagged *rpl-22(wbm58)* and NeuroRiboTag worms was performed of RNA captured from RiboTag co-IP eluates and respective total RNA input fractions. **a** PCA using log2(ratios) of RNA expression values comparing *rpl-22(wbm58)* and NeuroRiboTag samples. **b** Scatter plot showing mean log2(ratios) only of RNAs detected in both *rpl-22(wbm58)* and NeuroRiboTag samples. **c and d** From NeuroRiboTag animals only, expression values from RNA of IP elution fractions were compared to total RNA levels from IP input fractions, generating fold-change values of all genes with detectable expression. **c** TEA of the 5 % most up-regulated genes in NeuroRiboTag co-IP elution fractions compared to total RNA levels (neuronal terms are written in red; shown are the 15 most significant terms). **d** TEA of the 5 % most down-regulated genes in NeuroRiboTag co-IP elution fractions compared to total RNA levels (neuronal terms are written in red; shown are the 15 most significant terms).

results from co-IPs of NeuroRiboTag animals with those of the endogenous RiboTag line *rpl-22(wbm58)*. For each strain, the RiboTag IP RNA samples were normalised to total input RNA. Subsequently, the results for the endogenous and neuronal RiboTag strains were compared. As expected, the results of both sample sets differ regarding transcript identities and quantities (Fig. 28a, b). The shift in the scatter plot towards a higher log2 ratio on the y-axis shows that most of the mRNAs found in both sample sets were detected with a higher abundance in the NeuroRiboTag samples (Fig. 28b). We next directly compared total RNA levels from IP input fractions to RNA from co-IP elution fractions from NeuroRiboTag worms only. In other words, we used RNA from the same NeuroRiboTag strain and analysed (1) whole-animal RNA before the IP and (2) pulled down RNA after the IP. We calculated fold changes for genes with detectable expression and tested the top 5 % of changed mRNAs in the IP fraction for an enrichment of *C. elegans* anatomical terms, using the Tissue Enrichment Analysis (TEA) tool (Angeles-Albores et al., 2016). The genes corresponding to the highest fold-change values for the neuronal RiboTag IP RNA were significantly enriched for neuronal tissues. Of 49 significant tissue categories, 46 were neuron-specific (Fig. 28c, only the 15 most significant terms are depicted, full dataset see Tab. 5 in appendix). Using the top down-regulated genes for the same analysis, only one out of 23 significant terms corresponded to a neuronal cell class (BAG). Instead, many terms corresponding to the germ line were significantly enriched. In addition, the terms epithelial and muscular system were significantly enriched in the down-regulated genes comparing RNA sequencing data from NeuroRiboTag IPs to NeuroRiboTag total RNA (Fig. 28d, only the 15 most significant terms are depicted, full dataset see Tab. 6 in appendix). These data show that a co-IP from NeuroRiboTag worms purifies actively translated mRNAs specifically from neurons, one of the least abundant tissues in the worm. Collectively, we could show that the optimised RiboTag worms developed in this study enable the analysis of tissue-specific mRNA translation.

In follow-up studies, first, we aim to deeply characterise further tissue-specific RiboTag lines enabling us to also investigate translation in the soma, muscle or intestine on a transcript-specific level. Second, using the generated RiboTag toolbox, we will analyse the tissue-specific translatomes of worms with an inhibited ISR to gain further insights into the interplay of ISR regulation, selective translation and longevity. Together, this work will enable us to further analyse the process of mRNA translation during healthy ageing and longevity.

3 Discussion

In this study, we analysed a forward genetic screen for novel regulators of ageing and longevity. This work was distributed into three sequential sub-projects. First, from the forward longevity screen we identified over 100 worm lines with an extended lifespan of 18 % and more and sequenced their whole genomes. We built a pipeline to analyse the corresponding results in depth, leading to the identification of novel alleles of known longevity genes in a variety of pathways described before to extend lifespan, thereby validating our approach.

Second, by using this pipeline we identified mutations clustering in genes affecting the translation initiation key-factor eIF2 to be causative for longevity. These mutations were inhibiting the ISR without reducing overall protein synthesis rates. In this context, we found the selective translation of *kin-35* as required factor for the observed longevity. In sum, we could show that genetic and pharmacological ISR inhibition were causing longevity in *C. elegans* without generally reducing translation rates. We therefore found a novel, non-canonical role of the ISR and translation initiation pathways in longevity.

Third, we hypothesised that the selective translation observed upon the ISR inhibitory conditions in *ppp-1* mutants might be more pronounced in defined tissues. However, we did not have an optimal tool at hand that would enable the analysis of tissue-specific translation. We therefore worked in collaboration with the laboratory of Assoc. Prof. William Mair (Harvard T.H. Chan School of Public Health) to generate, validate and deeply characterise RiboTag worms, enabling the co-IP of fully assembled ribosomes and associated mRNAs from selected tissues. Ultimately, we aim to use this toolbox in the context of ISR inhibitory conditions to study tissue-specific translation.

3.1 The unbiased forward genetic longevity screen - success and boundaries

The successful performance of previous genetic screens for extended lifespan inspired us to set out a large-scale mutagenesis screen for increased survival in *C. elegans* (Klass, 1983; Lee et al., 2003; Hamilton et al., 2005; Hansen et al., 2005; Denzel et al., 2014). In contrast to previously performed genetic screens for longevity, this was the first fully unbiased longevity screen using random chemical mutagenesis combined with whole genome sequencing. This enabled not only an amino acid resolution, but also the identification of gain-of-function mutations next to loss-of-function ones in both essential and non-essential genes. The here performed forward genetic screen, its validation and analysis will be discussed in the following sections.

3.1.1 Success: Identification of alleles of old and new longevity genes

Previously performed RNAi-based screens for longevity in *C. elegans* led to the conclusion that most major longevity pathways activated by gene knockdown were already discovered (Lee et al., 2003; Hamilton et al., 2005; Hansen et al., 2005). Hence, our aim was to identify and analyse unknown longevity pathways, specifically focussing on the effect of gain-of-function mutations which have not been analysed in this context before. As opposed to the earlier phenotype- and RNAi-based screens, in this work the focus shifted towards an

advanced sequencing analysis. The large amount of induced mutations complicated the analysis and identification of phenotype-causing variants. Possible ways to ease the analysis of such data lie within the backcrossing of a mutant line to the wildtype strain while preserving the phenotype (Schneeberger, 2014). This idea was captured in the outcrossing of single long-lived worm lines from the screen. This approach reduced the background EMS SNPs by 87 % (see chapter 2.1.2). We concluded that in this particular strain, SNPs in the non-coding DNA were causing the longevity.

The most stringent way to identify causative mutations directly from sequencing data of forward genetic screens is the analysis of allelism by finding multiple alleles of the same gene in independent mutants with the same phenotype (Sarin et al., 2008; Denzel et al., 2014; Allmeroth et al., 2020). Previous forward genetic screens for longevity in *C. elegans* used this strategy, but were more targeted for example towards processes related to the protein quality control pathways: Genes modulating ageing through ER protein homeostasis could be identified using proxy phenotypes after EMS mutagenesis such as tunicamycin resistance. Together with the requirement of allelism for candidate causative mutations, in this particular screen candidate genes could be prioritised according to their potential function within the phenotype (Denzel et al., 2014). While this procedure can be complicated by looking at a very multifaceted phenotype such as longevity alone, using these strategies we were successful in identifying not only new alleles in known longevity genes but also in novel ones such as *ppp-1 / eIF2Bγ*.

Next to the identification of genes associated to the insulin signalling pathway and chemosensation using the allelism strategy, we further found a mutation in *iftb-1*, the β subunit of eIF2, causative for longevity. The *iftb-1* variant caused a reduction in overall translation rates. Perturbations in translation have been connected to lifespan extension before in a variety of studies and model organisms (Hansen et al., 2007; Syntichaki et al., 2007; Tohyama et al., 2008; Pan et al., 2007; Essers et al., 2016; Karunadharma et al., 2015). In one of the initial studies connecting reduced translation with longevity, RNAi-mediated knockdown of *iftb-1* was found to reduce protein production and therefore extended lifespan (Hansen et al., 2007). This is in accordance with the effects we see in the long-lived point mutant worm strain *iftb-1(wrm53)*. In sum, these results further validated the screening approach to identify several major longevity-associated pathways.

3.1.2 Boundaries: EMS mutations in the non-coding DNA

While successfully identifying novel longevity variants, our candidate longevity gene selection from the forward genetic screen was focussed on a collection of mutations within the coding sequences of all known *C. elegans* genes. Accordingly, longevity-causing mutations in regulatory sequences were disregarded. However, the preliminary experiments of backcrossing the long-lived strain MSD211 from the screen to wildtype animals and the corresponding results presented in chapter 2.1.2 indicated that, at least for this specific strain, the lifespan causing mutations reside within the non-coding fraction of the genome.

Cis-regulatory elements such as promoters and enhancers are located in the non-coding DNA and can modulate expression of genes in three-dimensional structures in distances of

up to hundreds of kilobases. Trans-acting factors regulate gene expression by interaction with cis-regulating elements, the regulated genes or their products and comprise for example non-coding RNAs. In the context of disease- and tissue-specific gene expression regulation, SNPs in regulatory elements have been identified to be causative for specific phenotypes in a variety of contexts (Coppola et al., 2016). An intronic SNP associated with melanocyte pigmentation was shown to modulate the enhancer activity of the distant gene *IRF4* by directly stabilising a corresponding chromatin loop structure (Visser et al., 2015). A SNP in the intronic region of the longevity-associated transcription factor *FOXO3* could be shown to provide a novel HSF-1 binding site, leading to induced FOXO3 expression upon stress conditions (Grossi et al., 2018). In sum, not only mutations in the coding sequence but also in other DNA elements can be considered as longevity variants.

One of the major advances of the screen performed in this study over previous RNAi screens is the variant coverage of the whole genome over the CDS only. Therefore, as of now, the limitations of this screen are within the analysis, that focussed on the identification of longevity-causing gain-of-function mutations in the CDS and not on mutations in the non-coding sequences. Together, the analysis of this screen shows that assigning mutations in regulatory elements to downstream phenotypic effects from forward genetic screens remains difficult, but at the same time outlines an intriguing possibility to identify novel longevity regulators. Thus, in-depth analysis of the SNPs in the non-coding sequence will be fundamental in the future.

3.2 Lifespan extension through ISR inhibition - a non-canonical longevity mechanism

By analysing the forward longevity screen, we discovered not only mutations for example in *iftb-1*/eIF2β, reducing translation and therefore prolonging life. Strikingly, we further identified a novel class of longevity genes, which affect translation initiation and ISR activity without generally reducing translation rates. Genetically dominant mutations in *ppp-1*/eIF2Bγ extended lifespan while partially inhibiting the ISR and selectively changing mRNA translation of specific transcripts such as *kin-35*. In addition, pharmacological ISR inhibition and a full impairment of the ISR in phospho-defective eIF2 worms carrying an S51A mutation caused an extension of lifespan. In all cases, the longevity was dependent on *kin-35* expression without a reduction of overall protein synthesis (Fig. 29). Both *ppp-1* and *eIF2*αS51A mutant strains further showed an improved resistance in response to toxic stresses, contributing to improved cellular and organismal health. In sum, our data show that ISR inhibition drives longevity and increased protein homeostasis in *C. elegans* dependent on the translation of *kin-35*.

3.2.1 Lessons from yeast (1): Gcn(-) mutations and eIF2B

The translation initiation process and the ISR have been intensely studied in yeast, leading to deep mechanistic insights of eIF2 modulation via its kinases and its guanine nucleotide exchange factor eIF2B, as well as the downstream consequences (Hinnebusch, 2005). In yeast, the ISR axis sensing amino acid starvation via Gcn2 is termed general control

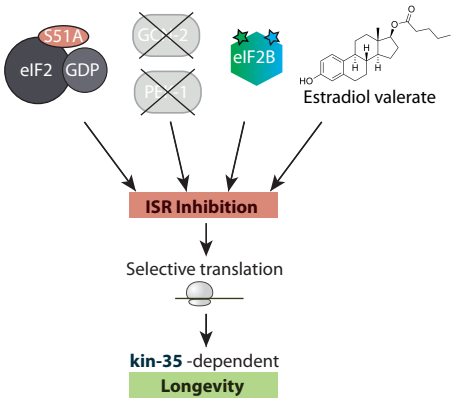

Figure 29: Lifespan extension through ISR inhibition. In *C. elegans*, a partial or full inhibition of the ISR is mediated through phospho-dead eIF2, a knock-down of the eIF2 kinases, mutations in the γ subunit of eIF2B or estradiol valerate treatment. Likewise, worms with an inhibited ISR are long-lived in dependence of the selective translation of *kin-35*.

pathway, where activation leads to the de-repression and therefore enhanced translation of *gcn4/atf-4* (Hinnebusch, 1988). In this context, mutants which are generally unable to activate uORF-regulated translation of *gcn4/atf-4* upon stress were classified as general control non-derepressible, in short Gcn(-). Typical Gcn(-) mutations therefore generally diminish the stress-induced translation of genes regulated by uORF structures, such as *atf-4*, and hence inhibit the ISR (Hinnebusch, 2005). We classified the *ppp-1*/eIF2Bγ alleles as Gcn(-) mutations, since they blunted the ER-stress induced expression of GFP under the uORF controlled promoter of *atf-4* (see Fig. 18). Therefore, they belong to the Gcn(-) class of mutations in the classical sense, as in these mutants *atf-4* is non-derepressible upon stress. Further, we assigned variants that reduce eIF2α phosphorylation levels, and thus inhibit the ISR, to the class of Gcn(-) mutations. ISR inhibition was observed in the worm lines with partial loss-of-function mutations in *gcn-2* and *pek-1* or the *eIF2*αS51A animals analysed in this study. Conveniently, in yeast, variants of different subunits of eIF2B have been described as Gcn(-) mutations before (Vazquez de Aldana and Hinnebusch, 1994). For example, mutations in eIF2Bβ and eIF2Bγ were reported to prevent the inactivation of the eIF2B complex by phosphorylated eIF2 (Vazquez de Aldana and Hinnebusch, 1994; Dev et al., 2010; Kashiwagi et al., 2019). As a consequence, one of the major regulatory mechanisms of the ISR, the inhibition of eIF2B by phosphorylated eIF2α, is lost in these mutants. We speculate that the mutations we found in *ppp-1*/eIF2Bγ might similarly render the eIF2B complex insensitive to the inhibition by phosphorylated eIF2 and consequently show a reduced ISR activity.

3.2.2 Lessons from yeast (2): Gcn(-) mutations and eIF2B bodies

Focussing on a more cell biological level, recent research on specific non-membrane-bound cellular compartments opened up further research directions regarding the interplay of ISR and translation initiation with eIF2B. Granules containing mRNAs stalled in translation initation, so-called messenger ribonucleoproteins (mRNPs), are known as dynamic mRNA storage compartments in a variety of cellular contexts (Protter and Parker, 2016). Exemplary, well-studied stress granules form from mRNAs stalled in translation, keeping them on hold.

So called P bodies more specifically contain mRNAs targeted for degradation. Still, mRNPs from both stress granules and P bodies can go back to an active translation state (Protter and Parker, 2016). Another highly specific non-membrane-bound cellular compartment that is gaining attention recently is the eIF2B body. eIF2B bodies were shown to be a site of eIF2B and eIF2 co-localisation in yeast and human cells. They might constitute a specific cellular locus where eIF2B GEF activity occurs. Therefore, eIF2B bodies might represent a specialised site of translational control (Campbell et al., 2005; Taylor et al., 2010). More recently, it could be shown in cells that, during stress, phosphorylated eIF2α localises to eIF2B bodies with a subsequent decrease of eIF2 shuttling, which could be rescued by ISR inhibiting drugs such as ISRIB (Hodgson et al., 2019; Norris et al., 2020). Interestingly, in yeast, different ISR inhibitory Gcn(-) class mutations in the α-subunit of eIF2B were shown to affect eIF2B body formation up to their complete loss. By the disappearance of eIF2B bodies and hence the cellular site of phospho-eIF2α interaction with eIF2B, the ISR-mediated translational control during stress might get lost in Gcn(-) mutants (Norris et al., 2020). In addition, mutations that were shown to decrease eIF2B GEF activity disrupt eIF2B bodies (Norris et al., 2020), suggesting that only fully intact eIF2B decamers form eIF2B bodies. These data are in line with another study using cryo-electronmicroscopy (cryo-EM) in yeast to show that the polymerisation of intact eIF2B decamers results in eIF2B body formation (Nüske et al., 2020). However, Hodgson *et al.* (2019) showed that eIF2B bodies can differ in their content: they reported that larger eIF2B bodies contain all eIF2B subunits, while smaller ones predominantly contain the catalytic subunits. The authors further showed that phosphorylated eIF2α mainly associates with large eIF2B bodies. These data indicate a more diverse role of eIF2B bodies during stress conditions (Hodgson et al., 2019). In sum, these results indicate a role of cellular eIF2B localisation in the regulation of translation initiation. It would be interesting to analyse our novel Gcn(-) class mutations in *ppp-1*/eIF2Bγ in regard to a potential impact on eIF2B body formation - a potential future perspective that is further discussed in the respective section of this thesis (see chapter 4.2.1).

3.2.3 A new mode: Tuning translation can lead to longevity

The processes of translation initiation and the ISR are tightly connected. We found a shift in the translatome of *ppp-1* mutants and could identify a role of selectively translated *kin-35* in the longevity of worms with reduced ISR activity (see Fig. 16). We further investigated the role of *kin-35* in *C. elegans* longevity and found that *kin-35* over-expression was not sufficient to extend worm lifespan. However, over-expression of other key factors that are required for lifespan extension is also not sufficient to induce longevity. One example is the FOXO worm ortholog *daf-16*. While *daf-2*/*IGF1R*-mediated longevity fully depends on *daf-16*, the over-expression of *daf-16* only causes a mild lifespan extension not comparable with the *daf-2*-mediated phenotype (Henderson and Johnson, 2001). Because it carries a putative protein kinase domain, we termed the identified mRNA, which was previously named M04F3.3, now *kin-35*. Its closest human and mouse orthologs are other kinases such as tau tubulin kinases, vaccinia related kinases and members of the protein kinase family CK1α. However, the percentages of matching sequences are low and do not meet the requirements for high-quality

orthologs (see supplementary Tab. 7). Therefore, *kin-35* is considered an undefined gene without biochemical evidence for its function or putative targets. Within the translationally changed mRNAs identified in the *ppp-1* animals, a GO term analysis showed an enrichment of genes related to phosphorylation functions. Nevertheless, we cannot conclude that a specific kinase activity of *kin-35* is responsible for the observed longevity phenotypes. Comprehensive biochemical and genetic analyses are needed to understand the downstream effects of *kin-35*, that go beyond the scope of this work.

The role of *kin-35* in our genetic and pharmacological models of ISR inhibition proved the connection between selective translation and longevity. Based on our results, we conclude that the translational switch and not the down-regulated ISR *per se* is responsible for the observed longevity phenotypes. That the variability of protein quantities is only partially reflected by fluctuations in mRNA expression was shown in several model organisms, including data suggesting that cellular protein levels are predominantly controlled translationally (de Godoy et al., 2008; Schwanhausser et al., 2011). The lifespan extension driven by Gcn(-) mutations being dependent on the selective translation of *kin-35* is an example of the role of post-transcriptional regulation in the context of ageing and longevity. However, how selective translation of *kin-35* is regulated in the Gcn(-) mutants remains unknown. Possible regulators of translation lie within cis-regulatory elements such as enhancers or promoters and trans-regulatory ones, for example microRNAs. Specific UTR characteristics were shown to affect translational efficiency of mRNAs such as RBP- and miRNA binding motifs, length, free-folding energy and GC-content (Rollins et al., 2019; Rogers et al., 2011; Zid et al., 2009). Thus, to better understand the regulation of selective translation, a deep characterisation of the 5'-UTRs of differentially translated mRNAs during different Gcn(-) conditions remains to be performed. In line with our data, the regulation of ageing at the translational level has been described before: long-lived *daf-2*/IGF1 mutant worms show changes on the translatome level (McColl et al., 2010). Further, in the context of synergistically mediated longevity in *daf-2*/IGF1; *rsks-1*/S6K double mutant worms, the selective translational repression of *cyc-2.1* was identified as key mediator of longevity (Lan et al., 2019). However, the translational efficiency of *cyc-2.1* was not altered in *ppp-1* mutants, supporting an independent mechanism. Moreover, in *C. elegans* it was shown that dietary restriction (DR) induces the translational regulation of specific subsets of genes involved in DR-mediated longevity (Rollins et al., 2019). It would be interesting to compare these genes to the transcripts displaying changed translational efficiency in *ppp-1* mutants in the future. While the mechanism behind the selective translation in *ppp-1* mutants remains unknown, we conclude that in Gcn(-) mutants, a translational switch is required for the observed lifespan extension.

3.2.4 Integrating the ISR (1): Ageing and disease

Data from this work suggest that ISR activity increases during ageing in *C. elegans*. Here, the ISR status was monitored through phosphorylated eIF2α from whole worm lysates. While we could not detect changes in eIF2α phosphorylation between wildtype and *ppp-1* mutant animals during ageing, phospho-eIF2α levels were consistently increased in old animals compared to young ones. These data stand in contradiction with published studies. Multiple

data indicate a decrease of ISR activity with ageing on the one hand. For example, the levels of eIF2α phosphorylation and ATF4 were reported to be decreased in the aged cerebral cortex of mice (Naidoo et al., 2008) and a variety of further tissues in aged rats (Hussain and Ramaiah, 2007). On the other hand, next to the data presented in this work, an increase of ISR activation during ageing was reported in the following studies: ISR activating GCN2 phosphorylation levels and ATF4 protein amounts were shown to be increased in brain lysates of old mice (Krukowski et al., 2020). Further, a study in the fruit fly showed elevated phospho-eIF2α levels with ageing (Brown et al., 2014). These data are in line with the report of reduced overall translation during ageing in *C. elegans* (Kirstein-Miles et al., 2013), which could be mediated by an increased ISR activity. In sum, the role of age-dependent changes in the ISR remains controversial. From the existing data, we speculate that ISR activity during ageing is regulated context-dependently, possibly in a tissue-specific manner.

In line with the conflicting data on ISR regulation during ageing, the ISR has been proven to play context-dependent roles in different age-associated diseases, often affecting the nervous system. The pharmacological activation of the ISR was shown to be protective in a Huntington mouse model by transiently lowering mRNA translation with a subsequent improvement of protein homeostasis (Krzyzosiak et al., 2018). Further, ISR activation has been described as protective in mouse models of Parkinson's disease and amyotrophic lateral sclerosis through the inhibition of eIF2α de-phosphatases (Colla et al., 2012; Jiang et al., 2014). However, also increased eIF2α levels were described in several diseases and in these contexts, the down-regulation of the ISR was shown to be beneficial. An upregulated ISR activation in pancreatic β-cells has been correlated with diabetes (Cnop et al., 2017). Further, an activated ISR was associated with neurodegenerative disorders. Elevated eIF2a phosphorylation levels were described in the brains of Alzheimer's disease patients (Ma et al., 2013). In mouse models of traumatic brain injury, down syndrome and prion disease, persistently high levels of eIF2 phosphorylation were detected (Chou et al., 2017; Jun Zhu et al., 2019; Halliday et al., 2015). In addition, mutations in genes directly associated with the ISR cause neurological disorders. In the genetic leukoencephalopathy Vanishing White Matter Disease (VWM), deleterious mutations in eIF2B cause a destabilisation of its complex formation and hence a down-regulation of eIF2B function, leading to myelin loss (van der Knaap et al., 2002; Li et al., 2004). In sum, these data undermine the role of the ISR in ageing and age-associated diseases.

The treatment of pathological conditions associated with an increased ISR can be achieved by the inhibition of eIF2α phosphorylation or by interfering with eIF2B function and inhibition. In a variety of neuronal disorders, the rescue of increased eIF2 phosphorylation leads to neuroprotection including the reversal of cognitive and long-term memory deficits (Chou et al., 2017; Jun Zhu et al., 2019; Halliday et al., 2015). In Alzheimer's disease mice, ISR down-regulation by genetic deletion of GCN2 and PERK prevented aberrant translation, low synaptic plasticity and memory defects. These results rendered the eIF2 kinases as potential therapeutic targets in the treatment of Alzheimer's disease (Ma et al., 2013). A similar reversal of disease-associated phenotypes could be observed during the knockout of PKR in Down syndrome mice (Jun Zhu et al., 2019). Further, direct genetic inhibition of the ISR

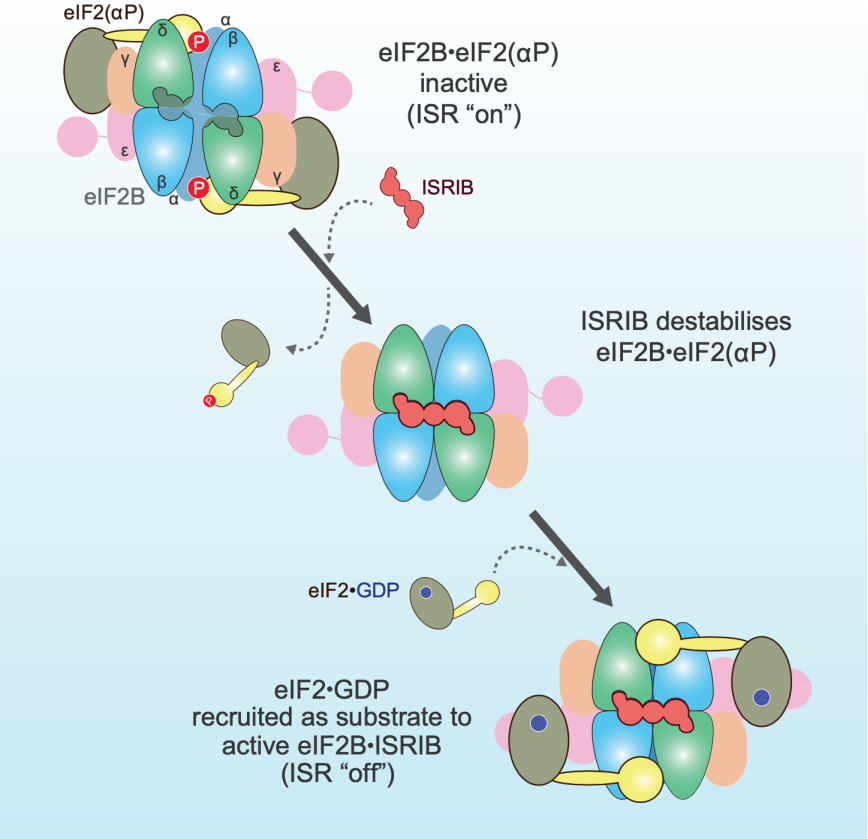

Figure 30: The biochemical mechanism behind ISRIB. ISRIB binds eIF2B in a deep binding pocket and counters the inhibiting effect of phospho-eIF2 on eIF2B through an allosteric structural rearrangement. Figure adapted from Zyryanova et al. (2020).

in heterozygous *eIF2α*S51A mice enhanced synaptic plasticity and memory in young 2- to 4-month-old mice compared to wildtype animals (Costa-Mattioli et al., 2007). Strikingly, directly inhibiting the ISR is possible using compounds such as ISRIB (ISR Inhibitor). This drug-like small molecule was described to reverse cognitive defects associated with traumatic brain injury and conferred neuroprotection in prion disease mouse models (Chou et al., 2017; Halliday et al., 2015). In lung adenocarcinomas, induced ATF4 levels could be blocked by the use of ISRIB (Albert et al., 2019). Further, in VWM cells, ISR inhibition using ISRIB rescued the activity of the mutant eIF2B complex (Wong et al., 2018). In line with the phenotypes of heterozygous *eIF2α*S51A mice, treatment with ISRIB further increased learning and long-term memory in young healthy mice (Costa-Mattioli et al., 2007; Sidrauski et al., 2013). Moreover, acute ISRIB treatment in old mice (19 months of age) was shown to reverse the decline in memory during ageing by resetting the ISR in the brain, causing an improvement of neuronal function towards the phenotypes of young mice of 3-6 months of age. Additionally, general age-related inflammation processes in the brain of old mice were shown to be reduced upon ISRIB administration (Krukowski et al., 2020). Overall, these data suggest the ISR as druggable target in health and disease.

ISRIB targets eIF2B and enhances its function by promoting eIF2B assembly and stabilising its decameric complex (Fig. 30; Sidrauski et al. (2015); Sekine et al. (2015)). In more detail, ISRIB acts as molecular staple by bridging eIF2B core oligomeric structures in a deep

binding pocket. Therefore, ISRIB counters the effect of eIF2α phosphorylation which inhibits eIF2B (Costa-Mattioli and Walter, 2020; Zyryanova et al., 2020; Schoof et al., 2021). The data on positive systemic effects of ISRIB mediated eIF2B activation in a variety of contexts converge with the enhanced survival and protein homeostasis observed in the *ppp-1*/eIF2Bγ mutants we assigned to the Gcn(-) class. The biochemical mechanism of ISRIB and its cellular consequences further strengthen the hypothesis that the *ppp-1* point mutations cause a gain-of-function effect in eIF2B. Earlier, we hypothesised that the identified *ppp-1* variants might diminish the inhibition of eIF2B by phosphorylated eIF2. In light of the ISRIB mechanism of action, an enhanced eIF2B complex stability through mutations in *ppp-1* would be another possible explanation for the observed phenotypes. In total, these data suggest a complex role of aberrant ISR activity in age-associated diseases that depends highly on the context. Further, they show that eIF2B gain-of-function mechanisms can overcome some of the disease-associated effects caused by an activated ISR.

3.2.5 Integrating the ISR (2): Longevity

Our data suggest that, next to the *ppp-1* variants, inhibitory amino acid substitutions in the worm eIF2 kinases GCN-2 and PEK-1 reduce ISR activity and extend lifespan. This stands in contradiction with published data showing that the knockout of these kinases via RNAi or deletion mutations does not cause longevity in the worm (Baker et al., 2012; Henis-Korenblit et al., 2010). Taken together, these results suggest that the kinases might have additional targets other than eIF2 or that they act in larger protein complexes. These functions could be affected by larger deletions or RNAi-mediated gene knockdown while being preserved in the point mutants analysed in this study. Indeed, it was reported that yeast Gcn2 has further targets including eIF2B and Gcn20. These physiologically relevant factors fine-tune translational control upon ISR activation (Dokladal et al., 2021). Futher, in different model organisms, yeast Gcn2 and mammalian GCN2 were reported to associate with additional proteins such as eEF1A and the ribosomal P-stalk, a complex that is part of the ribosomal GTPase-associated centre (Visweswaraiah et al., 2011; Inglis et al., 2019; Harding et al., 2019).

Although many studies show a connection between ISR deregulation and age-associated diseases (see chapter 3.2.4), the role of the ISR in longevity is still unclear. It has not formally been tested yet how a direct modulation of the ISR affects survival in higher organisms. Most studies connecting the ISR and longevity focussed on the role of ATF4. In yeast, the ATF4 homolog Gcn4 was shown to play a crucial role in longevity mechanisms related to down-regulated translation and dietary restriction (Steffen et al., 2008). This suggests a beneficial role of the activated ISR for longevity. Following this path, the activation of Gcn2 extended yeast lifespan in a Gcn4/ATF4-dependent manner. Moreover, the Gcn4/ATF4-mediated longevity relied on functional autophagy, making it a downstream target of active Gcn2 to extend lifespan (Hu et al., 2018). The relationship of ISR activation and longevity has further been investigated in mice. Liver-specific elevation of ATF4 could be observed in mice upon several interventions that extended their life (Li et al., 2014). Further, over-expression of a mammalian ATF4 target gene, *FGF21*, caused longevity in mice (Salminen et al., 2017). In

contrast to these findings, our data support a model in which partial or full ISR inhibition via Gcn(-) mutations causes lifespan extension in *C. elegans*. In addition, we showed that the longevity and increased protein homeostasis in Gcn(-) mutants is mediated by specific changes in the translatome. Our data also demonstrated, that in *C. elegans*, the ISR is clearly required to cope with acute stress, specifically during development. We conclude that while the activation of ATF4 extends lifespan and increases robustness mainly in conditions of reduced protein synthesis, we identified an independent, novel class of longevity mutations inhibiting the ISR without suppression of overall protein production. We show that lifespan extension by ISR inhibition is dependent on selective mRNA translation through a mechanism fully independent of ISR activation or ATF4 expression. In the future, investigation of this translational switch in mice will help to understand the role of ISR inhibition in mammalian longevity.

3.3 The RiboTag model - on the importance of studying tissue-specific translation

The consequences of translation initiation and ISR modulation in ageing, age-related diseases and longevity are still under investigation and many research directions point towards context- and tissue-specific effects (see chapters 3.2.4 and 3.2.5). Maintenance of translation in neurons was shown to be beneficial during ageing-associated diseases in mice caused by an over-active ISR. For example restoring protein synthesis rates in the brain of prion-diseased mice using ISRIB prevented neurodegeneration (Halliday et al., 2015). Therefore, investigating the effects of tissue-specific translation and its regulation is essential for understanding principal cellular processes during ageing. In detail, studying the here described Gcn(-) mutations with the relating selected translatome changes in a tissue-specific context would be of great interest. While we analysed mRNA translation extensively on the organismal level, tissue-specific changes in the translatome were not examined in Gcn(-) mutants yet. Given the large impact of eIF2B activation through ISRIB administration in the context of neuronal processes and neurodegenerative diseases (see chapter 3.2.4), we speculate that the Gcn(-) mutations identified in *C. elegans* might cause substantial effects on the level of neuronal translation.

Across diverge species, RiboTag models are used to investigate the tissue-specific regulation of mRNA translation in different physiological conditions. Most notably are studies on differences in the translatome of neuronal cell types (Heiman et al., 2008; Gracida et al., 2017; Koterniak et al., 2020). The RiboTag method is of specific importance in the *C. elegans* field. The worm is generally considered as an easy-to-handle post-mitotic model organism in the fields of genetics and biochemistry. However, tissue- and cell-type-specific studies are complicated by the physiology of the animal and worm dissociation is rarely reported due to its size (Hench et al., 2011; Zhang et al., 2011). Through the combination of a specialised worm disruption method with fluorescence-activated cell sorting, the neuronal transcriptome of *C. elegans* was studied for the first time by Kaletsky *et al.* in 2015. The results revealed neuron-specific changes of gene expression in insulin signalling mutants and demonstrate the crucial role of tissue-specific phenotype regulators in the context of longevity (Kaletsky et al.,

2015). In this regard, the tissue-specific RiboTag worms provide suitable models to study the translatomes of distinct tissues. The RiboTag methodology is using standard lab techniques such as worm homogenisation followed by co-IPs, making it very robust. Next to RiboTag mice (Heiman et al., 2008; Sanz et al., 2009), similar models have been developed in *C. elegans* recently. Tagging the ribosomal protein RPL-1 with enhanced green fluorescent protein (eGFP) enabled the tissue-specific analysis of actively translated mRNA from the nervous system, body-wall muscle, intestine and dopaminergic and serotonergic neurons each (Gracida et al., 2017; Gracida and Calarco, 2017). In a similar model, an HA-tag was added to RPL-22 and expressed specifically in serotonergic neurons (McLachlan and Flavell, 2019; Rhoades et al., 2019). In this work, we generated an optimised *C. elegans* RiboTag model.

3.3.1 RiboTag worms: Development, characterisation and goals

The *C. elegans* RiboTag model developed here was designed using the CRISPR/Cas9-based SKI-LODGE system (Silva-Garcia et al., 2019). The generated worms express ^{FLAG}RPL-22 from the genomic *rpl-22* locus or in a tissue-specific manner from different SKI-LODGE cassettes. To ensure that the FLAG tag does not generally interfere with mRNA translation, we used the control endogenous RiboTag line to characterise the effect of ^{FLAG}RPL-22 on translation and worm health in depth. We successfully co-immunoprecipitated assembled ribosomes and associated mRNAs not only from the endogenous RiboTag worms but also from the neuron-specific RiboTag line. Using the NeuroRiboTag worms, we proved the successful tissue-specific isolation of ribosome-associated mRNAs through RNA sequencing after RNA elution from a FLAG co-IP. To my knowledge, comparable deep characterisations of previous RiboTag worm lines have not been published yet.

While our RiboTag model compliments the existing *C. elegans* RiboTag lines (Gracida and Calarco, 2017; McLachlan and Flavell, 2019), we feel it provides important optimisations and advantages, specifically for studying the nervous system. In both previous approaches, the tagged ribosomal subunits were expressed via extrachromosomal arrays. These genetic constructs are not directly integrated to the worm genome but have a semi-stable form (Chen et al., 2016; Kadandale et al., 2009; Zanin et al., 2011). Using DNA mutagens, they can be randomly integrated to the genome, making it hard to predict copy numbers and locus-dependent effects on local gene expression (Hutter, 2012). In contrast, the CRISPR/Cas9-based SKI-LODGE system used here generates precise genome edits by homology directed repair. The so-generated transgenes are expressed under pre-defined tissue-specific promoters at known loci in a single copy (Silva-Garcia et al., 2019). Therefore, this system provides a clean genetic background. To minimise effects on ribosome functionality, our RiboTag model uses a 3xFLAG epitope, which is substantially smaller than eGFP. While here RPL-22 is not fluorescently tagged itself, transgene expression can be followed by the fluorescent wrmScarlet, that is included in the design of all tissue-specific SKI-LODGE lines. Further, we could decrease the needed number of worms for the successful isolation of pan-neuronally translated mRNA from the NeuroRiboTag system from 150 000 worms (Gracida et al., 2017; McLachlan and Flavell, 2019) to 30 000 worms, leading to a drastic reduction in consumables needed in the co-IP. Lastly, the SKI-LODGE cassette-driven neuronal expression of ^{FLAG}RPL-

22 is under the control of the *rab-3* 3'UTR, preventing leaky expression in the intestine that is common to other expression cassettes in *C. elegans*.

Existing RiboTag worm models have helped to successfully discover tissue-specific differences in alternative splicing (Koterniak et al., 2020), as well as translational alterations in serotonergic neurosecretory motor neurons, leading to the identification of novel sensory mechanisms for food sensing and stress-induced feeding (Rhoades et al., 2019; Gracida et al., 2017). These data demonstrate that tissue-specific RiboTag worms are a suitable model to study mRNA translation in diverse genetic backgrounds, during physiological manipulations and pharmacological treatments. In this work, we provide an optimised, clean neuronal RiboTag model that was characterised in depth for the *C. elegans* community. Similar strains will be designed and extensively tested for other tissues such as the soma, muscle and intestine. We are looking forward to use the so generated RiboTag lines to investigate the role of tissue-specific translation in the context of ageing and longevity in general and of Gcn(-) mutants specifically.

4 Future perspectives

As discussed in the previous section, the work of this thesis opens up several important questions and possibilities for follow up studies. This final section describes the future perspectives of the three main parts of my work.

4.1 The future of this and other forward longevity screens

4.1.1 Improving the strategy that identified *ppp-1* as novel longevity gene

As discussed previously, we were able to identify SNPs in the coding region of *C. elegans* genes to extend lifespan from the forward longevity screen. We used a stringent strategy for candidate gene identification from the pooled sequencing data of all long-lived EMS mutants. This approach found *ppp-1* mutations to be causative for longevity. However, many candidate genes remain to be un-analysed and the causative mutations for lifespan extension in several EMS-mutagenised worm lines stay unresolved. Hence, testing more potential longevity variants from the high confidence candidate list from the forward longevity screen would be of interest. The adaptation of CRISPR/Cas9-mediated gene editing in *C. elegans* was a game changer for the whole worm community and its efficiency is constantly being improved (Paix et al., 2014, 2017). While in our experience this system does work to generate specific SNPs in the worm by injection of all required components to the worm gonad, the success rate and time spent to receive the DNA change of interest highly differed between each edit in our hands. To generate defined SNPs using the CRISPR/Cas system, a repair template carrying the desired edit has to be inserted to the genome via homology directed repair (HDR). Efficient repair template design was analysed in depth to ensure precise HDR in *C. elegans* (Farboud et al., 2019). From these studies, repair template design should be further adapted to ensure highly efficient genome editing rates for our purposes. In addition to the originally identified endonuclease Cas9 derived from *Streptococcus pyogenes* for the use of targeted gene editing (Jinek et al., 2012), the nuclease Cas12a from *Acidaminococcus sp.* can also be used

within the CRISPR/Cas system. Compared to Cas9, it uses a different, thymine-rich target site sequence (protospacer-adjacent motif (PAM)). Hence, the use of Cas12a might increase the number of potential editing sites which were not accessible previously or only with a low editing efficiency. This might be of benefit particularly in adenine/thymine-rich organisms such as *C. elegans* (Zetsche et al., 2015; Consortium, 1998). Improving the CRISPR/Cas-mediated gene editing success rate by adapting the insights described above would be of great help to systematically replicate more potential longevity variants within a wildtype background.

Next to an increase in speed and efficiency of gene editing via the CRISPR/Cas system, another future direction might be to improve the strategy of candidate longevity gene identification. In their pipeline for the analysis of mutant genome sequences, Minevich *et al.* (2012) suggest to analyse forward genetic screen data with regard to certain classes of genes. Using lists comprising for example transcription factors or genes involved in transgene splicing, all genes on our high confidence candidate list could be analysed for an enrichment in such classes (Minevich et al., 2012). Using only genes that showed allelism might overcome the fact that the forward longevity screen originally aimed at a saturation of EMS SNPs in all existing *C. elegans* genes. This generally makes similar analyses, network approaches and multiple factor analyses for the identification of causal variants complicated. In sum, improving the strategy that was successfully used to identify *ppp-1* as novel longevity gene might ease the identification of further novel longevity variants within the coding sequence of the EMS mutagenised worms.

4.1.2 Improving the identification of longevity-causing SNPs by outcrossing

Are more targeted approaches successful to identify novel longevity variants from the forward genetic screen? To find the causative SNP from the analysis of separate mutagenised worm lines, we outcrossed one of the most long-lived strains from the screen to a wildtype line to reduce the background noise of EMS mutations. This strategy led to a decrease in EMS SNPs of 87 % while preserving the longevity phenotype. However, the only variant falling into a coding gene sequence was not causative for longevity. Since we did not get an enrichment of remaining EMS SNPs at a specific locus or chromosome, we had no point of reference which of the remaining 126 variants within the non-coding sequence might be causative. Because we pooled twelve long-lived worm lines with 2 outcrossing events each for the DNA sequencing, we did not achieve one outcrossed strain to keep working with. One option would be to repeat this approach with more original long-lived worm strains from the forward longevity screen, speculating that the lifespan extension of some of them is caused by a variation in a coding gene, such as the *ppp-1* mutations. To ease the downstream analysis of the phenotype-causing variants, we could further repeat this strategy in a linear way, performing one outcrossing event per crossing generation. Because we would need to follow the longevity phenotype in each crossing step, this would be very time consuming, but in the end generate one long-lived worm line with a drastically reduced amount of background mutations for further analyses. Another possibility to ease the separation of phenotype-causing mutations from other EMS SNPs might be the Hawaiian SNP mapping approach. The polymorphic Hawaiian *C. elegans*

isolate can be distinguished from the Bristol N2 line by 100,000 SNPs (Doitsidou et al., 2010). By backcrossing an EMS mutagenised worm line to the Hawaiian worm strain instead of our canonical Bristol N2 wildtype worms, the strongly increased amount of marker SNPs could enable the identification of loci associated with the causative mutation (Doitsidou et al., 2010). Together, making adjustments in the outcrossing strategy to reduce the burden of background EMS variants of separate long-lived worm strains might improve the investigation process of longevity causing mutations.

4.1.3 Initiating the analysis of longevity variants in the non-coding DNA

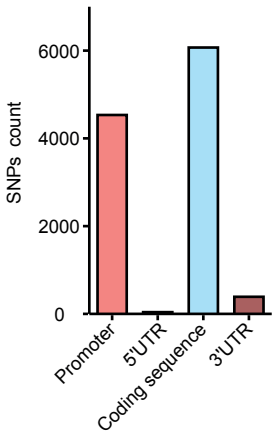

Figure 31: EMS SNPs from the forward longevity screen adjacent to coding sequences. Of over 30 000 EMS SNPs in 101 sequenced long-lived worms from the forward longevity screen, 6085 were mapped to the coding sequence, while 4548 EMS SNPs were assigned to promotor regions.

As mentioned before, we so far only analysed EMS SNPs within the coding sequence from the sequencing data of long-lived EMS mutant worms. Hence, there are several parts of the non-coding DNA sequence including for example promoters, introns and enhancers carrying EMS SNPs that we did not look at. The outcrossing following the phenotype of longevity of the strain MSD211 proved that the EMS mutagenesis produced long-lived worm lines that contain causative variants within the non-coding sequence. In this context, are we able to identify longevity-causing SNPs in the non-coding DNA from the forward longevity screen? A first step in the analysis of SNPs outside of the CDS from the here performed forward longevity screen could be the use of the existing WGS data to analyse SNPs in promoter regions, which make up a substantial proportion of the identified unique EMS SNPs (Fig. 31). Additionally, SNPs within intronic regions could potentially be analysed. Looking specifically at highly conserved elements in introns might ease the analysis, since these often include splice- or binding-site sequences (Kelly et al., 2015). The forward longevity screen was analysed successfully for novel longevity variants within the CDS. This could be used as a basis for further studies investigating the impact of SNPs in the non-coding DNA sequence on the ageing process. To my knowledge, this has not been done from a forward longevity screen in a strategic manner to date and hence shows considerable potential to identify novel regulatory nodes in the ageing gene network. However, analysing SNPs for example in promoters of estimated sizes and in large intronic sequences might lead to a reduction in specificity and potentially many false candidate genes, making the candidate gene list impractical. A further drawback in analysing an EMS-based mutagenesis screen for effects on regulatory regions might be the mutagen itself. While the SNP-induced amino acid variations often cause structural changes in proteins, regulatory elements might be rather influenced by larger genomic alterations such as deletions and inversions, as these regions have a higher tolerance for small sequence variations as compared to the coding sequence (Moresco et al., 2013). After all, the association of non-coding variants to phenotypic effects remains complicated and they stay under-diagnosed, not only in the here presented screen, but also in the context of diseases

and other complex phenotypic traits (Bronstein et al., 2020). However, the under-diagnosis of variations in the non-coding sequence generally and in the context of longevity research specifically provides an opportunity for novel discoveries regarding the regulation of ageing and lifespan extension.

While the longevity screen as performed here might not be designed specifically for the identification of phenotypic SNPs within non-coding sequences, developments in screening design, analysis strategies and software endorse the performance of a forward genetic screen for the identification of longevity regulators in the non-coding sequence. Targeted CRISPR/Cas9 screens using multiplexed single guide RNAs have been developed and performed in cell lines to investigate the function of specific enhancer sequences (Canver et al., 2015). Recently, also in *C. elegans* targeted parallel genome editing was described by Froehlich *et al.* (2021). Here, an inducible Cas9 was used in combination with multiplexed single guide RNAs to produce many targeted small indels in enhancers or promoters in parallel. Subsequently, regulatory genotypes could be associated with phenotypic traits in the worms (Froehlich et al., 2021). Further, deep learning algorithms through artificial neural networks were shown to model splicing from a genomic sequence. Such a system was able to identify cryptic splice mutations in the context of genetic diseases (Jaganathan et al., 2019). The combination of targeted CRISPR/Cas9 mutagenesis screens and enhanced analysis methods for example predicting splicing from genomic sequence variants might lead to the identification of longevity-causative mutations. Summarising, the analysis of SNPs in the non-coding region of the *C. elegans* genome from the here performed forward longevity screen might lead to new insights in the regulation of longevity. Further, novel technical developments in genetic screening approaches might enable more targeted screens for the identification of causative non-coding variants in complex phenotypes, providing a potential future direction when it comes to genetic screens in the field of longevity research.

4.2 Open questions regarding Gcn(-) mutations, selective translation and longevity

4.2.1 The mechanism of action behind the *ppp-1* mutations

Our studies on the fine-tuning of eIF2 positively affecting *C. elegans* survival through Gcn(-) mutations lead to several direct follow-up questions. While our results clearly assigned the *ppp-1*/eIF2Bγ variants to the Gcn(-) class of mutations through relating phenotypes in *atf-4* translation and eIF2α phosphorylation, the biochemical mode of action behind those mutations remains unknown. Its identification therefore prompts one of the most urging follow-up projects. There are two standing hypotheses that should be investigated. First, as discussed before, previous yeast studies confirmed eIF2B as potential carrier of Gcn(-) mutations. It was shown that mutations in eIF2Bβ and eIF2Bγ can overcome the inhibitory effect of eIF2α phosphorylation on eIF2B and its function (Vazquez de Aldana and Hinnebusch, 1994; Dev et al., 2010; Kashiwagi et al., 2019). Based on these data, we speculated that the mutations identified in *ppp-1*/eIF2Bγ might have a similar effect on eIF2B function, making it insensitive to the inhibiting association with phospho-eIF2α. Second, the small molecule ISRIB was shown to stabilise the eIF2B complex. The so generated gain-of-function effect

on eIF2B therefore antagonises the effect of eIF2 phosphorylation inhibiting eIF2B (Schoof et al., 2021; Zyryanova et al., 2020). Accordingly, the mutations in *ppp-1* potentially enhance eIF2B function through a stabilisation of the complex.

To directly study the effect of *ppp-1* mutations on the interaction between eIF2B and phosphorylated eIF2α, co-IP experiments could be performed pulling down eIF2B, subsequently testing the amount of bound phosphorylated eIF2 or *vice versa*. Since in the worm field no antibody is known to effectively detect *C. elegans ppp-1*, tagging the eIF2B subunit would be necessary for this approach. Tagged eIF2B would further enable the identification of further putative binding partners of the complex and their potential alteration in the *ppp-1* mutant form through a proteomics approach. Ultimately, structurally studying the effect of the mutations in *ppp-1* would be of great interest to understand the molecular mechanism and the downstream effects of the here identified variants. The structures of yeast and human eIF2B and eIF2-eIF2B complexes have been resolved with high resolutions and showed that different conformation and assembly states of eIF2B regulate the ISR (Adomavicius et al., 2019; Tsai et al., 2018; Schoof et al., 2021; Kashiwagi et al., 2019). Moreover, it was shown that the eIF2B complex-stabilising drug ISRIB can block the binding of phospho-eIF2 to eIF2B through an allosteric mechanism (Schoof et al., 2021; Zyryanova et al., 2020). The *C. elegans* structure of eIF2B has not been analysed yet. The lifespan-extending *ppp-1* mutations we identified in *C. elegans* are not conserved in human or yeast. Therefore, investigating the worm eIF2B and eIF2-eIF2B complex structures using cryo-EM is a future perspective of this project, to perspectively study the effect of *ppp-1* mutations on eIF2B and eIF2-eIF2B complex formation.

On a more cellular perspective, I earlier discussed the role of eIF2B bodies in ISR-mediated translational control. While eIF2B body formation has been intensely studied in yeast and cellular cultures, to my knowledge this was not analysed in *C. elegans* yet. Studying the putative role of the *ppp-1* mutations in eIF2B body formation depicts a promising future direction in understanding the mechanism of action behind the here identified mutations and the corresponding phenotypes. It would be necessary to ask if (1) eIF2B bodies exist in the nematode microscopically using fluorescently labelled eIF2B and (2) if the here identified mutations in *ppp-1* alter the eIF2B body formation or the shuttling of phosphorylated and un-phosphorylated eIF2 through these bodies. Using a not-yet existing cryo-EM structure of worm eIF2B to compare the effects of *ppp-1* mutations with mutations in yeast or human eIF2B subunits known to affect eIF2B body formation could bring further insights to this topic. Lastly, the general role of eIF2B bodies in ageing has not yet been studied to my knowledge. If eIF2B bodies are existent and visualisable in *C. elegans*, the nematode would depict an excellent model organism to further analyse the role of eIF2B bodies in development and ageing. Together, studying the structural and biochemical effects of the *ppp-1* mutations is of high interest to better understand the molecular mechanism behind the observed *ppp-1* phenotypes. Moreover, studying the *ppp-1* mutations in a more cellular context might increase our knowledge in eIF2B body formation and its regulation.

4.2.2 The mechanism of selective translation in Gcn(-) mutants

Another biochemical process that opens up further research questions is the selective translation of specific mRNAs in worms carrying *ppp-1* mutations. The here analysed translatome data were acquired by polysome profiling and subsequent RNA sequencing of mRNAs associated with polysomes, meaning highly translated mRNAs. While this approach is sufficient to quantify the translational status of single mRNAs in different conditions, few further conclusions can be drawn on the level of specific mRNAs and their mode of translation. As discussed earlier, a comprehensive analysis of the 5'-UTRs of differentially translated mRNAs would allow to unravel the role of promotors, enhancers and included specific motifs, e.g. for RNA binding proteins, in the regulation of selective translation in *ppp-1* mutants. For a deeper analysis of the observed translational changes, further experiments should be performed to better understand the factors that drive the selective translation, not only in *ppp-1* mutants but potentially also in other mutant animals belonging to the Gcn(-) class such as the *eIF2α*S51A worms.

Next to the here performed polysome profiling approach, the so-called ribosome footprinting method can give further insights into the translation process. Here, from a sample lysate, a nuclease digestion is degrading all mRNAs that are not protected by bound ribosomes. Subsequent purification and deep sequencing enable the identification of precise positions of ribosomes at specific mRNAs and the analysis of translational control at codon resolution in a genome wide context (Ingolia et al., 2009). This method allows the monitoring of translation elongation speed and ribosome stalling at specific mRNA sites. Further, alternative translation of specific mRNAs can be identified such as uORF translation, ORF frame selection and truncation or extension of ORF translation (Ingolia, 2016). Ribosome footprinting has successfully been used to study translational regulation of selected mRNAs in cells during mTOR inhibition (Olshen et al., 2013). In *C. elegans*, ribosome footprinting has been adapted and was used to prove the functional role of maternal ribosomes in translation during embryonic development (Cenik et al., 2019). In sum, performing ribosome footprinting in long-lived Gcn(-) mutant worms would enable an in-depth analysis of the translational status of selectively translated mRNAs that has not been reached yet. This approach has great potential to shed light onto the mechanism of selective translation mediated by Gcn(-) mutations generally and *ppp-1* variants specifically.

Many studies using the ISR inhibitory compound ISRIB showed a specific beneficial effect of ISR inhibition on neuronal phenotypes during ageing and disease (Halliday et al., 2015; Krukowski et al., 2020). Further, upon a maladaptive ISR activation during disease, ISRIB was shown to restore translation levels in the brain (Halliday et al., 2015). We therefore hypothesise, that in Gcn(-) mutant worms, a translational switch in neurons specifically mediates benefits of ISR inhibition on lifespan. Therefore, using the RiboTag worms developed in this work to study the effects of Gcn(-) mutations on neuron-specific translation is a compelling future perspective. Further, differential ribosomal composition was shown to play a role in selective translation of specific mRNAs (Shi et al., 2017; Ferretti et al., 2017). It would be compelling to analyse ribosomal heterogeneity in mutants that show changes in their translatome such as the *ppp-1* worms. This could be achieved by using the RiboTag animals

to pull down ribosomes followed by the application of proteomic approaches to study their composition. The hypothesis of specialised ribosomes is further discussed in chapter 4.3.1. Together, a deep analysis of the translational changes in animals carrying Gcn(-) mutations is needed to further understand the mechanism behind the observed phenotypes on ageing and longevity.

4.2.3 What is the role of KIN-35 in ageing and longevity?

While the selectively translated putative kinase *kin-35* was shown to be essential in the Gcn(-)-driven longevity, its specific role and function to date stay unknown. To understand the mechanism by which *kin-35* mediates an extension of lifespan in the Gcn(-) context, an extensive genetic and biochemical analysis of *kin-35* would be necessary. Several open questions remain to be answered. First, as indicated by its sequence including a kinase domain, is KIN-35 a functional kinase? Next, which are its catalytically active residues? And further, what are potential targets and is the putative kinase function required for the *ppp-1*-mediated longevity? From the existing data we cannot finally conclude that KIN-35 acts as kinase generally and in the context of longevity specifically. Hence, these questions remain hypothetical. Potential experiments defining the future perspective regarding the role of KIN-35 in longevity include the biochemical tagging of KIN-35, enabling the analysis of its protein levels and, in case of a fluorescent tag, its tissue-specific expression. Further, a genetic targeted knockout of the putative kinase motif might shed further light on the potential kinase function of KIN-35 and after crossing to respective mutants its effect on *ppp-1* phenotypes. More generally, the global protein phosphorylation status has been successfully analysed in *C. elegans* before (Zielinska et al., 2009; Huang et al., 2018). Since the GO-term analysis of all translationally changed genes in *ppp-1* worms showed an enrichment in phosphorylation processes, the analysis of the phosphoproteome of *ppp-1* mutants might generally lead to the identification of downstream mediators of longevity. More specifically, the analysis of potential *kin-35* deletion mutants might identify putative KIN-35 target proteins and therefore it might specify the role of KIN-35 as kinase, mediating longevity in Gcn(-) animals. The *in vitro* analysis of recombinant KIN-35 would enable further strategies to analyse potential kinase activities and active substrates, discussion of which exceeds the scope of this work (Swinney and Haubrich, 2016). Lastly, to investigate how *kin-35* is translationally enhanced in *ppp-1* animals, one could genetically modify its 5'-UTR and therefore investigate the involvement of 5'-UTR structure in the mechanism behind the selective translation process. In all, the function of KIN-35 is poorly understood und hence, its role in longevity remains elusive. These caveats show the need for further studies regarding KIN-35.

4.2.4 Fine-tuning the ISR and it's impact on longevity

The longevity caused by the potential gain-of-function mutations in *ppp-1* prompts further questions. First, is the over-expression of *ppp-1* sufficient to cause an extension in lifespan? And second, are the mediated *ppp-1* effects driven by specific tissues? We aim to answer both questions by using the previously mentioned SKI LODGE system enabling CRISPR/Cas9-mediated tissue-specific expression of selected transgenes (Silva-Garcia et al., 2019). By

over-expressing *ppp-1* in a controlled way on a whole-body level using a SKI LODGE cassette driven by an endogenous promoter, we plan to answer the question if increasing *ppp-1* expression is sufficient for lifespan extension. Expressing wildtype and mutant *ppp-1* in SKI LODGE cassettes under tissue-specific promoters will show the potential sufficiency of respective tissue-specific expression of the different gene versions for worm longevity. As mentioned earlier, to further study tissue-specific responses to ISR inhibition in *ppp-1* or *eIF2*αS51A mutant worms, the here proposed RiboTag model will enable the analysis of translation in a tissue-specific context.

Another open question is the following: How do different levels of ISR modulation affect the here described Gcn(-)-mediated phenotypes? In conditions of elevated eIF2α phosphorylation levels during prion disease, fine-tuning the ISR precisely with ISRIB mediated neuron-protective effects. Halliday *et al.* (2015) hypothesised that maintaining sufficient translation of key factors while keeping the protective aspects of a functional ISR to a certain degree might be the key to these observations (Halliday et al., 2015). We speculate that a similar sweet spot of ISR inhibition might be also a key to healthy ageing and longevity. To study the hypothesis that a specific degree of ISR inhibition might be beneficial for longevity, one should further analyse the effects of different levels of ISR modulation on lifespan and selective translation. In addition, potential negative effects such as increased sensitivity to stress should be investigated. The lifespan extension of the phospho-dead *eIF2*αS51A worms was in a similar range as the *ppp-1* mediated longevity. This indicates that full inhibition as seen in the *eIF2*αS51A animals is not further driving longevity when compared with a partial ISR inhibition as seen in the *ppp-1* animals, that show a residual ISR activity level. Moreover, in the *eIF2*αS51A worms we could observe a hypersensitivity towards ER stress during development, showing a down-side of low eIF2α phosphorylation levels. In contrast to ISR inhibition, worms with phospho-mimicking *eIF2*αS51D mutations were only viable in a heterozygous state, were short-lived and showed further detrimental phenotypes. This was in consistence with the use of the ISR activating compound propafenone hydrochloride and a corresponding reduced lifespan. On the pharmacological level, we further could show an ISR inhibiting effect of the drug estradiol valerate on ATF-4::GFP reporter and eIF2α phosphorylation levels that was correlated with longevity. However, we did not perform a comprehensive analysis of dose effects of ISR modulating drugs. Together, it would be of great interest to test more states of ISR activity analysing not only lifespan and translation but also stress sensitivity. This could be achieved using different doses of the here identified ISR activating and inhibiting drugs. We speculate that a sweet spot of ISR modulation elicits a translational switch that promotes robustness and longevity.

4.2.5 ISR activity and translation during healthy ageing

Are the effects mediated by the mutations in *ppp-1* persistent or changing throughout worm life and specifically during ageing? Inhibiting the ISR using ISRIB in old mice not only increased neuronal function and memory but also caused a reduction of inflammatory processes in the brain (Krukowski et al., 2020). Since the here identified *ppp-1* mutations at least partially phenocopy the ISRIB-mediated effects, it would be interesting to analyse similar

phenotypes in aged *ppp-1* animals. In the study of Krukowski *et al.* (2020), an increase of ISR activity was measured during ageing, analysing ATF4 and phosphorylated GCN2 levels. This is in line with our data showing high ISR activity levels during worm ageing as measured by phospho-eIF2α levels. However, the *ppp-1* mutations did not rescue the high ISR activity in old worms (see Fig. 14) as observed for ISRIB-treated old mice (Krukowski et al., 2020). To consistently compare phenotypes, it would be interesting to additionally measure *atf-4* levels in old nematodes. Furthermore, memory could be tested in *C. elegans* using published protocols (Kauffman et al., 2011).

Focussing on translation during ageing, overall protein synthesis rates were reported to decrease during worm ageing (Kirstein-Miles et al., 2013) and reduced protein production is a well-studied cause of longevity, specifically in the context of dietary restriction (Hansen et al., 2007; Syntichaki et al., 2007; Tohyama et al., 2008; Pan et al., 2007; Essers et al., 2016; Karunadharma et al., 2015). However, due to the beneficial effect of ISR inhibition by ISRIB administration during diseases and healthy ageing, one could speculate that partially rescuing the low translation during ageing might be of benefit for organismal health (Chou et al., 2017; Jun Zhu et al., 2019; Halliday et al., 2015; Krukowski et al., 2020). As mentioned above, maintaining translation to a certain degree that allows sufficient translation of key factors on the one hand and protective UPR function on the other hand might be beneficial, at least in selected tissues such as the neurons (Halliday et al., 2015). Therefore, studying the effects of Gcn(-) mutations on translation during ageing is a compelling future perspective. It would be interesting to evaluate the effect of *ppp-1* mutations on overall and selective translation during ageing using polysome profiling, ribosome footprinting and eventually proteomics. Furthermore, our data showed that ISR inhibition by estradiol valerate feeding extended lifespan, even if the treatment was initiated late in life. The effect of estradiol valerate treatments starting at different points of life should be investigated on the level of translation. If selected tissues are sufficient to drive the phenotypes mediated by *ppp-1* mutations generally, studying these tissue-specific effects during ageing would also be of enhanced interest; this could for example be achieved by measuring tissue-specific translation using the here developed RiboTag worms. Together, tissue-specific and age-related effects of Gcn(-) mutations should be investigated to enhance our understanding of the role of the ISR and the translation initiation process in healthy ageing and longevity.

4.2.6 Gcn(-) mutations, selective translation and longevity in higher organisms

The ISR and translation initiation are both evolutionary conserved intracellular mechanisms. From our data, we ultimately concluded that in the nematode, tuning eIF2 activity and translation through genetic or pharmacological ISR inhibition caused longevity without a suppression of overall protein biosynthesis. We therefore speculate, that fine-tuning of eIF2 and translation might be a therapeutic approach to modulate the ageing process, especially in the light of other research on ISR modulation during ageing and disease (see chapter 3.2.4). Our final future perspective is therefore to study if our observations can be recapitulated in higher organisms. We hence aim to test if the here observed beneficial consequences of Gcn(-) mutations for worm health and lifespan hold true in mammals. First, the conservation of the

molecular Gcn(-) phenotypes should be studied in mouse or human cellular culture systems. Because the *ppp-1* mutations are not conserved in sequence, other known eIF2B mutations with a Gcn(-) effect (Hinnebusch, 2005), the over-expression of different eIF2B subunits and finally the *eIF2α*S51A mutations are currently being recapitulated in cellular systems in Dr. Martin Denzel's laboratory. In addition, ISRIB-mediated ISR inhibition and the downstream effects on translation are being analysed in mammalian cells. More studies are planned to deeply analyse changes in ISR activity, the translatome and the proteome during Gcn(-) conditions in the mammalian system to investigate the conservation of our findings in the nematode.

To further analyse the conservation of the novel Gcn(-) phenotypes observed in *C. elegans*, we aim to test if ISR inhibition is causing longevity in mice. The heterozygous *eIF2α*S51A mice showing increased learning and memory phenotypes could further be analysed for potential changes in lifespan (Costa-Mattioli et al., 2007). Interestingly, respective homozygous mouse mutants are not viable and die shortly after birth due to hypoglycemia, indicating a more complex reaction in response to a full ISR inhibition in mice as compared to worms (Scheuner et al., 2005). More therapeutically relevant and closer to the *ppp-1* mutant worms, ISRIB was shown to inhibit the ISR via eIF2B and, amongst many other effects, to rescue an age-induced reduction in neuronal function and memory (see chapter 3.2.4; Costa-Mattioli and Walter (2020); Krukowski et al. (2020)). Therefore, one of the most urgent questions arising from this work is if ISRIB administration in mice can extend lifespan. More recently, 2BAct has been developed as enhanced small drug-like eIF2B activator with similar potency to ISRIB. 2BAct was shown to have improved solubility and pharmacokinetics as compared to ISRIB, leading to a higher bioavailability and enabling oral administration. In accordance with ISRIB effects, feeding of 2BAct reversed the chronic ISR activation during VWM and prevented related pathologies (Wong et al., 2019). Consequently, next to studying ISRIB effects on lifespan, 2BAct administration in mice is another strategy to test if ISR inhibition can cause longevity and other effects such as selective translation in mammals. We hypothesise that specifically modulating the ISR and fine-tuning translation initiation in healthy organisms can extend lifespan not only in worms, but potentially also in higher organisms. Studying the effect of ISR inhibitors on lifespan in mice might unravel novel insights in promoting the healthy mammalian ageing process. In the future, ISR inhibition might be a viable option to also promote healthy ageing in humans. These intriguing possibilities are yet to be discovered.

4.3 The future of RiboTag worms

As mentioned previously, studying translation specifically in selected tissues would be a promising future direction to further analyse the phenotypes mediated by Gcn(-) mutations in *C. elegans*. The here generated RiboTag worms will enable such analyses. We so far optimised endogenous and neuron-specific RiboTag tools for successful studies of the respective translatomes and plan to use them in the Gcn(-) context. We next aim to expand the RiboTag toolbox by adding soma-, muscle- and eventually intestine-specific RiboTag worms. We generated respective worm lines, which are currently being characterised in depth exactly

following the NeuroRiboTag example described in this work. To generate a RiboTag strain with somatic expression of ^{FLAG}RPL-22, we inserted the *rpl-22* sequence into a SKI LODGE cassette under the control of the *eft-3* promoter and the *unc-54* 3'UTR. This promoter drives ubiquitous gene expression in all tissues but the germline. The potential MuscleRiboTag worms express FLAG-tagged RPL-22 from a SKI LODGE cassette under control of a *myo-3* promoter and an *unc-54* 3'UTR. An intestinal RiboTag line expressing ^{FLAG}RPL-22 under the intestine-specific *nep-14* promoter is currently in the making. To finally be able to conclude that the co-IP of assembled ribosomes with translated mRNAs is working from these lines, we aim to analyse the mRNAs derived by the co-IPs using RNAseq and the same bioinformatic pipeline that was successfully used in the NeuroRiboTag analysis. Together, we aim to generate a RiboTag *C. elegans* toolbox including not only the here described endogenous and neuronal RiboTag lines, but prospectively also lines to investigate the soma-, muscle- and intestine-specific translatomes in depth. We plan to make the so generated optimised RiboTag toolbox, the corresponding deep characterisation and the RiboTag IP protocols available to the whole *C. elegans* community.

4.3.1 RiboTag worms in a wider context

Originally, we aimed to use the RiboTag worms to analyse overall mRNAa translation in distinct tissues. Moreover, from a methodical point of view it would be interesting to combine the RiboTag IPs from different tissues with other applications to tackle more diverse research questions. For example, we could apply the nuclease digestion step of the ribosome footprinting approach to tissue-specific ribosomes isolated from RiboTag worms. This might enable detailed analyses of translational control with sub-codon resolution within specific tissues (Ingolia et al., 2009). Furthermore, it would be interesting to study tissue-specific mRNA association with monosomes or polysomes specifically. We therefore aim to combine the separation of monosomes and polysomes on a sucrose gradient with a subsequent RiboTag IP or vice versa. This combination might not be easy due to the use of very specific buffers for each method and the low stability of ribosomal complexes depending on intact RNA throughout the experiments. However, both ribosome profiling and RiboTag IP methods are well established and to our knowledge, combining both has not been done in *C. elegans* before, making it a worthwhile goal. This is of particular interest since studying monosome- and polysome-specific translation has gained attention lately. Recent studies showed that effective mRNA translation occurred not only in polysomes, but also in monosomes (Heyer and Moore, 2016). Furthermore, Biever *et al.* (2020) could show a subtissue-specific role of monosomal translation in the production of synaptic proteins in neuropils as compared to neuronal cell bodies. These results were acquired through a specific neuronal cell culture method, allowing the microdissection of neurites from cell bodies. This enabled the analysis of translation in the specific cell parts via polysome profiling and ribosome footprinting (Biever et al., 2020). As mentioned earlier, accurately separating tissues from *C. elegans* is not an established technique within the worm field, making similar studies impossible in the worm. Therefore, enabling the tissue-specific analysis of mRNA distribution to monosomes or polysomes would be a great add-on for our RiboTag toolbox.

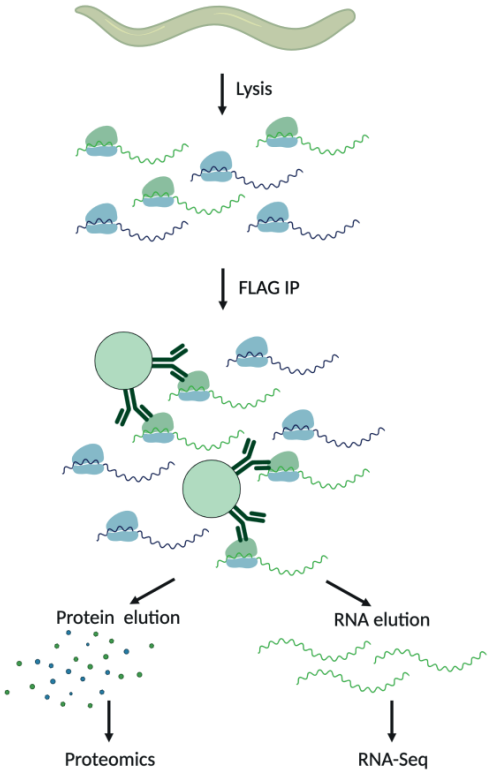

Figure 32: Schematic depiction of the RiboTag co-IP approach and possible downstream applications. While the elution of RNA from tissue-specific RiboTag co-IPs allows the analysis of mRNA translation from selected tissues, the elution of proteins for proteomic approaches might facilitate new research directions in the worm towards studying tissue-specific ribosomal heterogeneity.

Another topic that might be addressed with the RiboTag worms is the analysis of tissue-specific stoichiometries in ribosomal composition. By eluting fully assembled ribosomes from worm RiboTag co-IPs, tissue-specific ribosomal compositions could be analysed through subsequent quantification of ribosomal proteins by comparative proteomics (Fig. 32). The existence and role of specialised ribosomes in translation of selected mRNAs is more and more discussed recently. Ribosomes can be modified in several ways, for example through post translational modifications, rRNA modifications, different ribosome-associated proteins and presence or absence of core ribosomal proteins (Genuth and Barna, 2018). It has been shown that actively translating ribosomes can have different protein compositions and that heterogenous ribosomes translate different subpopulations of mRNAs (Shi et al., 2017; Simsek et al., 2017; Ferretti et al., 2017). For example, ribosomes enriched with specific proteins, such as RPL-10A, favour translation of mRNAs with internal ribosome entry sites (Shi et al., 2017). In ribosomes, RPS-26 is mediating Kozak sequence recognition. However, RPS-26 deficient ribosomes drive translation of selected mRNAs during stress (Ferretti et al., 2017). While these results can be seen as evidence of heterogeneous ribosomes translating selected mRNAs, many open questions remain: Which further ribosomal components and modifications enable specialised translation and how are specific mRNAs recognised by specialised ribosomes? Furthermore, do different tissues have distinct ribosomal compositions and might those change throughout different developmental stages or ageing? To identify specialised functions of heterogenous ribosomes, specific classes of mRNAs need to be biochemically matched with specific ribosomes (Haag and Dinman, 2019). We speculate that the tissue-specific RiboTag co-IP system from *C. elegans* combined with RNA sequencing and proteomic analyses will allow a careful biochemical characterisation of specialised ribosomes and their potential tissue-specificity. If we can show the *C. elegans* RiboTag system to be sufficient to identify heterogenous tissue-specific ribosomes, it would further be interesting to analyse ribosomal composition during ageing, as translation per se was shown to change during worm life (Kirstein-Miles et al., 2013). However, ribosome compositions were analysed during ageing in mice without showing any differences in ribosome protein stoichiometry in liver and three different brain tissues (Amirbeigiarab et al., 2019). Furthermore, an elegant study by Cenik *et al.* (2019) showed that during early larval development in *C. elegans*, tissue development occurs without specialised ribosomes. Instead, maternal ribosomes are sufficient for tissue diversification during embryogenesis (Cenik et al., 2019). Nevertheless, as described above, ribosome heterogeneity was shown to play a role in post-transcriptional control (Genuth and Barna, 2018). Ribosomal stoichiometry has not been investigated in depth for a wider range of tissues during ageing and upon conditions that alter translation such as the Gcn(-) mutations causing longevity through a translational switch, different cellular stresses or diseases that change translation rates. Therefore, the tissue-specific RiboTag worms might ease the systematic analysis of ribosome composition in different tissues during a variety of conditions from an *in vivo* model. In sum, we hypothesise that the isolation of fully assembled ribosomes and associated mRNAs from tissue-specific RiboTag worms will bring novel insights to the selective translation phenotype in Gcn(-) mutant worms. Further, the RiboTag toolbox has the potential to facilitate several new research directions regarding

translational regulation in *C. elegans*.

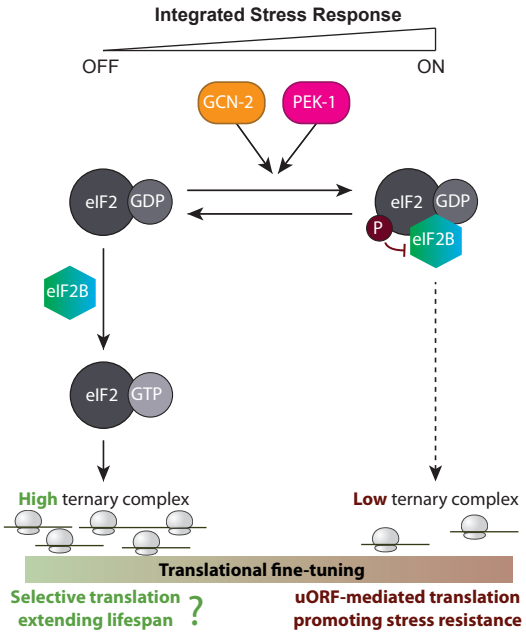

Figure 33: Regulation of ageing and longevity by a re-programming of translation. Fine-tuning of the ISR might enable different translational switches with distinct beneficial downstream effects.

4.4 Closing remarks

Shifting the balance from growth and reproduction to stress resistance is known to mediate longevity in a wide range of model organisms from yeast to mammals. Examples are the IIS and TOR pathways, which have antagonistic functions throughout life and serve as examples for the 'antagonistic pleiotropy theory' of ageing.

We found that ISR activity in *C. elegans* is crucial upon stress during development. However, if the animals are grown without the experimental application of cellular stress, genetic and pharmacological ISR inhibition caused an extension of lifespan that was independent of a down-regulation of overall mRNA translation. Based on our results, we speculate that a translational switch is mediating the observed lifespan extension rather than the ISR inhibition *per se*. Moreover, a permanent genetic or pharmacologic activation of the ISR shortened the lifespan of *C. elegans*.

From this, we propose that antagonistic ISR activity levels can facilitate cellular maintenance during stress or, unexpectedly, mediate a switch in translation that promotes longevity upon ISR inhibition (Fig. 33). The above mentioned future perspectives will elaborate on the role of the ISR and an ISR-mediated translational re-programming in ageing and longevity.

5 Materials and methods

5.1 Experimental Model: Worm Handling and Methods

5.1.1 *C. elegans* strains and culture

All *C. elegans* strains were maintained at 20 °C on nematode growth medium (NGM) agar plates seeded with the *Escherichia coli* (*E. coli*) strain OP50, unless indicated otherwise (Brenner, 1974). To provide an isogenic background in all mutant strains, they were outcrossed against the wildtype Bristol N2 strain. All strains used in this study are listed in chapter 5.4, including outcrossing information and source. Genotyping primers used in this study are listed in chapter 5.4. The strains *ppp-1(syb728)* II and *ppp-1(syb691)* II were generated by SunyBiotech (China) using CRISPR/Cas9; the correct sequence was verified by PCR and Sanger sequencing (Eurofins Genomics, Germany) All RiboTag strains including *rpl-22(wbm58)* II and *wbmIs99*[*rab-3p*::3xFLAG::*rpl-22*::SL2::wrmScarlet::*rab-3* 3'UTR] were generated by Anne Lanjuin, PhD, in the laboratory of assoc. Prof. William Mair (Harvard T.H. Chan School of Public Health).

5.1.2 Unbiased forward longevity screen

The longevity screen was performed with the temperature sensitive sterile strain CF512 *fer-15(b26)* II; *fem-1(hc17)* IV. L4 larvae were exposed to 0,3 % ethyl methane sulfonate (EMS, Sigma) in M9 buffer for 4 h at room temperature. After recovery overnight, young P0 adult animals were transferred to new plates. Singled F1 progeny were allowed to lay eggs overnight. In the next generation, singled F2 progeny were allowed to lay eggs for 16 h. After egg-laying, F2 worms were stocked at 15 °C. F3 eggs were heat shocked at 25 °C for 48 h to induce sterility and adult animals were scored twice a week for preliminary lifespan analysis. Mutants that outlived the non-mutagenized control by 20 % (maximum lifespan) were selected for regular demographic lifespan analyses to confirm the longevity phenotype. After the lifespan assays, mutants with a mean lifespan extension above 18 % compared to non-mutagenized CF512 controls were selected for whole genome sequencing.

5.1.3 Mutant mapping and sequence analysis

Genomic DNA of selected long-lived strains was prepared using the QIAGEN Gentra Puregene Kit. Whole genome sequencing was conducted on the Illumina HiSeq2000 platform. Paired-end 100 bp reads were used; the average coverage was larger than 16-fold. Sequencing outputs were analysed using the CloudMap Unmapped Mutant Workflow pipeline on Galaxy (Minevich et al., 2012). The WS220/ce10 *C. elegans* assembly was used as reference genome.

5.1.4 Lifespan assays

Gravid day 1 adults were allowed to lay eggs for 5 h. The offspring was used for lifespan analysis. The L4 stage was defined as day0 and more than 100 worms were used per strain and condition. Worms were kept at 20 °C on NGM plates seeded with OP50 *E. coli* at all times. The animals were transferred every second day to fresh plates until they reached

the post-reproductive stage. Scoring was performed every second day by monitoring (touch-provoked) movement and pharyngeal pumping. Animals in all RNAi lifespan assays were treated with RNAi from the young adult stage on and kept on NGM plates seeded with HT115 *E. coli* bacteria expressing control *luciferase* or candidate RNAi clones throughout the experiment. Animals in all lifespan assays on estradiol valerate (Est Val, Sigma), ISRIB (Sigma) or propafenone hydrochloride (Propa, Sigma) were transferred at the L4 stage to NGM plates containing 1 % DMSO (Sigma) and 20 μM Est Val/ISRIB/Propa or to control plates with 1 % DMSO only. Animals in lifespan assays on tunicamycin (TM, Sigma) were transferred on day 1 of adulthood to NGM plates containing 20 μg/mL TM and 1 % DMSO or control plates with 1 % DMSO only. Lifespan assays of heterozygous animals were performed on F1 hermaphrodites after crossing of mutant hermaphrodites to wildtype male animals. In all lifespan experiments, worms that had undergone internal hatching, vulval bursting, or worms crawling off the plates were censored. Throughout the experiment, strain and/or treatment was unknown to researchers. Data were assembled on completion of the experiment. Statistical analyses were performed with the Mantel-Cox log rank method in Prism (Version 8.2.0). All detailed statistics on the here performed lifespan assays are depicted in the appendix (see chapter 5.4, Tab. 8) or published in Derisbourg et al. (2021).

5.1.5 Outcrossing following longevity

To outcross EMS-mutagenised worm strains following the phenotype of longevity, a parental EMS-mutant CF512 worm line from the forward longevity screen was crossed to unmutagenised CF512 males. From successful crosses, 12 individually outcrossed strains in the F2 generation (that underwent two distinct outcrossing events each) were allowed to perform an egg lay on 12 new single plates each for lifespan analysis and on further plates for stocking at 15 °C. F3 eggs on a total of 144 plates for lifespan analyses were heat shocked at 25 °C for 48 h to induce sterility and adult animals were broadly scored twice a week for dead worms per plate. Analysing the maximum lifespan, mutants on plates that largely outlived the non-mutagenised control by at least two days were selected for whole genome sequencing. The genomic DNA of the respective stocked worms was prepared, pooled and a whole genome sequencing was performed and the results analysed as described earlier. Homozygous EMS SNPs were identified from the pooled data of the outcrossed worms and compared to the EMS SNPs from the original long-lived CF512 line. Only congruent EMS SNPs were further analysed. The number of remaining congruent SNPs divided by the number of EMS mutagenesis SNPs from the original long-lived CF512 strain indicated the success of this method.

5.1.6 The CRISPR/Cas9 generation of the *R160.6(wrm23)* allele

CRISPR/Cas9-mediated gene editing was performed using the recombinant Cas9 EnGen nuclease from *S. pyogenes* (NEB). Design of CRISPR guides was performed using the CRISPOR.org web tool specified for the use of Cas9 (Concordet and Haeussler, 2018). To induce SNPs via HDR, the repair template was designed following the recommendations of Paix et al. (2017). Single guide RNAs and tracrRNA were ordered from IDT genomics. In addition, linear repair templates were ordered as Ultramer DNA Oligos from IDT genomics. Guides targeting

the *dpy-10* gene were used as co-injection markers as recommended by Paix et al. (2017). Injections were performed using the following mix: 1 µL Cas9 (3.2 µg/µL), 2.5 µL tracrRNA (4 µg/µL), 0.4 µL *dpy-10* sgRNA (8 µg/µL), 0.5 µL target sgRNA (8 µg/µL), 1 µL target linear repair template (1 µg/µL), 0.25 µL KCl (1 M), 0.375 µL HEPES pH 7.4 (200 mM), H2O up to a total volume of 10 µL. The mix was incubated for 10 min at 37 °C to allow activation of the Cas9 enzyme.

Wildtype worms were used for injections of the CRISPR/Cas9 mix. L4 larvae or young adults were placed in a 20 µL drop of halocarbon oil (Sigma) on a 2 % agarose pad. Injections of the CRISPR/Cas9 mix were done using a Carl Zeiss Axio Imager Z1 microscope with a manual micromanipulator, connected to a microinjector (Femtojet4). When the offspring of injected worms showed a *dpy* phenotype in the F1 generation, siblings of the same parental animal were singled and genotyped for the desired gene edit.

Single guide RNA sequences:
dpy-10: CGCTACCATAGGCACCACG
R160.6(1): TCTACCACCGTAGTAAGACC
R160.6(2): CGCCTATACTCAAATAAATA

Repair template sequence *R160.6*:
gtaagtttttggaatttttgggaaagtaattaaaaatcgtatctatctgagCATAGGCAAACAAAATAGAATA-
TTACTCTATCATCGTAGCAAGACATGGAATACTATTAAAGTGGGCAAAAACGGGC

Red: Desired gene edit
Blue: Silent mutations to prevent re-cutting of Cas9
Green: (Mutated) PAM site
Underlined: Single guide RNA binding site

5.1.7 Thermotolerance assays

After an egg-lay, synchronised day 1 animals were transferred to 6 cm NGM plates containing OP50 *E. coli* and placed at 35 °C. Survival was scored for (touch-provoked) movement and pharyngeal pumping every two hours until no survivors were left. Worms with internal hatching, vulval bursting, and worms crawling off the plates were censored. Throughout the experiment, strain and/or treatment was unknown to the researcher. Unless stated otherwise, at least 3 independent experiments were performed, error bars represent means ±SD and assays were analysed by two-way ANOVA, Dunnett's or Sidak's post hoc test as indicated. All detailed statistics on the here performed thermotolerance assays are published in Derisbourg et al. (2021).

5.1.8 Dauer formation assays

Day 1 adult worms were allowed to lay eggs for 5 h at room temperature. For dauer formation assays, the offspring was kept at 27 °C for 60 h directly after the eggs were laid. Dauer and non-dauer animals were scored according to their appearance (with at least 50 animals per strain). Dauer and non-dauer stages were verified by performing microscopy of the worm cuticle (Zeiss Imager Z1, Axio Cam ICC5, Zen 2.3 pro software). Images were analysed with ImageJ.

5.1.9 Motility assays

Animals carrying the *unc-54P::Q35:YFP* (polyQ35) or the or the *unc-54P::α-syn* transgene were grown on NGM plates seeded with OP50 *E. coli*. For RNAi experiments, they were transferred at the L4 stage to plates seeded with HT115 bacteria expressing *luciferase* or candidate RNAi clones. On day 7 or day 8 of adulthood, motility was tested by transferring single worms to M9, where they were allowed to acclimatise for 30 sec, followed by the counting of body bends over 30 sec. At least 12 worms were scored per experiment, genotype and/or treatment. Throughout the experiment, strain and/or treatment was unknown to the researcher. Unless stated otherwise, at least 3 independent experiments were performed, error bars represent means ±SD and assays were analysed by one-way ANOVA, Dunnett's post hoc test.

5.1.10 RNAi experiments

For RNAi mediated knockdown of specific genes, HT115 bacteria carrying vectors for dsRNA of the target gene under a promotor inducible by isopropyl ß-D-1-thiogalactopyranoside (IPTG) and an ampicillin resistance were used. Bacteria were seeded on NGM plates containing 100 μg/μL ampicillin (Merck Millipore) and 1 mM IPTG (Roth). After egg-lay, worms were grown on regular NGM plates seeded with OP50 bacteria until the L4 stage and then transferred to RNAi plates. RNAi against *luciferase* was used as non-targeting control. All RNAi clones were obtained from the Ahringer and Vidal RNAi libraries (Kamath and Ahringer, 2003; Rual et al., 2004). Clones were validated by plasmid purification (QIAprep Spin Miniprep Kit, Qiagen) and sequencing using the L4440 seq RV primer.

5.1.11 Induction of endoplasmic reticulum stress with tunicamycin

To induce endoplasmic reticulum (ER) stress with tunicamycin, worms were transferred on NGM plates containing different tunicamycin concentrations and 1 % DMSO or control plates with 1 % DMSO only. Standard treatment was at 10 μg/mL tunicamycin for 6 h at day 1 of adulthood, unless stated otherwise. Treatments for lifespan experiments, the compound screen, and developmental tunicamycin resistance assays are specifically described in the respective methods subsections.

5.1.12 Induction of endoplasmic reticulum stress with dithiothreitol

Endoplasmic reticulum (ER) stress was induced by incubation of worms in dithiothreitol (DTT, Sigma). For the DTT treatment, an overnight culture of OP50 bacteria was 10-fold concentrated in S-basal medium. Worms were transferred into 250 μL S-basal medium, 200 μL 10-fold concentrated OP50 *E. coli* and 5 μL 1 M DTT diluted in S-basal. The volume was filled up to a total of 1 mL with S-basal (final DTT concentration: 5 mM). Worms were incubated for 2 h at 200 rpm. For further analysis by western blotting, worms were kept on ice after treatment and washed three times in M9 buffer. Finally, worms were shock-frozen in liquid nitrogen and kept at -80 °C until further use.

5.1.13 Developmental tunicamycin resistance assays

For developmental tunicamycin (TM) resistance assays, NGM plates supplemented with 10 μg/mL TM or indicated TM concentrations and control plates without TM were used (seeded with OP50 bacteria). 50 to 80 synchronised eggs per genotype and/or condition were added to the plates. Development to the adult stage was scored after 4 or 5 days. Unless stated otherwise, at least 4 independent experiments were performed, error bars represent means ±SEM and assays were analysed by two-way ANOVA, Sidak's post hoc test.

5.1.14 Selective RNAi screen for suppressors of *ppp-1* motility

Synchronised worms of the *ppp-1(wrm10)* strain crossed to *mLs133[unc-54P::Q35:YFP]* animals (*ppp-1* polyQ35) and control *mLs133[unc-54P::Q35:YFP]* worms (WT polyQ35) were grown to the L4 larval stadium. Animals were then placed on NGM plates containing 10 μM 5-Fluoro-2'-deoxyuridine (FUDR, Sigma) to inhibit the development of progeny. Plates were seeded with HT115 bacteria expressing selected RNAi clones to knock down specific genes in the nematodes. At day 8 of adulthood, the motility of *ppp-1* polyQ35 as well as WT polyQ35 worms was assessed on *luciferase* control RNAi and 66 RNAi treatments targeting mRNAs enriched in *ppp-1* polysomes. To test motility, 15 worms were picked into the center of a 10 mm circle on an unseeded NGM plate and their ability to leave the circle after one minute was scored. For more reliability, 4 experiments were performed for the control conditions (WT polyQ35 and *ppp-1* polyQ35 on *luciferase* RNAi; error bars represent means ±SD).

RNAi treatments rescuing the *ppp-1* polyQ35 motility phenotype to at least 50 % compared to the *ppp-1* polyQ35 control on *luciferase* RNAi were validated by full motility assays (without usage of FUDR) counting body bends over 30 seconds in liquid. In a counter screen, the effect of the RNAi treatments on WT polyQ35 animals was tested. To this end, young worms were treated as described before and the motility on day 6 of adulthood was scored as described above. If motility of WT polyQ35 worms treated with RNAi against candidate mRNAs was significantly lower compared to animals treated with *luciferase* RNAi, candidates were excluded from further analysis.

5.1.15 Worm imaging

For worm imaging, animals were arranged in stacks on unseeded NGM plates and kept on ice. Images were taken with a fluorescence microscope (Leica M165FC) and a camera (Leica DFC 3000G). Images were taken and analysed with the Leica Application Suite X (Version 3.4.1.17822), scale bars as indicated in the figures.

5.1.16 Compound screen

To identify compounds inhibiting the ISR, synchronised *atf-5P::GFP::unc-54 3'UTR* L4 animals were transferred to NGM plates without or with 4 μg/mL tunicamycin (TM). Furthermore, plates were supplemented with 1 % DMSO (Sigma) as control, or with 1 % DMSO and 20 μM estradiol valerate (Sigma), ISRIB (Sigma), GSK2606414 (Calbiochem), propafenone hydrochloride (Sigma), azadirachtin (Sigma) or estriol (Sigma), respectively. Day 1 animals were analysed by fluorescent microscopy as described above.

5.1.17 Pharyngeal pumping

Pharyngeal pumping rates of synchronised animals were measured at day 1 of adulthood by counting pharyngeal contractions per worm during 30 sec. Per experiment and genotype, at least 15 worms were analysed. Throughout the experiment, strain and/or treatment was unknown to the researcher. Error bars represent means ±SD.

5.1.18 Generation time

For generation time assays, synchronised eggs were allowed to develop to adult worms on single plates until they laid the first egg, which was defined as generation time. After 55 h, animals were scored every hour with 15 worms being analysed per experiment and genotype. Throughout the experiment, strain and/or treatment was unknown to the researcher. Error bars represent means ±SD.

5.1.19 Brood size assays

For brood size assays, synchronised L4 worms were placed on individual NGM plates seeded with OP50 bacteria. Worms were transferred to fresh plates every 24 h until no more eggs were laid. The number of viable progenies on each plate was counted and summed up per individual parental worm per day or in total. Per experiment, genotype and/or condition, at least 15 parental worms were analysed. Error bars represent means ±SD.

5.2 Molecular biology and biochemistry

5.2.1 RNA extraction and qRT-PCR (qPCR)

For qPCR analyses, day 1 worm samples or indicated samples from ribosome profiling were collected in TRI Reagent (Zymo) and frozen in liquid nitrogen. RNA extraction was performed using the Direct-zol RNA MicroPrep Kit (Zymo Research) according to the manufacturer's recommendations, followed by cDNA synthesis (iScript cDNA Synthesis Kit, BioRad).

qPCRs were performed using Power SYBR Green PCR Master Mix (Applied Biosystems) on a ViiA 7 Real-Time PCR System (Applied Biosystems). All primers used in this study can be found in chapter 5.4. Primers for the gene *act-1* were used as internal control. Unless stated otherwise, at least three independent experiments were performed, error bars represent means ±SEM and assays were analysed by two-way ANOVA, Tukey's post hoc test.

5.2.2 Western blotting

For Western blotting, day 1 worms were collected in M9 and snap frozen in liquid nitrogen. For protein extraction, worms were lysed in Ripa buffer (150 mM NaCl, 1 % NP40, 0.5 % sodium deoxycholate, 0.1 % SDS, 50 mM Tris-HCl, pH 8.0, completed with protease inhibitors), sonicated and spun down. The supernatant was taken to protein quantification by bicinchoninic acid assay (Pierce BCA Protein Assay Kit, Thermo Fisher). Equal amounts of protein were taken to NuPAGE LDS Sample Buffer (4X, ThermoFisher) containing 50 mM Dithiothreitol (DTT). Proteins were then separated by reducing sodium dodecyl sulfate-polyacrylamide gel electrophoresis (SDS-PAGE) and transferred to nitrocellulose membranes (AmershamTM Hybond ECL), followed by blocking with milk or bovine serum albumin (BSA) and antibody labelling with specific antibodies to phospho-eIF2α (Ser51) (Cell Signaling; 1:2.000 in 2 % BSA), puromycin (Merck Millipore; 1:10.000 in 5 % milk), Living Colors GFP (Clontech; 1:5.000 in 5 % milk), FLAG (Sigma; 1:5.000 in 3 % milk), RPS-6 (Abcam; 1:1.000 in 1 % BSA), α-tubulin (Sigma; 1:10.000 in 5 % milk) and histone H3 (Abcam; 1:10.000 in 5 % milk). Immunolabelling was visualised using chemiluminescence kits (ECL, Amersham Bioscience) on a Chemidoc MP Imaging System (Biorad) and analysed with the ImageLab Software (version 5.2, Biorad). Labelling was quantified with Image J (version 1.51) and Prism (version 8.2.0). For Western blot analyses of compound-feeding experiments, worms were fed after hatching with 20 μM Est Val and 1 % DMSO, or 1 % DMSO only. ER stress by DTT or TM was induced as described above. For Western blot analysis at day 6 of adulthood (and corresponding day 1 control experiments), worms were transferred to NGM plates containing 10 μM 5-Fluoro-2'-deoxyuridine (Sigma) at the L4 stadium. The collection of the Western blot samples was conducted at the same time for day 1 and day 6 animals. Unless stated otherwise, at least 4 independent experiments were performed, error bars represent means ±SEM and assays were analysed by one-way ANOVA, Tukey's or Dunnett's post hoc test as indicated.

5.2.3 35S-methionine labelling

To monitor translation rates, 35S-methionine labelling was performed based on Hansen et al. (2007). OP50 bacteria were cultured overnight in LB medium (1 mL/sample) containing 15 μCi of 35S-methionine and concentrated 10-fold. synchronised day 1 worms were added to the mix and incubated for 3 h at room temperature. Worms were washed twice with S-basal and incubated in non-radioactive OP50 (10-fold concentrated). Worms were washed twice with S-basal medium and flash frozen three times in liquid nitrogen. Worm pellets were boiled in 100 μL 1 % SDS and centrifuged 2 min at 2000 g to remove cuticles. Supernatants were submitted to trichloroacetic acid precipitation. Protein pellets were neutralized with 20 μL of

0,2 M NaOH. Proteins were solubilized with 180 μL of 8 M urea; 4 % chaps; 1 % DTT. Protein concentrations were measured using Bradford reagent and 35S radioactivity was measured by liquid scintillation. Unless stated otherwise, at least 5 independent experiments were performed, error bars represent means ±SEM and assays were analysed by one-way ANOVA, Dunnett's post hoc test.

5.2.4 Surface sensing of translation (SUnSET), puromycin incorporation

To monitor protein synthesis in a non-radioactive manner using puromycin incorporation and detection based on Schmidt et al. (2009), day 1 worms were collected in M9 and once washed into S-basal medium. For the puromycin treatment, an overnight culture of OP50 bacteria was 10-fold concentrated in S-basal medium. Worms were then transferred into 250 μL S-basal medium, 200 μL 10-fold concentrated OP50 and 50 μL 10 mg/mL puromycin diluted in S-basal. The volume was filled up to a total of 1 mL with S-basal (final puromycin concentration: 0,5 mg/mL). Worms were incubated for 3 h at 200 rpm. Afterwards, they were washed 3 times in S-basal and snap-frozen in liquid nitrogen. Worms were kept on ice after the puromycin treatment. Protein extraction and Western blot using anti-puromycin antibody (Merck Millipore) was performed as described before.

5.2.5 Polysome profiling

For the analysis of translation via polysome profiling based on Großhans and Ding (2009), synchronised gravid day 1 adults were grown on NGM plated seeded with OP50. Per genotype and replicate, ∼12000 worms were harvested and washed twice with M9, once with M9 supplemented with 1 mM cycloheximide (Sigma) and once with lysis buffer (20 mM Tris pH 8.5, 140 mM KCl, 1.5 mM MgCl2, 0.5 % Nonidet P40, 1 mM DTT, 1 mM cycloheximide). Worms were pelleted and resuspended in 350 μL cold lysis buffer supplemented with 1 % sodiumdeoxycholate (DOC, Sigma). Resuspended worms were lysed using a chilled Dounce homogenizer. Ribonuclease inhibitor RNasin (Promega) was added to samples used for RNA sequencing or quantitative PCR (qPCR) at a concentration of 0,4 U/μL. Samples were then mixed and incubated on ice for 30 min, followed by a centrifugation step (12000 g, 10 min, 4 °C) for clearance. The pellet was discarded and the RNA concentration of the supernatant was estimated by absorbance measurement at 260 nm.

To prepare sucrose gradients, 15 % (w/v) and 60 % (w/v) sucrose solutions were prepared in basic lysis buffer (20 mM Tris pH 8.5, 140 mM KCl, 1.5 mM MgCl2, 1 mM DTT, 1 mM cycloheximide). Linear sucrose gradients were produced using a Gradient Master (Biocomp). Equivalent amounts of sample (around 400 μg RNA) were loaded on the gradient and centrifuged at 39000 g for 3 h at 4 °C, using an Optima L-100 XP Ultracentrifuge (Beckman Coulter) and the SW41Ti rotor. To analyse the sample on the gradient during fractionation, absorbance at 254 nm was measured and recorded (Econo UV monitor EM-1, Biorad) using the Gradient Profiler software (version 2.07). Gradient fractionation was performed from the top down using a Piston Gradient Fractionator (Biocomp) and a fraction collector (Model 2110, Biorad). Gradients were fractionated in 20 fractions of equal volume. In an initial experiment, the ribosomal fractions were validated by analyzing RNA from each fraction via

agarose gel electrophoresis. The 18 S and 28 S rRNA signals were used as indicators for the 40 S ribosomal subunit, the 60 S ribosomal subunit and fully assembled ribosomes. Quantification of the ribosomal complexes was performed using Image J and statistically analysed with Prism. Unless stated otherwise, at least 4 independent experiments were performed, error bars represent means ±SD and assays were analysed by two-way ANOVA, Dunnett's post hoc test.

For more precise analysis of ribosomal fractions, they were collected by hand according to their absorbance profile; for RNAseq and qPCR analyses, one fraction for 80 S ribosomes and one for polysomes (excluding disomes) was collected per sample. RNA extraction from total lysates and from each fraction was performed using the Direct-zol RNA MicroPrep Kit (Zymo Research) according to the manufacturer´s recommendations.

5.2.6 Polysome sequencing

For polysome sequencing, monosome extracts, polysome extracts (without disomes), and corresponding total RNA were collected as detailed above. cDNA libraries were generated with ribosomal RNA depletion at the Cologne Center for Genomics and sequenced on the Illumina HiSeq2000 platform.

For data analysis, raw reads from all RNAseq and polysome sequencing replicates were mapped to the *C. elegans* reference genome (ENSEMBL 91) using HISAT2 (v2.1.0; Kim (2015)). After guided transcriptome assembly with StringTie (v1.3.4d), transcriptomes were merged with Cuffmerge and quantification was performed with Cuffquant (Pertea et al., 2015). The analysis for differential gene expression for total, monosomal and polysomal RNA was performed with Cuffdiff (Cufflinks v2.2.1; Trapnell et al. (2012, 2010)). To analyse the translatome, the abundance of each mRNA in the polysomal fraction was normalized to its abundance in the total input mRNA. Respective normalized values were used to identify changes between different conditions using Student's t-test. For further analyses, we only included the mRNAs that were found significantly changed in both *ppp-1* mutants. For each mRNA, the mean p-values and the mean log-2 fold change of both *ppp-1* mutants were used. David analysis was performed to identify significantly enriched gene ontology terms (Fresno and Fernandez, 2013). The RNA sequencing data from this work have been deposited in NCBI's Gene Expression Omnibus and are accessible through GEO Series accession number GSE144607. Furthermore, detailed analysed sequencing results are published in the supplementary materials in Derisbourg et al. (2021).

5.2.7 TCA protein precipitation from polysome profiling fractions

For trichloroacetic acid (TCA) precipitation of ribosomal proteins from polysome profiling experiments, fractions of 600 µL were collected from the polysome profiling. For protein precipitation of each 600 µL fraction, 100 µL of 100 % TCA and 800 µL cold acetone were added. Precipitation was performed at -80 °C over night. Samples were thawed carefully on ice and centrifuged at 16.000 g for 10 min at 4 °C. Precipitates were washed two times with 900 µL cold acetone. Acetone was removed by pipetting and evaporation for 1 h at room temperature. Subsequently, pellets were resuspended in 50 µL of 1x Laemmli Sample Buffer

(BioRad) with 2.5 % v/v β-mercaptoethanol, incubated for 10 min with constant shaking on 95 °C and sonicated twice for 2 min before analysis via SDS-PAGE and western blot as described earlier.

5.2.8 Immuno-precipitation of tagged ribosomes

Protein G coated dynabeads (ThermoFisher) were incubated with 0.1 μg monoclonal anti-FLAG antibody (Sigma) per μL of dynabeads at 4 °C and constant rotation over night. Per RiboTag co-IP, 30.000 synchronised day 1 worms were collected in M9 buffer and washed two times in M9 and one final time in M9 including 1 mM cycloheximide (Sigma). Samples were then washed with lysis buffer prepared in nuclease free water (10 mM 4-(2-hydroxyethyl)-1-piperazineethanesulfonic acid (HEPES) pH 7.4, 150 mM KCl, 5 mM MgCl2, 0.5 mM DTT, 1 mM cycloheximide, EDTA free Protease Inhibitor). Worms were pelleted at 2,000 g for 2 min and the supernatant was discarded. The residual 500 μL worm pellet was shock frozen by dropping it into liquid nitrogen in fractions of 20 μL. The resulting frozen worm pearls were carefully lysed using the TissueLyserII (Qiagen) for twice 1 min at 30 Hz using metal beads of 5 mm diameter. Keeping all parts and the samples RNase-free and ice-cold at all times was crucial. Lysed worm powder was thawed on ice in a final volume of 3.75 ml (with approximately 8 worms/ μL) lysis buffer including 0.5 % v/v NP-40 (Sigma), 0.4 U/μL RNasin (Promega), 10 mM ribonucleoside vanadyl complex (RVC by NEB), 33 mM 1,2-diheptanoyl-sn-glycero-3-phosphocholine (DHPC by Merck) and 1 % w/v sodium deoxycholate (Sigma). Samples were incubated for 30 min on ice. After centrifugation at 12.000 g for 10 min at 4 °C, the supernatant was further used and the pellet was discarded. As total RNA input sample, 200 μL of post-mitochondrial supernatant was mixed with 200 μL of RLT buffer (Qiagen RNeasy Kit) including 1 % v/v β-mercaptoethanol. This total RNA input sample was then vortexed, incubated for 10 min at room temperature and stored at -80 °C. The remaining post-mitochondrial supernatant was next pre-cleared with washed 10 μL protein G coated Dynabeads without coupled antibody for at least 1 h. Samples were then incubated with FLAG-antibody-coupled beads for at least 2 h at 4 °C and constant rotation. Supernatant was taken and frozen at -80°C as control. Beads were washed three times with wash buffer (10 mM HEPES pH 7.4, 350 mM KCl, 5 mM MgCl2, 1 % v/v NP-40, 0.04 U/μL RNasin). Afterwards, beads were either incubated with 50 μL of 1x Laemmli Sample Buffer (BioRad) including 2.5 % v/v β-mercaptoethanol, followed by elution of proteins at 95°C for 10 min and analysis by SDS-PAGE and Western blotting. Alternatively, the beads were incubated in 350 μL of RLT buffer (Qiagen RNeasy Kit) including 1 % v/v β-mercaptoethanol for 10 min at room temperature. The eluate was separated from the beads and RNA purification was performed using the Qiagen RNeasy Kit following the manufacturer's protocol and analysed using Agilent Technologies 2200 TapeStation System or further analysed in RNA sequencing experiments.

5.2.9 RNA sequencing from RiboTag co-IP samples

For RNA sequencing from RiboTag co-IP samples, RNA was eluted and purified as described above. RNA sequencing was performed in collaboration with the laboratory of assoc. Prof.

William Mair (Harvard T.H. Chan School of Public Health) and the Molecular Biology Core Facility at the Dana-Farber Cancer Institute (Boston). All RNA samples were processed using a Kapa mRNA library preparation and sequenced on an Illumina sequencing platform.

Raw reads were quantified using the alignment free quantification tool kallisto version 0.45.0 and the reference genome WBcel235 (Bray et al., 2015). Gene counts were imported to R version 3.5.1 and normalised to library size using DESeq2 version 1.22.2 (Love et al., 2014). General differential gene expression was determined using DESeq2. Functional enrichment of differentially expressed genes was performed using the DAVID API using all genes as background (Huang da et al., 2009). Polysome Fractionation or RiboTag IP samples were normalised to total input RNA by dividing data through total input for each replicate respectively. The Mann-Whitney-U test was performed for each gene comparing two groups using the scipy.stats python package. Functional enrichment of differentially expressed genes was performed using the DAVID API (background: all genes).

For the principle component analyses (PCAs), the principal components were calculated on individual log2(ratios) using only genes present in all samples relevant for the comparison using the R function prcomp. The first and second component were visualised as a scatterplot also indicating the variance depicted by each component on the axis label. The scatterplots show the average ratio after log2 transformation for the respective group. These figures only show genes present in both groups. The R function used for the plot is SmoothScatter. The Spearman Rank Correlation coefficient was calculated using only the genes represented by the scatterplot. The dotted green line represents the diagonal y = x. Darker blue represent a higher density of genes at this location.

For a normalisation of immuno-precipitation counts to input counts from NeuroRiboTag experiments, counts were normalised using EdgeR's upper quartlie normalisation. RPKMs were calculated for each group and genes were kept with an rpkm greater than 1 in both groups. The log2fc of input versus total RNA counts was calculated. The top 5 % of highest or lowest log2fc was submitted to a Tissue Enrichment Analysis (TEA, Angeles-Albores et al. (2016)). TEAs tested a *C. elegans*-specific tissue ontology for enrichment of specific terms.

5.3 Statistics

Unless stated otherwise, results are presented as means +/±SD or means +/±SEM. Unless noted otherwise, statistical tests were performed using one-way or two-way ANOVA with Sidak's, Dunnet's or Tukey's multiple comparison test. Significance levels are $*p<0.05$, $**p<0.01$, and $***p<0.001$ versus WT control unless otherwise noted. Experiments were carried out with at least three biological replicates unless noted otherwise.

5.4 Worm strains and primers used in this study

Table 1: Worm strains used in this study.

Strain name	Genotype	Backcrossed to N2	Source
MSD331	Bristol N2		CGC
CF512	*fer15(b26) II; fem-1(hc17) IV*	n/a	CGC
MSD383	*R160.6(wrm23) X*	n/a	this study
MSD283	*ppp-1(wrm10) II*	4x	this study
MSD310	*ppp-1(wrm15) II*	4x	this study
SYB691	*ppp-1(syb691) II* CR-N295I (wrm10)	n/a	Suny Biotech
SYB728	*ppp-1(syb728) II* CR-L216F (wrm15)	n/a	Suny Biotech
MSD513	*iftb-1(wrm53) I*	4x	this study
MSD275	*gcn-2(wrm4) II*	4x	this study
MSD302	*pek-1(wrm7) X*	4x	this study
MSD413	*gcn-2(wrm4) II; pek-1(wrm7) X*	n/a	this study
MSD535	*gcn-2(ok871) II*	2x	this study
MSD511	*pek-1(ok275) X*	2x	this study
MSD412	*gcn-2(ok871) II; pek-1(ok275) X*	2x	this study
MSD512	*gcn-2(wrm4) II; pek-1(ok275) X*	n/a	this study
MSD536	*gcn-2(ok871) II; pek-1(wrm7) X*	n/a	this study
MSD441	*mls133[unc-54p::Q35:YFP]*	2x	CGC
MSD442	*mls133[unc-54p::Q35:YFP]; ppp-1(wrm10)*	2x	this study
MSD457	*mls133[unc-54p::Q35:YFP]; ppp-1(wrm15)*	2x	this study
MSD505	*pkIs2386[Punc-54::alpha-synuclein::YFP; unc-119(+)]*	2x	this study
MSD506	*pkIs2386[Punc-54::alpha-synuclein::YFP; unc-119(+)]; ppp-1(wrm10)*	2x	this study
MSD507	*pkIs2386[Punc-54::alpha-synuclein::YFP; unc-119(+)]; ppp-1(wrm15)*	2x	this study
MSD406	*rsks-1(sv31) III*	2x	Hubbard lab
MSD538	*sybEx[M04F3.3P::M04F3.3::mCherry;unc-54 3'UTR]* line 1	n/a	Suny Biotech
MSD539	*sybEx[M04F3.3P::M04F3.3::mCherry;unc-54 3'UTR]* line 2	n/a	Suny Biotech
MSD540	*sybEx[M04F3.3P::M04F3.3::mCherry;unc-54 3'UTR]* line 3	n/a	Suny Biotech
MSD314	*ldIs(T04C10.4/atf-4P::GFP::unc-54 3'UTR)*	2x	Blackwell lab
MSD317	*ldIs(T04C10.4/atf-4P::GFP::unc-54 3'UTR); ppp-1(wrm10) II*	2x	this study
MSD456	*ldIs(T04C10.4/atf-4P::GFP::unc-54 3'UTR); ppp-1(wrm15) II*	2x	this study
SYB1385	*Y37E3.10a(syb1385) I*	2x	Suny Biotech
PHX1567	*Y37E3.10a(syb1567)/hT2[bli-4(e937)let-?(q782)qIs48] I*	2x	Suny Biotech
MSD498	*daf-2(e1370) III*	4x	this study
MSD340	*daf-16(mu86) I*	4x	this study
WBM	Bristol N2		Mair lab
WBM1344	*rpl-22(wbm58) II*	6x to WBM WT	Mair lab
WBM1340	*wbmIs99[rab-3p::3XFLAG::rpl-22::SL2::wrmScarlet::rab-3 3'UTR] IV*	6x to WBM WT	Mair lab
MSD211	EMS mutant strain used for outcrossing following longevity	n/a	this study
MSD104	EMS mutant strain containing a *daf-2* mutation	n/a	this study
MSD212	EMS mutant strain containing a *daf-2* mutation	n/a	this study
MSD305	EMS mutant strain containing a *daf-2* mutation	n/a	this study
MSD167	EMS mutant strain containing a *daf-2* mutation	n/a	this study
MSD055	EMS mutant strain containing a *daf-2* mutation	n/a	this study
MSD155	EMS mutant strain containing a *daf-2* mutation	n/a	this study
MSD121	EMS mutant strain containing a *che-3* mutation	n/a	this study
MSD202	EMS mutant strain containing a *che-3* mutation	n/a	this study
MSD097	EMS mutant strain containing a *che-3* mutation	n/a	this study
MSD215	EMS mutant strain containing a *che-3* mutation	n/a	this study
MSD009	EMS mutant strain containing an *osm-3* mutation	n/a	this study
MSD218	EMS mutant strain containing an *ife-2* mutation	n/a	this study
MSD306	EMS mutant strain containing an *ife-2* mutation	n/a	this study
MSD295	EMS mutant strain containing an *ifg-1* mutation	n/a	this study
MSD076	EMS mutant strain containing an *ifg-1* mutation	n/a	this study

Table 2: Genotyping methods and primers used in this study.

Genotype	Genotyping Method	Primer sequence
ppp-1(wrm10) II *ppp-1(wrm15) II* *gcn-2(wrm4) II* *pek-1(wrm7) X*	TaqMan SNP mapping	Manufactured by Applied Biosysems
ppp-1(syb691) II CR-N295I (wrm10)	PCR	For TCCTTGTCAATCTGAATGGA Rev CCATCGATCAAATTAACTTCA
ppp-1(syb728) II CR-L216F (wrm15)	PCR	For GCAGTTACAAATCCATTTT Rev CCTTAATAATTCTAATTTTTACA
iftb-1(wrm53) I	PCR	CGTAATGTGCCATACTTGCAAG CTCAAAACACGAATCGAATGAG
gcn-2(ok871) II	PCR	For GCATGACATGGCAATGATTCATCG Rev GTACTTTGCAATGATTTTGAGGCG
pek-1(ok275) X	PCR	For CTGAGAAGGCAACGCTCTCT Rev ATCACCGCTACTCTGGATGG
eIF2α(syb1385) I	PCR	For ATTGGTAGTTTATCTCATTTAAT Rev TTCTCCTTAATATCTGCACT
rpl-22(wbm58) [EndoRiboTag]	PCR	For CGTTTATTCCTGAAGATGCCG Rev GAGAATTCCATCCTCAACTGG
wbmIs99 [NeuroRiboTag]	PCR	For CTACAGTAGCCCTATTTTCAGATGAC Rev CGTGTCCGTTCATGGATCCCTCCATGTG-GACCTTGAAACGCATGAACTCCTTGATA

Table 3: RT-qPCR primers used in this study.

Target gene	RT-qPCR primer sequence
act-1	For CTACGAACTTCCTGACGGACAAG Rev CCGGCGGACTCCATACC
kin-35	For GGTTGAATATTGGTGAGGAGGTTGT Rev TGCCACCATGATCTCTCTTTCAATC
hsp-4	For GTGGCAAACGCGTACTGTGATGA Rev CGCAACGTATGATGGAGTGATTCT
crt-1	For TGTGGCAGGTCAAGTCAGGAAC Rev TTTCTTCGTCGGCCTTCTCCTTC
dnj-27	For GAGAGCTTGCAGAGGTTATTGGAG Rev GCATCATTGGCAAGCATCCATACG
T14G8.3	For GGATCAAGCTAATGAGCAGCAGAC Rev TGACAGGTTTACAGTTCCGATGC
dod-8	For ACAGGATGTCTTCAAAAGGAATATGG Rev TTGCTGGGGTGATAGCTTGG
sod-3	For CACGAGGCTGTTTCGAAAGG Rev GAATTTCAGCGCTGGTTGGA

References

Abastado, J. P., Miller, P. F., Jackson, B. M., and G., H. A. (1991). Suppression of ribosomal reinitiation at upstream open reading frames in amino acid-starved cells forms the basis for GCN4 translational control. *Molecular and Cellular Biology*, 11(1).

Achenbaum, W. A. and Levin, J. S. (1989). What Does Gerontology Mean? *The Gerontologist*, 29.

Adomavicius, T., Guaita, M., Zhou, Y., Jennings, M. D., Latif, Z., Roseman, A. M., and Pavitt, G. D. (2019). The structural basis of translational control by eIF2 phosphorylation. *Nat Commun*, 10(1):2136.

Ahmet, I., Wan, R., Mattson, M. P., Lakatta, E. G., and Talan, M. (2005). Cardioprotection by intermittent fasting in rats. *Circulation*, 112(20):3115–21.

Albert, A. E., Adua, S. J., Cai, W. L., Arnal-Estape, A., Cline, G. W., Liu, Z., Zhao, M., Cao, P. D., Mariappan, M., and Nguyen, D. X. (2019). Adaptive Protein Translation by the Integrated Stress Response Maintains the Proliferative and Migratory Capacity of Lung Adenocarcinoma Cells. *Mol Cancer Res*, 17(12):2343–2355.

Allmeroth, K., Horn, M., Kroef, V., Miethe, S., Muller, R. U., and Denzel, M. S. (2020). Bortezomib resistance mutations in PSMB5 determine response to second-generation proteasome inhibitors in multiple myeloma. *Leukemia*.

Amirbeigiarab, A., Kiani, P., Velazquez Sanchez, A., Krisp, C., Kazantsev, A., Fester, L., Schlüter, H., , and Ignatova, Z. (2019). Invariable stoichiometry of ribosomal proteins in mouse brain tissues with aging. *Proc Natl Acad Sci U S A*, 116(49):24907.

Angeles-Albores, D., RY, N. L., Chan, J., and Sternberg, P. W. (2016). Tissue enrichment analysis for C. elegans genomics. *BMC Bioinformatics*, 17(1):366.

Anisimov, V. N., Berstein, L. M., Egormin, P. A., Piskunova, T. S., Popovich, I. G., Zabezhinski, M. A., Tyndyk, M. L., Yurova, M. V., Kovalenko, I. G., Poroshina, T. E., and Semenchenko, A. V. (2008). Metformin slows down aging and extends life span of female SHR mice. *Cell Cycle*, 7(17):2769–73.

Apfeld, J. and Kenyon, C. (1999). Regulation of lifespan by sensory perception in Caenorhabditis elegans. *Nature*, 402(6763):804–9.

Apfeld, J., O'Connor, G., McDonagh, T., DiStefano, P. S., and Curtis, R. (2004). The AMP-activated protein kinase AAK-2 links energy levels and insulin-like signals to lifespan in C. elegans. *Genes Dev*, 18(24):3004–9.

Arantes-Oliveira, N., Apfeld, J., Dillin, A., and Kenyon, C. (2002). Regulation of Life-Span by Germ-Line Stem Cells in Caenorhabditis elegans. *Science*, 295.

Baker, B. M., Nargund, A. M., Sun, T., and Haynes, C. M. (2012). Protective coupling of mitochondrial function and protein synthesis via the eIF2alpha kinase GCN-2. *PLoS Genet*, 8(6):e1002760.

Basisty, N., Meyer, J. G., and Schilling, B. (2018). Protein Turnover in Aging and Longevity. *Proteomics*, 18(5-6):e1700108.

Ben-Shem, A., Garreau de Loubresse, N., Melnikov, N., Jenner, L., Yusupova, G., and Yusupov, M. (2011). The Structure of the Eukaryotic Ribosome at 3.0 A Resolution. *Science*, 334.

Ben-Zvi, A., Miller, E. A., and Morimoto, R. I. (2009). Collapse of proteostasis represents an early molecular event in Caenorhabditis elegans aging. *Proc Natl Acad Sci U S A*, 106(35):14914–9.

Biever, A., Glock, C., Tushev, G., Ciirdaeva, E., Dalmay, T., Langer, J. D., and Schuman, E. M. (2020). Monosomes actively translate synaptic mRNAs in neuronal processes. *Science*, 367.

Bjedov, I., Toivonen, J. M., Kerr, F., Slack, C., Jacobson, J., Foley, A., and Partridge, L. (2010). Mechanisms of life span extension by rapamycin in the fruit fly Drosophila melanogaster. *Cell Metab*, 11(1):35–46.

Bodkin, N., Alexander, T., Ortmeyer, H., Johnson, E., , and Hansen, B. (2003). Mortality and Morbidity in Laboratory-maintained Rhesus Monkeys and Effects of Long-term Dietary Restriction. *Journal of Gerontology*, 58A(3).

Bray, N., Pimentel, H., Melsted, P., and Pachter, L. (2015). Near-optimal RNA-Seq quantification. *arXiv preprint*.

Brenner, S. (1974). The genetics of Caenorhabditis elegans. *Genetics*, 77.1.

Bronstein, R., Capowski, E. E., Mehrotra, S., Jansen, A. D., Navarro-Gomez, D., Maher, M., Place, E., Sangermano, R., Bujakowska, K. M., Gamm, D. M., and Pierce, E. A. (2020). A combined RNA-seq and whole genome sequencing approach for identification of non-coding pathogenic variants in single families. *Hum Mol Genet*, 29(6):967–979.

Brown, M. K., Chan, M. T., Zimmerman, J. E., Pack, A. I., Jackson, N. E., and Naidoo, N. (2014). Aging induced endoplasmic reticulum stress alters sleep and sleep homeostasis. *Neurobiol Aging*, 35(6):1431–41.

Bundesamt, S. (2017). Gesundheit: Todesursachen in Deutschland. Report 2120400157004.

Bürger, M. (1960). Altern und krankheit als problem der biomorphose. *Edition Leipzig*.

Campbell, S. G., Hoyle, N. P., and Ashe, M. P. (2005). Dynamic cycling of eIF2 through a large eIF2B-containing cytoplasmic body: implications for translation control. *J Cell Biol*, 170(6):925–34.

Canto, C., Gerhart-Hines, Z., Feige, J. N., Lagouge, M., Noriega, L., Milne, J. C., Elliott, P. J., Puigserver, P., and Auwerx, J. (2009). AMPK regulates energy expenditure by modulating NAD+ metabolism and SIRT1 activity. *Nature*, 458(7241):1056–60.

Canver, M. C., Smith, E. C., Sher, F., Pinello, L., Sanjana, N. E., Shalem, O., Chen, D. D., Schupp, P. G., Vinjamur, D. S., Garcia, S. P., Luc, S., Kurita, R., Nakamura, Y., Fujiwara, Y., Maeda, T., Yuan, G. C., Zhang, F., Orkin, S. H., and Bauer, D. E. (2015). BCL11A enhancer dissection by Cas9-mediated in situ saturating mutagenesis. *Nature*, 527(7577):192–7.

Cenik, E. S., Meng, X., Tang, N. H., Hall, R. N., Arribere, J. A., Cenik, C., Jin, Y., and Fire, A. (2019). Maternal Ribosomes Are Sufficient for Tissue Diversification during Embryonic Development in C. elegans. *Dev Cell*, 48(6):811–826 e6.

Chen, X., Feng, X., and Guang, S. (2016). Targeted genome engineering in Caenorhabditis elegans. *Cell & Bioscience*, 6(1).

Chou, A., Krukowski, K., Jopson, T., Zhu, P. J., Costa-Mattioli, M., Walter, P., and Rosi, S. (2017). Inhibition of the integrated stress response reverses cognitive deficits after traumatic brain injury. *Proc Natl Acad Sci U S A*, 114(31):E6420–E6426.

Cnop, M., Toivonen, S., Igoillo-Esteve, M., and Salpea, P. (2017). Endoplasmic reticulum stress and eIF2alpha phosphorylation: The Achilles heel of pancreatic beta cells. *Mol Metab*, 6(9):1024–1039.

Colla, E., Jensen, P. H., Pletnikova, O., Troncoso, J. C., Glabe, C., and Lee, M. K. (2012). Accumulation of toxic alpha-synuclein oligomer within endoplasmic reticulum occurs in alpha-synucleinopathy in vivo. *J Neurosci*, 32(10):3301–5.

Concordet, J. P. and Haeussler, M. (2018). CRISPOR: intuitive guide selection for CRISPR/Cas9 genome editing experiments and screens. *Nucleic Acids Res*, 46(W1):W242–W245.

Consortium, S. (1998). Genome Sequence of the Nematode C. elegans: A Platform for Investigating Biology. *Science*, 282:2012.

Copeland, J. M., Cho, J., Lo, T., J., Hur, J. H., Bahadorani, S., Arabyan, T., Rabie, J., Soh, J., and Walker, D. W. (2009). Extension of Drosophila life span by RNAi of the mitochondrial respiratory chain. *Curr Biol*, 19(19):1591–8.

Coppola, C. J., R, C. R., and Mendenhall, E. M. (2016). Identification and function of enhancers in the human genome. *Hum Mol Genet*, 25(R2):R190–R197.

Costa-Mattioli, M., Gobert, D., Stern, E., Gamache, K., Colina, R., Cuello, C., Sossin, W., Kaufman, R., Pelletier, J., Rosenblum, K., Krnjevic, K., Lacaille, J. C., Nader, K., and Sonenberg, N. (2007). eIF2alpha phosphorylation bidirectionally regulates the switch from short- to long-term synaptic plasticity and memory. *Cell*, 129(1):195–206.

Costa-Mattioli, M. and Walter, P. (2020). The integrated stress response: From mechanism to disease. *Science*, 368(6489).

Crick, F. (1970). Central Dogma of Molecular Biology. *Nature*, 227.

Curran, S. P., Wu, X., Riedel, C. G., and Ruvkun, G. (2009). A soma-to-germline transformation in long-lived Caenorhabditis elegans mutants. *Nature*, 459(7250):1079–84.

de Godoy, L. M., Olsen, J. V., Cox, J., Nielsen, M. L., Hubner, N. C., Frohlich, F., Walther, T. C., and Mann, M. (2008). Comprehensive mass-spectrometry-based proteome quantification of haploid versus diploid yeast. *Nature*, 455(7217):1251–4.

Deegan, S., Saveljeva, S., Gorman, A. M., and Samali, A. (2013). Stress-induced self-cannibalism: on the regulation of autophagy by endoplasmic reticulum stress. *Cell Mol Life Sci*, 70(14):2425–41.

Deelen, J., Evans, D. S., Arking, D. E., Tesi, N., Nygaard, M., Liu, X., Wojczynski, M. K., Biggs, M. L., van der Spek, A., Atzmon, G., Ware, E. B., Sarnowski, C., Smith, A. V., Seppala, I., Cordell, H. J., Dose, J., Amin, N., Arnold, A. M., Ayers, K. L., Barzilai, N., Becker, E. J., Beekman, M., Blanche, H., Christensen, K., Christiansen, L., Collerton, J. C., Cubaynes, S., Cummings, S. R., Davies, K., Debrabant, B., Deleuze, J. F., Duncan, R., Faul, J. D., Franceschi, C., Galan, P., Gudnason, V., Harris, T. B., Huisman, M., Hurme, M. A., Jagger, C., Jansen, I., Jylha, M., Kahonen, M., Karasik, D., Kardia, S. L. R., Kingston, A., Kirkwood, T. B. L., Launer, L. J., Lehtimaki, T., Lieb, W., Lyytikainen, L. P., Martin-Ruiz, C., Min, J., Nebel, A., Newman, A. B., Nie, C., Nohr, E. A., Orwoll, E. S., Perls, T. T., Province, M. A., Psaty, B. M., Raitakari, O. T., Reinders, M. J. T., Robine, J. M., Rotter, J. I., Sebastiani, P., Smith, J., Sorensen, T. I. A., Taylor, K. D., Uitterlinden, A. G., van der Flier, W., van der Lee, S. J., van Duijn, C. M., van Heemst, D., Vaupel, J. W., Weir, D., Ye, K., Zeng, Y., Zheng, W., Holstege, H., Kiel, D. P., Lunetta, K. L., Slagboom, P. E., and Murabito, J. M. (2019). A meta-analysis of genome-wide association studies identifies multiple longevity genes. *Nat Commun*, 10(1):3669.

Dekanty, A., Lavista-Llanos, S., Irisarri, M., Oldham, S., and Wappner, P. (2005). The insulin-PI3K/TOR pathway induces a HIF-dependent transcriptional response in Drosophila by promoting nuclear localization of HIF-alpha/Sima. *J Cell Sci*, 118(Pt 23):5431–41.

Denzel, M. S., Lapierre, L. R., and Mack, H. I. D. (2019). Emerging topics in C. elegans aging research: Transcriptional regulation, stress response and epigenetics. *Mech Ageing Dev*, 177:4–21.

Denzel, M. S., Storm, N. J., Gutschmidt, A., Baddi, R., Hinze, Y., Jarosch, E., Sommer, T., Hoppe, T., and Antebi, A. (2014). Hexosamine pathway metabolites enhance protein quality control and prolong life. *Cell*, 156(6):1167–1178.

Derisbourg, M. J., Wester, L. E., Baddi, R., and Denzel, M. S. (2021). Mutagenesis screen uncovers lifespan extension through integrated stress response inhibition without reduced mRNA translation. *Nat Commun*, 12(1):1678.

Desplan, C., Chen, X., and Dickman, D. (2017). Development of a tissue-specific ribosome profiling approach in Drosophila enables genome-wide evaluation of translational adaptations. *PLOS Genetics*, 13(12):e1007117.

Dev, K., Qiu, H., Dong, J., Zhang, F., Barthlme, D., and Hinnebusch, A. G. (2010). The beta/Gcd7 subunit of eukaryotic translation initiation factor 2B (eIF2B), a guanine nucleotide exchange factor, is crucial for binding eIF2 in vivo. *Mol Cell Biol*, 30(21):5218–33.

Dever, T. E., Dinman, J. D., and Green, R. (2018). Translation Elongation and Recoding in Eukaryotes. *Cold Spring Harb Perspect Biol*, 10(8).

Dever, T. E. and Green, R. (2012). The elongation, termination, and recycling phases of translation in eukaryotes. *Cold Spring Harb Perspect Biol*, 4(7):a013706.

Dobson, C. M. (2003). Protein folding and misfolding. *Nature*, 426.

Doitsidou, M., Poole, R. J., Sarin, S., Bigelow, H., and Hobert, O. (2010). C. elegans mutant identification with a one-step whole-genome-sequencing and SNP mapping strategy. *PLoS One*, 5(11):e15435.

Dokladal, L., Stumpe, M., Pillet, B., Hu, Z., Garcia Osuna, G. M., Kressler, D., Dengjel, J., and De Virgilio, C. (2021). Global phosphoproteomics pinpoints uncharted Gcn2-mediated mechanisms of translational control. *Mol Cell*.

Erguler, K., Pier, M., and Deltas, C. (2013). A mathematical model of the unfolded protein stress response reveals the decision mechanism for recovery, adaptation and apoptosis. *BMC Systems Biology*, 7.

Essers, P., Tain, L. S., Nespital, T., Goncalves, J., Froehlich, J., and Partridge, L. (2016). Reduced insulin/insulin-like growth factor signaling decreases translation in Drosophila and mice. *Sci Rep*, 6:30290.

Estes, S., Ajie, B. C., Lynch, M., and Phillips, P. C. (2005). Spontaneous mutational correlations for life-history, morphological and behavioral characters in Caenorhabditis elegans. *Genetics*, 170(2):645–53.

Fabian, M. R., Sonenberg, N., and Filipowicz, W. (2010). Regulation of mRNA translation and stability by microRNAs. *Annu Rev Biochem*, 79:351–79.

Farboud, B., Severson, A. F., and Meyer, B. J. (2019). Strategies for Efficient Genome Editing Using CRISPR-Cas9. *Genetics*, 211(2):431–457.

Fawcett, T., Martindale, J., Guyton, K., Hai, T., and Holbrook, N. (1999). Complexes containing activating transcription factor (ATF)/cAMP-responsive- element-binding protein (CREB) interact with the CCAAT/enhancer-binding protein (C/EBP)–ATF composite site to regulate Gadd153 expression during the stress response. *Biochemical Journal*, 339.

Ferretti, M. B., Ghalei, H., Ward, E. A., Potts, E. L., and Karbstein, K. (2017). Rps26 directs mRNA-specific translation by recognition of Kozak sequence elements. *Nature Structural & Molecular Biology*, 24(9):700–707.

Fessler, E., Eckl, E.-M., Schmitt, S., Mancilla, I. A., Meyer-Bender, M. F., Hanf, M., Philippou-Massier, J., Krebs, S., Zischka, H., and Jae, L. T. (2020). A pathway coordinated by DELE1 relays mitochondrial stress to the cytosol. *Nature*.

Fire, A., Xu, S., Montgomery, M., Kostas, S., Driver, S., and C., M. (1998). Potent and specific genetic interference by double-stranded RNA in Caenorhabditis elegans. *Nature*, 391.

Fresno, C. and Fernandez, E. A. (2013). RDAVIDWebService: a versatile R interface to DAVID. *Bioinformatics*, 29(21):2810–1.

Friedman, D. B. and Johnson, T. E. (1988a). A Mutation in the age-1 Gene in Caenorhabditis elegans Lengthens Life and Reduces Hermaphrodite Fertility. *Genetics*, 118:75–86.

Friedman, D. B. and Johnson, T. E. (1988b). Three Mutants That Extend Both Mean and Maximum Life Span of the Nematode, Caenorhabditis Elegans, Define the Age-1 Gene. *Journal of Gerontology*, 43(4):B102–B109.

Froehlich, J. J., Uyar, B., Herzog, M., Theil, K., Glazar, P., Akalin, A., and Rajewsky, N. (2021). Parallel genetics of regulatory sequences using scalable genome editing in vivo. *Cell Rep*, 35(2):108988.

Garcia, M. A., Meurs, E. F., and Esteban, M. (2007). The dsRNA protein kinase PKR: virus and cell control. *Biochimie*, 89(6-7):799–811.

Gems, D., Sutton, A. J., Sundermeyer, M. L., Albert, P. S., King, K. V., Edgley, M. L., Larsen, P. L., and Riddle, D. L. (1998). Two pleiotropic classes of daf-2 mutation affect larval arrest, adult behavior, reproduction and longevity in Caenorhabditis elegans. *Genetics*, 150(1):129–55.

Genuth, N. R. and Barna, M. (2018). The Discovery of Ribosome Heterogeneity and Its Implications for Gene Regulation and Organismal Life. *Mol Cell*, 71(3):364–374.

Gracida, X. and Calarco, J. A. (2017). Cell type-specific transcriptome profiling in C. elegans using the Translating Ribosome Affinity Purification technique. *Methods*, 126:130–137.

Gracida, X., Dion, M. F., Harris, G., Zhang, Y., and Calarco, J. A. (2017). An Elongin-Cullin-SOCS Box Complex Regulates Stress-Induced Serotonergic Neuromodulation. *Cell Rep*, 21(11):3089–3101.

Großhans, X. C. and Ding, H. (2009). Repression of C. elegans microRNA targets at the initiation level of translation requires GW182 proteins. *The EMBO Journal*, 28.

Grossi, V., Forte, G., Sanese, P., Peserico, A., Tezil, T., Lepore Signorile, M., Fasano, C., Lovaglio, R., Bagnulo, R., Loconte, D. C., Susca, F. C., Resta, N., and Simone, C. (2018). The longevity SNP rs2802292 uncovered: HSF1 activates stress-dependent expression of FOXO3 through an intronic enhancer. *Nucleic Acids Res*, 46(11):5587–5600.

Guo, X., Aviles, G., Liu, Y., Tian, R., Unger, B. A., Lin, Y. T., Wiita, A. P., Xu, K., Correia, M. A., and Kampmann, M. (2020). Mitochondrial stress is relayed to the cytosol by an OMA1-DELE1-HRI pathway. *Nature*, 579(7799):427–432.

Haag, E. S. and Dinman, J. D. (2019). Still Searching for Specialized Ribosomes. *Dev Cell*, 48(6):744–746.

Halliday, M., Radford, H., Sekine, Y., Moreno, J., Verity, N., le Quesne, J., Ortori, C. A., Barrett, D. A., Fromont, C., Fischer, P. M., Harding, H. P., Ron, D., and Mallucci, G. R. (2015). Partial restoration of protein synthesis rates by the small molecule ISRIB prevents neurodegeneration without pancreatic toxicity. *Cell Death Dis*, 6:e1672.

Halliday, M., Radford, H., Zents, K. A. M., Molloy, C., Moreno, J. A., Verity, N. C., Smith, E., Ortori, C. A., Barrett, D. A., Bushell, M., and Mallucci, G. R. (2017). Repurposed drugs targeting eIF2alpha-P-mediated translational repression prevent neurodegeneration in mice. *Brain*, 140(6):1768–1783.

Hamanaka, R., Bennett, B., Cullinan, A., and Diehl, A. (2005). PERK and GCN2 Contribute to eIF2Phosphorylation and Cell Cycle Arrest after Activation of the Unfolded Protein Response Pathway. *Molecular Biology of the Cell*, 16.

Hamanaka, R. B., Bobrovnikova-Marjon, E., Ji, X., Liebhaber, S. A., and Diehl, J. A. (2009). PERK-dependent regulation of IAP translation during ER stress. *Oncogene*, 28(6):910–20.

Hamilton, B., Dong, Y., Shindo, M., Liu, W., Odell, I., Ruvkun, G., , and Lee, S. (2005). A systematic RNAi screen for longevity genes in C. elegans. *GENES & DEVELOPMENT*, 19.

Han, A. P., Yu, C., Lu, L., Fujiwara, Y., Browne, C., Chin, G., Fleming, M., Leboulch, P., Orkin, S., and J., C. J. (2001). Heme-regulated eIF2[U+0097] kinase (HRI) is required for translational regulation and survival of erythroid precursors in iron deficiency. *The EMBO Journal*, 20(23).

Hannan, R. D., Jenkins, A., Jenkin, A. K., and Brandenburger, Y. (2003). Cardiac hypertrophy: A matter of translation. *Clinical and Experimental Pharmacology and Physiology*, 30.

Hansen, M., Hsu, A. L., Dillin, A., and Kenyon, C. (2005). New genes tied to endocrine, metabolic, and dietary regulation of lifespan from a Caenorhabditis elegans genomic RNAi screen. *PLoS Genet*, 1(1):119–28.

Hansen, M., Taubert, S., Crawford, D., Libina, N., Lee, S. J., and Kenyon, C. (2007). Lifespan extension by conditions that inhibit translation in Caenorhabditis elegans. *Aging Cell*, 6(1):95–110.

Harding, H. P., Novoa, I., Zhang, Y., Zeng, H., Wek, R., Schapira, M., and Ron, D. (2000). Regulated Translation Initiation Controls Stress-Induced Gene Expression in Mammalian Cells. *Molecular Cell*, 6(5).

Harding, H. P., Ordonez, A., Allen, F., Parts, L., Inglis, A. J., Williams, R. L., and Ron, D. (2019). The ribosomal P-stalk couples amino acid starvation to GCN2 activation in mammalian cells. *Elife*, 8.

Hay, N. and Sonenberg, N. (2004). Upstream and downstream of mTOR. *Genes Dev*, 18(16):1926–45.

Hayflick, L. (1985). Theories of biological aging. *Experimental gerontology*, 20.

Heiman, M., Schaefer, A., Gong, S., Peterson, J. D., Day, M., Ramsey, K. E., Suarez-Farinas, M., Schwarz, C., Stephan, D. A., Surmeier, D. J., Greengard, P., and Heintz, N. (2008). A translational profiling approach for the molecular characterization of CNS cell types. *Cell*, 135(4):738–48.

Hellen, C. U. T. (2018). Translation Termination and Ribosome Recycling in Eukaryotes. *Cold Spring Harb Perspect Biol*, 10(10).

Hench, J., Bratic Hench, I., Pujol, C., Ipsen, S., Brodesser, S., Mourier, A., Tolnay, M., Frank, S., and Trifunovic, A. (2011). A Tissue-Specific Approach to the Analysis of Metabolic Changes in Caenorhabditis elegans. *PLoS ONE*, 6(12):e28417.

Henderson, S. T. and Johnson, T. E. (2001). daf-16 integrates developmental and environmental inputs to mediate aging in the nematode Caenorhabditis elegans. *Current Biology*, 11:1975–1980.

Henis-Korenblit, S., Zhang, P., Hansen, M., McCormick, M., Lee, S. J., Cary, M., and Kenyon, C. (2010). Insulin/IGF-1 signaling mutants reprogram ER stress response regulators to promote longevity. *PNAS*, 107(21).

Herndon, L., Wolkow, C., Driscoll, M., and Hall, D. (2018). Introduction to Aging in C. elegans. *In WormAtlas*.

Herranz, D., Munoz-Martin, M., Canamero, M., Mulero, F., Martinez-Pastor, B., Fernandez-Capetillo, O., and Serrano, M. (2010). Sirt1 improves healthy ageing and protects from metabolic syndrome-associated cancer. *Nat Commun*, 1:3.

Herskind, A. M., McGue, M., Holm, N. V., Sorensen, T. I. A., Harvald, B., and Vaupel, J. W. (1996). The heritability of human longevity: a population-based study of 2872 Danish twin pairs born 1870–1900. *Hum Genet*, 97.

Hetz, C., Zhang, K., and Kaufman, R. J. (2020). Mechanisms, regulation and functions of the unfolded protein response. *Nat Rev Mol Cell Biol*, 21(8):421–438.

Heyer, E. E. and Moore, M. J. (2016). Redefining the Translational Status of 80S Monosomes. *Cell*, 164(4):757–69.

Hinnebusch, A. G. (1988). Mechanisms of Gene Regulation in the General Control of Amino Acid Biosynthesis in Saccharomyces cerevisiae. *Microbiological Reviews*, 52:248–273.

Hinnebusch, A. G. (2005). Translational Regulation of GCN4 and the General Amino Acid Control of Yeast. *Annu. Rev. Microbiol.*, 59.

Hinnebusch, A. G., Ivanov, I. P., and Sonenberg, N. (2016). Translational control by 5′-untranslated regions of eukaryotic mRNAs. *Science*, 352.

Hodgkin, J. and Doniach, T. (1997). Natural Variation and Copulatory Plug Formation in Caenorhabditis elegans. *Genetics*, 146.

Hodgson, R. E., Varanda, B. A., Ashe, M. P., Allen, K. E., and Campbell, S. G. (2019). Cellular eIF2B subunit localisation: implications for the integrated stress response and its control by small molecule drugs. *Mol Biol Cell.*

Honjoh, S., Yamamoto, T., Uno, M., and Nishida, E. (2009). Signalling through RHEB-1 mediates intermittent fasting-induced longevity in C. elegans. *Nature*, 457(7230):726–30.

Horn, M., Kroef, V., Allmeroth, K., Schuller, N., Miethe, S., Peifer, M., Penninger, J. M., Elling, U., and Denzel, M. S. (2018). Unbiased compound-protein interface mapping and prediction of chemoresistance loci through forward genetics in haploid stem cells. *Oncotarget*, 9(11):9838–9851.

Houtkooper, R. H., Canto, C., Wanders, R. J., and Auwerx, J. (2010a). The secret life of NAD+: an old metabolite controlling new metabolic signaling pathways. *Endocr Rev*, 31(2):194–223.

Houtkooper, R. H., Williams, R. W., and Auwerx, J. (2010b). Metabolic networks of longevity. *Cell*, 142(1):9–14.

Howe, K. L., Achuthan, P., Allen, J., Allen, J., Alvarez-Jarreta, J., Amode, M. R., Armean, I. M., Azov, A. G., Bennett, R., Bhai, J., Billis, K., Boddu, S., Charkhchi, M., Cummins, C., Da Rin Fioretto, L., Davidson, C., Dodiya, K., El Houdaigui, B., Fatima, R., Gall, A., Garcia Giron, C., Grego, T., Guijarro-Clarke, C., Haggerty, L., Hemrom, A., Hourlier, T., Izuogu, O. G., Juettemann, T., Kaikala, V., Kay, M., Lavidas, I., Le, T., Lemos, D., Gonzalez Martinez, J., Marugan, J. C., Maurel, T., McMahon, A. C., Mohanan, S., Moore, B., Muffato, M., Oheh, D. N., Paraschas, D., Parker, A., Parton, A., Prosovetskaia, I., Sakthivel, M. P., Salam, A. I. A., Schmitt, B. M., Schuilenburg, H., Sheppard, D., Steed, E., Szpak, M., Szuba, M., Taylor, K., Thormann, A., Threadgold, G., Walts, B., Winterbottom, A., Chakiachvili, M., Chaubal, A., De Silva, N., Flint, B., Frankish, A., Hunt, S. E., GR, I. I., Langridge, N., Loveland, J. E., Martin, F. J., Mudge, J. M., Morales, J., Perry, E., Ruffier, M., Tate, J., Thybert, D., Trevanion, S. J., Cunningham, F., Yates, A. D., Zerbino, D. R., and Flicek, P. (2021). Ensembl 2021. *Nucleic Acids Res*, 49(D1):D884–D891.

Hsin, H. and Kenyon, C. (1999). Signals from the reproductive system regulate the lifespan of C. elegans. *Nature*, 399.

Hu, Z., Xia, B., Postnikoff, S. D., Shen, Z. J., Tomoiaga, A. S., Harkness, T. A., Seol, J. H., Li, W., Chen, K., and Tyler, J. K. (2018). Ssd1 and Gcn2 suppress global translation efficiency in replicatively aged yeast while their activation extends lifespan. *Elife*, 7.

Huang, J., Wu, Z., Wang, J., and Zhang, X. (2018). Quantitative phosphoproteomics reveals GTBP-1 regulating C.elegans lifespan at different environmental temperatures. *Biochem Biophys Res Commun*, 503(3):1962–1967.

Huang da, W., Sherman, B. T., and Lempicki, R. A. (2009). Systematic and integrative analysis of large gene lists using DAVID bioinformatics resources. *Nat Protoc*, 4(1):44–57.

Hussain, S. G. and Ramaiah, K. V. (2007). Reduced eIF2alpha phosphorylation and increased proapoptotic proteins in aging. *Biochem Biophys Res Commun*, 355(2):365–70.

Hutter, H. (2012). Fluorescent Protein Methods: Strategies and Applications. 107:67–92.

Hwang, A. B., Jeong, D. E., and Lee, S. J. (2012). Mitochondria and Organismal Longevity. *Current Genomics*, 13.

Inglis, A. J., Masson, G. R., Shao, S., Perisic, O., McLaughlin, S. H., Hegde, R. S., and Williams, R. L. (2019). Activation of GCN2 by the ribosomal P-stalk. *Proc Natl Acad Sci U S A*.

Ingolia, N. T. (2016). Ribosome Footprint Profiling of Translation throughout the Genome. *Cell*, 165(1):22–33.

Ingolia, N. T., Ghaemmaghami, S., Newman, J. R. S., and Weissman, J. S. (2009). Genome-Wide Analysis in Vivo of Translation with Nucleotide Resolution Using Ribosome Profiling. *Science*, 324.

Inoki, K., Corradetti, M., and Guan, K. L. (2005). Dysregulation of the TSC-mTOR pathway in human disease. *Nature Genetics*, 37.

Jaganathan, K., Kyriazopoulou Panagiotopoulou, S., McRae, J. F., Darbandi, S. F., Knowles, D., Li, Y. I., Kosmicki, J. A., Arbelaez, J., Cui, W., Schwartz, G. B., Chow, E. D., Kanterakis, E., Gao, H., Kia, A., Batzoglou, S., Sanders, S. J., and Farh, K. K. (2019). Predicting Splicing from Primary Sequence with Deep Learning. *Cell*, 176(3):535–548 e24.

Jiang, H. Q., Ren, M., Jiang, H. Z., Wang, J., Zhang, J., Yin, X., Wang, S. Y., Qi, Y., Wang, X. D., and Feng, H. L. (2014). Guanabenz delays the onset of disease symptoms, extends lifespan, improves motor performance and attenuates motor neuron loss in the SOD1 G93A mouse model of amyotrophic lateral sclerosis. *Neuroscience*, 277:132–8.

Jinek, M., Chylinski, K., Fonfara, I., Hauer, M., Doudna, J. A., and Charpentier, E. (2012). A Programmable Dual-RNA–Guided DNA Endonuclease in Adaptive Bacterial Immunity. *Science*, 337.

Johnstone, T. G., Bazzini, A. A., and Giraldez, A. J. (2016). Upstream ORFs are prevalent translational repressors in vertebrates. *EMBO J*, 35(7):706–23.

Jonas, S. and Izaurralde, E. (2015). Towards a molecular understanding of microRNA-mediated gene silencing. *Nat Rev Genet*, 16(7):421–33.

Jousse, C., Oyadomari, S., Novoa, I., Lu, P., Zhang, Y., Harding, H. P., and Ron, D. (2003). Inhibition of a constitutive translation initiation factor 2alpha phosphatase, CReP, promotes survival of stressed cells. *J Cell Biol*, 163(4):767–75.

Jun Zhu, P., Khatiwada, S., Cui, Y., Reineke, L. C., Dooling, S. W., Kim, J. J., Li, W., Walter, P., and Costa-Mattioli, M. (2019). Activation of the ISR mediates the behavioral and neurophysiological abnormalities in Down syndrome. *Science*, 366:843–849.

Kadandale, P., Chatterjee, I., and Singson, A. (2009). Germline transformation of Caenorhabditis elegans by injection. *Methods Mol Biol*, 518:123–33.

Kaletsky, R., Lakhina, V., Arey, R., Williams, A., Landis, J., Ashraf, J., and Murphy, C. T. (2015). The C. elegans adult neuronal IIS/FOXO transcriptome reveals adult phenotype regulators. *Nature*, 529(7584):92–96.

Kaletta, T. and Hengartner, M. O. (2006). Finding function in novel targets: C. elegans as a model organism. *Nat Rev Drug Discov*, 5(5):387–98.

Kamath, R. and Ahringer, J. (2003). Genome-wide RNAi screening in Caenorhabditis elegans. *Methods*, 30(4):313–321.

Kapahi, P., Chen, D., Rogers, A. N., Katewa, S. D., Li, P. W., Thomas, E. L., and Kockel, L. (2010). With TOR, less is more: a key role for the conserved nutrient-sensing TOR pathway in aging. *Cell Metab*, 11(6):453–65.

Karunadharma, P. P., Basisty, N., Dai, D. F., Chiao, Y. A., Quarles, E. K., Hsieh, E. J., Crispin, D., Bielas, J. H., Ericson, N. G., Beyer, R. P., MacKay, V. L., MacCoss, M. J., and Rabinovitch, P. S. (2015). Subacute calorie restriction and rapamycin discordantly alter mouse liver proteome homeostasis and reverse aging effects. *Aging Cell*, 14(4):547–57.

Kashiwagi, K., Yokoyama, T., Nishimoto, M., Takahashi, M., Sakamoto, A., Yonemochi, M., Shirouzu, M., and Ito, T. (2019). Structural basis for eIF2B inhibition in integrated stress response. *Science*, 364(6439):495–499.

Kauffman, A., Parsons, L., Stein, G., Wills, A., Kaletsky, R., and Murphy, C. (2011). C. elegans positive butanone learning, short-term, and long-term associative memory assays. *J Vis Exp*, (49).

Kelly, S., Georgomanolis, T., Zirkel, A., Diermeier, S., O'Reilly, D., Murphy, S., Langst, G., Cook, P. R., and Papantonis, A. (2015). Splicing of many human genes involves sites embedded within introns. *Nucleic Acids Res*, 43(9):4721–32.

Kenner, L. R., Anand, A. A., Nguyen, H. C., Myasnikov, A. G., Klose, C. J., McGeever, L. A., and Frost, A. (2019). eIF2B-catalyzed nucleotide exchangeand phosphoregulation by theintegrated stress response. *Science*, (364(6439)):491–495.

Kenyon, C. (2005). The plasticity of aging: insights from long-lived mutants. *Cell*, 120(4):449–60.

Kenyon, C., Chang, J., , Gensch, E., Rudner, A., and Tabtiang, R. (1993). A C. elegans mutant that lives twice as long as wild type. *Nature*, 366(6454):461-4.

Kenyon, C. J. (2010). The genetics of ageing. *Nature*, 464(7288):504–12.

Khoury, G. A., Baliban, R. C., and Floudas, C. A. (2011). Proteome-wide post-translational modification statistics: frequency analysis and curation of the swiss-prot database. *Sci Rep*, 1.

Kilberg, M. S., Shan, J., and Su, N. (2009). ATF4-dependent transcription mediates signaling of amino acid limitation. *Trends Endocrinol Metab*, 20(9):436–43.

Kim, D., L. B. S. S. L. (2015). HISAT: a fast spliced aligner with low memory requirements. *Nat Methods*, 12(4):357–60.

Kimura, K., Tissenbaum, H. A., Liu, Y., and Ruvkun, G. (1997). daf-2, an Insulin Receptor–Like Gene That Regulates Longevity and Diapause in Caenorhabditis elegans. *Science*, 277.

King, H. A. and Gerber, A. P. (2016). Translatome profiling: methods for genome-scale analysis of mRNA translation. *Brief Funct Genomics*, 15(1):22–31.

Kirkwood, T. B. (2017). The evolution of senescence in the tree of life. *The disposable soma theory*.

Kirstein-Miles, J., Scior, A., Deuerling, E., and Morimoto, R. I. (2013). The nascent polypeptide-associated complex is a key regulator of proteostasis. *EMBO J*, 32(10):1451–68.

Klass, M. R. (1983). A method for the isolation of longevity mutants in the nematode Caenorhabditis elegans and initial results. *Mechanisms of Ageing and Development*, 22(3):279–286.

Koterniak, B., Pilaka, P. P., Gracida, X., Schneider, L. M., Pritisanac, I., Zhang, Y., and Calarco, J. A. (2020). Global regulatory features of alternative splicing across tissues and within the nervous system of C. elegans. *Genome Res*, 30(12):1766–1780.

Kourtis, N. and Tavernarakis, N. (2011). Cellular stress response pathways and ageing: intricate molecular relationships. *EMBO J*, 30(13):2520–31.

Krukowski, K., Nolan, A., Frias, E. S., Boone, M., Ureta, G., Grue, K., Paladini, M. S., Elizarraras, E., Delgado, L., Bernales, S., Walter, P., and Rosi, S. (2020). Small molecule cognitive enhancer reverses age-related memory decline in mice. *Elife*, 9.

Kruse, A. and Wahl, H. W. (2010). *Zukunft Altern - Individuelle und gesellschaftliche Weichenstellungen*. Spektrum Akademischer Verlag.

Krzyzosiak, A., Sigurdardottir, A., Luh, L., Carrara, M., Das, I., Schneider, K., and Bertolotti, A. (2018). Target-Based Discovery of an Inhibitor of the Regulatory Phosphatase PPP1R15B. *Cell*, 174(5):1216–1228 e19.

Lan, J., Rollins, J. A., Zang, X., Wu, D., Zou, L., Wang, Z., Ye, C., Wu, Z., Kapahi, P., Rogers, A. N., and Chen, D. (2019). Translational Regulation of Non-autonomous Mitochondrial Stress Response Promotes Longevity. *Cell Rep*, 28(4):1050–1062 e6.

Lee, S., Liu, B., Lee, S., Huang, S. X., Shen, B., and Qian, S. B. (2012). Global mapping of translation initiation sites in mammalian cells at single-nucleotide resolution. *Proc Natl Acad Sci U S A*, 109(37):E2424–32.

Lee, S. S., Lee, R. Y., Fraser, A. G., Kamath, R. S., Ahringer, J., and Ruvkun, G. (2003). A systematic RNAi screen identifies a critical role for mitochondria in C. elegans longevity. *Nat Genet*, 33(1):40–8.

Lee, Y. Y., Cevallos, R. C., and Jan, E. (2009). An upstream open reading frame regulates translation of GADD34 during cellular stresses that induce eIF2alpha phosphorylation. *J Biol Chem*, 284(11):6661–73.

Lehman, S. L., Ryeom, S., and Koumenis, C. (2015). Signaling through alternative Integrated Stress Response pathways compensates for GCN2 loss in a mouse model of soft tissue sarcoma. *Sci Rep*, 5:11781.

Leon-Annicchiarico, C. L., Ramirez-Peinado, S., Dominguez-Villanueva, D., Gonsberg, A., Lampidis, T. J., and Munoz-Pinedo, C. (2015). ATF4 mediates necrosis induced by glucose deprivation and apoptosis induced by 2-deoxyglucose in the same cells. *FEBS J*, 282(18):3647–58.

Leroi, A. M., Bartke, A., De Benedictis, G., Franceschi, C., Gartner, A., Gonos, E. S., Fedei, M. E., Kivisild, T., Lee, S., Kartaf-Ozer, N., Schumacher, M., Sikora, E., Slagboom, E., Tatar, M., Yashin, A. I., Vijg, J., and Zwaan, B. (2005). What evidence is there for the existence of individual genes with antagonistic pleiotropic effects? *Mech Ageing Dev*, 126(3):421–9.

Li, W., Li, X., and Miller, R. A. (2014). ATF4 activity: a common feature shared by many kinds of slow-aging mice. *Aging Cell*, 13(6):1012–8.

Li, W., Wang, X., Van Der Knaap, M. S., and Proud, C. G. (2004). Mutations linked to leukoencephalopathy with vanishing white matter impair the function of the eukaryotic initiation factor 2B complex in diverse ways. *Mol Cell Biol*, 24(8):3295–306.

Lin, . J., Seroude, L., and Benzer, S. (1998). Extended Life-Span and Stress Resistance in the Drosophila Mutant methuselah. *Science*, 282.

Lin, J., Li, H., Yasumura, D., Cohen, H., Zhang, C., Panning, B., Shokat, K., LaVail, M., and Walter, P. (2007). IRE1 Signaling Affects Cell Fate During the Unfolded Protein Response. *Science*, 318.

Lin, J. H., Li, H., Zhang, Y., Ron, D., and Walter, P. (2009). Divergent effects of PERK and IRE1 signaling on cell viability. *PLoS One*, 4(1):e4170.

Lin, K., Dorman, J., Rodan, A., and Kenyon, C. (1997). daf-16: An HNF-3/forkhead Family Member That Can Function to Double the Life-Span of Caenorhabditis elegans. *Science*, 278.

Lin, S. J., Defossez, P. A., and Guarente, L. (2000). Requirement of NAD and SIR2 for Life-Span Extension by Calorie Restriction in Saccharomyces cerevisiae. *Science*, 289.

Lopez-Otin, C., Blasco, M. A., Partridge, L., Serrano, M., and Kroemer, G. (2013). The hallmarks of aging. *Cell*, 153(6):1194–217.

Love, M. I., Huber, W., and Anders, S. (2014). Moderated estimation of fold change and dispersion for RNA-seq data with DESeq2. *Genome Biol*, 15(12):550.

Lu, P. D., Harding, H. P., and Ron, D. (2004). Translation reinitiation at alternative open reading frames regulates gene expression in an integrated stress response. *J Cell Biol*, 167(1):27–33.

Ma, T., Trinh, M. A., Wexler, A. J., Bourbon, C., Gatti, E., Pierre, P., Cavener, D. R., and Klann, E. (2013). Suppression of eIF2alpha kinases alleviates Alzheimer's disease-related plasticity and memory deficits. *Nat Neurosci*, 16(9):1299–305.

Mair, W., Goymer, P., Pletcher, S. D., and Partridge, L. (2003). Demography of Dietary Restriction and Death in Drosophila. *Science*, 301.

Maklakov, A. A., Rowe, L., and Friberg, U. (2015). Why organisms age: Evolution of senescence under positive pleiotropy? *Bioessays*, 37(7):802–7.

Martina, J. A., Chen, Y., Gucek, M., and Puertollano, R. (2012). MTORC1 functions as a transcriptional regulator of autophagy by preventing nuclear transport of TFEB. *Autophagy*, 8(6):903–14.

Masoro, E. J. (2005). Overview of caloric restriction and ageing. *Mech Ageing Dev*, 126(9):913–22.

Mathew, R., Pal Bhadra, M., and Bhadra, U. (2017). Insulin/insulin-like growth factor-1 signalling (IIS) based regulation of lifespan across species. *Biogerontology*, 18(1):35–53.

Matsumoto, H., Miyazaki, S., Matsuyama, S., Takeda, M., Kawano, M., Nakagawa, H., Nishimura, K., and Matsuo, S. (2013). Selection of autophagy or apoptosis in cells exposed to ER-stress depends on ATF4 expression pattern with or without CHOP expression. *Biol Open*, 2(10):1084–90.

Mattson, M. P. and Wan, R. (2005). Beneficial effects of intermittent fasting and caloric restriction on the cardiovascular and cerebrovascular systems. *J Nutr Biochem*, 16(3):129–37.

McColl, G., Rogers, A. N., Alavez, S., Hubbard, A. E., Melov, S., Link, C. D., Bush, A. I., Kapahi, P., and Lithgow, G. J. (2010). Insulin-like signaling determines survival during stress via posttranscriptional mechanisms in C. elegans. *Cell Metab*, 12(3):260–72.

McLachlan, I. and Flavell, S. (2019). Cell Type-specific mRNA Purification in Caenorhabditis elegans via Translating Ribosome Affinity Purification. *Bio-Protocol*, 9(15).

Meneely, P. M., Dahlberg, C. L., and Rose, J. K. (2019). Working with Worms:Caenorhabditis elegansas a Model Organism. *Current Protocols Essential Laboratory Techniques*, 19(1).

Minevich, G., Park, D. S., Blankenberg, D., Poole, R. J., and Hobert, O. (2012). CloudMap: a cloud-based pipeline for analysis of mutant genome sequences. *Genetics*, 192(4):1249–69.

Mitteldorf, J. (2019). What Is Antagonistic Pleiotropy? *Biochemistry (Mosc)*, 84(12):1458–1468.

Moresco, E. M., Li, X., and Beutler, B. (2013). Going forward with genetics: recent technological advances and forward genetics in mice. *Am J Pathol*, 182(5):1462–73.

Morley, J. F., Brignull, H. R., Weyers, J. J., and Morimoto, R. I. (2002). The threshold for polyglutamine-expansion protein aggregation and cellular toxicity is dynamic and influenced by aging in Caenorhabditis elegans. *Proc Natl Acad Sci U S A*, 99(16):10417–22.

Morley, J. F. and Morimoto, R. I. (2004). Regulation of Longevity in Caenorhabditis elegans by Heat Shock Factor and Molecular Chaperones. *Molecular Biology of the Cell*, 15.

Moroz, N., Carmona, J. J., Anderson, E., Hart, A. C., Sinclair, D. A., and Blackwell, T. K. (2014). Dietary restriction involves NAD(+) -dependent mechanisms and a shift toward oxidative metabolism. *Aging Cell*, 13(6):1075–85.

Morris, J. Z., Tissenbaum, H. A., and Ruvkun, G. (1996). A phosphatidylinositol-3-0H kinase family member regulating longevity and diapause in Caenorhabditis elegans. *Nature*, 382.

Murphy, C. T. and Hu, P. J. (2013). Insulin/insulin-like growth factor signaling in C. elegans. *WormBook*, pages 1–43.

Naidoo, N., Ferber, M., Master, M., Zhu, Y., and Pack, A. I. (2008). Aging impairs the unfolded protein response to sleep deprivation and leads to proapoptotic signaling. *J Neurosci*, 28(26):6539–48.

Norris, K., Hodgson, R. E., Dornelles, T., Allen, K. E., Abell, B. M., Ashe, M. P., and Campbell, S. G. (2020). Mutational analysis of the alpha subunit of eIF2B provides insights into the role of eIF2B bodies in translational control and VWM disease. *J Biol Chem*.

Novoa, I., Zeng, H., Harding, H. P., and Ron, D. (2001). Feedback Inhibition of the Unfolded Protein Response by GADD34-mediated Dephosphorylation of eIF2α. *The Journal of Cell Biology*, 153(5).

Nüske, E., Marini, G., Richter, D., Leng, W., Bogdanova, A., Franzmann, T. M., Pigino, G., and Alberti, S. (2020). Filament formation by the translation factor eIF2B regulates protein synthesis in starved cells. *Biology Open*.

Ogg, S., Paradis, S., Gottlieb, S., Patterson, G., Lee, L., Tissenbaum, H. A., and Ruvkun, G. (1997). The Fork head transcription factor DAF-16 transduces insulin-like metabolic and longevity signals in C. elegans. *Nature*, 389.

Olshen, A. B., Hsieh, A. C., Stumpf, C. R., Olshen, R. A., Ruggero, D., and Taylor, B. S. (2013). Assessing gene-level translational control from ribosome profiling. *Bioinformatics*, 29(23):2995–3002.

Paix, A., Folkmann, A., and Seydoux, G. (2017). Precision genome editing using CRISPR-Cas9 and linear repair templates in C. elegans. *Methods*, 121-122:86–93.

Paix, A., Wang, Y., Smith, H. E., Lee, C. Y., Calidas, D., Lu, T., Smith, J., Schmidt, H., Krause, M. W., and Seydoux, G. (2014). Scalable and versatile genome editing using linear DNAs with microhomology to Cas9 Sites in Caenorhabditis elegans. *Genetics*, 198(4):1347–56.

Pakos-Zebrucka, K., Koryga, I., Mnich, K., Ljujic, M., Samali, A., and Gorman, A. M. (2016). The integrated stress response. *EMBO Rep*, 17(10):1374–1395.

Pakulski, J. (2016). Population ageing and Australia's future: Facing the challenges of an ageing society. *Population Ageing*, 111.

Palam, L. R., Baird, T. D., and Wek, R. C. (2011). Phosphorylation of eIF2 facilitates ribosomal bypass of an inhibitory upstream ORF to enhance CHOP translation. *J Biol Chem*, 286(13):10939–49.

Pan, K. Z., Palter, J. E., Rogers, A. N., Olsen, A., Chen, D., Lithgow, G. J., and Kapahi, P. (2007). Inhibition of mRNA translation extends lifespan in Caenorhabditis elegans. *Aging Cell*, 6(1):111–9.

Partridge, L. (2001). Evolutionary theories of ageing applied to long-lived organisms. *Experimental Gerontology*, 36.

Partridge, L., Pletcher, S. D., and Mair, W. (2005). Dietary restriction, mortality trajectories, risk and damage. *Mech Ageing Dev*, 126(1):35–41.

Pavitt, G., Ramaiah, K., Kimball, S., and Hinnebusch, A. G. (1998). eIF2 independently binds two distinct eIF2B subcomplexes that catalyze and regulate guanine–nucleotide exchange. *GENES & DEVELOPMENT*, 12.

Pertea, M., Pertea, G. M., Antonescu, C. M., Chang, T. C., Mendell, J. T., and Salzberg, S. L. (2015). StringTie enables improved reconstruction of a transcriptome from RNA-seq reads. *Nat Biotechnol*, 33(3):290–5.

Pitt, J. N. and Kaeberlein, M. (2015). Why is aging conserved and what can we do about it? *PLoS Biol*, 13(4):e1002131.

Plötzsch, O. and Rößger, F. (2015). *Statistisches Bundesamt: Bevölkerung Deutschlands 2060. 13. koordinierte Bevölkerungsvorausberechnung.* Wiesbaden.

Price, N. L., Gomes, A. P., Ling, A. J., Duarte, F. V., Martin-Montalvo, A., North, B. J., Agarwal, B., Ye, L., Ramadori, G., Teodoro, J. S., Hubbard, B. P., Varela, A. T., Davis, J. G., Varamini, B., Hafner, A., Moaddel, R., Rolo, A. P., Coppari, R., Palmeira, C. M., de Cabo, R., Baur, J. A., and Sinclair, D. A. (2012). SIRT1 is required for AMPK activation and the beneficial effects of resveratrol on mitochondrial function. *Cell Metab*, 15(5):675–90.

Protter, D. S. W. and Parker, R. (2016). Principles and Properties of Stress Granules. *Trends Cell Biol*, 26(9):668–679.

Proud, C. G. (2007). Signalling to translation: how signal transduction pathways control the protein synthetic machinery. *Biochem J*, 403(2):217–34.

Pyo, J. O., Yoo, S. M., Ahn, H. H., Nah, J., Hong, S. H., Kam, T. I., Jung, S., and Jung, Y. K. (2013). Overexpression of Atg5 in mice activates autophagy and extends lifespan. *Nat Commun*, 4:2300.

Raney, A., Law, G. L., Mize, G. J., and Morris, D. R. (2002). Regulated translation termination at the upstream open reading frame in s-adenosylmethionine decarboxylase mRNA. *J Biol Chem*, 277(8):5988–94.

Reichard, M. (2017). Evolutionary perspectives on ageing. *Semin Cell Dev Biol*, 70:99–107.

Rhoades, J. L., Nelson, J. C., Nwabudike, I., Yu, S. K., McLachlan, I. G., Madan, G. K., Abebe, E., Powers, J. R., Colon-Ramos, D. A., and Flavell, S. W. (2019). ASICs Mediate Food Responses in an Enteric Serotonergic Neuron that Controls Foraging Behaviors. *Cell*, 176(1-2):85–97 e14.

Richardson, C. E., Kinkel, S., and Kim, D. H. (2011). Physiological IRE-1-XBP-1 and PEK-1 signaling in Caenorhabditis elegans larval development and immunity. *PLoS Genet*, 7(11):e1002391.

Robida-Stubbs, S., Glover-Cutter, K., Lamming, D. W., Mizunuma, M., Narasimhan, S. D., Neumann-Haefelin, E., Sabatini, D. M., and Blackwell, T. K. (2012). TOR signaling and rapamycin influence longevity by regulating SKN-1/Nrf and DAF-16/FoxO. *Cell Metab*, 15(5):713–24.

Rogers, A. N., Chen, D., McColl, G., Czerwieniec, G., Felkey, K., Gibson, B. W., Hubbard, A., Melov, S., Lithgow, G. J., and Kapahi, P. (2011). Life span extension via eIF4G inhibition is mediated by posttranscriptional remodeling of stress response gene expression in C. elegans. *Cell Metab*, 14(1):55–66.

Rollins, J. A., Shaffer, D., Snow, S. S., Kapahi, P., and Rogers, A. N. (2019). Dietary restriction induces posttranscriptional regulation of longevity genes. *Life Sci Alliance*, 2(4).

Ron, D. (2002). Translational control in the endoplasmic reticulum stress response. *J Clin Invest*, 110(10):1383–8.

Roobol, A., Roobol, J., Bastide, A., Knight, J. R., Willis, A. E., and Smales, C. M. (2015). p58IPK is an inhibitor of the eIF2alpha kinase GCN2 and its localization and expression underpin protein synthesis and ER processing capacity. *Biochem J*, 465(2):213–25.

Rousakis, A., Vlassis, A., Vlanti, A., Patera, S., Thireos, G., and Syntichaki, P. (2013). The general control nonderepressible-2 kinase mediates stress response and longevity induced by target of rapamycin inactivation in Caenorhabditis elegans. *Aging Cell*, 12(5):742–51.

Rual, J. F., Ceron, J., Koreth, J., Hao, T., Nicot, A. S., Hirozane-Kishikawa, T., Vandenhaute, J., Orkin, S., Hill, D., van den Heuvel, S., and Vidal, M. (2004). Toward Improving Caenorhabditis elegans Phenome Mapping With an ORFeome-Based RNAi Library. *Genome Research*, 14.10b.

Ruby, J. G., Wright, K. M., Rand, K. A., Kermany, A., Noto, K., Curtis, D., Varner, N., Garrigan, D., Slinkov, D., Dorfman, I., Granka, J. M., Byrnes, J., Myres, N., and Ball, C. (2018). Estimates of the Heritability of Human Longevity Are Substantially Inflated due to Assortative Mating. *Genetics*, 210(3):1109–1124.

Salminen, A., Kaarniranta, K., and Kauppinen, A. (2017). Integrated stress response stimulates FGF21 expression: Systemic enhancer of longevity. *Cell Signal*, 40:10–21.

Santos, J., Leitao-Correia, F., Sousa, M. J., and Leao, C. (2016). Dietary Restriction and Nutrient Balance in Aging. *Oxid Med Cell Longev*, 2016:4010357.

Sanz, E., Yang, L., Su, T., Morris, D. R., McKnight, G. S., and Amieux, P. S. (2009). Cell-type-specific isolation of ribosome-associated mRNA from complex tissues. *Proc Natl Acad Sci U S A*, 106(33):13939–44.

Sarin, S., Prabhu, S., O'Meara, M. M., Pe'er, I., and Hobert, O. (2008). Caenorhabditis elegans mutant allele identification by whole-genome sequencing. *Nat Methods*, 5(10):865–7.

Schachter, F., Faure-Delanef, L., Guenot, F., Rouger, H., Froguel, P., Lesueur-Ginot, L., and Cohen, D. (1994). Genetic associations with human longevity at the APOE and ACE loci. *Nature Genetics*, 6.

Scheuner, D., Vander Mierde, D., Song, B., Flamez, D., Creemers, J. W., Tsukamoto, K., Ribick, M., Schuit, F. C., and Kaufman, R. J. (2005). Control of mRNA translation preserves endoplasmic reticulum function in beta cells and maintains glucose homeostasis. *Nat Med*, 11(7):757–64.

Schmidt, E. K., Clavarino, G., Ceppi, M., and Pierre, P. (2009). SUnSET, a nonradioactive method to monitor protein synthesis. *Nat Methods*, 6(4):275–7.

Schneeberger, K. (2014). Using next-generation sequencing to isolate mutant genes from forward genetic screens. *Nat Rev Genet*, 15(10):662–76.

Schoof, M., Boone, M., Wang, L., Lawrence, R., Frost, A., and Walter, P. (2021). eIF2B conformation and assembly state regulate the integrated stress response. *Elife*, 10.

Schwanhausser, B., Busse, D., Li, N., Dittmar, G., Schuchhardt, J., Wolf, J., Chen, W., and Selbach, M. (2011). Global quantification of mammalian gene expression control. *Nature*, 473(7347):337–42.

Sekine, Y., Zyryanova, A., Crespillo-Casado, A., Fischer, P. M., Harding, H. P., and Ron, D. (2015). Mutations in a translation initiation factor identify the target of a memory-enhancing compound. *Science*, 348(6238).

Selman, C., Tullet, J., Wieser, D., Irvine, E., Lingard, S., Choudhury, A., Claret, M., Al-Qassab, H., Carmignac, D., Ramadani, F., Woods, A., Robinson, I., Schuster, E., Batterham, R., Kozma, S., Thomas, G., Carling, D., Okkenhaug, K., Thornton, J., Partridge, L., Gems, D., and Withers, D. (2009). Ribosomal Protein S6 Kinase 1 Signaling Regulates Mammalian Life Span. *Science*, 326.

Sgro, C. and Partridge, L. (1999). A Delayed Wave of Death from Reproduction in Drosophila. *Science*, 286.

Shadyab, A. H. and LaCroix, A. Z. (2015). Genetic factors associated with longevity: a review of recent findings. *Ageing Res Rev*, 19:1–7.

Shama, S., Lai, C. Y., Antoniazzi, J., Jiang, J., and M., J. S. (1998). Heat Stress-Induced Life Span Extension in Yeast. *Experimental cell research*, 245.

Sheaffer, K. L., Updike, D. L., and Mango, S. E. (2008). The Target of Rapamycin pathway antagonizes pha-4/FoxA to control development and aging. *Curr Biol*, 18(18):1355–64.

Shen, X., Ellis, R. E., Sakaki, K., and Kaufman, R. J. (2005). Genetic interactions due to constitutive and inducible gene regulation mediated by the unfolded protein response in C. elegans. *PLoS Genet*, 1(3):e37.

Shi, Z., Fujii, K.and Kovary, K. M., Genuth, N. R., Röst, H. L., Teruel, M. N., and Barna, M. (2017). Heterogeneous Ribosomes Preferentially Translate Distinct Subpools of mRNAs Genome-wide. *Molecular Cell*, 67(1):71–83.e7.

Shimobayashi, M. and Hall, M. N. (2014). Making new contacts: the mTOR network in metabolism and signalling crosstalk. *Nat Rev Mol Cell Biol*, 15(3):155–62.

Sidrauski, C., Acosta-Alvear, D., Khoutorsky, A., Vedantham, P., Hearn, B. R., Li, H., Gamache, K., Gallagher, C. M., Ang, K. K., Wilson, C., Okreglak, V., Ashkenazi, A., Hann, B., Nader, K., Arkin, M. R., Renslo, A. R., Sonenberg, N., and Walter, P. (2013).

Pharmacological brake-release of mRNA translation enhances cognitive memory. *Elife*, 2:e00498.

Sidrauski, C., Tsai, J. C., Kampmann, M., Hearn, B. R., Vedantham, P., Jaishankar, P., Sokabe, M., Mendez, A. S., Newton, B. W., Tang, E. L., Verschueren, E., Johnson, J. R., Krogan, N. J., Fraser, C. S., Weissman, J. S., Renslo, A. R., and Walter, P. (2015). Pharmacological dimerization and activation of the exchange factor eIF2B antagonizes the integrated stress response. *Elife*, 4:e07314.

Silva-Garcia, C. G., Lanjuin, A., Heintz, C., Dutta, S., Clark, N. M., and Mair, W. B. (2019). Single-Copy Knock-In Loci for Defined Gene Expression in Caenorhabditis elegans. *G3 (Bethesda)*, 9(7):2195–2198.

Simsek, D., Tiu, G. C., Flynn, R. A., Byeon, G. W., Leppek, K., Xu, A. F., Chang, H. Y., and Barna, M. (2017). The Mammalian Ribo-interactome Reveals Ribosome Functional Diversity and Heterogeneity. *Cell*, 169(6):1051–1065 e18.

Son, H. G., Altintas, O., Kim, E. J. E., Kwon, S., and Lee, S. V. (2019). Age-dependent changes and biomarkers of aging in Caenorhabditis elegans. *Aging Cell*, 18(2):e12853.

Sonenberg, N. and Hinnebusch, A. G. (2009). Regulation of translation initiation in eukaryotes: mechanisms and biological targets. *Cell*, 136(4):731–45.

Statzer, C., Venz, R., Bland, M., Robida-Stubbs, S., Meng, J., Patel, K., Emsley, R., Petrovic, D., Liu, P., Morantte, I., Haynes, C., Filipovic, M., Mair, W. B., Longchamp, A., Blackwell, T. K., and Ewald, C. Y. (2020). ATF-4 and hydrogen sulfide signalling mediate longevity from inhibition of translation or mTORC1. *bioRxiv preprint*.

Steffen, K. K., MacKay, V. L., Kerr, E. O., Tsuchiya, M., Hu, D., Fox, L. A., Dang, N., Johnston, E. D., Oakes, J. A., Tchao, B. N., Pak, D. N., Fields, S., Kennedy, B. K., and Kaeberlein, M. (2008). Yeast life span extension by depletion of 60s ribosomal subunits is mediated by Gcn4. *Cell*, 133(2):292–302.

Swinney, B. A. and Haubrich, D. C. (2016). Enzyme Activity Assays for Protein Kinases: Strategies to Identify Active Substrates. *Curr Drug Discov Technol.*, 13(1).

Syntichaki, P., Troulinaki, K., and Tavernarakis, N. (2007). Protein synthesis is a novel determinant of aging in Caenorhabditis elegans. *Ann N Y Acad Sci*, 1119:289–95.

Tacutu, R., Thornton, D., Johnson, E., Budovsky, A., Barardo, D., Craig, T., Diana, E., Lehmann, G., Toren, D., Wang, J., Fraifeld, V. E., and de Magalhaes, J. P. (2018). Human Ageing Genomic Resources: new and updated databases. *Nucleic Acids Res*, 46(D1):D1083–D1090.

Tatar, M., Bartke, A., and Antebi, A. (2003). The Endocrine Regulation of Aging by Insulin-like Signals. *Science*, 299.

Taylor, E. J., Campbell, S. G., Griffiths, C. D., Reid, P. J., Slaven, J. W., Harrison, R. J., Sims, P. F. G. and Pavitt, G. D., Delneri, D., and Ashe, M. P. (2010). Fusel Alcohols Regulate Translation Initiation by Inhibiting eIF2B to Reduce Ternary Complex in a Mechanism That May Involve Altering the Integrity and Dynamics of the eIF2B Body. *Molecular Biology of the Cell*, 21:2202–2216.

Taylor, R. C. and Dillin, A. (2013). XBP-1 Is a Cell-Nonautonomous Regulator of Stress Resistance and Longevity. *Cell*, 153(7):1435–1447.

Thomas, A., Lee, P.-J., Dalton, J. E., Nomie, K. J., Stoica, L., Costa-Mattioli, M., Chang, P., Nuzhdin, S., Arbeitman, M. N., and Dierick, H. A. (2012). A Versatile Method for Cell-Specific Profiling of Translated mRNAs in Drosophila. *PLoS ONE*, 7(7):e40276.

Timmons, L., Court, D. L., and Fire, A. (2001). Ingestion of bacterially expressed dsRNAs can produce speci®c and potent genetic interference in Caenorhabditis elegans. *Gene*, 263.

Tissenbaum, H. A. and Guarente, L. (2001). Increased dosage of a sir-2 gene extends lifespan in Caenorhabditis elegans. *Nature*, 410.

Tohyama, D., Yamaguchi, A., and Yamashita, T. (2008). Inhibition of a eukaryotic initiation factor (eIF2Bdelta/F11A3.2) during adulthood extends lifespan in Caenorhabditis elegans. *FASEB J*, 22(12):4327–37.

Trapnell, C., Hendrickson, D. G., Sauvageau, M., Goff, L., Rinn, J. L., and Pachter, L. (2012). Differential analysis of gene regulation at transcript resolution with RNA-seq. *Nature Biotechnology*, 31(1):46–53.

Trapnell, C., Williams, B. A., Pertea, G., Mortazavi, A., Kwan, G., van Baren, M. J., Salzberg, S. L., Wold, B. J., and Pachter, L. (2010). Transcript assembly and quantification by RNA-Seq reveals unannotated transcripts and isoform switching during cell differentiation. *Nat Biotechnol*, 28(5):511–5.

Trepanowski, J. F., Canale, R. E., Marshall, K. E., Kabi, M. M., and Bloomer, R. J. (2011). Impact of caloric and dietary restriction regimens on markers of health and longevity in humans and animals: a summary of available findings. *Nutrition Journal*, 10.

Tsai, J. C., Miller-Vedam, L. E., Anand, A. A., Jaishankar, P., Nguyen, H. C., Renslo, A. R., Frost, A., and Walter, P. (2018). Structure of the nucleotide exchange factor eIF2B reveals mechanism of memory-enhancing molecule. *Science*, 359(6383).

Urry, L., Cain, M., Wasserman, S., Minorsky, P., and Reece, J. (2016). *Campbell Biology, 11th.* Lisa Urry, Michael Cain, Steven Wasserman, Peter Minorsky, Jane Reece.

van den Berg, N., Beekman, M., Smith, K. R., Janssens, A., and Slagboom, P. E. (2017). Historical demography and longevity genetics: Back to the future. *Ageing Res Rev*, 38:28–39.

van der Knaap, M. S., Leegwater, P. A., Konst, A. A., Visser, A., Naidu, S., Oudejans, C. B., Schutgens, R. B., and Pronk, J. C. (2002). Mutations in each of the five subunits of translation initiation factor eIF2B can cause leukoencephalopathy with vanishing white matter. *Ann Neurol*, 51(2):264–70.

van Ham, T. J., Thijssen, K. L., Breitling, R., Hofstra, R. M., Plasterk, R. H., and Nollen, E. A. (2008). C. elegans model identifies genetic modifiers of alpha-synuclein inclusion formation during aging. *PLoS Genet*, 4(3):e1000027.

van Heemst, D., Beekman, M., Mooijaart, S. P., Heijmans, B. T., Brandt, B. W., Zwaan, B. J., Slagboom, P. E., and Westendorp, R. G. (2005). Reduced insulin/IGF-1 signalling and human longevity. *Aging Cell*, 4(2):79–85.

Vander Haar, E., Lee, S. I., Bandhakavi, S., Griffin, T. J., and Kim, D. H. (2007). Insulin signalling to mTOR mediated by the Akt/PKB substrate PRAS40. *Nat Cell Biol*, 9(3):316–23.

Vanderperre, B., Lucier, J. F., Bissonnette, C., Motard, J., Tremblay, G., Vanderperre, S., Wisztorski, M., Salzet, M., Boisvert, F. M., and Roucou, X. (2013). Direct detection of alternative open reading frames translation products in human significantly expands the proteome. *PLoS One*, 8(8):e70698.

Vattem, K. M. and Wek, R. C. (2004). Reinitiation involving upstream ORFs regulates ATF4 mRNA translation in mammalian cells. *Proc Natl Acad Sci U S A*, 101(31):11269–74.

Vazquez de Aldana, C. R. and Hinnebusch, A. G. (1994). Mutations in the GCD7 subunit of yeast guanine nucleotide exchange factor eIF-2B overcome the inhibitory effects of phosphorylated eIF-2 on translation initiation. *Molecular and Cellular Biology*, 14.5.

Vazquez de Aldana, C. R., Wek, R. C., Segundo, P. S., Truesdell, A. G., and Hinnebusch, A. G. (1994). Multicopy tRNA genes functionally suppress mutations in yeast eIF-2 alpha kinase GCN2: evidence for separate pathways coupling GCN4 expression to unchanged tRNA. *Molecular and Cellular Biology*, 14(12).

Visser, M., Palstra, R. J., and Kayser, M. (2015). Allele-specific transcriptional regulation of IRF4 in melanocytes is mediated by chromatin looping of the intronic rs12203592 enhancer to the IRF4 promoter. *Hum Mol Genet*, 24(9):2649–61.

Visweswaraiah, J., Lageix, S., Castilho, B. A., Izotova, L., Kinzy, T. G., Hinnebusch, A. G., and Sattlegger, E. (2011). Evidence that eukaryotic translation elongation factor 1A (eEF1A) binds the Gcn2 protein C terminus and inhibits Gcn2 activity. *J Biol Chem*, 286(42):36568–79.

Wang, M. C., O'Rourke, E. J., and Ruvkun, G. (2008). Fat Metabolism Links Germline Stem Cells and Longevity in C. elegans. *Science*, 322.

Weingarten-Gabbay, S., Elias-Kirma, S., Nir, R., Gritsenko, A. A., Stern-Ginossar, N., Yakhini, Z., Weinberger, A., and Segal, E. (2016). Comparative genetics. Systematic discovery of cap-independent translation sequences in human and viral genomes. *Science*, 351(6270).

Wek, R. C. (2018). Role of eIF2alpha Kinases in Translational Control and Adaptation to Cellular Stress. *Cold Spring Harb Perspect Biol*, 10(7).

Wilkie, G. S., Dickson, K. S., and Gray, N. K. (2003). Regulation of mRNA translation by 5′- and 3′-UTR-binding factors. *Trends in Biochemical Sciences*, 28(4):182–188.

Wong, Y. L., LeBon, L., Basso, A. M., Kohlhaas, K. L., Nikkel, A. L., Robb, H. M., Donnelly-Roberts, D. L., Prakash, J., Swensen, A. M., Rubinstein, N. D., Krishnan, S., McAllister, F. E., Haste, N. V., O'Brien, J. J., Roy, M., Ireland, A., Frost, J. M., Shi, L., Riedmaier, S., Martin, K., Dart, M. J., and Sidrauski, C. (2019). eIF2B activator prevents neurological defects caused by a chronic integrated stress response. *Elife*, 8.

Wong, Y. L., LeBon, L., Edalji, R., Lim, H. B., Sun, C., and Sidrauski, C. (2018). The small molecule ISRIB rescues the stability and activity of Vanishing White Matter Disease eIF2B mutant complexes. *Elife*, 7.

Ye, J., Kumanova, M., Hart, L. S., Sloane, K., Zhang, H., De Panis, D. N., Bobrovnikova-Marjon, E., Diehl, J. A., Ron, D., and Koumenis, C. (2010). The GCN2-ATF4 pathway is critical for tumour cell survival and proliferation in response to nutrient deprivation. *EMBO J*, 29(12):2082–96.

Yoon, M. S. (2017). The Role of Mammalian Target of Rapamycin (mTOR) in Insulin Signaling. *Nutrients*, 9(11).

Zanin, E., Dumont, J., Gassmann, R., Cheeseman, I., Maddox, P., Bahmanyar, S., Carvalho, A., Niessen, S., Yates, J. R., r., Oegema, K., and Desai, A. (2011). Affinity purification of protein complexes in C. elegans. *Methods Cell Biol*, 106:289–322.

Zetsche, B., Gootenberg, J. S., Abudayyeh, O. O., Slaymaker, I. M., Makarova, K. S., Essletzbichler, P., Volz, S. E., Joung, J., van der Oost, J., Regev, A., Koonin, E. V., and Zhang, F. (2015). Cpf1 is a single RNA-guided endonuclease of a class 2 CRISPR-Cas system. *Cell*, 163(3):759–71.

Zhang, Q., Nogales-Cadenas, R., Lin, J. R., Zhang, W., Cai, Y., Vijg, J., and Zhang, Z. D. (2016). Systems-level analysis of human aging genes shed new light on mechanisms of aging. *Hum Mol Genet*, 25(14):2934–2947.

Zhang, S., Banerjee, D., and R., K. J. (2011). Isolation and Culture of Larval Cells from C. elegans. *PLoS ONE*, 6(4):e19505.

Zhou, G., Myers, R., Li, Y., Chen, Y., Shen, X., Fenyk-Melody, J., Wu, M., Ventre, J., Doebber, T., Fujii, N., Musi, N., Hirshman, M. F., Goodyear, L. J., and Moller, D. E. (2001). Role of AMP-activated protein kinase in mechanism of metformin action. *Journal of Clinical Investigation*, 108(8):1167–1174.

Zid, B. M., Rogers, A. N., Katewa, S. D., Vargas, M. A., Kolipinski, M. C., Lu, T. A., Benzer, S., and Kapahi, P. (2009). 4E-BP extends lifespan upon dietary restriction by enhancing mitochondrial activity in Drosophila. *Cell*, 139(1):149–60.

Zielinska, D. F., Gnad, F., Jedrusik-Bode, M., Wisniewski, J. R., and Mann, M. (2009). Caenorhabditis elegans Has a Phosphoproteome Atypical for Metazoans That Is Enriched in Developmental and Sex Determination Proteins. *Journal of Proteome Research*, 8:4039–4049.

Zyryanova, A. F., Kashiwagi, K., Rato, C., Harding, H. P., Crespillo-Casado, A., Perera, L. A., Sakamoto, A., Nishimoto, M., Yonemochi, M., Shirouzu, M., Ito, T., and Ron, D. (2020). ISRIB Blunts the Integrated Stress Response by Allosterically Antagonising the Inhibitory Effect of Phosphorylated eIF2 on eIF2B. *Mol Cell*.

Appendix

Supplementary material

Table 4: The high-confidence candidate gene list from the forward longevity screen. Depicted are the the first and last gene from the list sorted by a score integrating the coding size of the gene with the number of independent alleles in long-lived worms generated by the EMS mutagenesis. The lower the score, the more likely the mutation in the gene has an effect. Identified novel *daf-2* alleles are shown as reference. Furthermore, genes that were tested are depicted. Mutations in the shown genes were re-created using CRISPR/Cas9 (orange) or respective lines were outcrossed for corresponding mutations (blue). The outcrossing of defined alleles in *ppp-1*, *gcn-2* and *pek-1* caused longevity (green).

Ranking	Gene name	CDS size (nt)	Alleles	Score
1	*F16H11.2*	174	5	0,01
2	*C08H9.4*	324	3	0,03
3	*C27B7.9*	273	2	0,04
5	*spp-5*	312	2	0,04
9	*F41F3.3*	471	2	0,06
10	*T03D8.2*	474	2	0,06
16	*C55B6.1*	900	3	0,08
20	*ife-2*	687	2	0,09
21	*srh-118*	1059	3	0,10
23	*eif-6*	741	2	0,10
30	*Y39G8C.2*	831	2	0,11
34	*col-106*	891	2	0,12
47	*srh-129*	1005	2	0,14
52	*W06B4.2*	1566	3	0,14
66	*ppp-1*	1215	2	0,16
136	*tsn-1*	2745	3	0,25
x	***daf-2***	**251**	**6**	**0,25**
139	*toe-2*	1866	2	0,25
155	*clr-1*	4335	4	0,29
156	*tat-1*	3270	3	0,29
213	*pek-1*	3234	2	0,44
215	*pqn-85*	6612	4	0,45
250	*mrp-2*	4578	2	0,62
257	*gcn-2*	5100	2	0,69
282	*lrk-1*	7182	2	0,97
303	*dig-1*	36753	3	3,31

Table 5: TEA of the 5 % most up-regulated genes in NeuroRiboTag co-IP elution fractions compared to total RNA levels. Shown are all significantly enriched *C. elegans* tissue terms.

Term	Expected	Observed	Enrichment Fold Change	P value
ventral nerve cord WBbt:0005829	61	199	3,3	3,30E-49
RIS WBbt:0005045	25	109	4,3	2,70E-38
hook sensillum WBbt:0006930	15	75	5,1	4,00E-32
CEM WBbt:0005246	15	74	5,1	7,50E-32
inner labial sensillum WBbt:0005116	20	85	4,3	1,20E-30
ray WBbt:0006941	18	76	4,1	2,50E-26
ASE WBbt:0005663	79	165	2,1	4,30E-19
lateral ganglion WBbt:0005105	100	197	1,9	9,00E-19
BAG WBbt:0006825	21	64	3,1	7,60E-16
AVE WBbt:0006819	29	71	2,4	4,30E-12
retrovesicular ganglion WBbt:0005656	58	113	2	9,30E-12
AVK WBbt:0006823	70	126	1,8	1,50E-10
amphid sensillum WBbt:0005391	160	242	1,5	7,30E-10
pharyngeal interneuron WBbt:0003668	45	88	2	1,10E-09
PVD WBbt:0006831	120	190	1,6	1,50E-09
outer labial sensillum WBbt:0005501	120	192	1,5	2,20E-09
thermosensory neuron WBbt:0005838	96	155	1,6	2,70E-09
nerve ring WBbt:0006749	38	74	1,9	3,40E-08
RID WBbt:0003938	8	25	3,1	1,20E-07
posterior lateral ganglion WBbt:0005465	8	22	2,7	7,00E-06
tail WBbt:0005741	84	123	1,5	1,50E-05
preanal ganglion WBbt:0005448	10	24	2,5	1,60E-05
FLP WBbt:0006828	13	30	2,2	1,70E-05
ASK WBbt:0005668	6	18	2,8	2,10E-05
ALA WBbt:0003955	1	7	5	5,40E-05
touch receptor neuron WBbt:0005237	83	119	1,4	6,00E-05
AUA WBbt:0006817	2	7	4,6	0,00011
head mesodermal cell WBbt:0004697	130	177	1,3	0,00011
HSN WBbt:0006830	6	15	2,7	0,00013
ASI WBbt:0005666	10	22	2,2	0,00019
PHA WBbt:0007807	6	14	2,5	0,00045
ASJ WBbt:0005667	5	13	2,5	0,00062
ASG WBbt:0005664	3	9	3,1	0,00062
BDU WBbt:0006826	2	7	3,6	0,00063
corpus WBbt:0003733	90	120	1,3	0,00065
SDQL WBbt:0004993	2	6	3,6	0,0011
SMD WBbt:0005353	2	7	3,1	0,0016
AWCL WBbt:0003827	5	12	2,3	0,0019
AWCR WBbt:0003826	5	12	2,3	0,0019
AVB WBbt:0005841	1	5	3,6	0,0024
RIC WBbt:0006834	2	5	3,4	0,0032
AVG WBbt:0003850	13	23	1,8	0,0035
dorsal nerve cord WBbt:0006750	26	39	1,5	0,0042
ALN WBbt:0006851	2	5	3,2	0,0043
ADF WBbt:0005660	4	9	2,4	0,0047
URX WBbt:0006846	3	7	2,6	0,0054
AVD WBbt:0006818	13	22	1,7	0,007
AIM WBbt:0006814	2	5	2,9	0,0072
SDQR WBbt:0004991	2	5	2,8	0,0081

Table 6: TEA of the 5 % most down-regulated genes in NeuroRiboTag co-IP elution fractions compared to total RNA levels. Shown are all significantly enriched *C. elegans* tissue terms.

Term	Expected	Observed	Enrichment Fold Change	P value
germ line WBbt:0005784	170	328	2	2,80E-31
reproductive system WBbt:0005747	200	338	1,7	1,30E-20
oocyte WBbt:0006797	4	27	6,6	1,60E-15
head mesodermal cell WBbt:0004697	76	146	1,9	1,00E-13
Psub3 WBbt:0006875	2	16	10	2,40E-13
Psub1 WBbt:0006874	6	27	4,7	7,70E-12
Z2 WBbt:0004576	1	13	10	2,80E-11
Z3 WBbt:0004575	1	13	10	2,80E-11
AB WBbt:0004015	3	18	6,3	8,20E-11
EMS WBbt:0006876	2	14	8,2	1,30E-10
BAG WBbt:0006825	12	35	3	6,00E-09
PSub2 WBbt:0006873	1	9	8	1,50E-07
Z4.a WBbt:0007025	15	35	2,4	1,60E-06
Z1.p WBbt:0007023	15	35	2,4	1,60E-06
male distal tip cell WBbt:0006864	15	35	2,3	1,80E-06
accessory cell WBbt:0005762	35	62	1,8	7,70E-06
reproductive tract WBbt:0005744	45	75	1,7	1,30E-05
cephalic sheath cell WBbt:0008406	18	37	2,1	1,40E-05
muscular system WBbt:0005737	170	217	1,3	7,30E-05
C WBbt:0003810	1	6	5,7	8,10E-05
epithelial system WBbt:0005730	120	163	1,3	0,00021
hermaphrodite WBbt:0007849	55	79	1,4	0,00073
E WBbt:0004804	1	4	4,9	0,0012

Table 7: Human and mouse orthologs of *C. elegans kin-35*. Orthologs determined using Ensembl 2021 (Howe et al., 2021).

Species	Orthologue	Target %id	Query %id	High Confidence
Homo sapiens	VRK2	13.58 %	15.72 %	No
Homo sapiens	VRK1	14.96 %	15.26 %	No
Homo sapiens	VRK3	11.60 %	12.53 %	No
Homo sapiens	TTBK2	5.22 %	19.59 %	No
Homo sapiens	CSNK1G2	17.35 %	16.40 %	No
Homo sapiens	TTBK1	7.72 %	23.23 %	No
Homo sapiens	CSNK1G1	15.37 %	16.63 %	No
Homo sapiens	CSNK1A1L	22.26 %	17.08 %	No
Mus musculus	Vrk3	12.14 %	12.53 %	No
Mus musculus	Csnk1g2	16.52 %	16.63 %	No
Mus musculus	Ttbk1	7.80 %	23.23 %	No
Mus musculus	Vrk1	15.68 %	15.72 %	No
Mus musculus	Csnk1g1	15.84 %	16.63 %	No
Mus musculus	Vrk2	14.51 %	16.63 %	No
Mus musculus	Ttbk2	7.55 %	22.55 %	No

Replicate	Strain	Mean LS (days)	Difference (%)	dead/censored animals	P value; Mantel-Cox log rank method	Reference control	Figure
1 (15 11 15)	CF512	18,04	0	71/80			Fig. 10b
	MSD211	26,34	46	78/57	p<0,0001	vs WT	
1 (13 02 18)	WT	20,23	0	102/30			Fig. 10d
	R160.6(wrm)	20,09	-1	89/30	p = 0,09	vs WT	
1 (22 6 20)	WT WBM	21,35	0	93/36			
	rpl-22(wbm58)	21,46	1	62/41	p = 0,55	vs WT WBM	Fig. 24a
	wmbIs99	21,22	-1	62/39	p = 0,89	vs WT WBM	Fig. 27a
2 (22 6 20)	WT WBM	21,94	0	80/21			
	rpl-22(wbm58)	21,77	-1	53/46	p = 0,91	vs WT WBM	Fig. 24a
	wmbIs99	21,24	-3	46/42	p = 0,61	vs WT WBM	Fig. 27a

Table 8: Lifespan statistics.

All other lifespan statistics are published under:

M Derisbourg, L Wester, R Baddi, M Denzel.

Mutagenesis screen uncovers lifespan extension through integrated stress response inhibition without reduced mRNA translation.

Nature Communications, 2021.

DOI: 10.1038/s41467-021-21743-x

Contributions

Table 9: Experimental work contributions.

Experimental work contributions:	
Figure 8: Unbiased forward longevity screen in C. elegans.	M.J.D., R.B., L.E.W.
Figure 9: Outcrossing for longevity.	L.E.W.
Figure 10: Mutations in known longevity genes identified through a mutagenesis screen for longevity.	L.E.W.
Figure 11: Mutations in ISR components identified in the forward longevity screen in C. elegans.	M.J.D., L.E.W., R.B.
Figure 12: Mutations in ppp-1 do not attenuate global protein synthesis.	M.J.D., L.E.W
Figure 13: ISR analysis in aged ppp-1 mutants.	M.J.D., L.E.W
Figure 14: Translational efficiency is altered in ppp-1 mutants.	L.E.W., M.J.D.
Figure 15: kin-35 translation is required for ppp-1 longevity.	M.J.D., L.E.W., R.B.
Figure 16: eIF2B activity is required for the longevity phenotype of ppp-1 mutants	M.J.D., R.B.
Figure 17: Mutations in ppp-1 and in eIF2 kinases reduce ISR activity.	L.E.W., M.J.D.
Figure 18: Inhibiting the ISR through ppp-1 mutations does not activate UPR or insulin signaling pathways.	L.E.W., M.J.D.
Figure 19: Estradiol Valerate inhibits the ISR and extends lifespan.	L.E.W., M.J.D., R.B.
Figure 20: Direct ISR inhibition through phospho-defective eIF2αS51A mutations mimicks ppp-1 mutations and extends lifespan.	M.J.D., L.E.W., R.B.
Figure 21: eIF2αS51A mutant longevity depends on kin-35 and ppp-1; constitutive ISR activation via phospho-mimic eIF2αS51D/+ mutations shortens C. elegans lifespan.	M.J.D., L.E.W., R.B.
Figure 23: Adding an N-terminal FLAG tag to RPL-22 does not impact worm health or overall mRNA translation.	L.E.W., E.H.W.B., A.L.
Figure 24: RiboTag co-IP from endogenously FLAG-tagged rpl-22(wbm58) animals and analysis of eluted protein and RNA.	L.E.W., E.H.W.B., A.L.
Figure 26: Neuron-specific expression of FLAGRPL-22 does not impact worm health or overall translation and is sufficient for RiboTag co-IPs.	L.E.W., E.H.W.B., A.L.
Figure 27: Co-IPs from NeuroRiboTag worms are sufficient to isolate and analyse mRNAs specifically translated in neuronal tissues.	L.E.W., E.H.W.B., A.L.

L.E.W.	Laura Elisabeth Wester (MPI for Biology of Ageing, Cologne)
M.J.D.	Maxime Joel Derisbourg (MPI for Biology of Ageing, Cologne)
R.B.	Ruth Baddi (MPI for Biology of Ageing, Cologne)
E.H.W.B.	Emanuel Hans Walter Bruckisch (MPI for Biology of Ageing, Cologne)
A.L.	Anne Lanjuin (Harvard T.H. Chan School of Public Health, Boston)

Bioinformatic analyses were performed in collaboration with the Bioinformatics Core Facility at the MPI for Biology of Ageing, Cologne.

Acknowledgements

I want to say thank you to **Dr. Martin Denzel**. First of all, thank you for giving me the opportunity to perform my PhD in your lab. During a career event, I heard that choosing goodness and kindness is a crucial part to become a good scientist. I am happy that I did my PhD in a lab where these values are cherished. Thank you for always lending an ear whenever needed, giving advice, being about science or beyond, and always seeing the science AND the person. The time in your lab made me a scientist by passion.

I want to thank **Prof. Linda Partridge**, **Prof. Andreas Beyer** and **Dr. Maxime Derisbourg** for being part of my thesis advisory committee. You were giving me valuable input during the course of my PhD.

Thank you to my thesis committee members, **Prof. Andreas Beyer** and **Prof. Ulrich Baumann**, for taking your time to evaluate my work.

I want to thank **assoc. Prof. William Mair** for the collaborative work on the RiboTag project. Moreover, you gave me so much advice on my career path - this really encouraged me to further pursue a scientific career. Thank you! I also want to thank **Dr. Anne Lanjuin** for the collaboration on the RiboTag project. Even though we never met in person, your passion for science crosses Zoom borders and is contagious.

Dr. Franziska Metge and **Dr. Jorge Boucas** as well as all members of the **bioinformatics core facility** at MPI AGE, thank you for supporting the work of this thesis with your analyses and for always vitally discussing and explaining your approaches.

I want to thank you, **Maxime**, for always having my back on a daily basis. No matter how crazy my thoughts or questions were, you answered all of them and helped me whenever I was struggling. You did not hesitate a minute to include me into 'team *ppp-1*' and I appreciated that a lot. We really were partners in crime on this and I think we rocked it. You always helped me to keep the big picture in mind when science was giving me a hard time. Thank you for being 'my' postdoc, teaching me science!

A big thank you to the whole **Denzel lab**! Dear Martin, Maxime, Ruth, Emi, Kira, Eike, Marco, Mati, Virginia, Felix, Sabine, Moritz and everyone past and present in the Denzel lab, you made the time that I spent doing my PhD not only work but so much beyond. Whenever I did not want to come back to the worms for scientific reasons, I enjoyed coming to the Institute for your company. I have so many amazing memories with all of you, I cannot thank you enough for that! I also want to thank all of you for always supporting and helping me, scientifically and personally. I further want to thank everybody in the **Antebi lab** for their support.

Ruthi, you taught me so much about worms and working with you was a great pleasure. Thank you so much for not only being part of 'team *ppp-1*' but also for becoming a friend. You always were there and listening, no matter what I needed to get off my chest. I enjoyed working with you a lot and without you, 'team *ppp-1*' and the Denzel lab would not have been the same!

Emi, it was a pleasure working with you on a scientific and personal level! Thank you for all the great work on the RiboTag project, but more importantly for being such an open, curious and positive person. I wish you all the best for your own PhD, I am sure you are

rocking it!

Dr. Kira, you supported me so much on a personal and a scientific level. Your ability to keep track of projects that are not even close to your own amazes me. And that not being enough, you are always willing to help others during hard times, even if that means you have to stay at the FACS until midnight. Thank you for always being helpful, scientifically and personally!

Dear **Mati**, thank you for always being involved, kind and fun, even though living on another continent. Thank you so much for helping me out when you had enough on your own plate!

Virginia, **Miri** and **Kira**, you became not only inevitable as PhD support group, but I was lucky enough to find true friends in you. Thank you for all the coffee breaks, pep talks, fun at carnival and Christmas parties and just being there, whenever needed!

Thank you to the **CGA class of 2016**. You made the CGA curriculum a blast and I was always looking forward to see all of you during all the courses, journal clubs, lectures and events. It was great to share the PhD journey with you.

I want to thank the **CGA coordination** team and specifically **Jenny Ostermann** and **Dr. Daniela Morick** for always being on our side. **Dany**, you helped me a lot with your calm and positive way of thinking when I had a hard time believing in myself. Thank you!

I lastly want to thank the important people that shaped my way towards pursuing a PhD. **Dr. Mara Werwie**, thank you for being my first scientific role model with your passion and love for science. The **Paulsen lab** showed me, how fun research groups can be to work in. **Prof. Hans Zischler** and **Dr. David Rosenkranz**, thank you for endorsing me to pursue a PhD.

Last but not least, mein herzlicher Dank gilt...

... meinen **Eltern** Martina und Martin. Zuerst möchte ich meiner Mutter Martina für das tolle Titelbild danken! Mama und Papa, Ihr unterstützt mich immer und seid immer auf meiner Seite, egal was kommt – das ist ein unglaublich gutes Gefühl. Ich danke Euch von ganzem Herzen für alles! Auch meinen **Großeltern** Karl und Gretel möchte ich ganz herzlich für ihre Unterstützung danken!

... meinen **Freunden**. Ich möchte Euch dafür danken, dass Ihr mich immer unterstützt habt und auch dann für mich da wart, wenn ich mich in stressigen Phasen seltener gemeldet habe oder hin und wieder zu viel über Würmer gesprochen habe. Liebe Valentina, wir sehen uns zwar nicht so häufig, aber zu wissen, dass Du immer da bist, ist einfach toll. Liebe Laura, die Studienzeit hätte schöner und lustiger nicht sein können als mit Dir – ich bin froh, dass unsere Freundschaft das Studium überdauert hat! Liebe Caro, lieber Malte, dass Ihr nach Köln gezogen seid ist eine riesige Bereicherung und die vielen tollen Treffen mit Euch waren wie kleine Urlaube in mitten einer manchmal anstrengenden Doktorzeit! Lieber Freddy, liebe Laura, mit Euch unterwegs zu sein ist immer eine große Freude und Eure entspannte und optimistische Art ist einfach ansteckend! Eure Freundschaften haben mich immer auf den Boden der Tatsachen gebracht, dass selbst die aufregendste Forschung nichts wert ist, wenn man niemanden hat, mit dem man seine Freude teilen kann!

... meinem Partner **Paul**. Lieber Paul, der größte Dank gilt wohl Dir. Du hast so viele Verrücktheiten von mir ertragen, hast Dir so viele Probe-Vorträge über meine Forschung angehört, hast mit mir über Würmer diskutiert und benutzt nun selbstverständlich Begriffe wie *ppp-1* und Dauer Zustand. Du hast mir immer den Rücken frei gehalten, wenn es stressig wurde. Mit Dir an meiner Seite kann nichts schief gehen! Tausend Dank für alles!

Erklärung

Ich versichere, dass ich die von mir vorgelegte Dissertation selbständig angefertigt, die benutzten Quellen und Hilfsmittel vollständig angegeben und die Stellen der Arbeit − einschließlich Tabellen, Karten und Abbildungen −, die anderen Werken im Wortlaut oder dem Sinn nach entnommen sind, in jedem Einzelfall als Entlehnung kenntlich gemacht habe; dass diese Dissertation noch keiner anderen Fakultät oder Universität zur Prüfung vorgelegen hat; dass sie − abgesehen von unten angegebenen Teilpublikationen − noch nicht veröffentlicht worden ist, sowie, dass ich eine solche Veröffentlichung vor Abschluss des Promotionsverfahrens nicht vornehmen werde. Die Bestimmungen der Promotionsordnung sind mir bekannt. Die von mir vorgelegte Dissertation ist von Dr. Martin Denzel betreut worden.

Köln, Mai 2021
Laura Wester

Teile dieser Arbeit wurden bereits veröffentlicht:

M Derisbourg, **L Wester**, R Baddi, M Denzel. Mutagenesis screen uncovers lifespan extension through integrated stress response inhibition without reduced mRNA translation. *Nature Communications*. DOI: 10.1038/s41467-021-21743-x. **2021**. Equal contribution.